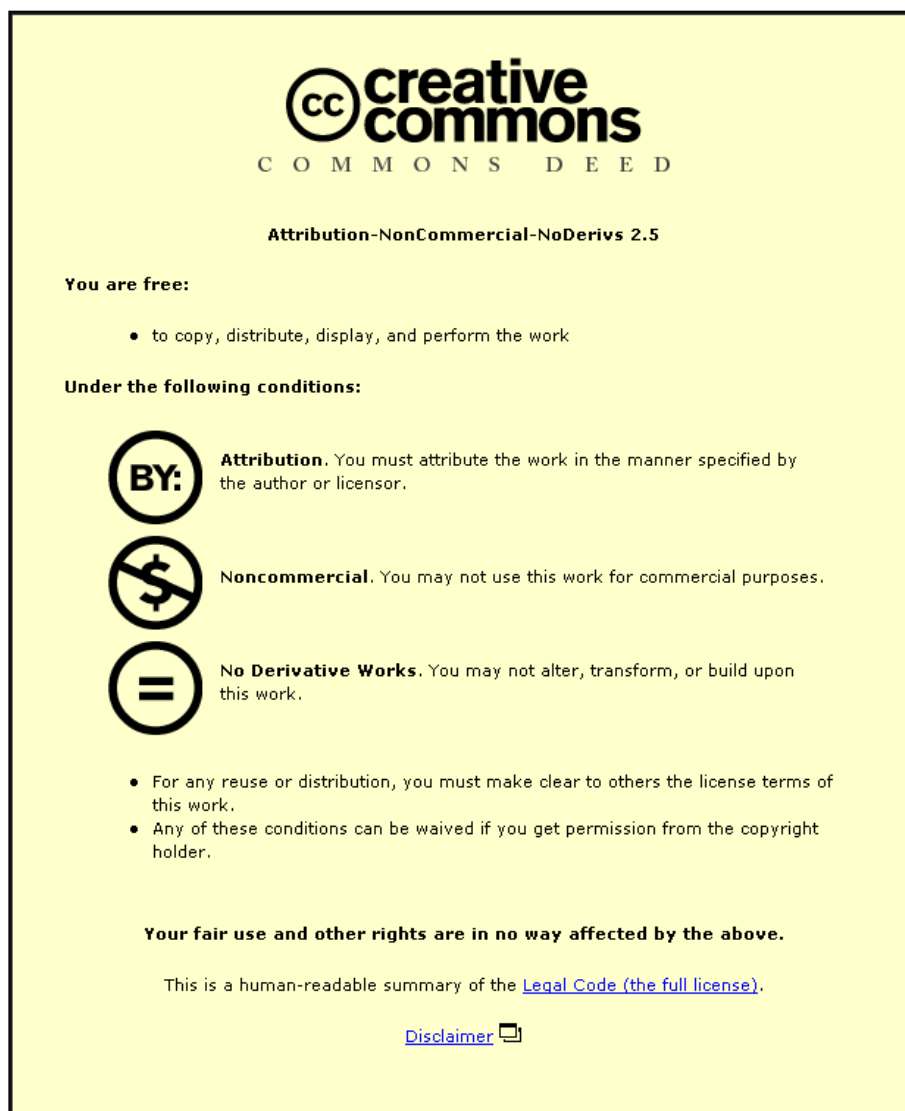


This item was submitted to Loughborough University as a PhD thesis by the author and is made available in the Institutional Repository (<https://dspace.lboro.ac.uk/>) under the following Creative Commons Licence conditions.



For the full text of this licence, please go to:
<http://creativecommons.org/licenses/by-nc-nd/2.5/>

BLL ID NO.: DS7228/85

LOUGHBOROUGH
UNIVERSITY OF TECHNOLOGY
LIBRARY

AUTHOR/FILING TITLE

BASIR, K B bin

ACCESSION/COPY NO.

008473/01

VOL. NO.

CLASS MARK

T

LOAN COPY

- 6 JUL 1990

30 JUN 1995

- 6 JUL 1990

- 3 OCT 1997

- 3 JUL 1992

- 3 JUL 1987

- 1 JUL 1988

30 JUN 1989

- 2 JUL 1993

- 1 JUL 1994

000 8473 01



This book was bound by

Badminton Press

18 Half Croft, Syston, Leicester, LE7 8LD

Telephone: Leicester (0533) 602918.

**INFLUENCE OF MACHINE AND MATERIAL VARIABLES
ON FUNDAMENTAL RHEOLOGICAL PROPERTIES OF
RUBBER MIXES**

by

**KAMARUL BAHARAIN BIN BASIR
B.Sc. (Mechanical Engineering)**

A Doctoral Thesis

**Submitted in partial fulfilment of the requirements for
the award of Doctor of Philosophy of the
Loughborough University of Technology.**

Loughborough, April 1985.

Director of research : Professor A.W. Birley

Supervisor: Mr. P.K. Freakley

Institute of Polymer Technology

© by Kamarul Baharain bin Basir (1985)

Loughborough University of Technology Library	
Date	July '85
Class	
Acc.	
No.	008473/01

I certify that neither my thesis nor my original work contained therein has been submitted to this or any other institution for consideration of a degree.

ACKNOWLEDGEMENT

First and foremost I should be grateful to Allah (God) for with His mercy He has given me the life and sustenance in this world. For Allah is indeed All-Mighty and All-Wise.

I wish to express my gratitude to Mr. P.K. Freakley for the supervision, guidance and assistance throughout the period of this work. Also to Mr. J.R. Buxton and Dr. J. M. Holt of Engineering Mathematics Department for their help in statistical and computing aspects in this study.

My thanks extend to the staff of IPT and the staff of Special Project Group, Avon Rubber Company, Melksham. In addition, to the Government of Malaysia and my employer, Rubber Research Institute of Malaysia, for their sponsorship.

Finally my appreciation goes to my wife Rosita and children Siti Rohayu, Amir Siddiq and Siti Aishah for their tolerance, patient and moral support throughout the years of my higher education.

ABSTRACT

In rubber product manufacturing the processability of a compound is highly dependent upon the internal mixing operation. The mixer operating variables and the ingredients of the compound influence strongly the quality of the compound coming out from the mixer. In this study, which is based on a natural rubber compound, a total of eight variables, comprising five mixer variables and three material variables were changed systematically using a statistical experimental design technique; and the resulting rheological properties and carbon black dispersion levels of the mixed batches were evaluated.

A prototype variable speed rotational viscometer known, as the TMS rheometer, was used in investigating the flow properties and wall slip behaviour of the rubber compounds. Rheological characterization of these compounds was based on the power-law dashpot Maxwell mechanical model. In addition, dark field reflected light microscopy (DFRLM) system was utilised in determining the carbon black dispersion level of the compounds.

A second order polynomial function was used to model the relationship between the measured properties of the rubber mixes and the independent variables. A statistical computer package performed curvilinear regression analysis for such a multivariable process. A newly developed technique, known as Interactive Graphics for Process Simulation, enables the measured responses to be represented pictorially in the form of shading diagrams. By inspecting the shading diagrams, the responses can be correlated with one another, consequently establishing an optimum level of the mixer operating variables and the material variables, for meeting both the process productivity and mixed product specification objectives.

CONTENTS

Page

Abstract

CHAPTER 1: AN INTRODUCTION TO THE MIXING OF RUBBER COMPOUNDS

1.1 Historical Development of Rubber Mixers	1
1.2 The Mixing Process	3
1.2.2 The Mixing of Particulate Additives	3
1.2.2 Mastication and Viscosity Reduction	10
1.2.3 The Mixing of Liquid Additive	11
1.3 Mixing Equipment and Systems	12
1.3.1 Batch Mixers	12
1.3.2 Continuous Mixers	19
1.3.3 Mixing Systems and Methods	22
1.3.4 Rubber Mixer Development	27
1.4 Objective of Research	29
Literature Cited	30

CHAPTER 2: MATERIAL CHARACTERISTICS AND VARIABLES

2.1 General Consideration	32
2.2 Raw Polymer Characteristics	34
2.2.1 Molecular Properties	34
2.2.2 Polymer Blends	37
2.3 Carbon Black Morphology and its Characterization	40
2.4 The Effect of Carbon Black in Rubber	42
2.4.1 Carbon Black Rubber Interaction	42
2.4.2 Rheological Behaviour of Black Filled Mixes	46
2.5 Viscosity Reduction by Processing Oil	50
Literature Cited	52

CHAPTER 3: FACTORS AFFECTING INTERNAL MIXER PERFORMANCE

3.1 Mixer Geometry	55
3.2 Mixer Operating Variables	60
3.3 Process Control System	67
Literature Cited	70

CHAPTER 4: CHARACTERIZATION OF MIXED COMPOUND

4.1 Introduction	71
4.2 Vulcanizates Properties	72

4.2.1 Static Tests	72
4.2.2 Dynamic Tests	76
4.3 Processability of Mixed Compound	81
4.3.1 Rheological Characterization	81
4.3.2 Viscoelasticity	91
4.3.3 Temperature Dependence	100
4.3.4 Rheological Measurements	102
4.4 Carbon Black Dispersion	113
4.4.1 Introduction	113
4.4.2 Transmitted Light Microscopy	116
4.4.3 Reflected Light Microscopy	119
Literature Cited	126

CHAPTER 5: STATISTICAL ANALYSIS OF MULTIVARIABLE INTERNAL MIXING PROCESS

5.1 Introduction	130
5.2 Experimental Design and Modelling	131
5.2.1 Experimental Design	131
5.2.2 Empirical Modelling	139
5.3 Multivariable Regression Analysis	140
5.4 Response Surfaces	149
5.4.1 Introduction	149
5.4.2 Shading Diagrams	151
Literature Cited	155

CHAPTER 6: COMPOUND SELECTION AND PREPARATION OF NR MIXES

6.1 Introduction	156
6.2 Experimental Work	157
6.2.1 Compounding Materials	157
6.2.2 Mixing Equipment and Method	158
Literature Cited	164

CHAPTER 7: RHEOLOGICAL BEHAVIOUR OF THE NR MIXES

7.1 Rheological Testing Methods	165
7.1.1 TMS Rheometer	165
7.1.2 Determination of Viscous Flow Behaviour	167
7.1.3 Measurement of Wall Slip	169
7.1.4 Measurement of Stress Relaxation	172

7.2 Analysis of Viscoelastic and Slip Behaviour	175
7.2.1 Mechanical Modelling of Viscoelastic Behaviour	175
7.2.2 Wall Slip Analysis in TMS Rheometer	177
7.3 Discussion of Results	180
7.3.1 General Form of Rheological and Slip Behaviour	180
7.3.2 General Form of Viscoelastic Behaviour	192
7.3.3 Effect of Temperature	195
7.3.4 Influence of Mixer Operating Variables	200
7.3.5 Influence of Compounding Variables	209
7.3.6 Combined Influence of Mixer Variables and Compounding Variables	217
Summary	220
Literature Cited	223

CHAPTER 8: DISPERSION OF CARBON BLACK IN THE NR MIXES

8.1 Carbon Black Dispersion Testing Methods	225
8.2 Determination and Analysis of Carbon Black Dispersion	228
8.2.1 Dispersion Analysis by Photometric Method	228
8.2.2 Automatic Dispersion Analysis by Microcomputer	229
8.3 Discussion of Results	233
8.3.1 General Form of Dispersion Analysis	233
8.3.2 Influence of Mixer Operating Variables	233
8.3.3 Influence of Compounding Variables	236
Summary	241
Literature Cited	243

CHAPTER 9: CORRELATION BETWEEN RHEOLOGICAL PROPERTIES AND CARBON BLACK DISPERSION WITH REGARD TO MIXER RESPONSES AND MIXER PERFORMANCE

9.1 Measurement of Mixer Responses	244
9.2 Discussion of Results	245
9.2.1 General Form of Variation of the Mixer Responses	245
9.2.2 Influence of Mixer Variables and Material Variables on Dump Temperature	246
9.2.3 Influence of Mixer Variables and Material Variables on Mixing Time	250

9.2.4 The Variation of Rheological Properties with Respect to the Mixer Responses and its Performance	256
9.2.5 The Variation of Carbon Black Dispersion with Respect to the Mixer Responses and its Performance	260
Summary	264
Literature Cited	266

CHAPTER 10: SUMMARY AND CONCLUSION	267
------------------------------------	-----

APPENDICES

Appendix I	270
Appendix II	271
Appendix III	273
Appendix IV	275
Appendix V	277
Appendix VI	278
Appendix VII	280

CHAPTER 1

AN INTRODUCTION TO THE MIXING OF RUBBER COMPOUND

1.1 Historical Development Of Rubber Mixers.

In rubber product manufacturing industries, the initial primary process which is extremely important in determining the end-product qualities and the ease of subsequent downstream processes is mixing. Mixing is an operation whereby the ingredients which have been decided by the compounder are incorporated into the base polymer to give a homogenously mixed compound. The operation is generally carried out in a batch process using two-roll mills or internal mixers.

Two-roll mills were used extensively in the rubber mixing process during the nineteen century. The impact of the growing automobile industry in the opening years of the twentieth century had shown the need for major advances in rubber technology, particularly in high demand and quality of rubber products, leading to increased production.

Handling of large volumes of fine carbon black and hazardous additives made mill mixing no longer desirable. A return to enclosed mixing of the type utilized by Thomas Hancock¹ in 1820 was thus necessary. Hancock's 'pickle' machine was the forerunner of the internal mixer, and its set-up is as shown in figure 1.1.

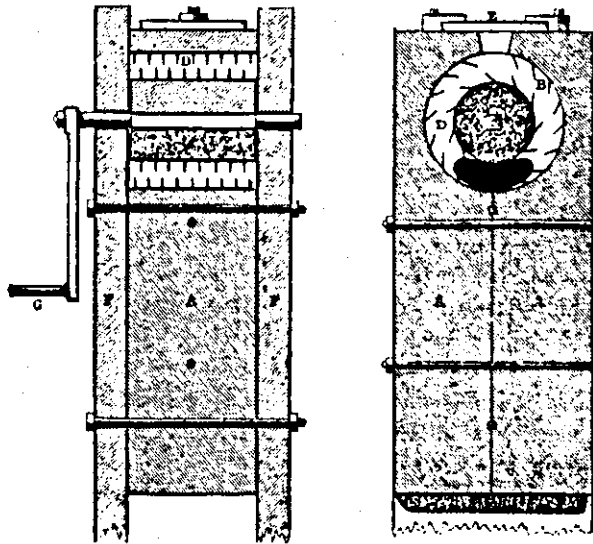


Figure 1.1 - Hancock's 'pickle' machine¹.

During the early years of the twentieth century, a number of companies, including Werner and Pfleiderer attempted to build internal mixers. A major breakthrough in design was in 1913-5 by Fernley H. Banbury, a mechanical engineering graduate who obtained a patent for his mixer. Banbury attempted to get his employer Werner and Pfleiderer to exploit his invention, but failing to do so, he joined the Birmingham Iron Foundry of Derby, Connecticut in April 1916. It was this company which developed and commercialized the Banbury mixer, with the first machine, size No.3, being sold to Goodyear in 1917.

In succeeding years larger machines with greater capacities were developed, with the size No. 27 machine first being sold in 1923. Since then the Banbury mixer has been widely used in most areas of the rubber products manufacturing industry. The other main mixer in use today was developed in the early 1930s by Francis Shaw, commonly known as the Intermix. In

the Intermix, intermeshing rotors are used with specially shaped flat topped nogs. Werner and Pfleiderer promote their own mixers which are primarily different in the rotor configuration.

The basic concepts of internal mixers have changed very little, but research and development continues, particularly in areas where elements which are critical to obtaining the best dispersion and most uniform product are being optimised and controlled in each machine. The incorporation of electronics and microprocessors into the mixer control systems² has made possible great advances in the performances and reliability of these machines.

On the other hand, the mixing of rubber compounds can be done in a continuous process. In the late 1940s, Francis Shaw developed their Double R continuous mixer³, which was based on a three-roll mill design. After the 1950s, there was a change in concept, screw extruder designs were incorporated into the continuous mixers set-up. Frequently these machines are used in-line with the internal mixer output.

1.2 The Mixing Process.

1.2.1 The Mixing Of Particulate Additives.

Generally a mixture consists of two or more identifiable components⁴. In a rubber compound, the base polymer is considered to be the major component, fillers and other additives are the minor components.

Mixing in its restricted sense, is the process whereby the particles of the minor components are dispersed into the

polymer matrix to give a uniform and homogeneously mixed compound. The mixing of carbon black particles in polymers has been widely investigated and will be outlined briefly in this study. The mixing of other particulate additives with rubber is similar to that of carbon black.

However, in mixing these particulate additives into rubber, a number of elementary stages are involved⁵, as depicted simply in figure 1.2.

Subdivision - When carbon black is first added, it is in the form of large agglomerates or pellets which are first subdivided into smaller ones purely by the physical forces generated within the mixer. These subdivided agglomerates are then readily incorporated into the rubber.

Incorporation/Wetting - At this early stage of mixing, the reduction in viscosity of rubber due to chain extension and temperature rise initiates the coalescent of rubber and black together to form a single coherent mass. According to flow visualisation studies⁶, this formation is achieved by the folding of the deformable rubber over the filler agglomerates completely enclosing the latter. Further incorporation occurs when the rubber penetrates into the voids of the agglomerates. Experiments have confirmed that rubbers which can fracture easily and ones with low elasticity will enhance incorporation and will accept black readily⁷. The viscous flow of rubber has the effect of increasing the surface area for black to rubber interaction thus increasing wetting. Moreover, the reduction of voids in the agglomerates minimises compressibility of the stock resulting in higher forces being applied to it for dispersive mixing.

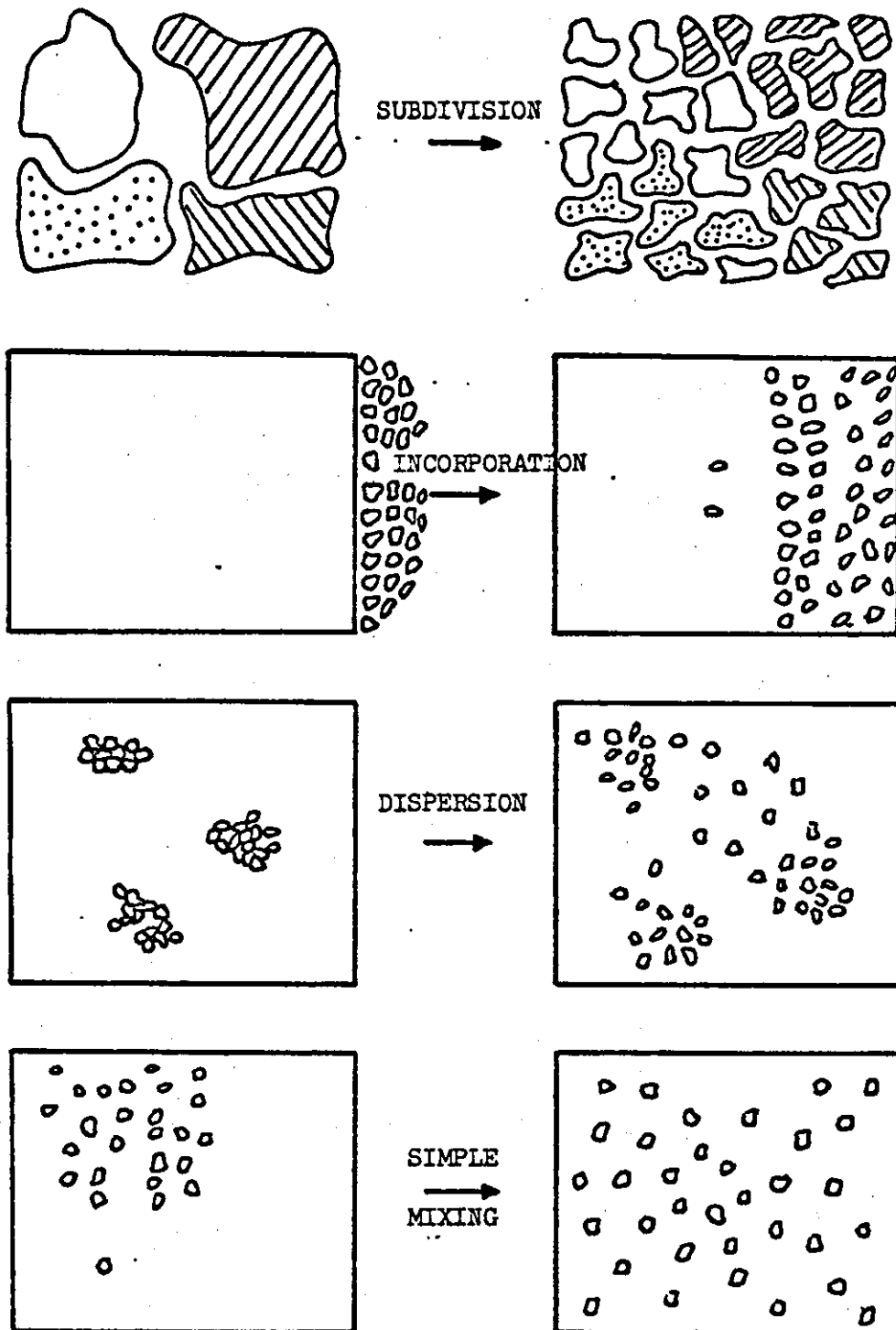


Figure 1.2 - Steps in rubber mixing process⁵.

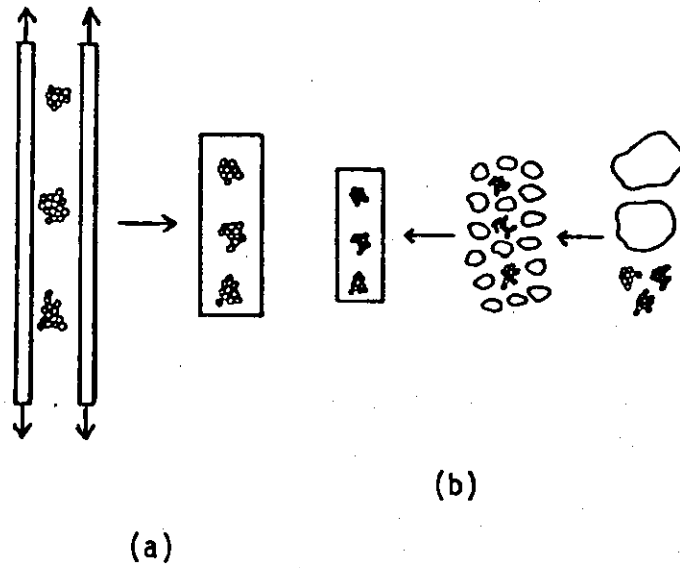


Figure 1.3 - Postulated incorporation model^{8,9}.

Nakajima^{8,9} has postulated that the incorporation stages has two mechanisms, as depicted in his idealized model in figure 1.3. In the first, the rubber undergoes large deformation, increasing the surface area for accepting carbon black; and subsequent relaxation of the rubber will sandwich and seal the black inside the rubber matrix, figure 1.3 (a). In the second, the rubber breaks down into small pieces, mixes with the carbon black and on re-coalescence seals it inside the rubber matrix, figure 1.3 (b). Both mechanisms may take place simultaneously throughout the mixing cycle.

The incorporation stage is important for effective mixing to take place, without which the ingredients are tumbled around in the mixer, with little energy being spent and practically no mixing taking place⁵.

Dispersion - The term dispersion or dispersive mixing applies to the process of reducing the size of the incorporated agglomerates to smaller aggregates. The aggregate is a solid entity of carbon and represents essentially the finest state of subdivision into which carbon black can be dispersed¹. Also, aggregates of filler will form a maximum surface area for optimum reinforcement activity.

In dispersive mixing, a certain force level has to be reached to overcome the cohesive forces between the filler aggregates^{4,11-13}. At any point in the mixing process, the system of filler and rubber may be idealized into an agglomerate suspended in a viscoelastic medium, figure 1.4. The application of a shearing strain will generate a hydrodynamic drag force acting on the agglomerate tending to separate it at its weakest link.

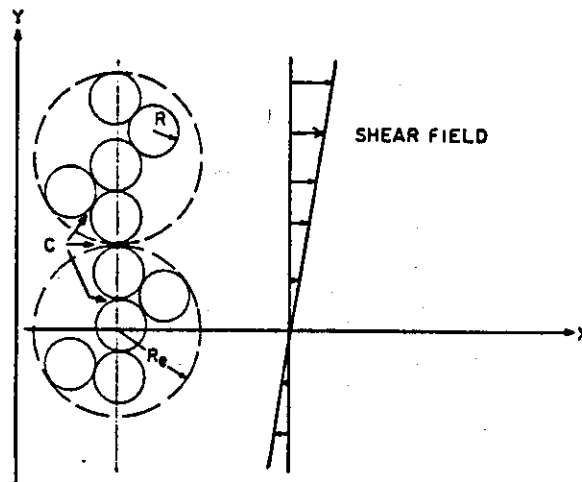


Figure 1.4 - Interactive forces in dispersive mixing of carbon black. C - interaggregate cohesive force¹¹.

Theoretical analysis have been developed to explain the dispersion phenomenon. Bolen and Colwell¹⁴ were the first to propose that agglomerates rupture occurs when hydrodynamic separating forces exceed the interaggregate cohesive forces. Dizon et.al¹¹ used the theory developed by McKelvey⁴ to illustrate the balance of forces that are involved in the dispersion of carbon black aggregates. The magnitudes of the separating forces can be approximated by Stoke's Law and depend on the effective diameter and orientation of the agglomerate, the viscosity of the suspended medium and the rate of strain^{11,10}.

Tadmor's¹² theory extended to consideration of the rupture of unequal agglomerates due to both shear and elongational deformation. The maximum force which tends to cause rupture at the same rate of deformation for elongational flow is twice that obtained in shear flow.

Recently I. Manas - Zloczower et.al¹³ proposed a mathematical model of the dispersive mixing process in Banbury type internal mixer. The good initial agreement between theory and experiment of the model used may have captured the key elements of the dispersive mixing process.

However, the common fundamental conclusions derived from this investigations are ; the smaller the aggregates clustered in the filler agglomerate, the more difficult it is for dispersive mixing, the cohesive force is directly proportional to the contact area between filler aggregates, and dispersive mixing is largely dependent on the stress level imparted on the filler agglomerates.

Distributive Mixing - It refers to an operation employed to increase the randomness or entropy of the spatial distribution of the minor constituent within the major base with no change in the size of the minor particles^{4,15,16}. With material of high viscosity which is the case for rubber, it is impossible to achieve the turbulence state of motion of the mixture components. Consequently, laminar flow dominates the distribution process. Distributive mixing is largely dependent on the amount of strain imparted on the mix continuum, where high stress level is unnecessary. For effective distribution, the interfacial area between the mixture components must be increased^{4,15,16}. The increase in interfacial area leads to a decrease in the average striation thickness¹⁶.

The degree of distributive mixing can be assessed either by total interfacial area or the average striation thickness¹⁶. In linear distributive mixing, the increase in interfacial areas is proportional to the amount of strain. However, in exponential distributive mixing, the increase in interfacial areas is exponential to the amount of strain. Gale¹⁶, Barry¹⁸ adopted this principle and developed the Cavity Transfer Mixer, whereby the mix continuum is systematically cut and rotated before being subjected to further strain, anticipating the exponential increase of the interfacial areas.

Distributive mixing is also termed as homogenization, but it is commonly known as simple mixing or blending in dry powder applications.

1.2.2 Mastication and Viscosity Reduction.

Mastication can be briefly described as the operations of softening and viscosity reduction of the rubber either mechanically¹ or by mechanochemical degradation^{19,20}. At the early stage of mastication, the reduction in rubber viscosity is primarily due to chain extension under the action of the applied stress²¹. Continued stressing may cause rupture to the rubber molecules, decreasing the molecular weight. Moreover, the temperature rise during the operation has great influence on the molecular breakdown and viscosity reduction²². The combined effects will consequently reduce the elasticity of the rubber and the viscous component starts to dominate.

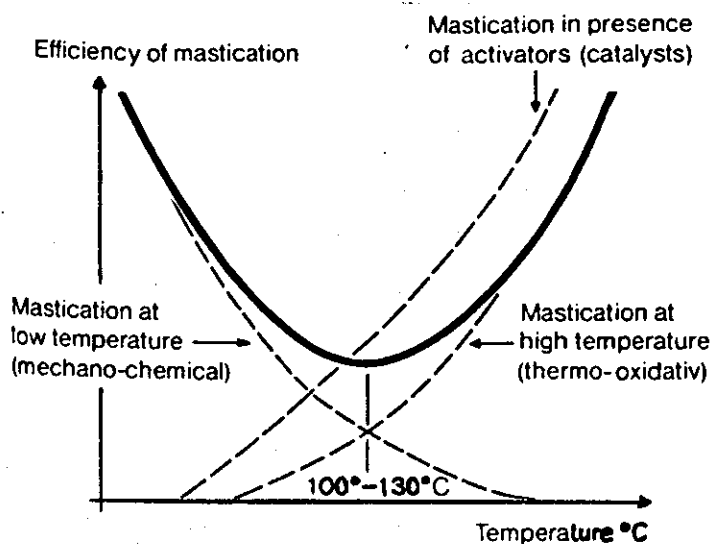


Figure 1.5 - Influence of temperature on the mastication effect¹⁹.

Molecular breakdown of rubber during mastication depends on two factors; the stresses generated during the process and

the influence of oxidation at higher temperature, the two separate factors corresponding to the mastication conditions are shown in figure 1.5. Adding to the chain breakdown, Pike and Watson¹⁹ showed that during mastication free rubber radicals were formed. Bristow²⁰ investigated the influence of radical acceptor (1 % thio-B-naphthol), on viscosity reduction of natural rubber during cold mastication.

1.2.3 The Mixing of Liquid Additives.

The presence of liquid additives in a rubber compound will primarily aid the processing operations leading to the product. Several investigations were made with regards to their influence on the physical properties of rubber compounds^{2,23}. Petroleum oils are widely used as plasticisers during rubber processing, causing a reduction in viscosity and easing filler incorporation.

The compatibility between the rubber and the oil is essential to ensure good physical and processing properties. Compatibility is quite dependent on molecular characteristics which are manifested in solubility parameters of the polymer and of the processing oils^{2,24}. The compatibility is greatest when these solubility parameters of the rubber and the oil are similar.

In addition to compatibility, the viscosity difference between the oil and rubber can be an important factor for liquid mixing⁴. The difference in the amount of shear exhibited by each component, determines the level of interfacial areas created, thus indicating the degree of mixing. McKelvey⁴ showed that the amount of shear is dependent on the geometrical configuration of the mixer and the velocity at which the boundaries between the rubber and oil are deformed.

1.3 Mixing Equipment and System.

1.3.1 Batch Mixers.

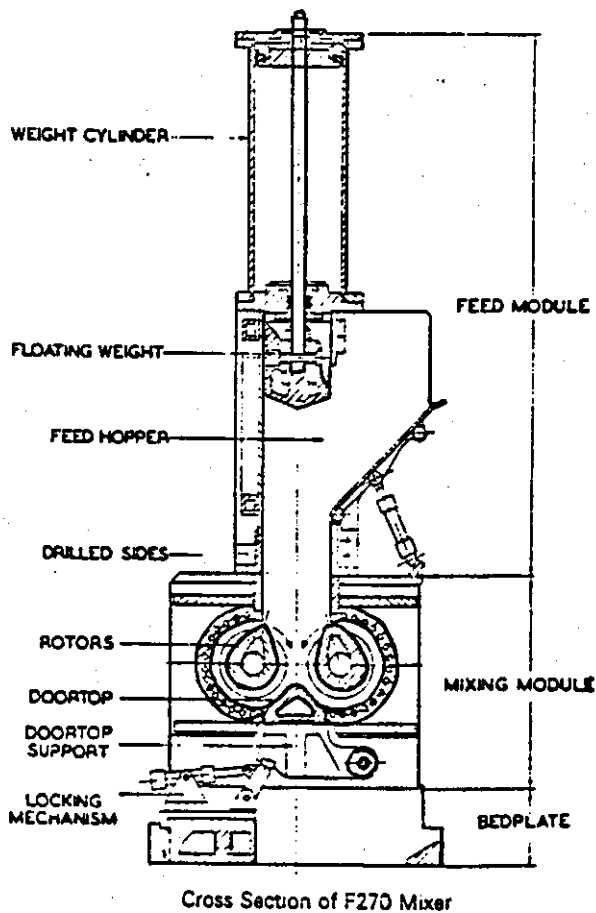
A two-roll mill may be used for the first two stages in rubber products manufacturing, namely mastication and mixing; but where the volume of work justifies the capital outlay, these operations may usually be more efficiently performed by an internal mixer. However, rubber mills are still an important component of the industry for sheeting dumps from internal mixers, and for small batches of special high value products.

Mixing on two-roll mills is effected by adding the compounding ingredients on to the rubber bank formed between the nip of the rolls. They are gradually absorbed by the masticated rubber, cut and folded from time to time by the mill operator. A mixing schedule is employed for the various operations throughout the mixing cycle.

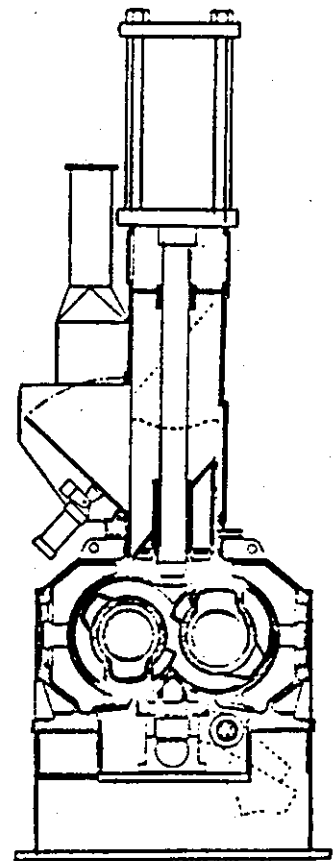
The two rolls on a mill are mostly of the same diameter, but one roll may rotate at a higher rate than the other. A friction ratio between 1.0 to 1.4 is common for most mills. Diameter of rolls ranges from 0.15 to 0.7 m, and with a working length of 0.3 to 2.1 m respectively. The power drives are from 5.6 to 180.0 kW for the 0.15 m and 0.7 m mills respectively. Water cooling or steam heating is incorporated into the machine for any particular mixing operations.

Internal mixers are essentially enclosed rubber mixing equipment suited to large output. The basic differences in internal mixers are in their rotor geometry, being either tangential or intermeshing. Banbury and Werner Pfleiderer mixers are with tangential rotors, Shaw Intermix mixers are of the

intermeshing configuration, with a recent introduction of an intermeshing rotor machine by Werner Pfleiderer. A sectional view of the mixers are shown in figure 1.6.



Farrel - Bridge
Banbury



Francis Shaw
Intermix

Figure 1.6 - Schematic diagrams of internal mixers²⁹.

In Banbury mixer, the rotors rotate in opposite direction with 1:1.2 friction ratio. The Francis-Shaw Intermix, however, has the rotors running at even speeds with the nogs designed to produce a friction ratio between themselves.

The material to be mixed is contained within the mixing chamber by pressure applied through the ram. A swing or drop door is positioned at the bottom of the chamber to permit rapid discharge of the mixed compound.

Internal mixers are available in a variety of sizes which are classified according to the volume of the mixing chambers. The net chamber volumes ranges from 0.057 to 0.62 m³ in Banbury mixers and 0.029 to 0.33 m³ for Werner Pfleiderer mixers. The chamber size for Intermix is from 0.018 to 0.85 m³. The power drives of these mixers ranges from 25.0 kW in the smaller machines up to 3300.0 kW for the bigger machines. Palmgren⁵ has made a detailed review on the characteristics of internal mixers.

The rubber compound to be mixed in an internal mixer depends entirely on the processors' need. Each compound is not alike and does not mix equally well at preset machine conditions. Moreover, it has been long recognized that the operating variables of an internal mixer have a strong influence on the properties of the rubber compounds^{25,26}. Thus it is necessary at this stage to be familiar with these operating variables before pursuing any internal mixing study. The influence of the variables on the mixed compound will be discussed in chapter 3.

Fill factor (F) - This refers to the fraction of the free mixer volume occupied by a rubber stock, and it indicates the degree of loading in the mixer chamber. Fill factor can be determined by the expression

$$\text{Fill factor} = \frac{\text{mixed batch size (kg)}}{\text{mixer volumes (l) x finished batch density (kg/l)}} \quad \dots 1.1$$

Generally, a factor of 0.6 to 0.85 has been an acceptable range²⁵⁻²⁷. The optimum degree of filling depends on the mix viscosity, mixer geometry, type and level of rubber, filler and processing oil.

Ram pressure (P) - Initially ram pressure was used as a floating weight to stuff the materials into the mixing chamber. It was later realised that the amount of force exerted by the ram has an important influence on mixing^{26,27}. The effect of ram pressure is primarily to maintain the 'hydrostatic' condition in the mixing chamber. 'Hydrostatic' pressure in the chamber is directly proportional to the applied ram pressure. Ram pressure must be sufficient to prevent the upward movement of the ram which allows material to reside in the throat of the mixer, where it can stagnate.

The increase in ram pressure will decrease the voids leading to an increase in areas of contact between the compounding materials^{26,28}. With low ram pressure, the ram oscillates up and down in the throat of the mixer allowing the mixer rotors to slip past the rubber where shredding cannot take place.

Coolant temperature (T) - During mixing the stresses and deformations imparted onto the stock generate a considerable amount of frictional heat due to the presence of dry particulate additives and the relative motion of the mixing materials against the rotor surfaces and the chamber wall²⁹. In addition, the hysteristic heat loss during deformation also contributes to the temperature rise of the mixing stock^{28,30}.

The flow properties of rubber are known to be temperature dependent. The exponential drop in viscosity with temperature can be described by the established Arrhenius relationship⁴

$$\eta_a = A \exp (E/RT) \quad \text{.....1.2}$$

where η_a - apparent viscosity

A - material constant

R - the gas constant

E - the activation energy

T - the absolute temperature °K

The viscosity drop has an adverse effect on the stress level during mixing. On the other hand, the mix ingredients are temperature sensitive, too high a temperature may either degrade the polymer or likely to cause premature vulcanization in the presence of curatives. Consequently, effective temperature control is necessary for the mixing operation of a rubber compound.

Nakajima et.al³¹ reported that out of the total mechanical energy input into the compound, 41.0 - 46.0 % went to raise the temperature of the compound and 41.0 - 45.0 % was removed by the cooling water. For efficient mixing³⁰ the heat removal by the

coolant must be high enough to reduce the temperature rise of the mixing stock.

The construction of the internal mixer is extremely important in determining the amount of heat transfer. Banbury internal mixers are equipped with a drilled sides chamber which significantly improves the cooling efficiency over previous methods. In Shaw Intermix, the side bodies, ends, top ram and bottom door are of water jacketed construction. Cooling efficiency in the Intermix is claimed to be higher than for the Banbury, mainly due to the greater cooling area^{10,32}.

However, the coolant temperature control system is essential for the control of starting temperature for a particular mixing operation. Accordingly, its influence on flow properties of the rubber compound has been acknowledged^{26,33}.

Rotor speed (S) - The rate of deformation of materials in the mixer is directly related to the rotor speed. A close approximation of the amount of shear above the rotor tip can be represented by⁵

$$\dot{\gamma} = V / h \quad \dots\dots\dots 1.3$$

where V - linear velocity at tip of rotor wing
 h - the clearance between rotor tip and wall
 $\dot{\gamma}$ - the shear rate

In a high speed mixer a shear rate of up to 500.0 s^{-1} is observed whilst for low speed mixer it is between 100.0 to 250.0 s^{-1} . A rotor speed of 40.0 rpm is often used for rubber mixing in large internal mixers. The speed of mixing is limited by the

maximum allowable temperature, that is by the balance between heat generation and heat removal^{32,34}.

With increase in rotor speed, shear rate above the rotor tip increases proportionally, but the corresponding increase in shear stress is much lower as evident from the power law expression

$$\tau = \eta_a \dot{\gamma}^n \quad \dots\dots\dots 1.4$$

where η_a - apparent viscosity

τ - corresponding shear stress

$\dot{\gamma}$ - shear rate

n - power law index

A doubling of shear rate will only lead to approximately a 20 % increase in shear stress. The shear rate increase will lead to heat buildup in the material, reducing its viscosity. This explains why no improvement in dispersion is noted with increase in rotor speed^{30,35}, which would otherwise be expected from an increase in shear stress.

Unit work (W) - One of the problems in mixing operations is to determine the criteria for terminating the process. Rubber compounds have been traditionally mixed according to time-temperature specifications. These specifications, however, are dependent on the mixer type, size and condition. Control specifications of time-temperature do not always assure batch to batch uniformity in the same type of mixer, due to the differences in the mixer's cooling system. These specifications are certainly difficult to translate to different type of equipment.

Mixing according to a work input specification has been shown to accurately predict material properties and improve batch to batch uniformity, independent of mixer type and condition^{25,26,36}. The total energy input to a mixer per unit volume of the material, based on the density of the finished mix, is termed as unit work or specific energy input.

Unit work is the combined effect of power and time during mixing. This is indicated by the cumulative area under the power time curve as shown in figure 1.10. In addition to the batch uniformity, work input control can improve efficiency by decreasing mixing cycle time^{36,37}. Throughout the work reported in this thesis unit work is the dump criterion; and hence mixing time and dump temperature depend on unit work.

1.3.2 Continuous Mixers.

Continuous mixers have been developed, either as a complete replacement of an internal mixer or for use in conjunction with an internal mixer. Initially the response from rubber industries for continuous mixing were lacking³⁸. However, progress is made in this area where substantial energy reduction and lower capital expenditure are observed, and this is attractive as compared to batch mixing^{50,51}. Continuous mixers are favourable for mixing powdered rubber than those of bale rubber. In cases where bale rubber is used, bale granulation is necessary prior to feeding into the continuous mixer. Wheelans⁵¹ showed that the high cost of granulation needs to be carefully considered with respect to any possible savings in continuous mixers, when making comparison to mixing in internal mixers.

Nevertheless, continuous mixers are not more common as

compared to batch mixers. This is so basically due to the high capital investment of the existing batch mixers, contributing to the unwillingness of the rubber processors to change over to continuous mixers. Furthermore, changing over for one compound to another is generally more difficult than with batch mixing. In addition the ancillary equipment for material handling, metering and weighing which are associated with continuous mixing has not yet been satisfactorily sorted out. Though a complete automation and a cleaner mixing operation is possible with the continuous process³⁹.

The commercially available continuous mixers are Werner Pfleiderer EVK single screw mixer extruder⁴⁰, Farrel Bridge MVX⁵⁰ and the Uniroyal Transfermix⁴². The Farrel Bridge MVX and the Transfermix are shown in figure 1.7 (a) and figure 1.7 (b) respectively.

Whilst the developements in continuous mixing have been going on, the manufacturers and users of batch mixers have not been idle. Both have progressively uprating the performance of their conventional machines. On the whole, the internal mixers will still be in use for some time to come.

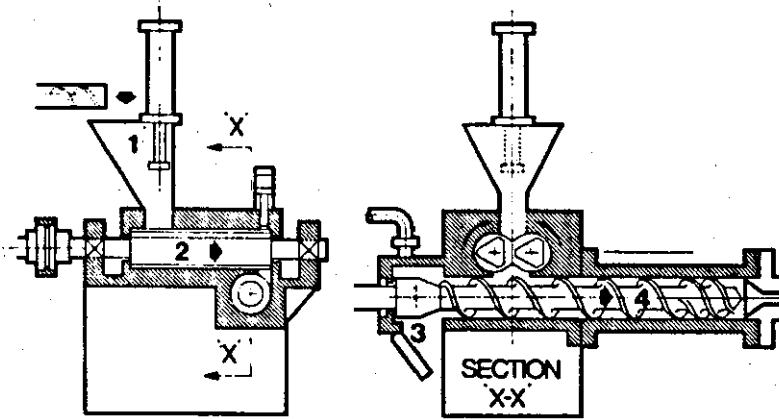


Figure 1.7 (a) - The Farrel Bridge MVX mixer⁵⁰.

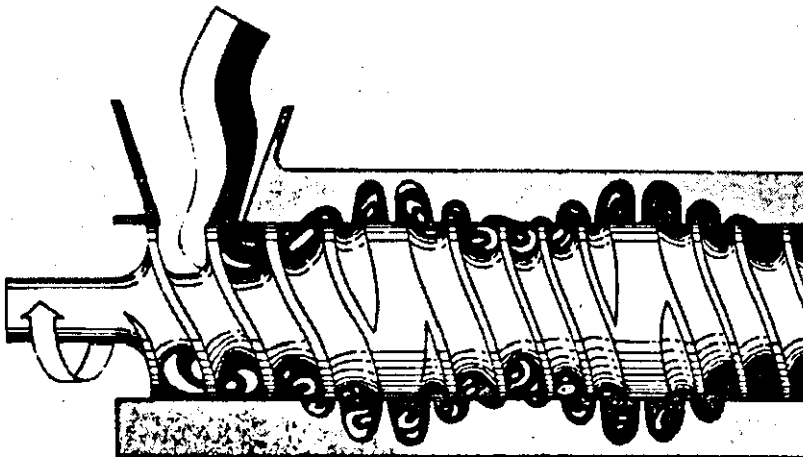


Figure 1.7 (b) - The Transfermix mixer⁴².

1.3.3 Mixing System and Methods.

The final mix of a rubber compound can be prepared by several processing routes. Single stage, two stage and multiple stage systems can be adopted depending on the type of compounds, the availability of machineries and the amount of throughput³⁰. The flow diagram of such systems are as shown in figure 1.8 and 1.9 respectively.

In a single stage system, the rubber and all its compounding ingredients are mixed together to completion in a single mixer. Variable speed mixing is sometimes used so that the temperature rise can be checked by the use of lower speed. The dump could be on a two-roll mill or extruder. There may be compounds which cannot be mixed in one stage. This system is such that the unit can be used as a masterbatch unit and final mix unit and any special compound needing two or more stages can be mixed in this way^{29,30}.

Alternatively, in two-stage system, a carbon black masterbatch is initially produced. Masterbatching is necessary where high degree of dispersion is required such as in the manufacture of tyre tread and other reinforcing compounds³. Curatives are then added in the next stage, where the masterbatch are converted to the final compound. However, multiple-stage mixing systems are not uncommon, and more handling of material is required³⁰.

On the other hand, different techniques are employed for a complete mixing cycle. In the conventional mixing method, the rubber is added at the beginning of the cycle followed by the filler and other dry additives. The increase in viscosity at

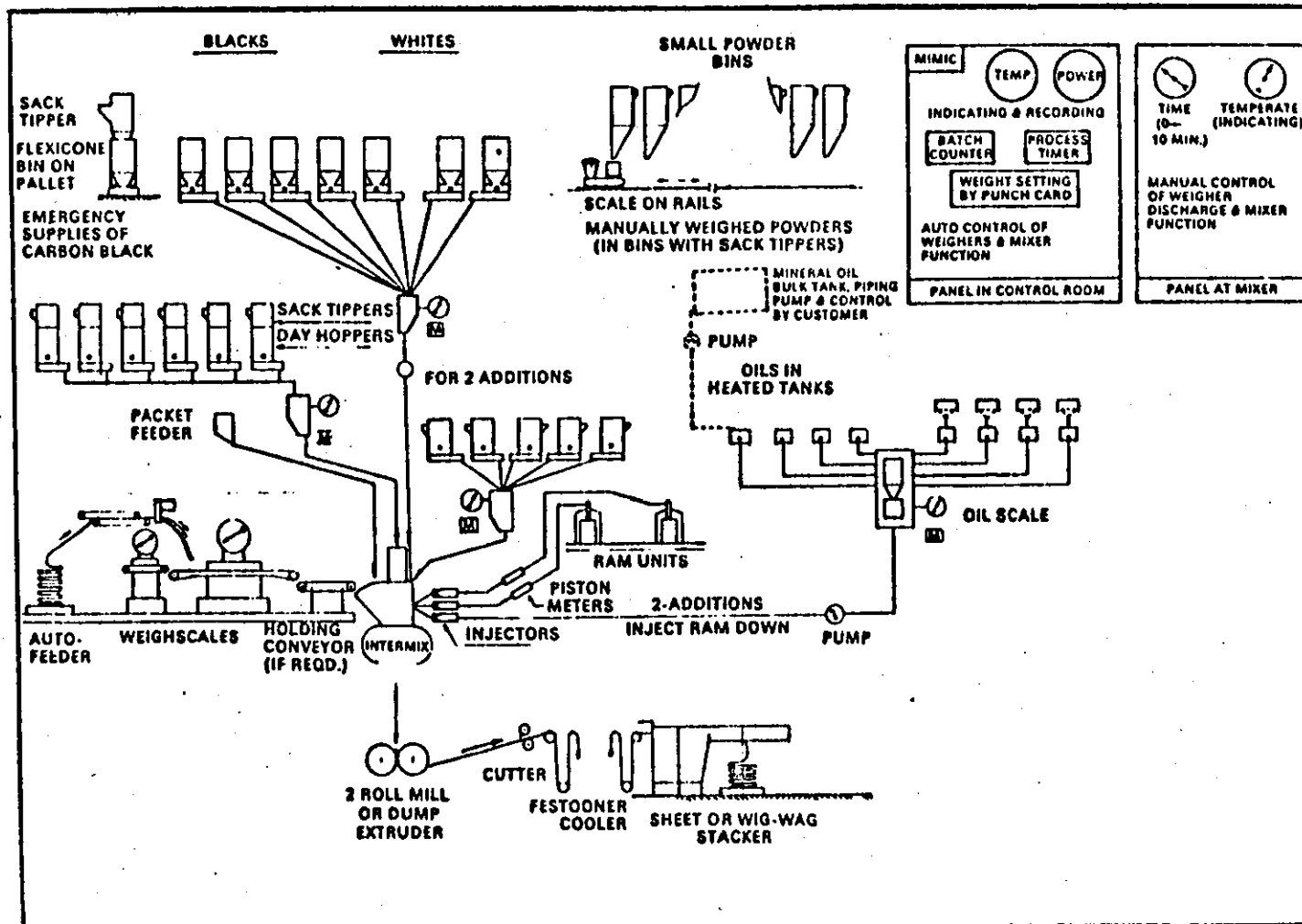


Figure 1.8 - Flow Diagram For A Single Stage Mixing System
(Francis Shaw Technical Literature).

this stage demands higher power, thus increasing the stress level, which is favourable to dispersive mixing. Plasticizers and processing oil that tend to reduce the viscosity of the mixing stock are added towards the end of the mixing period when most of the additives are already incorporated and dispersed²⁹.

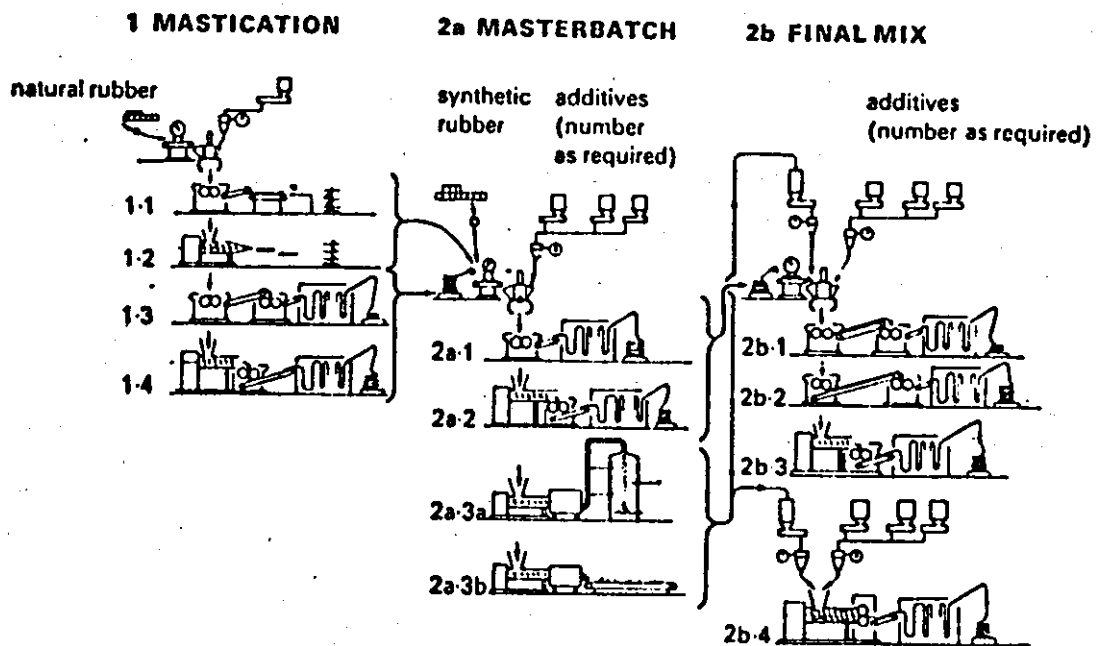


Figure 1.9 - Flow diagram of a multiple stage mixing system³⁰.

In contrast, early oil addition is advocated in the case of polychloroprene to retard the heat buildup in mixing and keep the rubber in the temperature region where it is less thermoplastic. Alternatively, half the oil and half the black can be added at the start of the mixing cycle to avoid great rise in temperature and peak power loads^{44,45}.

With low viscosity compounds, the sequential addition of ingredients in conventional mixing technique produces a better result⁴⁶. Figure 1.10(a) shows the general power-time curve of a conventional mixing cycle.

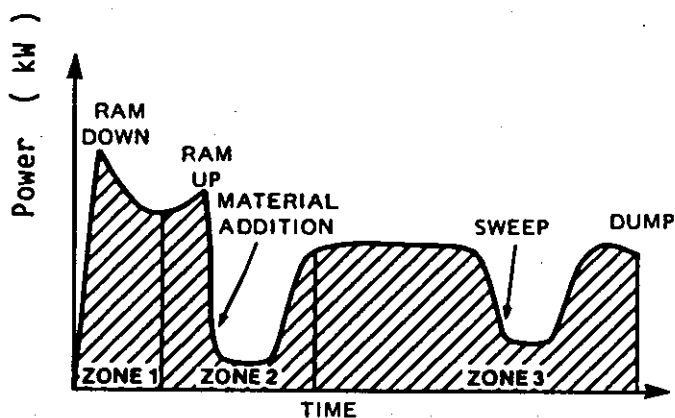


Figure 1.10 (a) - Generalised power curve of conventional mixing⁴⁶.

As the case for upside-down mixing technique, all the ingredients of a batch are introduced into the mixer at the same time. The ram is immediately applied, developing a high energy input to the stock at the start of the mixing cycle^{29,46}. The

uninterrupted high stress level over the cycle promotes dispersion of the filler, as shown in figure 1.10(b).

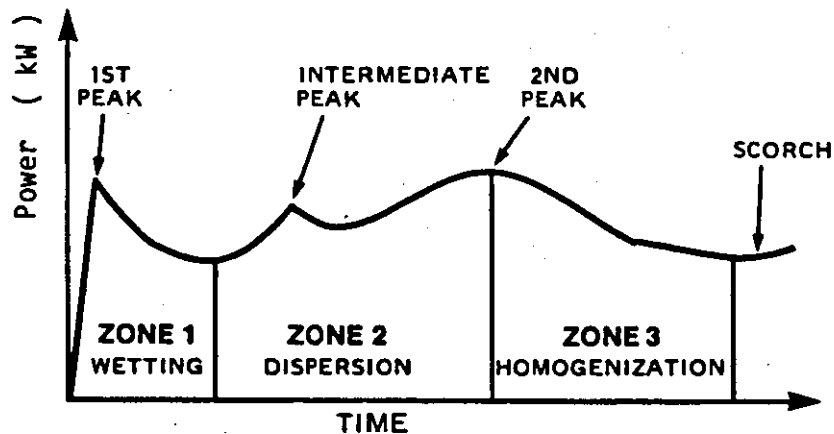


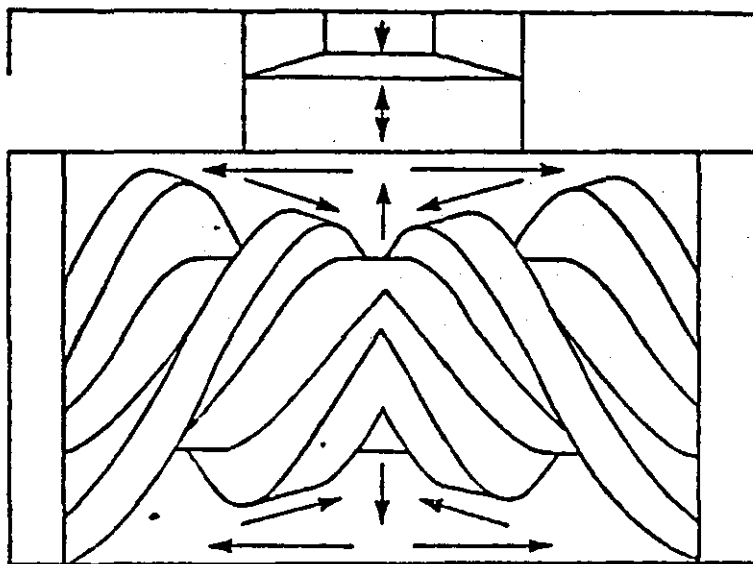
Figure 1.10 (b) - Generalised power curve of upside-down mixing⁴⁶.

Upside down mixing is the preferred method for high viscosity compound⁴⁶. Studebaker and Beatty⁴⁵ advocated that the upside-down technique is deemed suitable for high structure blacks compounds. However, upside-down has also proved to be very successful with compounds containing large quantities of oil and filler. The oil and filler are normally blended for a short period in the mixer before the rubber is added, avoiding lubricating the rotors by the oil⁴⁹.

1.3.4 Rubber Mixer Developments.

The Rutital Monomix⁴⁷ differs from the basic design of Shaw Intermix and Banbury mixer. It has a single bi-conical rotor in the form of two tapered screws with the helices moving in towards the centre of the cylindrical mixing chamber, as shown in figure 1.11.

Rotation of the rotor with the mix in the chamber and the ram down, imparts a recirculatory motion to the material, which is drawn down the rotor into the centre of the chamber and then forced out against the chamber walls and back to the outer extremities of the rotor. The high shear imparted to the mix by this motion is aided by the shear forces generated within the flights of the rotor as the material passes between the high and low pressure areas generated in the inter-flight spaces.



Mixing action with the ram down

Figure 1.11 - The Rutital Monomix²¹.

The manufacturer has claimed that the Monomix can mix faster and homogenously than the twin-rotor machines, although no results are available to support this claim.

Another design of single rotor mixer was recently developed by Scheisser⁴⁸. In this design a slotted rotor rotates in a cylindrical mixing chamber, as shown in figure 1.12. The rotor shaft moves the rotor back and forth through the compound in the mixing chamber and simultaneously rotates it. In order to pass the moving rotor, the compound is forced through the higher stress region, the slots in the rotor disc. It is also claimed that this mixer can achieve faster, more homogeneous mixing than other designs.

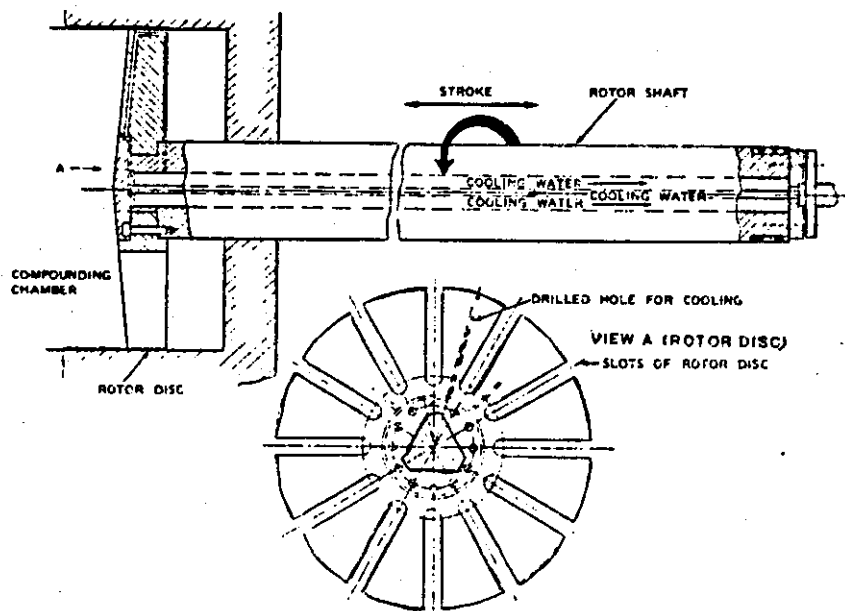


Figure 1.12 - The Scheisser I.M.I. Mixer¹⁹.

1.4 General Objective of Research.

Having reviewed the mixing process and its variables, it is essential at this stage to realise that a large number of variables influence the mixing operation. The subsequent processes in rubber product manufacturing are highly dependent on the quality of the compounds coming out from the mixer. Thus a relationship between the input variables of a mixer and the properties of the output mixes have to be established in order to give sufficient understanding of the subsequent mixing process and processability of the rubber compounds. Consequently, the main objectives of this research emerge and are outlined below;

a) To examine the combined influence of mixer operating variables and the material variables on the rheological properties and carbon black dispersion level of natural rubber compounds. The operating variables are fill factor (F), ram pressure (P), coolant temperature (T), rotor speed (S) and unit work (W). The material variables are types of carbon black (B), i.e. N220 (ISAF), N330 (HAF), N660 (GPF) and N762 (SRF) and their loading levels (L). In addition, material variable includes the loading level (O) of an aromatic processing oil.

b) To utilise statistical experimental design and analysis techniques, computer graphics presentation methods, and to evaluate their usefulness in such a multi-variables process.

Literature Cited.

(Chapter 1)

1. T. Hancock, 'Personal Narrative of the origin and progress of the Caoutchoue or India Rubber Manufacture in England'. Longmans and Roberts, London (1857)
2. L.A. Acquarulo Jr. and A.J. Notte, *Elastomerics*, Nov. (1983)
3. C.M. Blow, 'Rubber Technology And Manufacture', Butterworth Group, England (1977)
4. J.M. McKelvey, 'Polymer Processing' Wiley, New York (1962)
5. H. Palmgren, *Rubb. Chem. Tech.*, 48, 462, (1975)
6. P.K. Freakley and W.Y. Wan Idris, *Rubb.Chem.Tech.*, 52, 134 (1979)
7. N. Tokita and I. Pilskin, *Rubb.Chem.Tech.*, 46, 1166, (1973)
8. N. Nakajima, *Rubb.Chem.Tech.* 54, 266, (1981)
9. *ibid.* 55, 931, (1982)
10. A.I. Medalia, *Rubb.Chem.Tech.*, 47, 411, (1974)
11. E.S. Dizon et.al., *J.Elast.Plast.*, 8(4), 414 (1976)
12. Z. Tadmor, *Ind.Eng.Chem.Fund.*, 15, 346, (1976)
13. I. Manas-Zloczover et.al., *Rubb.Chem.Tech.*, 55, 1250 (1982)
14. W.R. Bolen and R.E. Colwell, *SPE J.* 14(8), 24, (1958)
15. E. Bernhardt, 'Processing of Thermoplastic Materials' Van Nostrand, New York (1959)
16. G.M. Gale, *Plast.Rubb.Process.Appl.*, 2, 4 (1982)
17. L. Erwin, *Polym.Eng.Sci.*, 18(7) May (1978)
18. J.P. Berry, *Plast.Rubb.Inter.*, 9(2) April (1984)
19. M. Pike and W.F. Watson, *J.Polym.Sci.*, 9, 229 (1952)
20. G.M. Bristow, *Trans.Inst.Rubb.Ind.*, 38, T29, T104 (1962)
21. F.T. Borzenski, ACS Rubb.Div. 111th Meeting, Chicago, May (1977)
22. W.F. Busse, *Ind.Eng.Chem.*, 24, 140 (1923)
23. W.L. Dunkel et. al, *Ind.Eng.Chem.*, 46, 578 (1954)
24. M.L. Studebaker and J.R. Beatty, 'Science and Technology of

Rubber' Academic Press, New York, (1978)

25. P.R. Van Buuskirk et.al., Rubb.Chem.Tech., 48,577 (1975)
26. P.C. Ebell, Ph.D Thesis Loughborough University (1981)
27. S.E. Pelberg, Rubb. World, 150(2)17,(1964)
28. Anon, Rubb. Journal 151(2),27(1964)
29. W.Y. Wan Idris, Ph.D Thesis Loughborough University (1978)
30. P. Whitaker, J. I.R.I., 4(4),153, August (1970)
31. N. Nakajima et.al, Rubb.Chem.Tech., 55,456 (1982)
32. P.S. Johnson, Elastomerics 9, January (1983)
33. K.B. Basir and P.K. Freakley, Kaut.Gummi Kunst., 35,205(1982)
34. M.G. Peakman, J. I.R.I. 4,(1),35, February (1970)
35. J.R. Bourne, New Scientist, 33,334(1967)
36. G.E. O Connor and J.B. Putman, Rubb.Chem.Tech., 51,799 (1978)
37. S.W. Newell et.al, Rubb.Chem.Tech.,48,1098 (1975)
38. 'The Mixing Process-An Analysis', Rubb.Jr.,151,48,Oct. (1969)
39. M.C. Hewitt, Rubb.Journal, 149(11),18, November (1967)
40. G. Schwarz, Eur.Rubb.J., 159(9),28, September (1977)
41. R.N. Comes et.al, ACS Rubb.Div.Meeting, April (1972)
42. C.M. Parshall and A.J. Saulmo, Rubb. World, 156(2),78 (1967)
43. J.T. Matsuoka, Rubb. World, 172(4) July (1975)
44. S.H. Morell, Prog.Rubb.Tech., 41,97 (1978)
45. M.L. Studebaker and J.R. Beatty, Rubb. Age, 107(5),31 (1976)
46. P.T. Dolezal and P.S. Johnson, Rubb.Chem.Tech., 53,252(1980)
47. 'Mixing Review', Eur.Rubb.J., 159(9), 27, September (1977)
48. A.G. Scheisser, ACS Rubb.Div.Meeting, Cleveland, October(1981)
49. P.K. Freakley, private communication.
50. C.W. Evans, Elastomerics, 30, March (1981)

CHAPTER 2

MATERIAL CHARACTERISTICS AND VARIABLES

2.1 General consideration.

It is recognized that the characteristics of both raw rubbers and compounding ingredients have a strong influence on processing and the physical properties of the final mix^{1,2}. In mixing, the ease with which the ingredients can be incorporated and dispersed in the rubber matrix is extremely important, in order to produce a homogeneously mixed compound³. However, the criteria for choosing the rubber and other ingredients used in a compound will certainly depend on the end product and its applications.

The origin of raw polymers are from two sources; firstly natural rubber which is obtained from *Hevea Brasiliensis* trees and secondly the synthetic rubber produced by polymerisation of hydrocarbon molecules⁴. Technical progress has resulted in a proliferation of the number of grades of both natural and synthetic rubbers, with increasingly detailed specifications. The various types and grades of rubber and their application are reported in several textbooks^{2,5,6}.

The reinforcement ability of particulate fillers such as carbon black has known to increase the strength of the vulcanized rubber more than ten fold⁷. In addition particulate fillers notably carbon black is recognized to have strengthening action similar in several respects to that conferred by

crystallization. During deformation, particularly stretching, substantial increase in strength of non-crystallizing rubber such as SBR were observed, and in some cases comparable with that of crystallizing rubbers such as NR, neoprene and butyl^{8,9}. Thus it is hardly surprising that relatively very few applications of elastomers utilize the polymer in the unfilled state.

The reinforcing fillers most widely used in rubber are carbon blacks and silicas. Silicates, clays, whiting (calcium carbonate) and other 'mineral fillers' are used extensively where a high degree of reinforcement is not essential.

The degree of reinforcement of a filler depends mainly on the interaction at the polymer-filler interface⁷. This is directly related to the level of dispersion of the filler in the polymer matrix developed during mixing^{7,10}. Focussing our attention particularly to carbon blacks, there are different types of varying characteristics and properties. A knowledge of their influence during mixing of rubber compounds is beneficial to rubber products manufacturing.

Similarly processing aids of different characteristics are also added into the mixing stock. Presently, very little information has been reported on their influence on the mixing process.

2.2 Raw Polymer Characteristics.

2.2.1 Molecular properties.

Polymers contain molecules with a wide range of molecular weights³, i.e. less than 10^4 to greater than 10^7 . The average magnitude^{3,11} may be described by the number average (M_n), the weight average (M_w), and the so called z-average (M_z). The molecular weight distribution (MWD) or heterogeneity index (H.I.)¹² is described by the ratio of $M_w : M_n$ or $M_z : M_n$. The molecular parameters are commonly determined by the gel permeation chromatography (GPC) technique, where extensive progress in instrumentation has been made¹³.

The effect of molecular parameters on the processing properties (viscosity and elasticity) of a rubber compound were reported by several researchers¹⁴⁻¹⁹. At low molecular weight, polymers are Newtonian fluids. However, at higher molecular weight, non-Newtonian viscosity is observed, with viscosities decreasing with increasing shear rates and the non-Newtonian behaviour becomes more pronounced¹⁵.

The viscous properties of polymer depend upon the distribution of molecular weight as well as the absolute molecular weight. In the studies of Fox and co-workers²¹, weight average molecular weight (M_w) was used in characterizing the viscosity and molecular weight relationship expressed by

$$\eta_o = k M_w^{3.4} \quad \text{.....2.1}$$

where η_o - the zero shear viscosity

k - temperature dependence constant

The above expression was expanded by Ferry²¹ to include its temperature dependence and takes the form as

$$\eta_o = [\exp (a / (T - T_g) + b)] \times M_w^{3.4} \dots 2.2$$

where a,b - universal constant

T - temperature

T_g - glass transition temperature

The influence of molecular weight distribution on the viscosity-shear rate behaviour is such that narrow molecular weight distribution elastomers are more Newtonian at low shear rates but at high shear rates the deviation to non-Newtonian behaviour persists²¹. Tokita and Pilskin¹⁷ have shown that the broader the distribution, the more non-Newtonian is the flow behaviour i.e. the stress is less sensitive to the shear rate. Accordingly, in figure 2.1 it is clear that at high shear rate as encountered in processing, the narrow distribution polymer will be in a much higher stress field compared with the broader molecular weight distribution polymers.

The influence of the degree and type of branching of polymer has also been recognized. Branching was found to decrease the magnitude of the low shear rate viscosity²². The viscosity is lower than that of linear polymers with the same molecular weight, only in the lower molecular weight ranges. Beyond a critical molecular weight, the branched polymers increase rapidly in viscosity with molecular weight and surpass the linear viscosity exhibiting a cross-over^{23,24}. However, the relationship between the type and amount of branching with processability is qualitative at present.

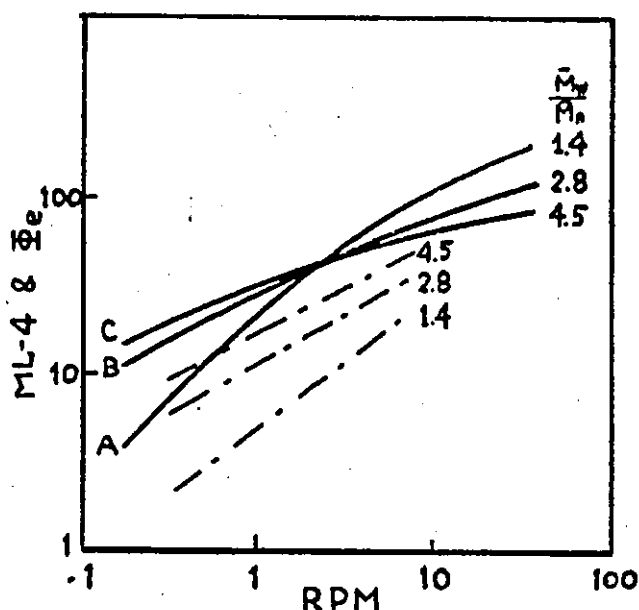


Figure 2.1 - Mooney torque (—) and Mooney recoil (---) of BR with different MWD¹⁷.

Molecular weight and its distribution have shown to influence the viscoelastic properties of polymers, particularly stress relaxation¹⁴, elastic memory and its elastic recovery properties²⁵. The normal stress difference is another important viscoelastic property, which increases with increase in molecular weight distribution²⁶.

During mixing of the carbon black loaded batches, the rupture of rubber molecules give rise to a reduction in molecular weight. The longest rubber molecules are much more prone to rupture, and since they affect the weight average molecular weight (M_w) much more than the number average molecular weight (M_n), their ratio ($M_w : M_n$) decreases as observed in SBR compounds with different types of carbon black. The changes in the heterogeneity index for a given mix is an indication of how far the breakdown has progressed^{11,10}.

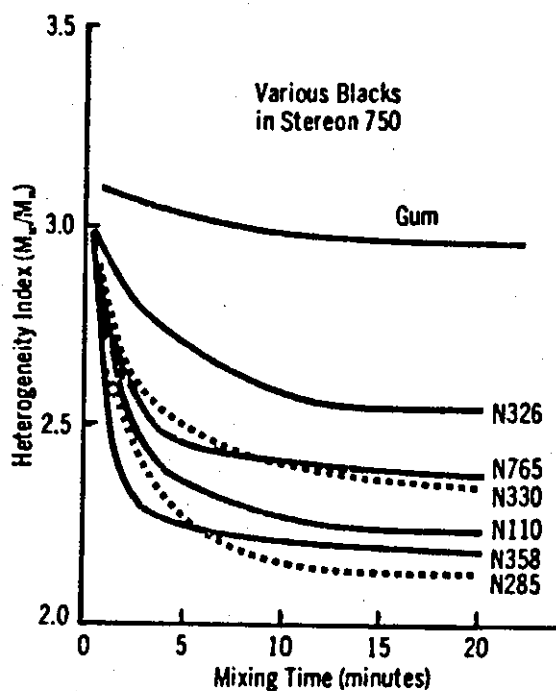


Figure 2.2 - Reduction in heterogeneity index (H.I.) with mixing time¹².

2.2.2 Polymer Blends.

Blends of two or more elastomers are widely used at present, especially in tyres. In general, polymers are incompatible on a molecular level and each polymer form zones of finite colloidal dimensions^{27,28}. In some cases, one polymer may be the dispersed phase and the other the continuous phase. While in other cases the phases are mostly interconnected, forming an interpenetrating two-phase network.

Corish and Powell²⁹ and Kruse³⁰ have reviewed the nature of blends and methods of studying them. Walters and Kaye³¹ were the first to carry out comprehensive studies on elastomer

blends. Their works covered a number of blends including NR/SBR, NR/BR and SBR/BR. Their results indicated that few, if any, elastomers can be blended on a molecular scale. They also provide direct evidence that fillers and curing agents do not necessarily distribute proportionately in the blends.

Blending is less effective when the polymers are of widely different viscosities³². Most studies³²⁻³⁴ have shown that the flow properties of elastomer blends are found to be non-additive of the flow properties of the homopolymers comprising the blends. Minimum and/or maximum viscosities for specific blend ratios are observed for a given rate of shear, showing the existence of a complex phenomenon³³, as illustrated in figure 2.3. Briefly good blending is favoured by a similarity of solubility parameters and viscosities of the homopolymers.

The addition of fillers to elastomer blends can significantly alter the state of the polymer phase³². The distribution of carbon black between the polymer phases depends on the relative viscosity of the polymers, their different affinity for carbon black (which may depend on the surface properties of the black), and the formation of bound rubber (which will be discussed in section 2.4). Depending on the temperature and mixing history of the batch, the black may form bound rubber predominantly with one of the polymers, in which it then tends to remain, or may partially transfer to the interface or to the other polymer³².

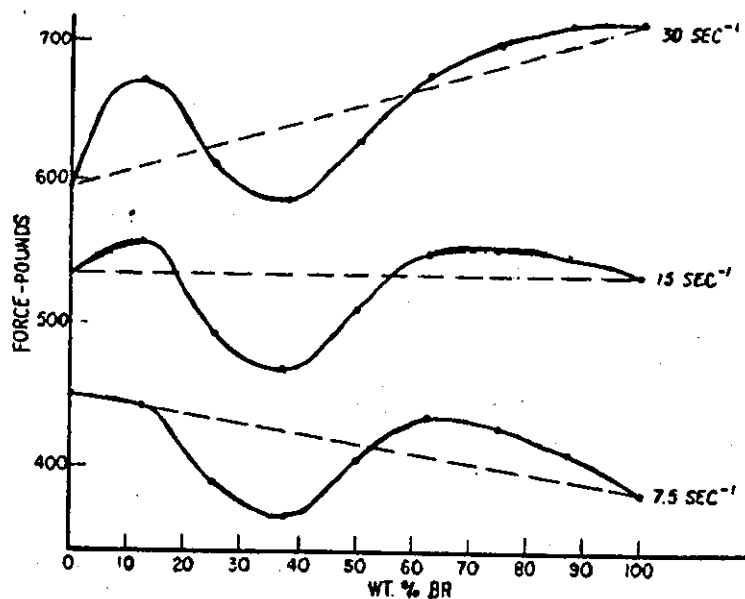


Figure 2.3 - Capillary extrusion force as a function of blend composition at various shear rates³³.

In blends, carbon black migrates from one polymer to another during mixing³⁵. Hess and coworkers²⁸ found that in blends of NR/BR, ISAF black migrated to the BR component and that the affinity of ISAF black to BR is a function of its viscosity. Similarly, Walters and Keyte³¹ found that both carbon black and zinc oxide often preferred one component in a blend. Presently there are many unanswered questions in the field of filled elastomer blends and this may lead to fruitful research in the coming future.

2.3 Carbon Black Morphology and Its Characterization.

Carbon black is an elemental carbon consisting of particles with paracrystalline graphitic layers which are aligned in a concentric fashion³⁶. The particles or nodular subunits⁷ are firmly fused together by the continuous network of the graphitic layers to form the primary aggregates. The aggregate is found to be the smallest discrete entity of carbon black existing in a rubber compound³⁶. The extent of interparticle fusion in an aggregate refers to the structure of a carbon black. High structure black consists of a large number of particles in its aggregate^{7,36}. Structure also refers to the bulkiness of the carbon black aggregate.

The great variety of sizes and shapes of the primary aggregates makes it a very difficult task to characterize the aggregate morphology. However, it is adequate for most purposes to describe filler morphology by two parameters, one related to the mean particle size and one to its structure⁷. The traditional particles count by electron micrograph for particle size determination has lost its favour in recent years. Adsorption methods are adopted whereby the specific surface area of the carbon black can be determined. The specific surface area is closely related to the particle size of the filler^{7,36}. The nitrogen adsorption³⁷ method measures the total specific area. Iodine adsorption³⁸ is affected by the surface chemical effects. It does not furnish an accurate description of either the total or non-pore surface of the carbon black^{40,41}. However, the surfactant adsorption method, using hexadecyltrimethyl ammonium bromide (CTAB) as the adsorbate, holds the most promise as a precise measure of non-pore surface area^{39,40}. Consequently the difference between the nitrogen and surfactant surface area

becomes a measure of area contained in micropores of the carbon black^{40,41}.

The specific surface area of carbon black is generally expressed in m^2/g . It is often considered to be inversely proportional to the particle size diameter⁴². This is roughly true for carbon black, although there is no accurate objective way of measuring the particle size. Most rubber grades of carbon black range from 30.0 - 130.0 m^2/g surface area. Thermal blacks are in the 6.0 - 12.0 m^2/g range⁴².

The structure of carbon black can be determined quantitatively by vehicle demand. The amount of vehicle adsorbed by the filler is a measure of its void volumes, which is related to the filler structure^{7,43}. Dibutylphthalate (DBP) is often used as the vehicle, and it is added to the carbon black in an adsorptometer⁴³. The volume of DBP per unit mass of carbon black is the DBP adsorption number or abbreviated as DBPA. Most grades of carbon black range in DBPA number from 59.0 - 140.0 $\text{cm}^3/100\text{g}$. Thermal black values are about 32.0 $\text{cm}^3/100\text{g}$.

High pressure mercury penetrometry has been proposed by Moscou et.al⁴⁴, as another technique for carbon black structure assessment. In essence this also furnishes a specific void volume measurement. Other morphological aspects of carbon black aggregates which can be classified as 'secondary' properties⁴⁵ include the aggregate size distributions⁴⁶ and anisometry^{47,48}. Moreover, characterization of carbon black can include tinting strength. The tint strength of a black increases with increasing specific surface area and decreasing structure level⁴⁹.

The classification of carbon blacks used in rubber products according to ASTM⁵⁰ are as shown in table 2.1. The first character 'N' or 'S', refer to the normal or slow rate of cure of a typical rubber compound containing the black. The second is an arbitrary figure designating the typical average particle size of the black, which is divided into ten groups. The third and fourth characters are arbitrarily assigned digits.

2.4 The Effect of Carbon Black in Rubber.

2.4.1 Carbon Black Rubber Interaction.

The mechanism by which carbon black reinforces rubber is one of the most interesting problems of modern technology and is still a subject of much speculation^{7,51-53}. Boonstra⁵¹ and Dannenberg⁵³ explained reinforcement by their molecular slippage model. The homogeneous stress distribution of the chains between carbon black particles gives the high improvement in strength. Kraus⁷ has viewed this phenomenon as due to the grafting of carbon black functional groups with the free radicals of rubber, formed during processing and vulcanization. Recently, Rigbi⁵² described reinforcement by reference to stress softening, which he attributed to the saltation of the rubber macromolecules onto the carbon black aggregates. This causes the applied stresses to be uniformly redistributed along the macromolecules, resulting in an increase in strength.

However, it is generally agreed that reinforcement improves the vulcanizate properties (particularly abrasion resistance, tear and tensile strength) to a very considerable degree, but such effects are not necessarily an indication of the level of reinforcement by the filler⁵². On the other hand,

Carbon Blacks								Vulcanizates Containing Carbon Black	
ASTM Designation	Iodine Adsorption No., ^a D 1510, g/kg	CTAB, D 3765, m ² /g	Nitrogen Adsorption, D 3037, m ² /g	DBP No. D 2414, cm ³ /100 g	DBP No. Compressed Sample, D 3493, cm ³ /100 g	Tint Strength, D 3265	Pour Density, D 1513, kg/m ³ (lb/ft ³)	Δ Stress ^b at 300 % Elongation MPa (psi) cured at 145°C (293°F) D 412, D 3182, and D 3192	
								15 min	30 min
N110	145	126	143	113	98	124	335 (21.0)	-2.6 (-375)	-2.5 (-365)
N121	120	121	132	130	112	121	320 (20.0)	+0.3 (+45)	+1.0 (+145)
S212	117 ^c	119	117	86	82	115	400 (25.0)	...	-5.5 (-800)
N219	118	107	116	78	75	123	440 (27.5)	-5.4 (-785)	-5.8 (-840)
N220	121	111	119	114	100	115	345 (21.5)	-1.8 (-260)	-1.6 (-230)
N231	125	108	117	91	86	117	390 (24.5)	-4.3 (-625)	-4.1 (-595)
N234	118	119	126	125	100	124	320 (20.0)	+0.5 (+70)	+0.8 (+115)
N242	123	111	125	126	106	116	330 (20.5)	-0.4 (-60)	-0.3 (-45)
N293	145	114	130	100	92	117	375 (23.5)	-4.2 (-610)	-3.6 (-520)
N299	108	104	108	124	105	113	335 (21.0)	+1.6 (+240)	+1.7 (+250)
S315	86 ^c	95	88	79	75	...	450 (28.0)	...	-6.3 (-915)
N326	82	83	84	71	69	112	465 (29.0)	-4.5 (-655)	-4.1 (-595)
N330	82	83	83	102	88	103	375 (23.5)	-0.7 (-100)	-0.7 (-100)
N332	84	102	90	118	375 (23.5)	-0.5 (-70)	-0.2 (-30)
N339	90	95	96	120	101	110	345 (21.5)	+0.7 (+100)	+1.0 (+145)
N341	67	72	73	112	90	100	350 (22.0)	+0.5 (+70)	+0.8 (+115)
N347	90	88	90	124	100	103	335 (21.0)	+0.6 (+85)	+0.4 (+60)
N351	67	74	73	120	97	100	345 (21.5)	+1.2 (+175)	+1.2 (+175)
N356	90	93	90	160	118	104	305 (19.0)	+4.8 (+700)	+4.8 (+700)
N358	84	88	87	150	112	99	290 (18.0)	+3.8 (+550)	+3.9 (+565)
N375	90	98	100	114	97	115	345 (21.5)	+0.2 (+30)	+0.7 (+100)
N472	270	145	270	178	114	...	255 (16.0)	-4.2 (-610)	-4.7 (-680)
N539	42	41	41	109	84	...	385 (24.0)	-0.9 (-130)	-1.4 (-200)
N550	43	42	42	121	88	...	360 (22.5)	-0.4 (-60)	-0.7 (-100)
N568	45	41	41	132	335 (21.0)	-0.3 (-45)	-0.4 (-60)
N630	36	38	38	78	62	...	465 (29.0)	-2.6 (-375)	-3.7 (-535)
N642	36	37	37	64	62	...	513 (32.0)	-4.1 (-595)	-4.6 (-665)
N650	36	38	38	125	87	...	370 (23.0)	-0.4 (-60)	-1.0 (-145)
N660	36	35	35	91	75	...	425 (26.5)	-2.7 (-390)	-3.3 (-480)
N683	30	39	37	132	335 (21.0)	-0.7 (-100)	-1.2 (-175)
N754	25	29	...	58	57	...	495 (31.0)	-5.6 (-810)	-5.4 (-785)
N762	26	29	28	62	57	...	505 (31.5)	-4.9 (-710)	-5.8 (-840)
N765	31	33	31	111	86	...	375 (23.5)	-1.8 (-260)	-2.0 (-290)
N774	27	29	29	70	62	...	495 (31.0)	-4.4 (-640)	-5.0 (-725)
N785	25	36	...	126	82	...	335 (21.0)	-1.1 (-160)	-1.4 (-205)
N787	31	32	30	81	74	...	450 (28.0)	-4.2 (-610)	-4.0 (-575)
N907	11	42	-7.1 (-1030)	-8.3 (-1205)
N908	-8.1 (-1175)	-9.2 (-1335)
N990	...	9	9	42	40	-7.1 (-1030)	-8.3 (-1205)
N991	10	8	7	...	38	-8.1 (-1175)	-9.2 (-1335)
IRB No. 4	82	97	86	107	...	-1.2 (-175)	-0.9 (-130)
IRB No. 5	82	102	90	102	388 (24.2)	0	0

Table 2.1 - Typical Properties Of Carbon Blacks (ASTM D1765).

reinforcement gives rise to some undesirable effects in the rubber compound such as increase in relaxation and creep rates, compression or tensile set and hysteresis.

Bound rubber is often used as a criterion for rubber-carbon black interaction. Carbon black is a free radical acceptor, the rubber radicals can attach themselves to its surface, forming attached rubber molecules which are insoluble and known as the bound rubber or gel^{12,54}. Bound rubber is the percentage of polymer resisting extraction by a solvent, usually benzene, in a rubber-filler mix⁷.

It has long been assumed that bound rubber is intimately associated with reinforcement. Unfortunately, the amount of gel in a filled rubber mix is likely to have little significance to reinforcement, unless the sample is prepared under carefully controlled and well defined conditions⁷. In any case, bound rubber is the result of several possible phenomena; physical adsorption, chemisorption and physical entrapment of free molecules⁷.

Nevertheless, gel values can be plotted against mixing variables^{6,55,56}. A typical relationship is as shown in figure 2.4. Several researchers^{6,57,58} reported that bound rubber increased to a plateau with increasing mixing time. However, Watson⁵⁹ and Ebell⁴⁵ noted that for NR mixes, bound rubber attains a maximum value and then drops slightly with mixing time. Similarly Wan Idris⁵⁵ noted that the bound rubber drops rapidly after 1000.0 MJ/m³ mixing energy.

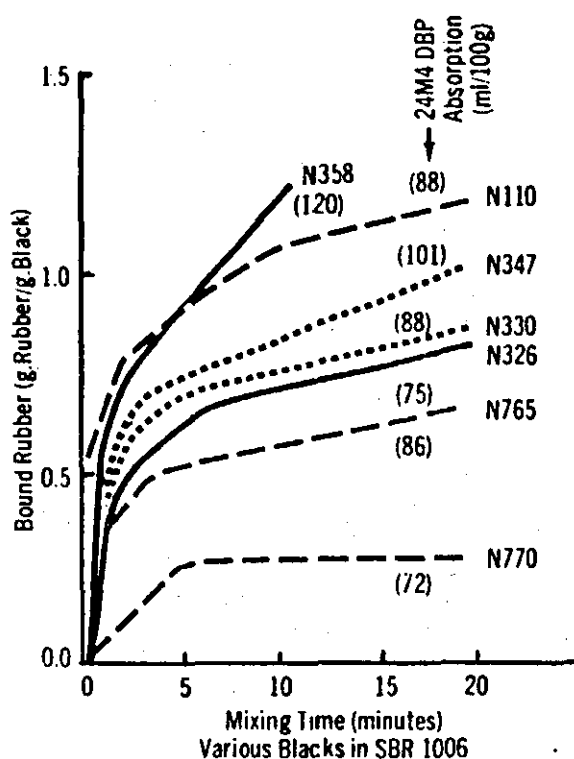


Figure 2.4 - Bound rubber increases with carbon black structure¹².

The adsorption of rubber segments onto the filler may lead to some loss of mobility of the chains^{7,36}. This immobilization is primarily due to the formation of occluded rubber, which penetrates into the internal void space of the structure aggregate. The occluded rubber is partially shielded from deformation when the rubber is strained. This shielding results in effective immobilization of a portion of the occluded rubber^{7,32}, which thereby acts as part of filler rather than the rubber matrix. It would be totally incorrect to identify the immobilized rubber with bound rubber⁷. Generally, the amount of occluded rubber increases with filler structure and it contributes to high viscosity and lower melt elasticity (low die swell) of the rubber compound⁷.

At the early stage of mixing, rubber penetrates into the

void of carbon black to form a coalesced mass as mentioned in chapter 1 (section 1.2). For a series of blacks of the same particle size but increasing in void volume (structure), the penetration of polymer is easier as the void volume increases and more layers of black will be contacted by the polymer. The black concentration in these layers is less for a high structure black than for a low structure black. Consequently, incorporation of high structure blacks are rapid as compared to low structure blacks⁵⁶.

The rate of penetration at a given pressure, which is the depth of the layer of the black contacted by polymer in a given time, does not only depend on structure but also on the particle size of the black, since particle size determines the size of the interstices between particles. This accounts for the well known fact that finer particle size blacks are more difficult to incorporate than coarse one⁵⁶.

2.4.2 Rheological Behaviour of Black Filled Mixes.

The rheological properties of unvulcanized rubber compounds containing fillers are of great interest in connection with processing. In particular, one is interested in the viscosity and elastic response of the compounds. They are markedly affected by filler morphology and rubber-filler interaction. The rheological behaviour of filled rubbers is so complex that to date there is no theory which describes it successfully.

Generally the viscosity of a rubber compound increases with a decrease in filler particle size. The dependence on particle size is a consequence of their larger interfacial area and closer proximity in the mix. Similarly it is observed that

viscosity increases with decrease in the black structure. Also viscosity increases with the concentration of carbon black^{7,11,36}. Increases in the non-Newtonian behaviour (shear rate dependence) are also observed with increase in filler content. The increase in viscosity caused by the filler is greatest at low shear rates^{11,60}. Rubber with high black content may be highly thixotropic, a phenomenon known as the Mullin's effect⁶¹. However, an apparent decrease in elastic memory is noticeable with increase in filler concentration^{11,17}.

The viscous behavior of filled rubbers is normally associated with the well known hydrodynamic theory of Einstein, Guth and Gold⁶². But experimental studies have shown that the influence of fillers on the viscosity do not follow the hydrodynamic theory expressed by

$$\eta_f = \eta_u (1 + 2.5\phi + 14.1 \phi^2) \dots\dots 2.3$$

where η_f - viscosity of filled rubber

η_u - viscosity of unfilled rubber

ϕ - volume fraction of fillers

This equation has been shown to apply reasonably well to large particle 'inactive' fillers, such as micron size glass beads or the coarser thermal blacks but it fails badly for compound with reinforcing fillers^{7,63}. Moreover, in determining the volume fraction of fillers, Tokita and Pilskin¹⁷ showed that the effective volume is a function of time which is given by

$$\phi_e(t) = \phi + \phi_{or}(t) \dots\dots\dots 2.4$$

where $\phi_e(t)$ - effective volume fraction at time t
 ϕ - filler volume fraction
 $\phi_{or}(t)$ - occluded rubber volume fraction at time t

The effective volume fraction (ϕ_e) in the early stage of mixing is high and it decreases with the mixing time. Consequently the poorly dispersed compound always has a higher viscosity than the well dispersed compound of the same filler loading¹⁷.

The hydrodynamic equation 2.3 usually underestimates the viscosity of filled rubber. Experimental studies⁶⁴⁻⁶⁶ have shown that the influence of types of carbon black on the viscosity of filled rubber can be generally expressed by

$$\eta(\text{SAF}) > \eta(\text{ISAF}) > \eta(\text{HAF}) > \eta(\text{FEF}) > \eta \left(\begin{matrix} \text{Guth} \\ \text{Gold} \\ \text{Simha} \end{matrix} \right) \dots 2.5$$

On the other hand, occluded rubber which is shielded from deformation has an effect on the elastic response of the filled compound. The total mass capable of undergoing large reversible deformation will be decreased by the occlusion of part of the rubber. This results a decrease of elastic recovery of the composite which is manifested by the reduction in extrusion shrinkage and lower die swell⁷.

For a given formulation of SBR compound, Kraus⁷ has shown that a good correlation exists between the rheological properties and the carbon black structure, irrespective of its specific surface area. This is illustrated in figure 2.4 (a) and 2.4 (b) for the Mooney viscosity and extrusion shrinkage

respectively at 50.0 phr carbon black loading level.

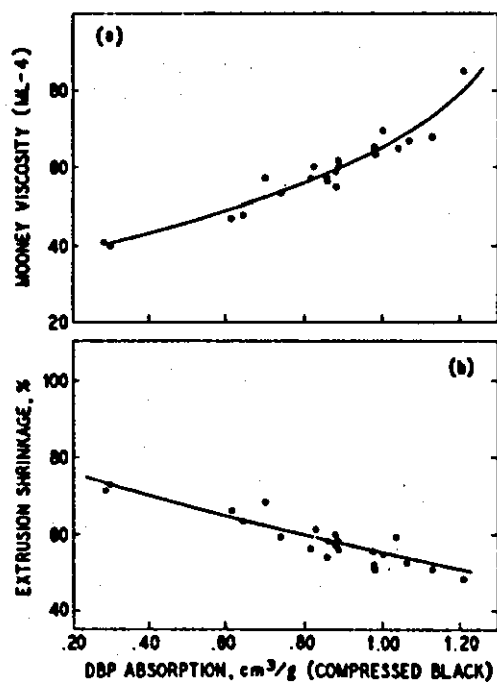


Figure 2.5 - (a) Mooney viscosity and (b) extrusion shrinkage as a function of carbon black structure. Black specific surface area ranges from 14.0-164.0 m^2/g .

2.5 Viscosity Reduction by Processing Oil.

The addition of oil into a rubber compound generally decreases the compound viscosity. Physically it hinders the development of excessive temperature and peak power during processing. The types of processing oils can be classified as paraffinic, naphthenic and aromatic². Aromatic oils give best processability but are likely to have detrimental effects on staining, colour stability and ageing resistance. Paraffinic oils are less effective whilst naphthenic oils fall between aromatic and paraffinic types in their processing effects with rubber.

Kraus and Gruver⁶⁷ suspected that the effect of plasticizer in polymer is the loosening of the entanglement network and the agitation of chain configuration by the diluent, leading to the reduction in viscosity. They postulated the Newtonian viscosity of plasticizer filled rubber by an approximation equation

$$\eta_a(\phi) = \eta_N \phi^{3.4} \quad \dots\dots\dots 2.6$$

where η_a - apparent viscosity

η_N - Newtonian viscosity at 1.0 s^{-1} shear rate

ϕ - volume fraction of plasticizer

For non-Newtonian viscosity

$$\eta_a(\dot{\gamma}, \phi) = \eta_N [\phi^{3.4} \times F(\dot{\gamma}, \phi^{3.4})] \quad \dots\dots 2.7$$

where $\dot{\gamma}$ - shear rate

F - material function

The above expressions contain no parameter/s related to the characteristic of the plasticizer. However, they showed a good approximation existed over a range of shear rates regardless to the type of diluent used.

The combined effect of oil and carbon black in a rubber compound was investigated by Hopper⁶⁸. Black and oil have an opposing effect, particularly on the viscosity of the compound. At a constant shear rate, an increase in oil level decreases the compound viscosity whilst an increase in black level increases viscosity. However, Derringer⁶⁹ extended the work to developing a unifying viscosity model capable of postulating the individual effects of plasticizer and filler. Naturally, a knowledge of this behaviour is essential in order to produce an optimum processable rubber compound.

Literature Cited.

(Chapter 2)

1. P.S. Johnson, *Elastomerics*, 9, January (1983)
2. C.M. Blow and C Hepburn, 'Rubber Technology and Manufacture'
Chp. 6. Butterworth Group, England (1977)
3. R.H. Norman and P.S. Johnson, *Rubb.Chem.Tech.*, 54, 493 (1981)
4. '100 years of Rubber', *Eur.Rubb.J.*, 164, (5), 27, June (1982)
5. M. Morton, 'Introduction to Rubber Technology', Chapman
and Hall, London (1959)
6. M.L. Studebaker and J.R. Beatty, 'Science and Technology of
Rubber', Chp. 9, Academic Press, New York, (1978)
7. G. Kraus, 'Science and Technology of Rubber', Chp. 8,
Academic Press, New York, (1978)
8. L. Bateman, 'The Chemistry and Physics of Rubber like
Substances', Chp. 10, McLaren & Sons, London (1963)
9. D. Parkinson, 'Reinforcement of Rubbers', Monograph IRI (1957)
10. A.I. Medalia and Heckman, *J.Coll.Inst.Sci.*, 36, 173 (1971)
11. J.L. White, 'Science and Technology of Rubber', Chp. 6,
Academic Press, New York (1978)
12. M.L. Studebaker and J.R. Beatty, *Rubb. Age*, 103, (5) 21 (1976)
13. A.C. Quano, *Rubb.Chem.Tech.*, 54, 535 (1983)
14. J.P. Berry et. al, *Plast.Rubb.Proc.*, 2, 97 (1977)
15. B.R. Smith, *Rubb.Chem.Tech.*, 49, 278 (1976)
16. D.P. Mukherjee, *Polym.Eng.Sci.*, 17, 788 (1977)
17. N. Tokita and I. Pilskin, *Rubb.Chem.Tech.*, 46, 1166 (1977)
18. A.V. Tobolsky, 'Properties and Structure of Polymers',
Wiley, New York (1960)
19. G.R. Cotten, *Rubb.Chem.Tech.*, 48, 548 (1975)
20. F.G. Fox and S. Loschack, *J.Appl.Phys.*, 26, 1082 (1955)
21. J.D. Ferry, 'Viscoelastic properties of polymers',
Wiley and Sons, New York (1970)

22. J.R. Shaefgen and P.J. Flory, J.Am.Chem.Soc., 70,2709(1948)
23. G. Kraus and J.T. Gruver, J.Polym.Sci.,Pt.A, 3,105(1965)
24. V.L. Folt, Rubb.Chem.Tech., 42,274(1969)
25. H. Leaderman et.al, J.Polym.Sci., 36,233(1959)
26. K. Oda et.al, Polym.Eng.Sci., 18,25(1978)
27. A.I. Medalia, Rubb.Chem.Tech., 51,437(1978)
28. W.M. Hess et.al, Rubb.Chem.Tech., 40,371(1967)
29. P.J. Corish and B.D.W. Powell, Rubb.Chem.Tech., 47,481(1974)
30. J. Kruse, Rubb.Chem.Tech., 46,653(1973)
31. M.H. Walters and P.N. Keyte, Trans.IRI., 38,40(1962)
32. A.M. Gessler et.al, Plast.Rubb.Proc., Vol.(37), March,June,
September, (1978)
33. V.L. Folt and R.W. Smith, Rubb.Chem.Tech., 46,1193(1973)
34. R.T. Seward, Rubb.Chem.Tech., 43,11(1970)
35. J.E. Callan and W.M. Hess, Rubb.Chem.Tech., 44,814(1971)
36. A.I. Medalia, Rubb.Chem.Tech., 47,411(1974)
37. ASTM Designation, D3037, 09.01
38. ASTM Designation, D1501, 09.01
39. ASTM Designation, D3765, 09.01
40. J. Janzen and G. Kraus, Rubb.Chem.Tech., 44,1287(1971)
41. R.A. Klyne et.al, Rubb.Chem.Tech., 46,192(1973)
42. A.I. Medalia, Rubb.Chem.Tech., 51,437(1978)
43. ASTM Designation, D3493 and D2414, 09.01
44. L. Moscou et.al, Rubb.Chem.Tech., 44,805(1971)
45. P.C.Ebell, Ph.D Thesis Loughborough University (1981)
46. A.I. Medalia, Rubb. Age, 93,580(1963)
47. K.A. Burgess et.al, Rubb.Chem.Tech., 44,230(1971)
48. W.M. Hess et.al, Rubb.Chem.Tech., 46,204(1973)
49. A.I. Medalia and L W Richards, J.Coll.Int.Sci., 40,233(1972)
50. ASTM Designation D1765 09.0
51. B.B. Boonstra, 'Rubber Technology and Manufacture', Chp. 7,
Butterworth Group,England (1977)

52. Z. Rigbi, Rubb.Chem.Tech., 55,1180(1982)
53. E.M. Dannenberg, Rubb.Chem.Tech., 48,410(1975)
54. P.B. Stickney and R.D. Falb, Rubb.Chem.Tech., 37,1299(1964)
55. W.Y. Wan Idris, Ph.D Thesis Loughborough University (1978)
56. B.B. Boonstra and A.I. Medalia, Rubb.Chem.Tech., 36,115(1963)
57. P.A. Bittel, Elastomerics,44, April (1980)
58. S.B. Turetzky et.al, Rubb.Chem.Tech., 49,1(1976)
59. W.F. Watson, Ind.Eng.Chem., 47,1281(1955)
60. N. Minagawa and J.L. White, Appl.Polym.Sci., 20,501(1976)
61. L. Mullin, J.Phys.Chem., 54,239(1950)
62. E. Guth and O. Gold, Phys.Rev. 53,322(1950)
63. G. Kraus, Rubb.Chem.Tech., 38,1070(1965)
64. E.A. Collins and J.T. Oetzel, Rubb. Age, 102,64(1970)
65. P.P.A. Smit, Rheol.Acta, 8,277(1969)
66. J.L. White, Rheol.Acta, 14,1600(1975)
67. G. Kraus and J.T. Gruver, Rubb.Chem.Tech., 40,734(1967)
68. J.R. Hopper, Rubb.Chem.Tech., 40,463(1967)
69. G.C. Derringer, Rubb.Chem.Tech., 47,825(1974)

CHAPTER 3

FACTORS AFFECTING INTERNAL MIXER PERFORMANCE

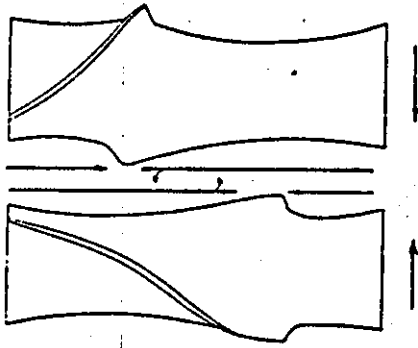
3.1 Mixer Geometry.

The throughput of an internal mixer is largely dependent on the batch size. It is inversely proportional to the mixing cycle time and the number of stages in the operation. Obviously batch size relates to the chamber empty volume (with rotors fitted) of the machine, and the fill factor during mixing. Cycle time and the number of stages depend on rotor geometry and the other mixer operating variables. Certainly material parameters should also be included when talking about the performance of each mixing operation¹⁻³.

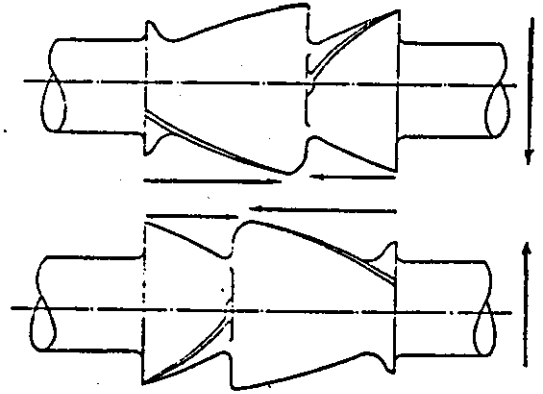
As mentioned in chapter 1.0 (section 1.3), the primary variation of an internal mixer is on its rotor geometry. There are two types of rotor design being tangential or intermeshing as shown in figure 3.1 . Each has its own advantages over the other. However, whatever the design, the rotors must have the ability to impart an adequate level of stresses and deformations onto the mixing stock, together with an efficient heat transfer capability^{1,4,5}.

Tangential rotors can either be of the two-wing or the four-wing rotor geometry^{3,6}. The wings on the rotor facilitate the axial and lateral movements of the compound. The narrow regions between the tip of the rotor and the chamber wall are

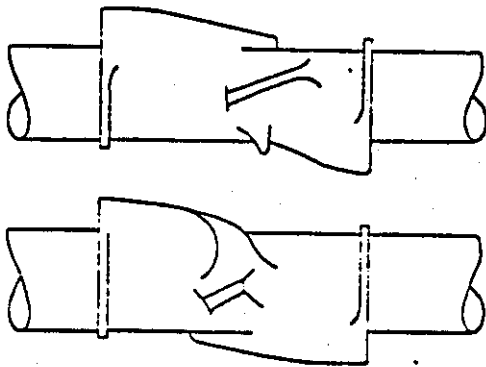
the high stress or the milling zone. Accordingly, Freakley⁷ observed that a sharp increase in pressure was generated when the rotor tip swept across the pressure transducer point. The relative directions of the compound movements in the mixing chamber are as shown in figure 3.2.



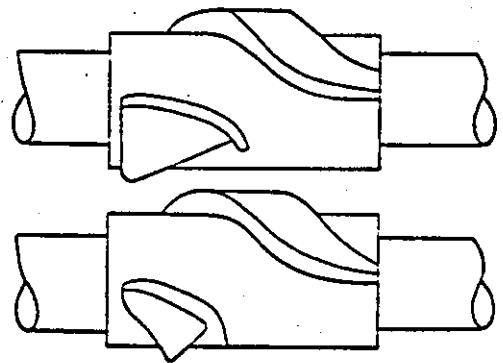
Banbury 2 - Wing



Banbury 4 - Wing



Werner Pfleiderer



Shaw Intermix

Figure 3.1 - Rotor Geometry of a few internal mixers⁵.

The space between the two rotors is involved with kneading and longitudinal cut-back of the rubber compound. Incorporation and distributive mixing are presumably taking place here⁸.

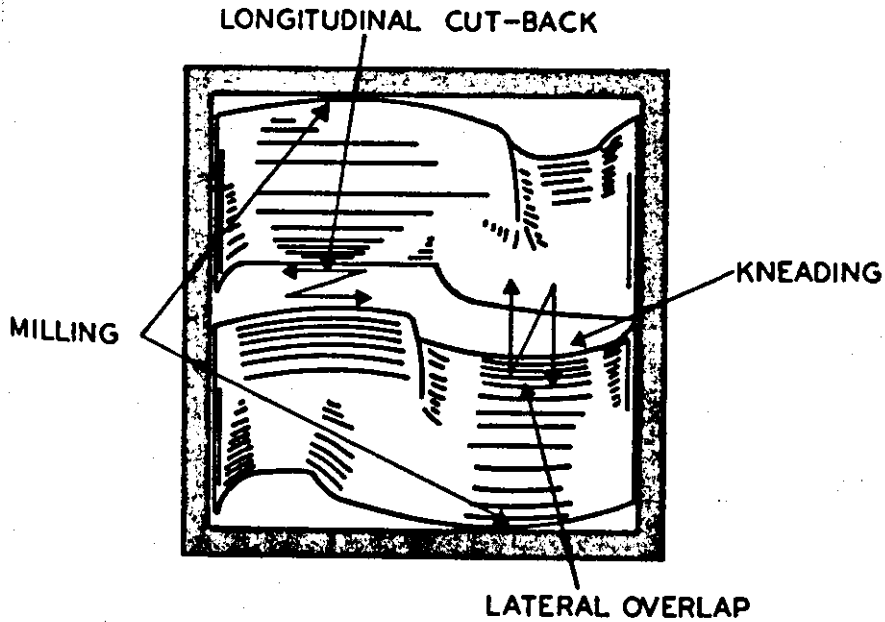


Figure 3.2 - Behaviour of compound in the internal mixer⁸.

As for intermeshing rotors, the clearance between the nogs on one rotor and the shaft of the other rotor is small. This is where the milling zone develops^{8,9}. Also the nogs or the wing surfaces have a much larger proportion of the total area of the rotor. Consequently increasing the residence time of the compound in the high stress region⁶.

Wiedman and Schmid¹⁰ made a comparative study of internal mixers fitted with the different types of rotor geometry. The intermeshing rotor mixers have larger empty volume than the tangential rotor mixers of the same rotors' centre distance. In spite of the greater empty volume, the useful working volume in the intermeshing rotor mixer is similar or only a little greater

than for the tangential rotor machines. Generally the intermeshing mixers operate at a lower fill factor. As capital cost is roughly proportional to chamber size, this is a significant disadvantage for intermeshing rotor machines¹¹.

The tangential rotor mixers are recognized for their fast feeding and emptying ability. They are also suitable for short mixing cycles and for multi-stage operation, which are all essential for high throughput process¹⁰.

Energy balance studies^{6,8,12} have shown that a high percentage of the total energy input is spent on increasing the temperature of the compound. Thus it is necessary to have sufficient cooling facilities in the mixer construction.

Rotor geometry has a substantial influence on the amount of heat transferred from the rubber compound to the mixer chamber wall and to the cooling system^{10,13,14}. The action of the intermeshing rotors generates new rubber surfaces leading to a rapid thermal homogenization of the compound. Consequently a better overall heat transfer is obtained in intermeshing mixers as compared to the tangential rotor mixers.

Figure 3.3 illustrates the overall heat transfer coefficient with mixing time. The high value of heat transfer coefficient early in the process may be related to the carbon black that is exposed to the chamber wall¹⁴. As the carbon black becomes incorporated, the heat transfer is then between the rubber and the chamber wall. This explains the decrease in the coefficient as mixing progresses, and it eventually reaches a constant level when the carbon black is completely incorporated^{6,12,14}.

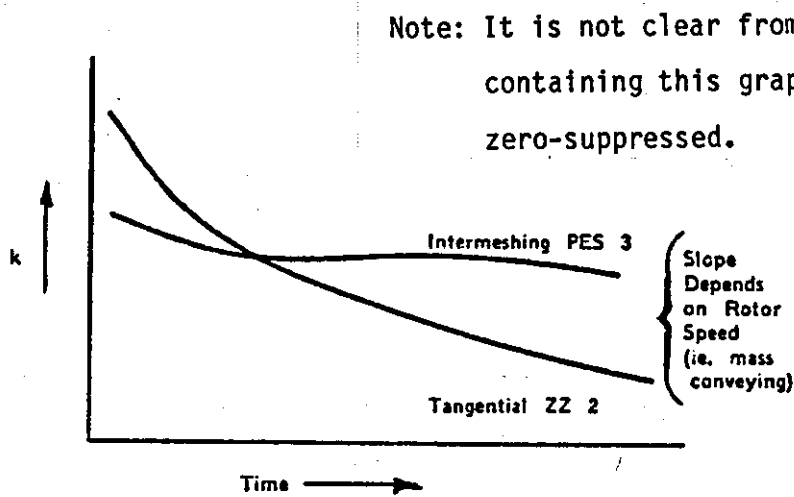


Figure 3.3 - Rotor design and heat transfer¹¹.

The energy efficiency of a mixing process is also dependent on the rotor geometry. Considering the Banbury mixer with tangential rotor design, the effective mixing takes place only in the milling zone, within a sickle shape space occupying about one quarter of the circumference of the chamber^{6,12}. In the back side of the rotor, little mixing takes place. This has lead to the developement of rotors with a larger number of wings whereby higher mixing efficiency is anticipated.

For example, a four-wing rotor shortened the mixing time by 25 % and improved the energy efficiency by 8 % as compared to the two-wing rotor. Therefore, higher throughput is obtained in the former machine. More recently, a new type of four-wing rotor was developed, resulting in an increase of 16 % in the energy efficiency as compared to the conventional four-wing rotor¹².

3.2 Mixer Operating Variables.

The internal mixer operating variables have a strong influence on the properties of a mixed rubber compound. An understanding of the effects of these variables on mixture behaviour is necessary to enable uniform feedstocks to be supplied to downstream processes. The variables have been introduced in chapter 1 (section 1.3), and the author feels it is worth mentioning them again i.e. fill factor (F), ram pressure (P), coolant temperature (T), rotor speed (S) and unit work or specific energy (W).

Strong interactions between the variables above have been shown to exert a significant influence on the properties of the rubber compound¹⁵⁻¹⁷. Consequently, attempting to determine the influence of each variable separately is difficult and basically incorrect. The importance of interaction between variables is further explained by the complex non-steady state nature of mixing operations.

The main effect of a variable should be individually interpreted only if there is no evidence that the variable interacts with other variables. When there is evidence of one or more such interaction effects, the interacting variables should be considered jointly^{18,19}.

The effects of operating variables on the properties of rubber compounds have been evaluated by statistical technique. Contour plots were widely used to give a pictorial representation of the relationship between the measured properties and the operating variables^{10,15-17}. This technique has proved to be a powerful tool in evaluating the multivariable

process of rubber mixing. The same approach is adopted in this study and it will be discussed in chapter 5.

Recently, Ebell¹⁶ analysed the effects of mixing variables using the mathematical desirability function²⁰. In a desirability function, the transformation of several responses to a single quantitative index can be achieved. The index known as desirability index is a measure of the overall mixing quality. A high desirability index, close to unity, indicates a better mixing quality.

In a mixing cycle, the specific energy input increases with an increase in fill factor and ram pressure, and also with lengthening of mixing time¹⁶. A reduction in the energy with increasing fill factor at low level of ram pressure was commonly noted^{6,16,21}. This may be due to the compound being pushed up into the throat of the mixer where it can stagnate, reducing the proportion for effective mixing.

The batch or dump temperature of a compound is influenced by coolant temperature and fill factor^{10,15-17}. A strong interaction between unit work and rotor speed was noted, with higher dump temperature when both variables were increased, as shown in figure 3.4. Obviously with high energy, more heat is being generated causing a rise in stock temperature. Similarly this applies to the increase in rotor speed.

Wiedman and Schmid¹⁰ showed that the change in dump temperature was lesser as compared to the change in the circulating coolant temperature. An increase by 30.0°C of the circulating coolant in the chamber and rotor, would result in between 15.0°C and 11.0°C increase in the dump temperature. This

change was for a 7 litre and a 6 litre mixer respectively. However, at low coolant temperature (30.0°C), dump temperature decreases with increase in ram pressure of up to 0.41 MPa irrespective of the rotor speed (45.0-75.0 rpm). This is true for SBR compound evaluated by Ebell¹⁶. At higher coolant temperature (50.0°C), the increase in dump temperature was more pronounced.

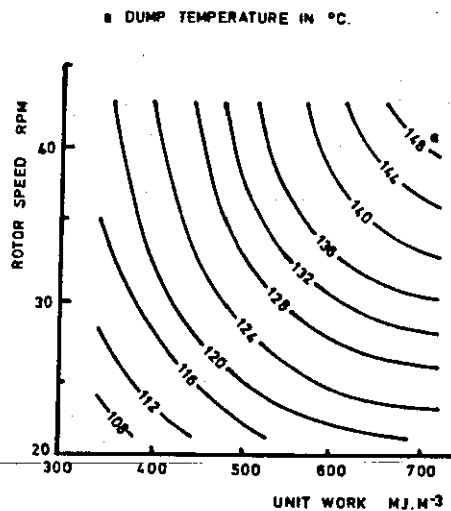


Figure 3.4 - The variation of dump temperature with rotor speed and unit work¹⁷.

Increase in fill factor cause an increase in dump temperature which may may be due to the simultaneous increase in specific energy input.

As for mixing time, a strong interaction between unit work and rotor speed was also observed^{15,16}. Mixing time increases with increase in unit work and decreases with increasing rotor speed, as shown in figure 3.5. At constant unit work, increasing fill factor will decrease mixing time irrespective of rotor

speed. A lesser decrease in mixing time was observed at these conditions for higher coolant temperature¹⁶. Low ram pressure prolonged the mixing time, which was due to low stress being imparted causing an increase in slippage of the compound¹⁶.

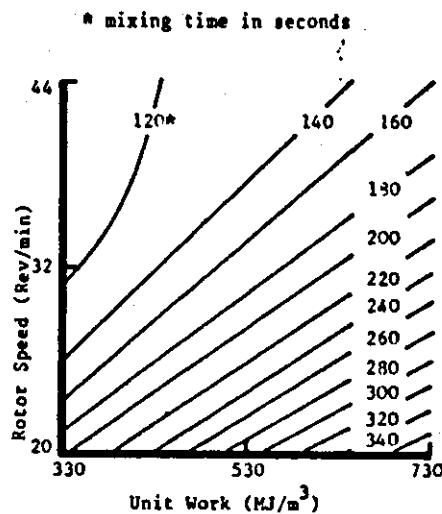


Figure 3.5 - The variation of mixing time with rotor speed and unit work¹⁵.

The level of carbon black dispersion in rubber determines the quality of the mixed compound. There are various methods of measuring the degree of dispersion, either directly or indirectly. However, at this stage, the influence of mixer variables on dispersion is our main interest and its method of determination, which will be discussed in the next chapter, can be disregarded here.

Dispersion of carbon black increases with increase in fill factor, unit work and at low coolant temperature^{16,22}. With high coolant temperature and high fill factor, a rapid rise in temperature of the compound occurs, resulting in the lowering of

its viscosity and stresses imparted. Ebell¹⁶ showed that the high coolant temperature is not conducive to improving mixing efficiency.

Wiedman and Schmid¹⁰ reported that with all variation in the mixer operating parameters, carbon black dispersion depends primarily on the amount of unit work input. This is illustrated in figure 3.6. This is so considering that unit work is closely related to fill factor and ram pressure¹⁶.

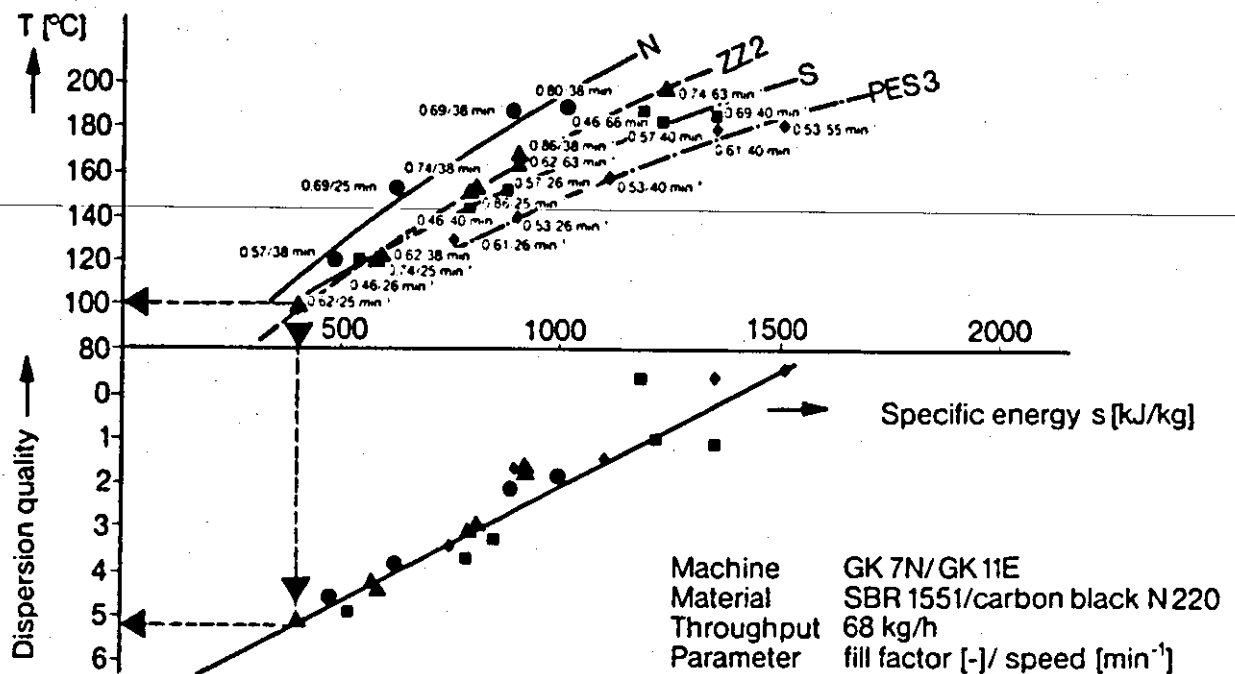


Figure 3.6 - Influence of rotor geometry on dump temperature, specific energy and dispersion level¹⁰.

The effect of changing ram pressure on dispersion is also very dependent on the levels of other variables. Ebell¹⁶, Wiedman and Schmid¹⁰ indicated that ram pressures greater than 0.57 MPa may well be unnecessary if other operating conditions are favourable.

In conjunction with high fill factor, low coolant temperature and adequate ram pressure, the effect of increasing mixing time is to improve carbon black dispersion.

On the other hand, the desirability function approach has shown that several interactions between the variables were observed. This is anticipated considering the combination of several responses to indicate the overall mixing quality¹⁶. The interaction between fill factor and unit work FW, exhibited a strong influence, with increases in the desirability index as the level of both variables increases.

Within the experimental regime, separate interactions between ram pressure, coolant temperature and rotor speed with fill factor (RF, TF and SF) affect the response significantly. Furthermore, third order interactions were noted affecting the overall mixing quality, such as PSW, PFW and TFS.

At low coolant temperature, the mixing quality improves with increases in fill factor, unit work and ram pressure. Increase in rotor speed has an adverse effect on the quality at constant fill factor and unit work regardless of ram pressure level.

At high coolant temperature, the increase in fill factor

and unit work has a negative effect on mixing. The decrease in viscosity of the compound is unfavourable to dispersive mixing leading to a decrease in the desirability index. Moreover, more unit work was needed in order to attain the same level of mix quality when compared to the amount of unit work at low coolant temperature. Ebell¹⁶ noted that at high coolant temperature, the disastrous effect of increase in rotor speed on mixing quality was magnified.

However, the best mixing conditions for SBR compound were found to be at low rotor speed (30.0 rpm), high unit work (1500.0 MJ/m³) and low coolant temperature (30.0°C). The worst mixing conditions were at high rotor speed (75.0 rpm), low unit work (300.0 MJ/m³) and high coolant temperature (50.0°C). The same finding was indicated by Wiedman and Schmid¹⁰ on their SBR compound.

In summary, the desirability function approach has confirmed that interactions between the mixer operating variables are important and to analyse the effects of each variable in isolation is incorrect.

3.3 Process Control System.

Effective control system are providing the solution to industry's ever increasing demands on production, higher quality and energy conservation. This effectiveness is made possible not only by incorporating microprocessor and electronic technology within newly designed polymer processing equipment, but also by adopting such technology to older, previously installed machinery such as the internal mixer.

The complexity of rubber mixing has been acknowledged, and it is imperative that the process be operated at a level compatible with the sophistication of the materials being compounded.

The basic control systems can be found in most internal mixers, provide manual control over the machine operating variables such as rotor speed, ram pressure and circulating coolant temperature. They respond to the level of energy, temperature (batch) and time over a mixing cycle. Alternatively, automatic control systems can be installed so as to monitor the machine responses and subsequently control the operating variables to the desired mixing operation. Present control philosophy is based on time, batch temperature and energy input override system^{10,23,24}.

The batch process control as found in internal mixing of rubber is not as straight forward as a continuous process²³. The controlled variables usually never have a chance to stabilize during the mixing operation, while a continuous system is allowed to stabilize before satisfactory output is expected. The limited time of batch process is often a handicap to effective

control. This requires a higher speed of sensing and actuating mechanisms, which has to be considered in the control philosophy as mentioned earlier. The development of infra-red optic probe has shown some promise in this aspect for temperature measurements.

Most systems do not concentrate on the control of mixing process alone, but include material handling and weighing¹¹. A schematic diagram of the input and output of a mixer control system is as shown in figure 3.7.

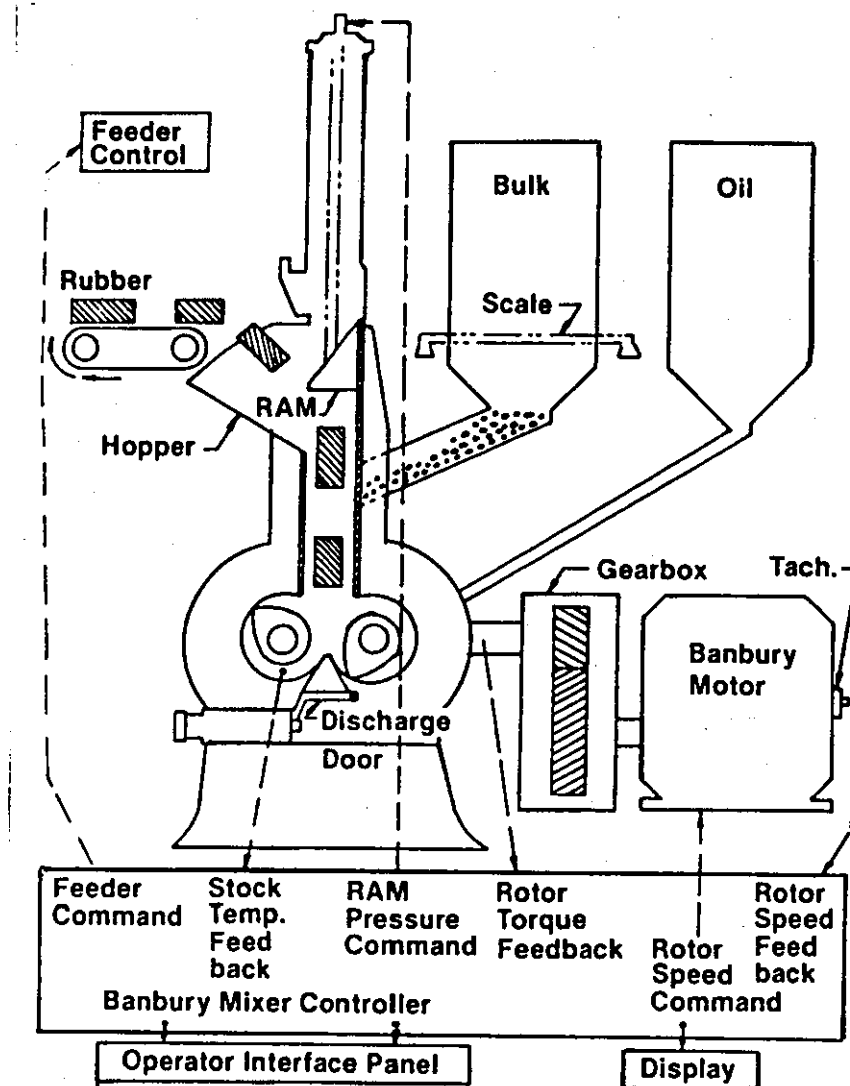


Figure 3.7 - Schematic diagram showing inputs and outputs on Banbury mixer control²³.

The adaptation of microcomputers in the system allow programable mixing operations to be effected. In addition, when an optimized mixing condition has been obtained, the computer can memorize the condition and then to run subsequent batches in the same way making consistent operation possible from batch to batch.

Furthermore, each operation can be stored or transmitted to other computers for statistical analysis and useful manipulation of information to generate processing histories, correlation to physical testing or long term storage^{23,25}. Recently, software has been developed to enable the microcomputer to manage the operation of a mixer and regulate the mixing process via a feedback loop to obtain the required compound properties²⁶.

Literature Cited.

(Chapter 3)

1. J.L. White and N. Tokita, J.Appl.Polym.Sci., 12,1589(1968)
2. N. Tokita and I. Pilskin, Rubb.Chem.Tech., 46,1166(1973)
3. W.M. Wiedman and H.M. Schmid, Eur.Rubb.J., 33,March(1982)
4. W.R. Bolen and R.E. Colwell, SPE J., 8(14),24, August(1958)
5. J.M. Funt, 'Mixing of Rubber', RAPRA Publications, England(1977)
6. H. Palmgren, Rubb.Chem.Tech., 48,462(1975)
7. P.K.Freakley and W.Y. Wan Idris, Rubb.Chem.Tech.,52,266(1981)
8. N. Nakajima, Rubb.Chem.Tech., 54,266(1981)
9. P. Whitaker, J. IRI 4,(4),153 August (1974)
10. W.M. Wiedman and H.M. Schmid, Rubb.Chem.Tech., 55,363(1982)
11. P.S. Johnson, Elastomeric 9,January(1983)
12. N. Nakajima, Rubb.Chem.Tech., 55,931(1982)
13. H. Ellwood, Eur.Rubb.J., 159,17,Jan/Feb(1977)
14. N. Nakajima et.al, Rubb.Chem.Tech., 55,546(1982)
15. P.K. Freakley, Int.Rubb.Conf.,Harrogate,England, June(1981)
16. P.C. Ebell, Ph.D Thesis Loughborough University (1981)
17. K.B. Basir and P.K. Freakley, Kaut.Gummi.Kunst., 35,205(1982)
18. G.E.P. Box et.al 'Statistic For Experimenters' Wiley and Sons
New York (1978).
19. O.L. Davies, 'Statistical Methods in Research and Production'
ICI (Oliver and Boyd) (1957).
20. E.C. Harrington, Ind.Qual.Cont., 21(10),494(1965)
21. J. Carver, Rubb. Age, 102,60(1970)
22. B. Boonstra and A.I. Medalia, Rubb.Chem.Tech., 36,115(1963)
23. L.A. Acquarulo Jr. and A.J. Notte, Elastomerics,17,Nov.(1983)
24. F.W. Hetzel et.al, Elastomerics,34, May (1981)
25. P.K. Freakley, Private Communication
26. Rubberex '84, Conference, NEC Birmingham, England
12 - 16 March (1984).

CHAPTER 4

CHARACTERIZATION OF MIXED COMPOUND

4.1 Introduction.

Most testing of rubber or rubber compound is conducted to determine its processing characteristics or to measure physical properties. Processing characteristics are generally divided into two areas, processability and vulcanization. Processability of an elastomeric compound is dependent on the compound's viscosity and elasticity^{1,2}. Vulcanization is the cross-linking of the compound which is dependent on its chemical composition³. Generally the physical properties of rubber vulcanizates are measured by static and dynamical tests, designed to simulate the mechanical conditions imposed on the finished rubber products.

In rubber testing there is a wide diversity of material characteristics, together with a large number of testing methods. However, certain characteristics and test methods have been generally accepted as the 'yardsticks'. They have been standardized and documented by the American Society of Testing and Material (ASTM), the British Standard Institution (BSI) and the International Standards Organization (ISO).

The importance of processability testing after the mixing stage is well recognized, especially for high output rubber products manufacturing. Moreover, bearing in mind that the various stages of processing are irreversible operations, the decision whether to accept or reject a mixed stock is mainly

dependent on this test. It acts as a batch control, where a mixed compound within a required specification is fed into subsequent downstream processes. In addition processability testing is essential for compound development, where a critical limit of processability is required which cannot be exceeded under any known circumstances. Furthermore, it is necessary to know whether fluctuation of processing conditions can prevent the material from being processed uniformly. Generally processability indicates the level of viscous and elastic behaviour, which is strongly affected by the level of carbon black in a rubber compound^{4,5}.

The physical properties of rubber vulcanizates will be described briefly in this chapter. However, processability and rheological behaviour of unvulcanized rubber compounds are the subjects of this study. Consequently a review of these topics is necessary in order to understand particularly the influence of mixing operations on flow characteristics.

4.2 Vulcanizates Properties.

4.2.1 Static tests.

The physical properties of vulcanizates are quite dependent upon the mixing operations. Initially, during incorporation of carbon black, there is a rapid change from the properties of a gum rubber, to those of the carbon black filled stock. When the dispersion level is improving, the physical properties of the corresponding vulcanizate follows a rather ragged pattern which smooths out when the dispersion reaches a plateau⁴⁻⁶. Figure 4.1 shows these features in the results of a typical mixing study. Generally the degree of carbon black

dispersion influences strongly the level of vulcanizate properties.

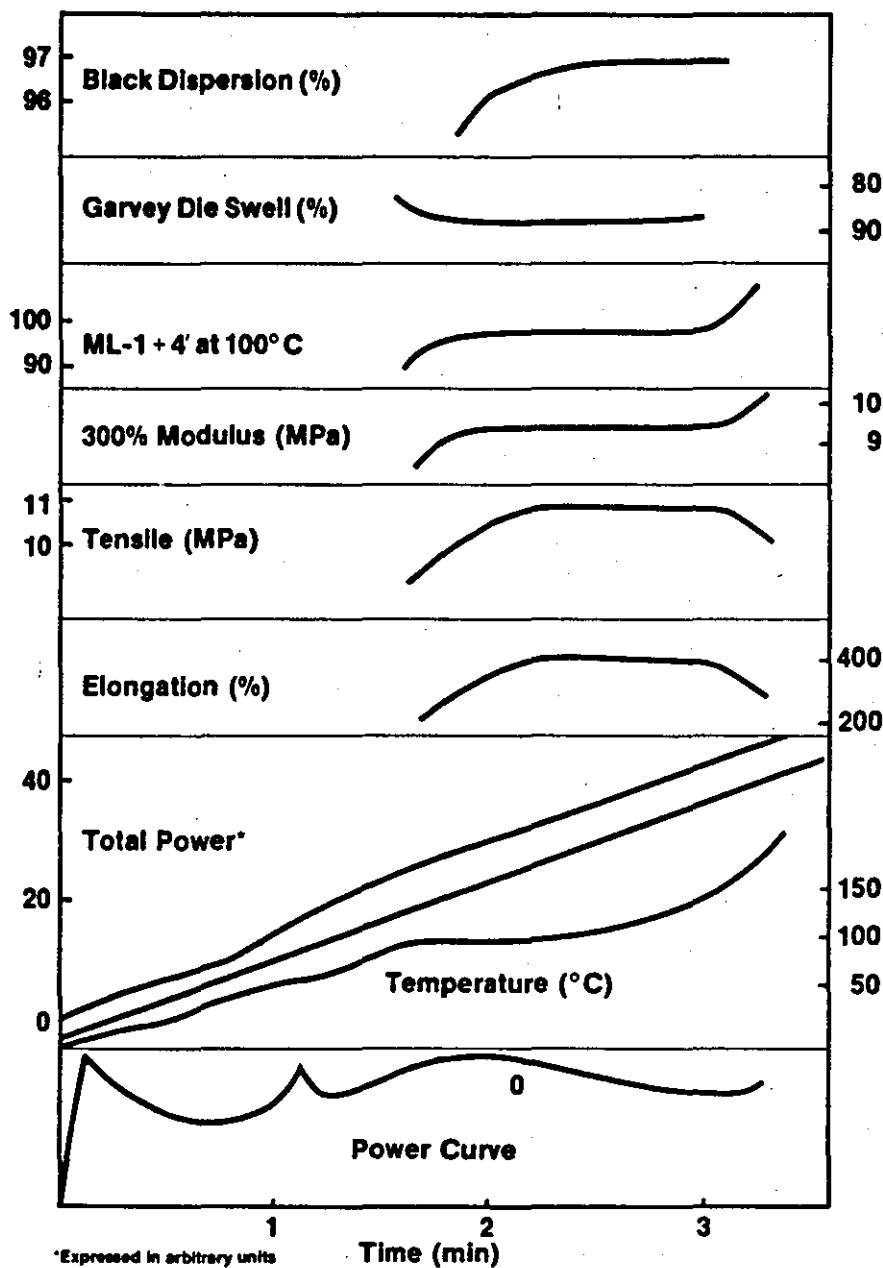


Figure 4.1 - Mixing profile for high viscosity Butyl compound⁵.

The majority of researchers⁴⁻⁹ have found that tensile strength increases with increase in mixing time. A plateau can be reached when the amount of energy input⁹ is between 1600.0 to

2100.0 MJ/m³. However, a gradual drop in tensile strength was noted when lengthening the mixing time¹⁰. Boonstra and Medalia⁶ reported that maximum tensile strength was reached in 3.0 minutes for a single stage mixing of SBR compound. Baker¹¹ investigated the influence of carbon black on tensile strength of NR, and concluded that tensile strength decreases as particle size of carbon black increases.

Williamson¹² indicated that tensile strength is influenced strongly by a strong interaction between rotor speed and circulating coolant temperature (ST), for PVC/Nitrile rubber blends. Increasing the amount of energy input onto the compound increased tensile strength considerably, which is attributed to improving dispersion.

Elongation at break is another property which is measured concurrently with tensile strength. An increase in the percentage of elongation is observed with increase in mixing time, which is similar trend to the tensile strength. Drogin⁹ reported a drop in elongation at break after prolonged mixing of over 20 minutes.

Tear strength has been used to measure the adequacy of mixing^{6,8}. It measures the tear resistance of a nicked sample when tension is applied¹³. Boonstra and Medalia⁶ reported that mixer operating variables did not affect tear strength. However, Dannenberg¹⁴ and Williamson¹² claimed that an increase in tear strength was observed with better mixing.

Other physical properties are the stresses at 100 %, 200 % and 300 % extensions, termed 'moduli' by rubber technologists. Among them, the modulus at 300 % elongation is widely used as

the criteria for vulcanizate stiffness. Most workers^{4,5,8,10} have shown that the modulus increases with mixing time a particular level, where it remains constant, as depicted in figure 4.1. However, the phenomenon of modulus decrease with improving dispersion has been established in most dispersion studies^{6,8,15,16}. Consequently, the decrease in modulus with mixing is based on this finding. Obviously there are additional factors which govern the modulus of a compound, such as the elastomer properties, rubber-filler interaction and the vulcanization reaction¹⁶.

Hardness¹⁷ refers to the ability of rubber vulcanizate to resist indentation. It is an indication of the modulus at low deformation. Consequently, hardness obeys the same arguments as applied to the modulus property. The level of hardness decreases with mixing^{4,6,8,16}. Williamson¹² observed that the hardness of PVC/Nitrile rubber decreases with increasing unit work.

Wear properties, particularly abrasion resistance are closely related to the level of carbon black dispersion. The influence of mixing conditions on dispersion will obviously reflect the resistance to wear of a rubber vulcanizate. Increase in abrasion resistance was observed with mixing^{6,9,15}. However, abrasion measurements were found to be the most difficult to evaluate, mainly due to the clogging of the abrasive surface¹⁷. Great care is needed in comparing results obtained on different machines or even the same machine at different times.

4.2.2 Dynamic Tests.

Dynamic testing of rubber vulcanizates can be performed by destructive or non-destructive methods. In non-destructive testing, dynamic properties refer to the response of vulcanizates to periodic or transient forces which do not cause failure or permanent change of properties during investigation¹⁸. Generally this is limited to small deformation not exceeding about 25 %¹⁹. As for destructive testing, it refers to the degree of surface cracking of a nicked vulcanizate when subjected to cyclic flexing. This test is commonly known as fatigue testing^{20,21}.

The dynamic properties of rubber are best visualized in terms of a specimen undergoing sinusoidal shear deformation as shown in figure 4.2. The plot of stress against time is sinusoidal for linear viscoelastic material, but is out of phase with the strain. The measured stress leads the strain by the angle δ .

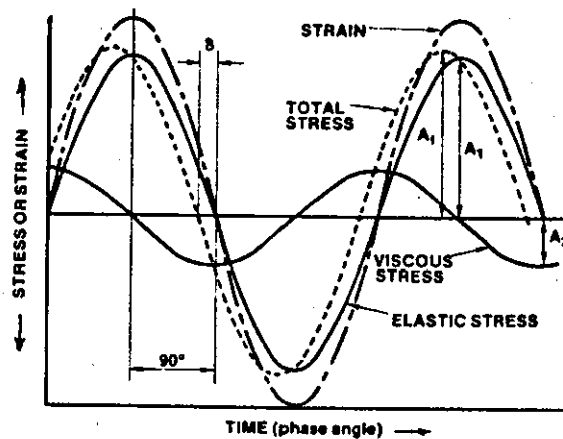


Figure 4.2 - Sinusoidal strain and stress components¹⁹.

This stress can be resolved into two sinusoidal components, the elastic stress which is in phase with the strain and the viscous stress which is out of phase. At any time the measured stress is the algebraic sum of its two components. Since the components are 90 degrees out of phase, there exist a simple relation between the maximum values of the components and the measured stress. They can be represented by the phase diagram as shown in figure 4.3.

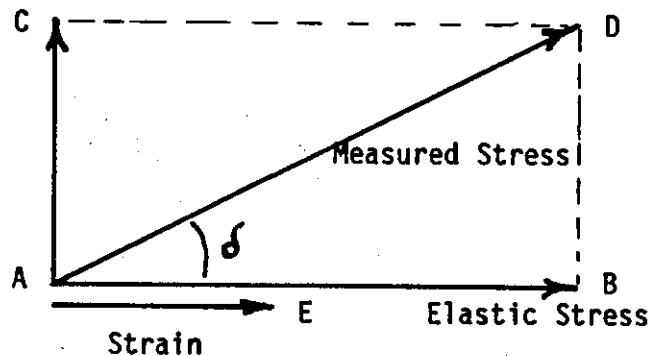


Figure 4.3 - Stress components and phase angle.

where AB - elastic stress component
 AC - viscous stress component
 AD - the resultant or the measured stress
 AE - strain amplitude
 and δ - loss angle

Sinusoidal motion can be expressed in terms of its real and imaginary component by

$$AD = AB + jAC \quad \dots\dots\dots 4.1$$

Dividing equation 4.1 by the strain amplitude AE , gives the modulus components represented by G , in shear and E in compression or extension. The complex modulus in shear can be expressed as

$$G^* = G' + jG'' \quad \text{.....4.2}$$

where G^* - dynamic shear modulus
 G' - the elastic modulus or storage modulus
 G'' - the viscous modulus or loss modulus
and j - the complex number operator

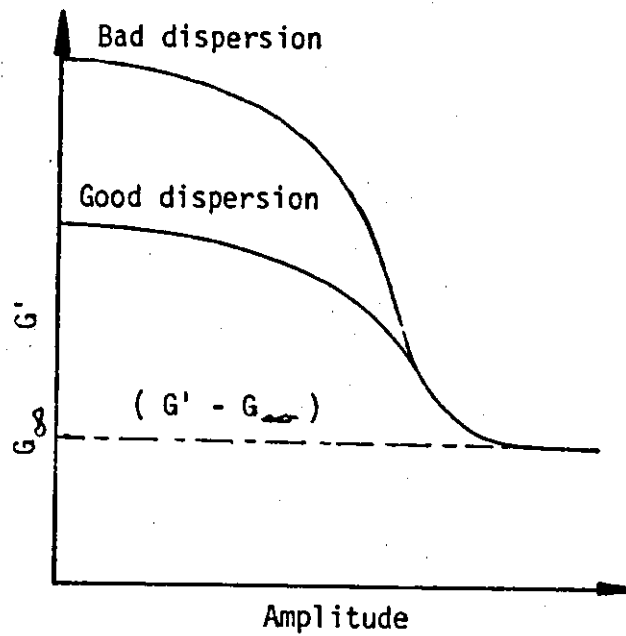
The loss tangent is expressed by

$$\tan \delta = \frac{G''}{G'} \quad \text{.....4.3}$$

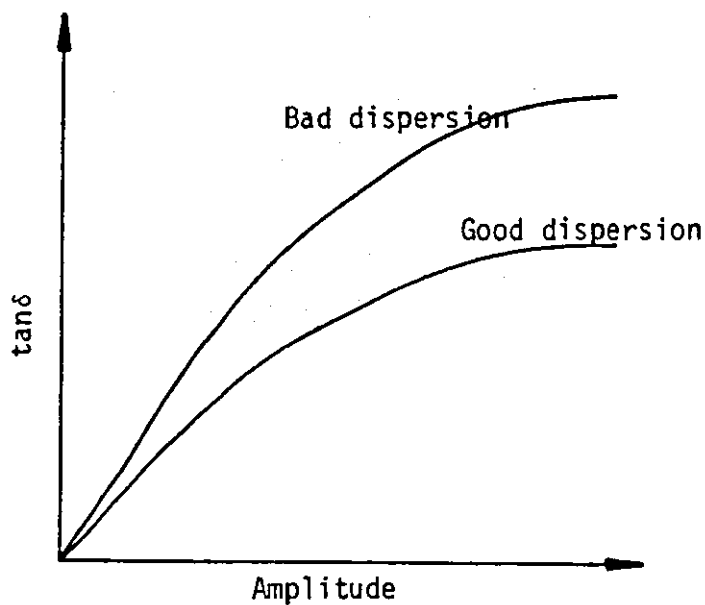
Generally dynamic properties of a material are specified by the storage modulus (elastic modulus) and the loss tangent. Storage modulus is closely related to the dynamic modulus¹⁹, thus the effect of various parameters on G^* can generally be applied to G' .

Many researchers^{4,7,8,22-24} have used dynamic properties as an assessment for carbon black dispersion in a compound. A drop in $\tan \delta$ (or δ) was observed as mixing progressed^{7,24}. The difference between ($G' - G_{\infty}$) as shown in figure 4.4 (a) represents the region of interaggregate interaction²⁵. A drop in its value indicates the extent of carbon black dispersion in the rubber matrix. Payne and Whittaker²² reported that at constant strain, a decrease in loss modulus demonstrated improved

dispersion. A graphical representation of dynamic properties with carbon black dispersion is as shown in figure 4.4 (a),(b)⁸.



(a)



(b)

Figure 4.4 - (a) Dispersion/amplitude dependence of G'
(b) Dispersion/amplitude dependence of δ ⁸.

Hysteresis, is another measurement that can be derived from dynamic testing. It measures the fractional amount of mechanical energy input converted to heat, which is also related to the loss tangent²⁶. Drogin¹⁰ and Boonstra et.al⁶ noted that hysteresis decreases with increasing mixing time. Heat buildup measurement, which is allied to hysteresis, was found to decrease with mixing^{6,15}. Also closely related to dynamic properties is the resilience of a rubber compound. The higher the loss tangent, the lower is also the resilience¹⁸.

One of the major causes of failure in rubber products under dynamic service condition arises from the development of cracks. The growth of these cracks under repeated deformation can lead to failure, known as fatigue. Fatigue resistance and cut growth are highly dependent on the level of carbon black dispersion²⁷. A slow down in cut growth was observed as mixing improves⁶. Wood²⁸ noted that rapid tread groove cracking occurs in a poorly dispersed tyre stock. Drogin¹⁰ reported that mixing time affects fatigue resistance variably, depending on rubber and type of carbon black.

4.3 Processability Of Mixed Compound.

4.3.1 Rheological Characterization.

Rheology has been defined as the science and mechanism of flow of deformable materials. The importance of rheology has been acknowledged by most researchers mainly in the field of processing and characterization of material properties. It encompasses the study of deformation of materials under the influence of applied stresses.

When a stress is applied on a solid, a deformation will begin and continue, until internal (molecular) stresses are developed which just balance the external stresses, establishing an equilibrium state of deformation. Most solids exhibit some degree of elastic response whereby the deformation is directly proportional to the applied stress. Upon removal of the applied stress, complete recovery of the deformation occurs. Materials exhibiting such linear behaviour are termed as Hookean solids. Elastic response may also be shown by non-Hookean materials for which the deformation is not linearly related to the applied stress.

Not all materials reach an equilibrium state of deformation. If an external stress is applied to a fluid, irrecoverable continuous deformation will occur until the stress is removed. Internal frictional forces (viscosity) retard the rate of deformation until an equilibrium state can be reached. The constant rate of deformation and its related internal frictional forces describe the viscous properties of the fluid. A fluid in which the rate of deformation is directly proportional to the applied stress is termed as Newtonian fluid.

However, most fluids exhibit non-linear response to the applied stress and they are collectively called the non-Newtonian fluids.

Most polymeric materials exhibit neither the idealized Hookean solid nor the Newtonian fluid properties. They possess a broad spectrum of behaviour from liquid-like to solid-like. Unvulcanized rubber can give both highly viscous and highly elastic behaviour and are generally considered as viscoelastic materials²⁹⁻³¹.

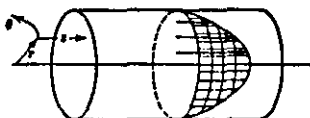
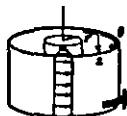
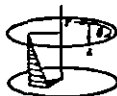
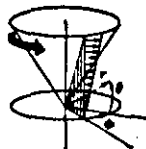
Under constant stress a viscoelastic material does not maintain constant deformation, but goes on slowly deforming with time, commonly known as creep. When constant deformation is constrained on the material, the stress required to hold it diminishes gradually or relaxes. Such material which is not quite liquid; and while flowing under constant stress, stores some of the energy input, instead of dissipating it all as heat and it may recover part of the deformation when the stress is removed (elastic recoil). As previously mentioned, when viscoelastic materials are subjected to sinusoidally oscillating stress, the strain is neither exactly in phase with the stress nor 90 degrees out of phase but is somewhere in between. Some of the energy input is stored and recovered in each cycle, and some is dissipated as heat.

The rheological properties of viscoelastic materials are a function of applied stress, degree and rate of deformation, time and their dependence on temperature and chemical composition²⁹⁻³¹. The relationship between stress and strain or strain rate and the dependence of this relationship on factors such as temperature is generally described by a constitutive

equation or a rheological equation. Rheological characterization of viscoelastic material should incorporate both the viscous and elastic components. When a clear distinction is made between the viscous and elastic behaviour of a polymer, a better understanding can be obtained of how molecular parameters, material variables and processing conditions affect processing properties³⁸⁻⁴⁰.

Perhaps the most important class of deformation for polymer are laminar shear flows, sometime known as the viscometric flows³⁵. This form of deformation corresponds to simple shear flow as illustrated in figure 4.5. Simple shear flows include Couette flow between co-axial cylinders³⁶, Poiseuille flow in a tube³¹, torsional flow between rotating disk³⁷ and flow between a cone and a plate³⁸. The flow notation in simple shear is as shown in table 4.1.

Table 4.1 - Simple shear flow notation²⁹.

Flow Geometry	Coordinate Notation			
	1	2	3	
1. Poiseuille Flow		z	r	θ
2. Couette Flow		θ	r	z
3. Parallel Plate Torsion		θ	z	r
4. Cone and Plate Torsion		ϕ	θ	r

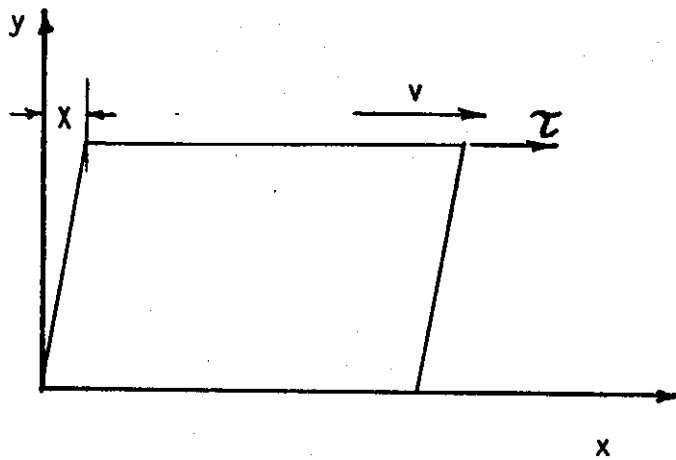


Figure 4.5 - Simple shear of Newtonian fluid.

Consider firstly the rheological response of a Newtonian fluid under simple shear mode of deformation. Referring to figure 4.5, a constant shear stress τ (acting in x-direction and perpendicular to y-plane) is applied on the top surface of the cube, setting its upper surface in motion until a steady velocity v (in the x-direction) is reached. The rheological equation of the Newtonian fluid is represented by³⁹

$$\tau = \eta_N \frac{dv}{dy}$$

$$\tau = \eta_N \frac{d}{dy} \frac{dX}{dt} \quad \dots\dots\dots 4.2$$

$$\tau = \eta_N \frac{d}{dt} \frac{dX}{dy} \quad \dots\dots\dots 4.3$$

where η_N - Newtonian viscosity of fluid
 v - velocity in x-direction

and $\frac{dx}{dy}$ is the strain in x-direction , represented by δ .

Therefore, rewriting equation 4.3 and it becomes

$$\begin{aligned}\tau &= \eta_N \frac{d\delta}{dt} \\ \tau &= \eta_N \dot{\delta} \quad \text{.....4.4}\end{aligned}$$

and $\dot{\delta}$ is the shear rate (time derivative of the strain δ)

However, as mentioned earlier many fluids deviate from the Newtonian behaviour and commonly known as non-Newtonian fluid. In non-Newtonian fluid, the shear stress is not proportional to the shear rate, whilst proportionality exists in Newtonian fluid as shown in figure 4.6. As such, it is more common to refer to the 'apparent viscosity' η_a , defined as the ratio of shear stress to the shear rate and can be expressed as

$$\eta = \frac{\tau}{\dot{\delta}} \quad \text{.....4.5}$$

However, apparent viscosity decreases with rate of shear for pseudoplastic fluid and it increases with rate of shear for dilatant fluid. For Newtonian fluid the apparent viscosity is independent of rate of shear. The apparent viscosity at 1.0 s^{-1} is called the reference viscosity.

Frequently a logarithmic plot of the shear stress and shear rate known as the 'flow curve' will show concisely the flow behaviour of the fluid. The curves A, B, C and D in figure 4.6 illustrates the deviation and non-linearity of flow from the idealized Newtonian fluid. When the shear rate increases more in

proportion than the shear stress (curve B), the fluid is known as pseudoplastic. As the case for shear stress increase is more than the shear rate (curve A), the fluid is known as dilatant^{31,39}.

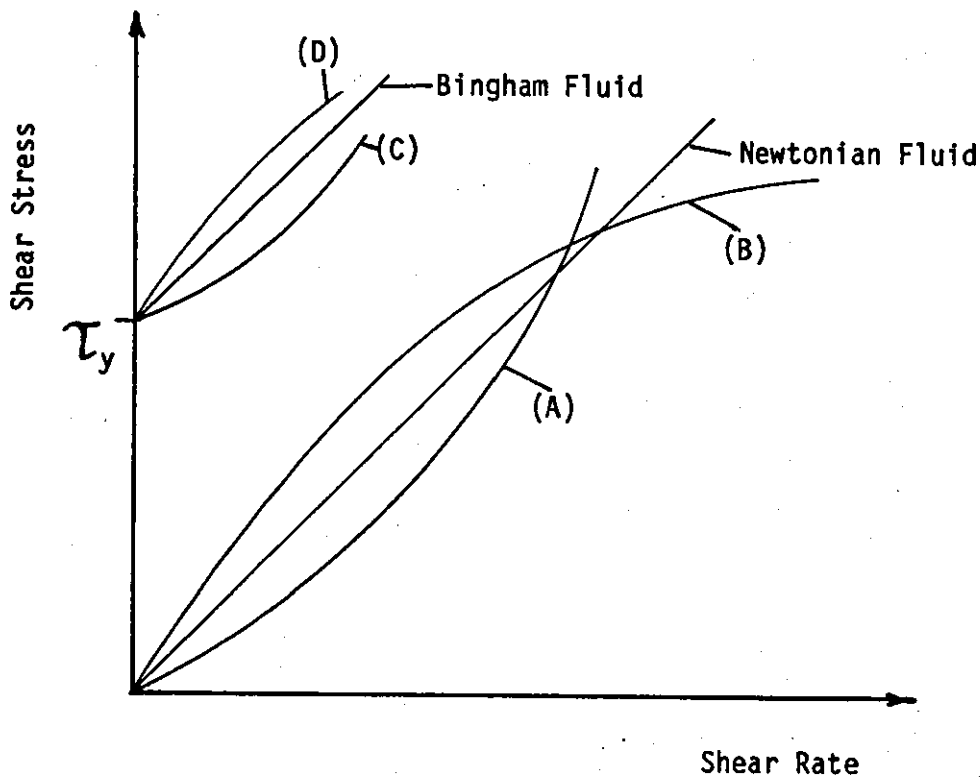


Figure 4.6 - Flow curves of different fluids³¹.

Some fluids will only start to flow if sufficient stress is applied. This is exhibited by Bingham fluid or the ideal plastic. A rheological equation similar to equation 4.5 with the yield stress term, τ_y , included can be written as

$$(\tau - \tau_y) = \eta_a \dot{\gamma} \quad \text{.....4.6}$$

where $\tau > \tau_y$

Pseudoplasticity and dilatancy also can exist in such fluids, as shown by the curves C and D in figure 4.6.

Many rheological equations have been proposed to describe the non-Newtonian behaviour of fluid flows. The Ostwald-de-Waele or power law equation relates the viscosity, shear rate and shear stress of the fluid in the form

$$\tau = \eta_0 \dot{\gamma}^n \quad \text{.....4.7}$$

where η_0 - the reference viscosity
n - the power law index

Equation 4.7 can be expressed in terms of the apparent and reference viscosities

$$\eta_a = \eta_0 (\dot{\gamma})^{n-1} \quad \text{.....4.8}$$

$$\eta_a = \eta_0 \left(\frac{\tau}{\tau_0} \right)^{\frac{n-1}{n}} \quad \text{.....4.9}$$

where τ_0 - shear stress at 1 s^{-1} shear rate.

A plot of $\log \tau$ versus $\log \dot{\gamma}$ will give a straight line, with slope n if the fluid obeys the power law equation. However, for rubber compounds this is normally only true for one or two decades of shear rate, but when extended over several decades, significant non-linearity becomes apparent³⁹⁻⁴². When the index $n < 1$, the viscosity of the fluid decreases with increasing shear rate, as found in pseudoplastic fluid. Dilatant fluids can be described when $n > 1$. Consequently, the extent of deviation of n from unity (Newtonian fluid $n = 1$), is an indication of the non-Newtonian behaviour of a fluid.

A summary of other derived empirical equations relating the viscosity and shear stress (or shear rate) is as shown in table 4.2.

Table 4.2 - Summary of viscosity relations for non-Newtonian fluids in simple shear³⁹.

(1) Newton	$\eta = \mu$
(2) Power law	$\eta = \eta^0 \left \frac{\dot{\gamma}}{\dot{\gamma}^0} \right ^{n-1} = \eta^0 \left \frac{\tau}{\tau^0} \right ^{(n-1)/n}$
(3) Reiner-Philippoff	$\eta = \mu_{\infty} + \left[\frac{\mu_0 - \mu_{\infty}}{1 + (\tau/A)^2} \right]$
(4) Ellis	$\eta = \frac{\mu_0}{1 + \frac{\mu_0}{\eta^0} \left \frac{\tau}{\tau^0} \right ^{m-1}}$
(5) Powell-Eyring	$\eta = \mu_0 \left[\frac{(\tau/B)}{\sinh(\tau/B)} \right]$ $\eta = \mu_0 \left[\frac{\operatorname{arcsinh}(\mu_0 \dot{\gamma}/B)}{(\mu_0 \dot{\gamma}/B)} \right]$
(6) Bueche	$\eta = \mu_0 f(x \dot{\gamma})$
(7) Rouse	$\eta = \mu_0 g(\beta \dot{\gamma})$

Some fluids undergo structural buildup or breakdown with either increasing or decreasing shear rate. The process of structural changes is time dependent and reversible, as found in thixotropic and rheopectic fluids. The rapid breakdown of the structure can reduce the final apparent viscosity of thixotropic fluid several times below its initial value^{39,40}. It was found difficult to quantify thixotropic behaviour with a single index^{40,43,44}. The temporary reduction in viscosity with time and shear rate shows a close resemblance to pseudoplastic fluids^{31,40}. However, there is a limiting reduction until the

viscosity reduces an equilibrium value. Mooney⁴⁰ reported that, the addition of carbon black in rubber increases thixotropic behaviour.

Rheopexy is an inverse to the previous phenomena, whereby, structural buildup is faster than the structural breakdown^{31,39}. The increase in apparent viscosity with time will eventually reach an equilibrium value at a particular shear rate.

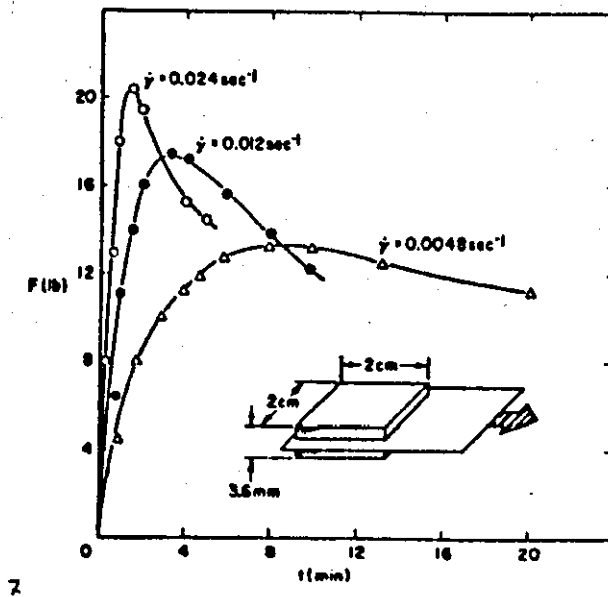


Figure 4.7 - Transient shear force buildup and stress overshoot⁴⁶.

Another aspect of non-linear viscoelastic effect is the variation of shear stress with time at the start-up of flow^{45,46}. At low shear rates, the stress monotonically increases to a steady state. However, at higher shear rates, it overshoots the steady state as shown in figure 4.7. Dillon and Cooper⁴⁴ reported in their investigation that, this time dependent non-linear viscoelastic effect exists in rubber. Recently Turner and Bickley⁴² observed the same phenomenon in SBR compound. However, Nakajima and Collins⁴⁷ expounded this transient

behaviour and derived a constitutive equation for the non-linear viscoelastic characteristics.

When polymeric material is under shear deformation, the response includes not only a shearing stress but unequal normal stresses in the direction perpendicular to the direction of flow^{48,49}. These normal stresses give rise to the stirring-rod climbing or Weissenberg normal stress effect. Generally the normal stresses are expressed in terms of the primary normal stress difference and the secondary stress difference^{29,48,49}.

The present of solid-like characteristics in viscoelastic materials give rise to elastic phenomena such as die swell, shark skin, melt fracture, frozen-in stresses and draw-downs^{29,31}. However, Metzner et.al⁵⁰ attempted to relate these elastic effects to the normal stresses developed when the material undergoes deformation.

In addition to shear flow, another important class of deformation is elongational flow. Cogswell⁵¹ showed that extensional (elongational) flow occurs whenever there is a convergence of flow lines such as an approach to the nip of two roll mill, and also between the rotor tip to the chamber wall of an internal mixer.

The elongational viscosity, like the shear viscosity may be a function of the rate of deformation. For the Newtonian fluid, however, one may established a relationship between η_0 (reference viscosity) and η_e (elongational viscosity). Viscosity is basically the ratio of stress to the rate of strain. To keep one of these quantities constant, while measuring the other is found to be difficult for extensional

experiments^{29,51,52}. For this reason, elongational viscosity is expressed in term of its total stress and not the dynamic stress

$$\eta_e = \frac{T}{\dot{\epsilon}} \quad \text{.....4.11}$$

where T - total stress (force/original X-sectional area of specimen)

$\dot{\epsilon}$ - elongational strain rate

At low strain rate, the elongational viscosity is related to the shear viscosity of Newtonian fluid by

$$\eta_e = 3 \eta_o \quad \text{.....4.12}$$

Elongational viscosity is sometimes referred to as the Trouton viscosity.

4.3.2 Viscoelasticity.

Linear viscoelastic behaviour is exhibited in material undergoing small (infinitesimal) deformation. For large (finite) deformation as encountered in polymer processing, non-linear viscoelastic behaviour develops. The dividing line between 'small' and 'large' depends of course, on the level of precision under consideration, and it varies greatly from one material to another³⁰. Linear viscoelastic theories are amenable to mathematical treatment^{30,53,54}. However, constitutive equations for non-linear viscoelasticity were later developed, though their applicability to highly filled material such as rubber compound is dubious⁵⁵.

Generally linear viscoelastic behaviour of a material is specified by constant stress (creep) or/and by the constant strain (stress relaxation) experiment, thereby measuring its compliances and moduli respectively^{29,30,56}. In addition, sinusoidal (dynamic) experiments, as described earlier are frequently used to characterize the viscoelastic properties²⁹.

In creep experiment, under constant stress the material deforms continuously with time. The ratio of the strain to the stress is known as the creep compliance. In simple shear the compliance, $J(t)$ takes the form

$$J(t) = \frac{\gamma(t)}{\tau} \quad \text{.....4.13}$$

where τ - constant stress

The creep behaviour of an uncrosslinked polymer can be shown schematically as in figure 4.8. After a sufficiently long time (but before the stress is removed at t_2), the creep strain is the sum of the deformation approaching a constant value (the response slope becomes constant) plus the viscous flow contribution^{30,56}, and expressed by

$$\gamma(t) = \tau \left(J_e + \frac{t}{\eta_N} \right) \quad \text{.....4.14}$$

where J_e - steady state compliance

η_N - Newtonian viscosity of material

Here, the steady state compliance is a measure of the elastic deformation during steady flow. Both J_e and η_N can be obtained from the geometry of a linear plot in this region. Whereas the strain recovery at time t is given by

$$\gamma_r(t) = \tau_e \left[J_e + \frac{t}{\eta_N} - J(t - t_2) \right] \quad \dots 4.15$$

The recovery approaches a final value of (t/η_N) . However, at high stress and strain rates these linear equations do not hold, and the elastic recovery is formulated in a more complicated manner^{30,56}.

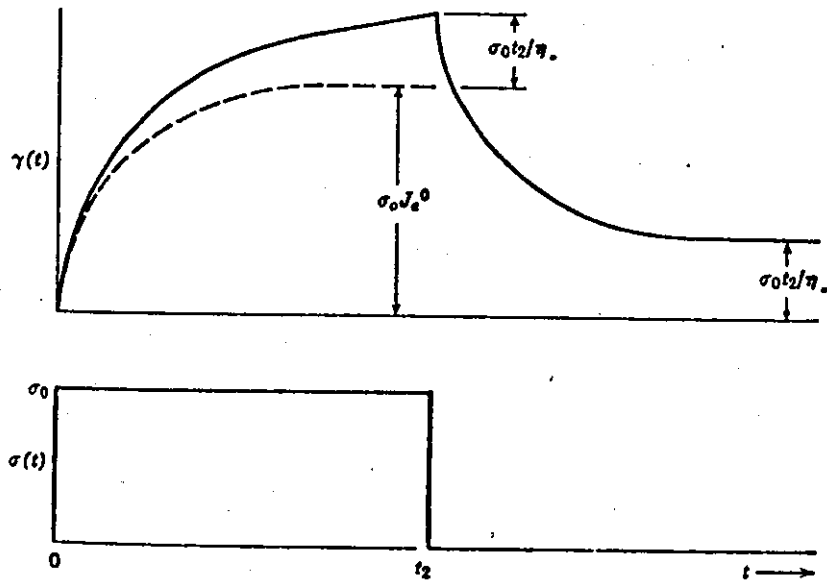


Figure 4.8 - Shear creep and creep recovery shown schematically of an uncrosslinked polymer³⁰.

Another aspect of viscoelastic behaviour is stress relaxation. When a deformation is applied and held constant, the stress gradually decays with time. Again, if the strain is small, the stress at any time t , after application of the strain γ , is proportional to the magnitude of the strain. The ratio of the stress to the strain is known as the relaxation modulus. For shear deformation, the modulus is

$$G(t) = \frac{\tau(t)}{\gamma} \quad \dots\dots\dots 4.16$$

where $G(t)$ - shear relaxation modulus
 $\tau(t)$ - shear stress at time t
 γ - constant shear strain

Figure 4.9 illustrates the relaxation modulus curve of crosslinked and uncrosslinked polymer. At long time, $G(t)$ for the crosslinked polymer approaches constant values. For uncrosslinked polymers, $G(t)$ falls rapidly and eventually vanishes. The relaxation and compliance moduli over a certain region can be equated as

$$G(t) = \frac{1}{J(t)} \quad \text{.....4.17}$$

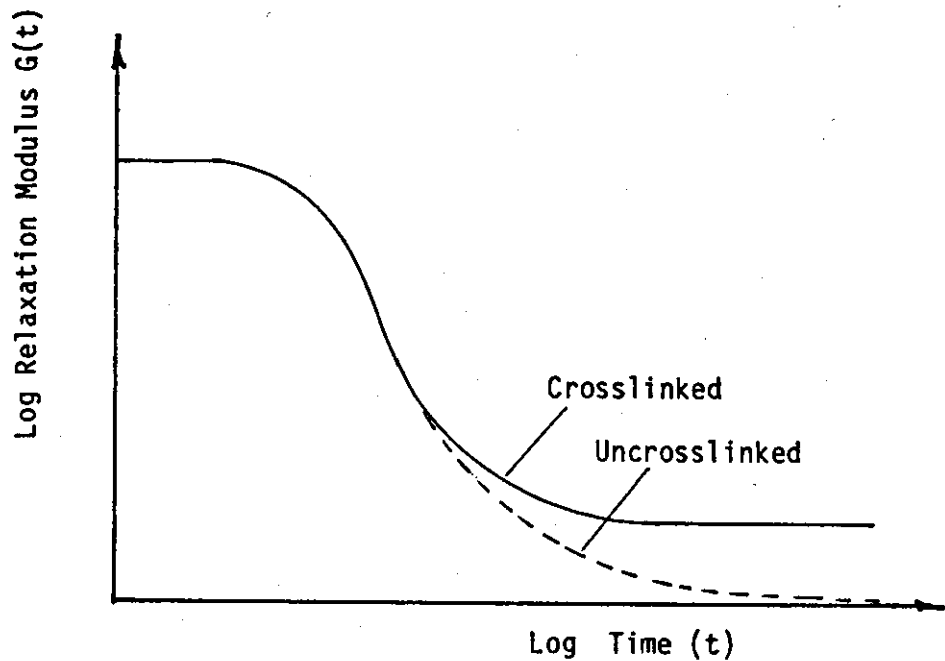


Figure 4.9 - Relaxation modulus curves of crosslinked and uncrosslinked polymer⁵¹.

Generally the superposition principle attributed to Boltzman^{30,55,56} gives a superior formulation of the mechanical behaviour in viscoelastic material. The linear constitutive equation derived from this principle is expressed as

$$\tau(t) = \int_0^t G(t-s) \frac{d\gamma}{ds} ds \quad \text{.....4.18}$$

where $\tau(t)$ - stress at time t

$G(t-s)$ - relaxation modulus integrated over all
past time s , up to the current time t

$d\gamma/ds$ - shear rate at time s

However, instead of deriving viscoelastic parameters from the constitutive equations, mechanical models are frequently used to simulate the viscoelastic phenomena^{29,30,55,56}. The simplest mechanical model analogous to a viscoelastic system is one spring combined with one dashpot.

The elastic component is represented by a Hookean spring and the viscous component by a Newtonian dashpot. When they are connected in series, a Maxwell model is obtained, whilst in parallel we get a Voigt (Kelvin) model as shown in figure 4.10 (a) and (b) respectively.

It is observed that the basic model is insufficient to describe the actual behaviour of the material. Generalized Maxwell and generalized Voigt model are used with an infinite number of the basic models connected in parallel and in series respectively. Combination of the basic Maxwell and Voigt models have been adopted, whereby dual networks were incorporated such

as the TMS model⁵⁷, in figure 4.11.

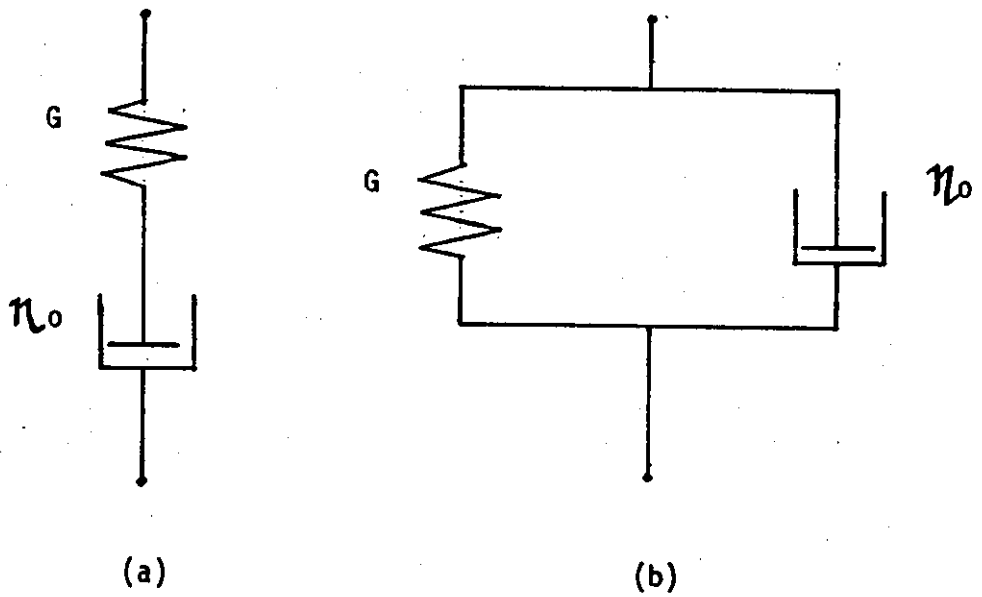


Figure 4.10 - (a) Maxwell model
 (b) Kelvin (Voigt) model

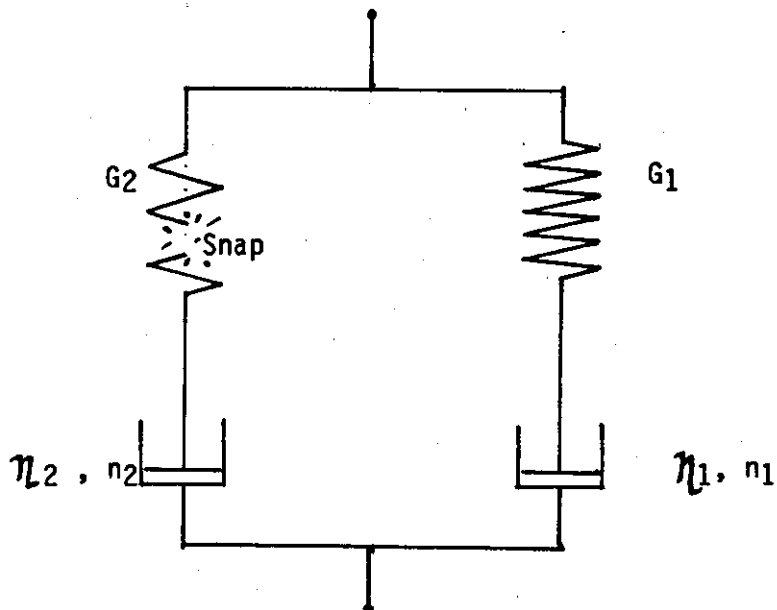


Figure 4.11 - The TMS model⁵⁷.

For the Maxwell model, the rate of deformation of a viscoelastic material under simple shear, would be the sum of rate of deformation due to the Newtonian flow and the elastic response

$$\begin{aligned}\dot{\gamma}_T &= \dot{\gamma}_D + \dot{\gamma}_S \\ &= \frac{\tau}{\eta_0} + \frac{1}{G} \frac{d\tau}{dt}\end{aligned}\quad \text{.....4.19}$$

where $\dot{\gamma}_T$ - total shear rate
 $\dot{\gamma}_D$ - shear rate in dashpot
 $\dot{\gamma}_S$ - shear rate in spring
 G - constant shear modulus

If the material is subjected to a constant strain i.e. zero shear rate, the equation 4.19 becomes

$$\frac{d\tau}{\tau} = - \frac{G}{\eta_N} \cdot dt$$

Upon integration, the solution obtained is as

$$\tau(t) = \tau_0 \exp(-t/\lambda) \quad \text{.....4.20}$$

where τ_0 - the stress at time $t = 0$
 λ - the relaxation time i.e. η/G

Dividing equation 4.20 by the constant strain γ ,

$$G(t) = G \exp(-t/\lambda) \quad \text{.....4.21}$$

The parameter λ , plays the role of a relaxation time and is therefore a measure of how rapidly stress relaxes in a Maxwellian material²⁹⁻³¹. The relaxation time is equal to the

time required for the stress to relax to $1/e$ of its initial value.

However, stress relaxation is not only given by the exponential equation above. The generalized Maxwell model^{58,59} can be used and expressed as

$$G(t) = \sum_{p=1}^N G_p \exp(-t/\lambda_p) \quad \text{.....4.22}$$

where p - number of basic Maxwell model

λ_p - discrete spectrum of relaxation time
of p models

Alternatively, if the number of elements in the Maxwell model is increased without limit, the stress relaxation behaviour can be replaced by a continuous function^{29-31,55}.

Similarly, viscoelastic behaviour can be described by the Voigt model. Under any external force the strain in the dashpot and the strain in the spring are equal. The total stress is the sum of the stress in the spring and in the dashpot

$$\begin{aligned} \tau_T &= \tau_D + \tau_S \\ &= \eta_0 \dot{\gamma} + G \dot{\gamma} \end{aligned} \quad \text{.....4.23}$$

where τ_T - total stress

τ_D - stress in dashpot

τ_S - stress in spring

From equation 4.23, if the material is subjected to constant strain the stress would remain constant, contrary to

the stress relaxation phenomena of a viscoelastic material. Furthermore, if the Voigt model is subjected to a constant stress τ , the solution of equation 4.23 is

$$\gamma(t) = \frac{\tau_0}{G} [1 - \exp(-t/\lambda)] \quad \dots\dots 4.24$$

Dividing equation 4.24 by the constant stress

$$J(t) = J_0 [1 - \exp(-t/\lambda)] \quad \dots\dots 4.25$$

The parameter $(\tau_0/G) = \lambda$, is defined as the retardation time which is significant in creep recovery experiments. The strain decay after the removal of stress follows an exponential relation with time. The retardation time λ , becomes the time required for the strain to fall to $1/e$ of its original value. For a group of Voigt elements in series, a spectrum of compliance and retardation time can be expressed as

$$J(t) = \sum_{p=1}^N J_p [1 - \exp(-t/\lambda_p)] \quad \dots\dots 4.26$$

Consequently by mathematical treatment, a continuous spectrum of retardation times can be derived^{29,30,59}.

It should be kept in mind that these models give a description of the phenomenological behaviour of a material and in general tell nothing of the detailed mechanisms that underlie the viscoelastic behaviour. Mechanical models do not necessarily imply anything concerning the molecular mechanism responsible for the observed viscoelastic behaviours⁵⁹.

4.3.3 Temperature Dependence.

It is well known that temperature has an important effect on the rheological properties of polymers^{30,39}. The variation of viscosities with temperature is a problem of major importance in polymer processing. Frequently, the Arrhenius equation is used to relate viscosity with temperature, which was previously mentioned in chapter 1.0 (section 1.3.1).

$$\eta = A \exp (E / RT) \quad \text{.....4.27}$$

Another empirical equation relating viscosity and temperature is

$$\eta = a \exp (- b T) \quad \text{.....4.28}$$

where a and b are derived constants.

A plot of $\log \eta$ against $1/T$ as shown in figure 4.12 for equation 4.27 or $\log \eta$ against T for equation 4.28 will show the temperature dependence of the polymer viscosity at a constant shear rate. Palmgren⁶⁰ observed that a transformation point occurs within a temperature range of 50.0 to 100.0° C, whereby a steeper slope at lower temperature changes to gradual slope at this point as temperature increases.

McKelvey³⁹ characterized the viscosity-temperature variation by the number of degrees that the temperature of the polymer must be raised at constant shear rate in order to decrease the viscosity by the factor $1/e$.

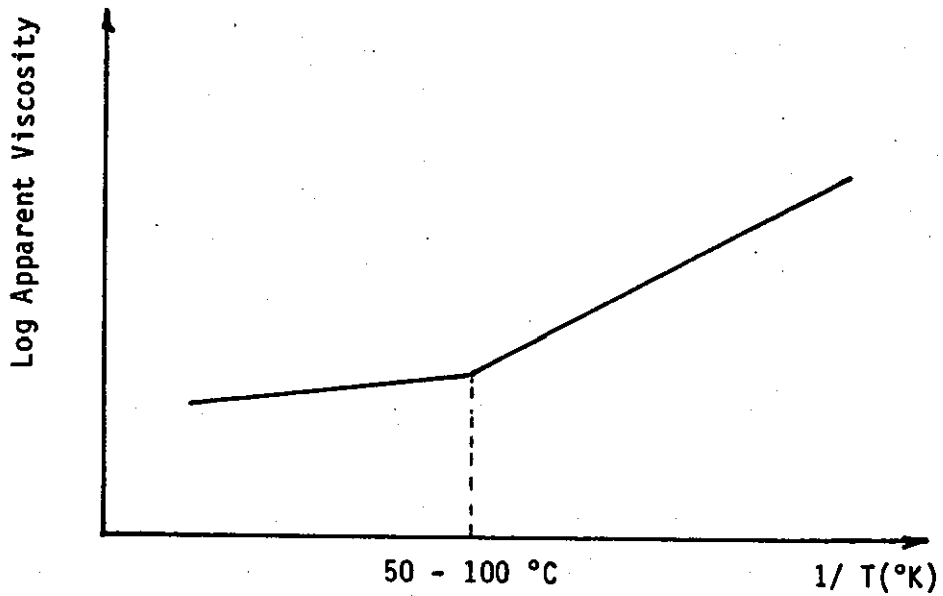


Figure 4.12 - Typical apparent viscosity-temperature curve⁶⁰.

As in the case for non-Newtonian fluid, the viscosity is a function of the state of shear (i.e. shear rate and shear stress) as well as a function of temperature³⁹. This is expressed by the functional equations

$$\eta = \eta (\tau, T) \quad \text{.....4.29}$$

$$\eta = \eta (\dot{\gamma}, T) \quad \text{.....4.30}$$

Therefore the variation of viscosity with temperature can be expressed whether at constant shear stress or constant shear rate. Bestul and Belcher⁶⁰ reported that for pseudoplastic fluids

$$\left(\frac{d\eta}{dT} \right)_{\tau} > \left(\frac{d\eta}{dT} \right)_{\dot{\gamma}} \quad \text{.....4.31}$$

Similarly, activation energy derived at constant stress is

different from that derived from constant strain. However, for Newtonian fluids the activation energies are equal for both conditions³⁹. Philippoff and Gaskins⁶¹ derived the activation energy of polythylene at constant shear stress and constant shear rate. White and Tokita⁶² computed the energy for SBR, polyisobutylene and NR at constant shear rate. In addition, Zahrenko⁶³ evaluated the influence of carbon black concentration on the constant shear rate activation energy. Constant shear rate activation energy is preferred because it measures viscosity under constant kinematic conditions and is thus most readily interpretable in terms of processing operations, and furthermore it is most adaptable into constitutive equations³⁹.

4.3.4 Rheological Measurements.

Though the industrial manufacture of rubber products dated to the third decade of the nineteenth century, it was not until the 1920's that rheological instruments were used to quantify the processability of uncured rubber⁶⁴. Extrusion⁶⁴ and compression⁶⁵ rheometers were initially developed followed by rotational instruments introduced by Mooney and others^{66,67}. These basic types of instruments remain today as the important methods of rheological analysis of filled and unfilled rubbers⁴⁰. However, each type of instrument has a different mode of deformation, and its potentiality depends on its capability, to measure linear and non-linear viscoelastic behaviours of rubber over a range of times, strains, strain rates and temperatures.

Extrusion or capillary rheometers are widely used in determining the rheological characteristics of polymers at high

rates of deformation⁶⁹⁻⁷¹. The amount of pressure drop across the die, and the extrusion rate are correlated with the shear stress and shear rate at the capillary wall respectively (refer to figure 4.13)

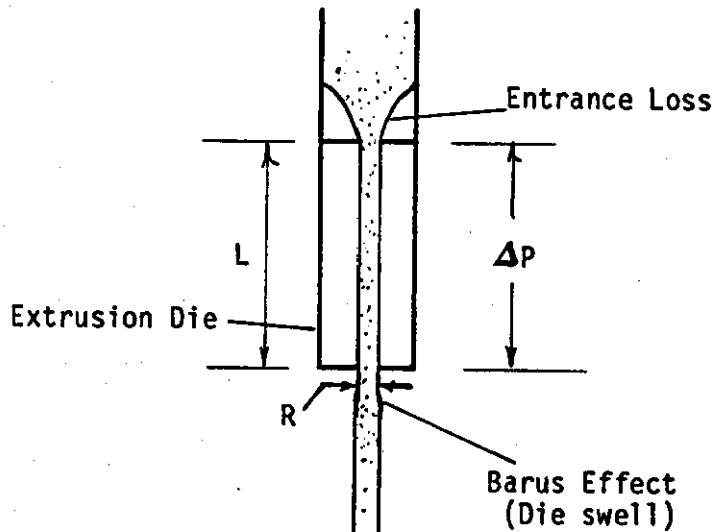


Figure 4.13 - Schematic diagram of capillary rheometer³¹.

The shear rate has been derived and known as Rabinowitsch equation takes the form

$$\dot{\gamma}_w = \left(\frac{3n' + 1}{4n'} \right) \frac{4Q}{\pi R^3} \quad \text{.....4.32}$$

where

$$n' = \frac{d \log (R \Delta P / 2L)}{d \log (4Q / \pi R^3)}$$

R - radius of die

Q - extrusion rate

ΔP - pressure drop across die

$\dot{\gamma}_w$ - shear rate at wall

L - length of die

In most cases the pressure drop is taken as between the pressure in the barrel and the atmospheric pressure. This ignores the effect of viscous and elastic deformations at the entrance and exit of the capillary. The large pressure losses due to this effect were reported by Mooney and Black⁷¹. Bagley⁷² proposed a correction factor for the deviation and established the true shear stress at the capillary wall by

$$\tau_{tw} = \frac{R \Delta P}{2 (L + eR)} \quad \text{.....4.33}$$

where τ_{tw} - true shear stress at wall

e - Bagley correction factor

Hence the true apparent viscosity is then given by

$$\eta_a = \tau_{tw} / \dot{\gamma}_w \quad \text{.....4.34}$$

The elastic properties of the material are indicated by the extrudate dimensions. Die swell or extrusion shrinkage which is the ratio of cross sectional area of the extrudate to that of the capillary, indicates the extent of the elastic behaviours. Significant studies by Cotten⁷³⁻⁷⁴ gave a better understanding of die swell phenomenon, which is related to molecular orientation and entanglement network of the elastomer.

During the past decade, sophisticated electronic, microcomputer and laser technology has been incorporated into the capillary rheometers such as the Monsanto Processability Tester⁷⁵ making them useful both for research and process problem solving. Obviously moving into automation of this

instruments will eliminate operator errors, giving reliable and reproducible results, leading to a better understanding of material behaviour.

In compression instruments, a cylindrical test piece is compressed axially between two plates or discs. Under constant compressive force and time the plasticity number of unvulcanized rubber is determined, represented by the thickness of the sample at this fixed condition⁷⁶. Alternatively, in the Deformeter test⁷⁷, the force required to compress the sample to a given thickness in a given time is measured. However, both are arbitrary figures and the compression produced by a fixed force is as good as the force for a fixed compression³.

The same principle is applied in measuring the oxidative resistance or breakdown of natural rubber⁷⁸, expressed by the plasticity retention index (PRI). The viscosity before and after ageing of the sample at 140°C is measured using the Wallace Rapid Plastimeter, and the retention index is calculated by

$$\text{Plasticity retention index} = \frac{\text{Viscosity after ageing}}{\text{Viscosity before ageing}} \times 100 \quad \dots 4.35$$

A high value of the index denotes a rubber of high resistance to oxidation and a guide to the degree of breakdown during mastication and mixing. The Wallace Rapid Plastimeter is noted for its simplicity and rapidity of measurement and the convenience of the constant volume sample preparation.

Scott⁷⁹ derived empirical equations to explain the flow characteristics under compressive forces. But due to its complexity, the theoretical equations are usually ignored. Only the height of samples and compressive forces at a given time are considered.

Recently, by adopting the same basic principle of compression plastimeter, stress relaxation parameters can be determined⁸¹. The Stress Relaxation Processability Tester (SRPT) as shown in figure 4.14 was developed by RAPRA (Rubber and Plastics Research Association) is capable of monitoring the stress decay in the compound. Leblanc⁸⁰ describes the relaxation behaviour by a power law function as expressed by

$$P = K t^{-a} \quad \text{.....4.36}$$

where

- P - decaying pressure
- K - stiffness of the material taken at $t = 1$
- t - the time
- a - relaxation rate

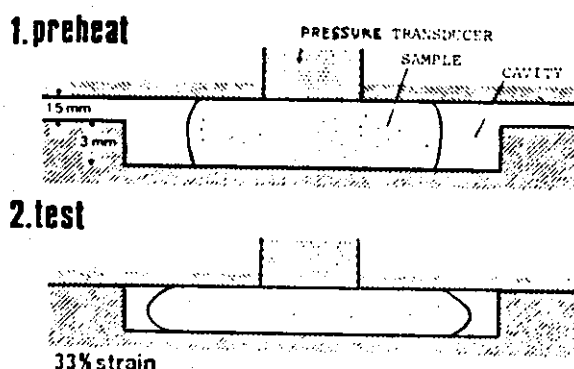


Figure 4.14 - The RAPRA Stress relaxation processability tester⁸⁰.

The parameter 'K' correlates well with Mooney viscosity ML (1 + 4). The relaxation rate 'a' characterizes the viscoelastic behaviour of rubber and consequently is a combination of its viscous and elastic responses. As 'a' tends

to zero the relaxation becomes slower and the viscosity increases.

A point to mention is that most compressive plastimeters work at low shear rate of less than 1 s^{-1} , which is well away below the processing shear rate of well above 100 s^{-1} as encountered in rubber mixing.

Extensional rheometers can either be of the constant stress or constant strain rate types. Meissner⁸², Stevenson⁸³, Vinogradov and co-workers⁸⁴ and White¹ adopted the constant strain rheometer to investigate the extensional viscosity of polyethylene and polyisobutylene. Cotten and Thiele⁵² investigated the flow of SBR with the same type of rheometer as in figure 4.15. Constant stress extensional rheometers have been described by Cogwell⁵¹ and Vinogradov et.al⁸⁴ for polyethylene and polystyrene.

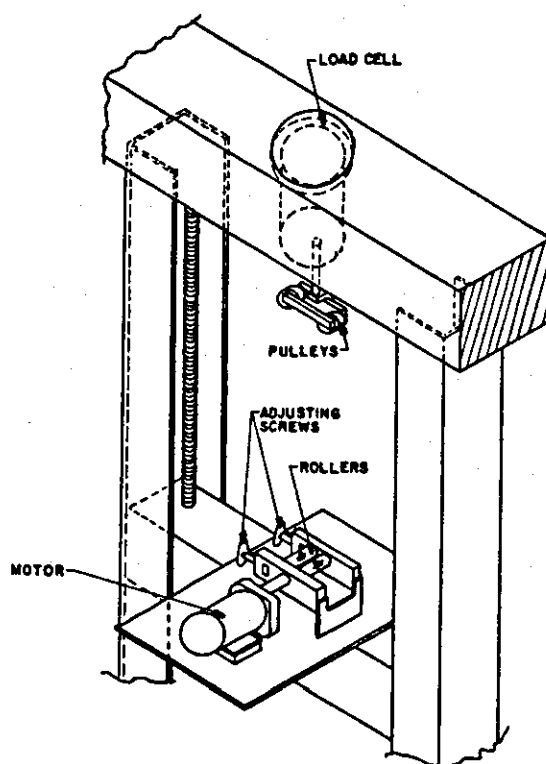


Figure 4.15 - Schematic diagram of extensional rheometer⁵².

The extensional viscosity of polymer may increase or decrease as stress is increased and the factors determining this behaviour have yet to be understood. Both stress relaxation and recovery behaviour has been investigated by use of extensional rheometers⁸⁴.

One reason for the apparent neglect of study in extensional flow is particularly due to the absence of cheap and simple apparatus for measurement of extensional viscosity, compared to shear viscosity. Furthermore other experimental difficulties arise, which have been acknowledged by Cogswell⁵¹.

For rheological characterization of steady state simple shear flow, parallel plate rheometer is most ideal⁸⁵. Unfortunately, problems of leakage, end effects and low shear rates have impaired the usefulness of this viscometric geometry.

Rotational instruments have been developed to resemble closely the flow pattern which exists in the ideal parallel-plate rheometers. Three basic simple shear flow geometries have been found to be practical for rotational rheometers: i) tangential flow between concentric cylinders, ii) tangential flow between co-axial cones having common vortex or between cone and plate, and iii) tangential flow between parallel disks.

Co-axial cylinder or Couette viscometers are widely used for low viscosity fluids^{61,86}, such as emulsions and suspensions. The material is sheared between the concentric cylinders as shown in figure 4.16 (a). However, Mooney⁶⁶ used such instrument to obtain a quantitative rheological data on raw

rubber. Krienger⁸⁷ showed that a co-axial viscometer can give the true shear rate and shear stress values of power law fluids, whereby the viscosity-shear rate relationship can be established. The phenomenon of stress overshoot has been investigated using the co-axial cylinder viscometer⁸⁸.

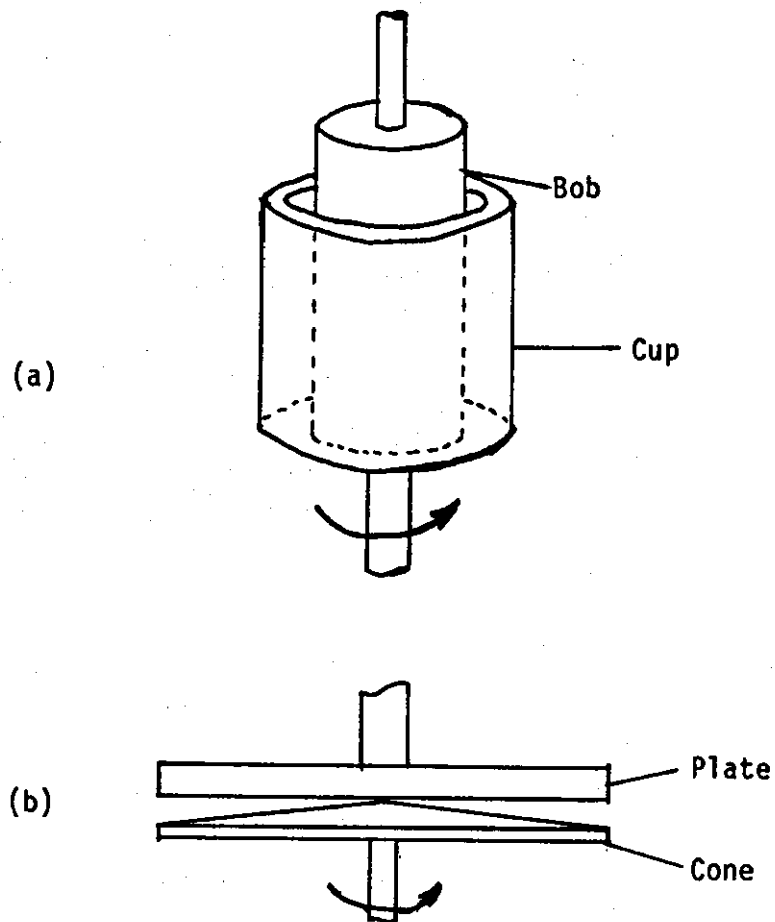


Figure 4.16 - Schematic diagram of a) co-axial cylinder rheometer, b) cone and plate rheometer.

Initially the development of cone and plate rheometer was to eliminate the edge effect observed in the Coutte viscometer⁸⁹. However, it's geometry as shown in figure 4.16 (b) has made it suitable for normal stress measurement³⁸. Both the

Weissenberg rheogoniometer and Mechanical Spectrometer are cone and plate instruments, and they are widely used to determine both the viscosity and normal stresses for polymer solutions and melts but not for rubber. The great advantage of this instrument is that for small cone angles, the shear rate is constant throughout the gap between the cone and the plate. Piper and Scott⁶⁷ adopted this principle to the biconical rotor viscometer which is suitable for rubber.

Of the various types of rotational instruments introduced, the most popular at present is the Mooney shearing disc viscometer³⁷. It has been widely used for measuring the processability of rubber and rubber compounds for control of factory processing. The Mooney viscosity, or viscosity in Mooney units is defined as the torque required to rotate the disc at two revolution per minute (average shear rate about 1.6 s^{-1}) at a fixed temperature usually 100.0°C . The misapplication of the term Mooney viscosity for torque has become standardized and well accepted⁹².

The material is sheared in a cylindrical cavity by a knurled disc rotor as shown in figure 4.17. The Mooney viscosity is commonly specified as ML 1 + 4 (100°C), indicating the testing condition and type of rotor used. However, over the years, several improvements have been made on the basic Mooney viscometer. Controls and instrumentation are incorporated to allow for multispeed^{47,61} operation and elastic recovery measurement⁴⁰.

The thixotropic effect⁴⁷ and the viscosity over a wide range of shear rate is essential as compared to the single point

Mooney value. Multispeed Mooney viscometer has been used to study the slip behaviour of rubber^{71,90}.

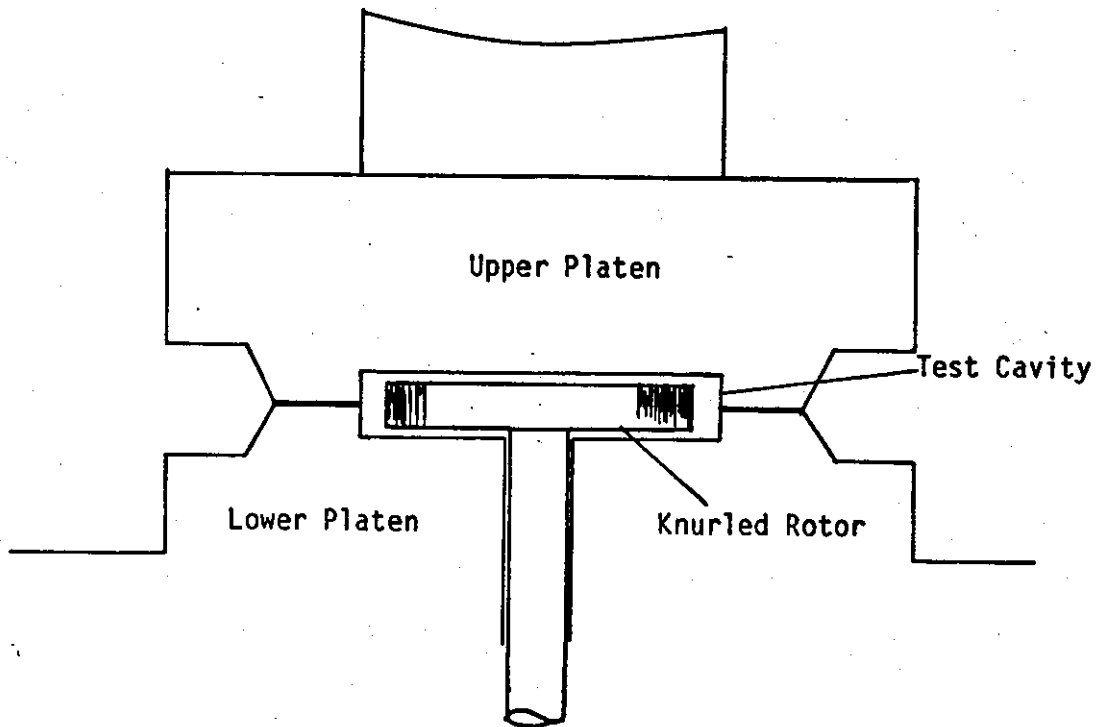


Figure 4.17 - Schematic diagram of Mooney viscometer⁴⁰.

To make headway in rotational rheometry, Piper and Scott⁶⁷ developed the variable speed shearing cone instrument which differed mainly in rotor configuration as compared to Mooney viscometer. The biconical rotor shape, as shown in figure 4.18, has the advantage of producing uniform shear rate over the rotor surface.

In this study, a shearing cone viscometer basically similar to the Piper and Scott⁶⁷ instrument is used. It is known as the TMS rheometer and will be described in chapter 7 (section 7.1)

Instrumented miniature internal mixer or the torque

rheometer can be used as processability testers. The amount of work input to the machine may be used with some success to assess the state of mixedness during a mix cycle^{4,9}. In addition dispersion ratings on the response chart indicate the dispersibility of carbon black in the polymer⁹². Torque rheometers, such as Brabender Plastograph have been used extensively for processability testing⁹³ and for rubber mixing studies⁴. High shear rates of up to 300 s^{-1} can be obtained from a torque rheometer⁹⁴. However, it does not measure rational rheological parameters, chiefly because the rubber is not deformed at any one shear rate but at a spectrum of shear rates³.

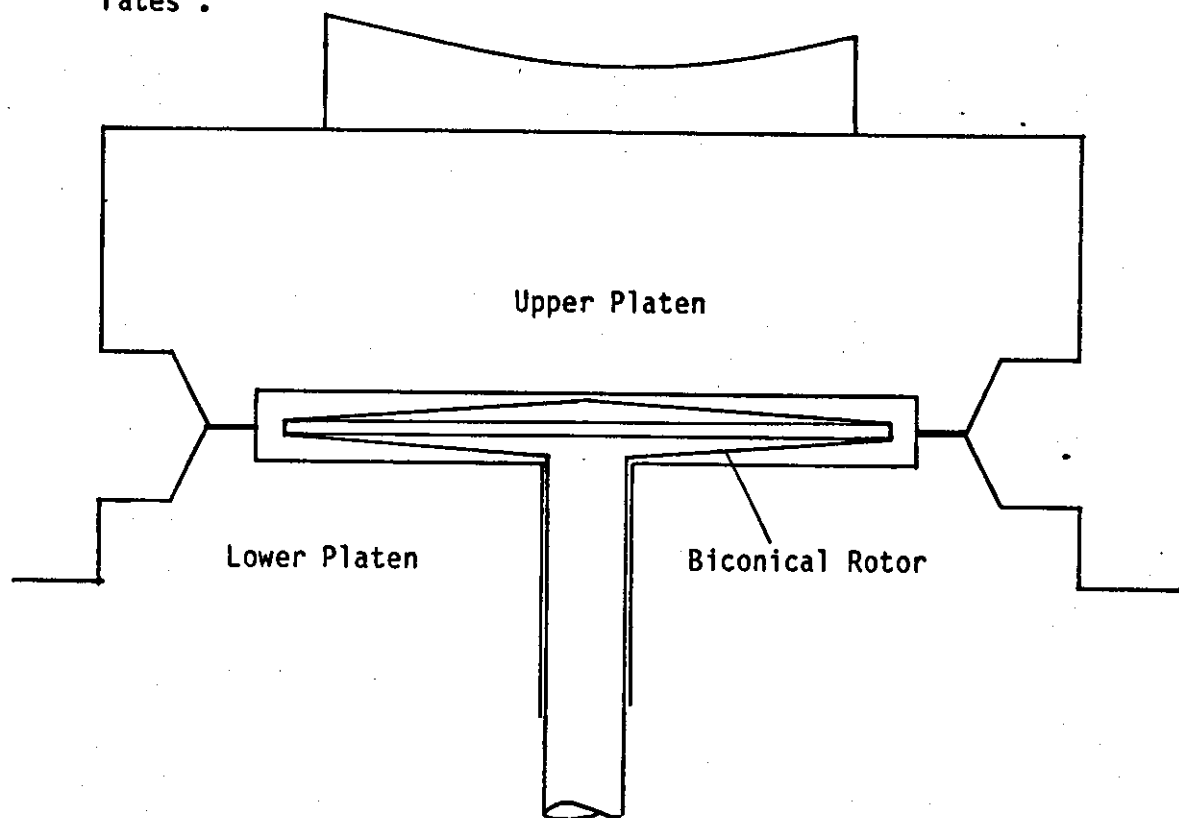


Figure 4.18 - Schematic diagram of biconical rotor rheometer⁶⁷.

4.4 Carbon Black Dispersion.

4.4.1 Introduction.

The method of assessing carbon black dispersion in rubber compounds may be broadly classified into two categories; i) those which employ direct visual or microscopical observation, or the mechanical surface analyses technique and ii) the indirect methods, whereby compounds' properties which are closely related to dispersion are measured. The first category includes the analyses of surfaces prepared by tearing, cutting and polishing, as well as the examination of thin sections by means of light or electron microscopy. Carbon black dispersion is indirectly related to the rubber vulcanizate properties as mentioned in section 4.2. Dispersion is also related to the electrical conductivity of the compound¹⁰¹. However, changes in these properties should not be totally relied on as an indication to the changes in dispersion¹⁰⁴.

The fact that carbon black rubber composite (whether vulcanizate or unvulcanize), when cut leaves a surface indicating the nature of filler dispersion in the polymer has been known for some time⁹². Carbon black agglomerates deflect the cut path, because of their hardness relative to the surrounding matrix. Thus, good dispersion gives a smooth surface texture whilst badly dispersed compound is rougher.

The roughness of a cut surface can be determined mechanically by a stylus type device, tracking across the sample surface. This method is widely used for surface roughness measurement in other industrial applications. However, Vegravi and co-workers^{95,96}, and recently Ebell⁸ adopted the same principle to assess carbon black dispersion in rubber compounds.

They used the mean peak heights and the frequency of peaks as the parameters, to characterize the surface roughness of the compounds. The frequency and size of the roughness peaks decrease as carbon black dispersion improves. Ebell⁸ showed that an exponential decrease in the mean peak heights occurs with mixing time, levelling off after 2.5 minutes mixing.

This method offers great versatility and is applicable to both vulcanized and unvulcanized rubber samples. In addition it is not limited to carbon black application alone. Nevertheless, since this technique does not involve visual examination at all, artefacts such as blade marks and air bubbles may be erroneously be included in the analysis⁸.

Carbon black dispersion can be evaluated directly by means of light and electron microscopes. Both of which can either be in the form of incident or transmitted illumination. Rubber is sufficiently opaque to both light and electrons, that only thin sections can be studied with transmitted illumination¹⁰⁴. Alternatively surface examination of thick specimens can be useful but it will not reveal the interior of the specimens. Moreover, carbon black and rubber mixtures give a fairly high contrast system, which is favourable to microscopical examinations.

The high magnification of electron microscopy is rarely necessary for carbon black dispersion analysis. Such fine scale has been found to have little effect on rubber properties¹⁰³. Moreover, with small field of vision the results obtained may be statistically misleading⁸. In addition, to prepare an extremely thin sample of 100 Å is found difficult for the transmitted

electron microscopy (TEM)¹⁰⁵. Sweitzer et.al¹⁰⁶ have used this method to evaluate black dispersion in SBR compounds.

On the other hand scanning electron microscopy (SEM) utilizes the reflected electrons from the surface of a specimen to produce a topographical image¹⁰⁷. SEM operates at a much lower voltage (1.0 - 20.0 kV) than the transmitted electron microscopy (10.0 - 1000.0 kV). Recently Ebell⁸ used scanning electron microscope to compare the topography of rubber compound surfaces. He observed that the smoothness of the surface increases as mixing progresses. Ebell⁸ utilized this method to substantiate his findings on carbon black dispersion as determined by dark field reflected light microscopy, which will be discussed later. Generally electron microscopy frequently resolves the differences in dispersion when other methods fail to provide the ultimate answer^{104,106}.

Although light microscopy shows dispersion on a much coarser scale, the conclusions it lead to are more useful and reliable. Furthermore, the techniques employed are simpler and easier. A larger field of view can be studied and the variation between such fields is smaller. On the other hand numerical estimates of dispersion can be made^{8,100,104,106,108}.

In this study the dispersion levels of carbon black in rubber mixes are determined by means of a light microscopy technique. Consequently a short review on this subject is deemed necessary.

4.4.2 Transmitted Light Microscopy.

Assessment of carbon black dispersion by transmitted light microscopy was initially performed by Tidmus and Parkinson¹⁰⁹. This method was originally proposed for qualitative estimation of the degree of dispersion. However, a quantitative calculation was subsequently developed by Leigh-Dugmore^{100,104}, whereby the percentage of carbon black dispersed was calculated.

As mentioned earlier, observation by transmitted light microscopy requires thin samples of about 2 μm . This is frequently done by using a microtome equipped either with a steel or glass knife¹⁰⁴. Before a thin section can be cut from a piece of rubber, the whole piece must be frozen by either liquid nitrogen or liquid carbon dioxide^{97,104}. Stretching or squeezing methods do not produce samples that are thin enough. Furthermore they are liable to be distorted and uneven in thickness.

The thin sections are examined by transmitted light microscope with magnification of about 70 to 100 X. A micrometer containing a graticules of squares each of 10 μm or 13 μm sides^{97,100}, is contained in the eye piece of the microscope. The total number of graticule squares that are at least half filled with carbon black are to be counted for the estimation of percentage dispersion. The percentage of carbon black that has been dispersed below 5 μm or 6.5 μm ^{97,100} agglomerate size is expressed by

$$\text{Dispersion (\%)} = 100.0 - \frac{u \cdot s}{L} \quad \text{.....4.37}$$

(D)

where u - Average of 5 graticule counts on the section containing at least half filled with carbon black.

s - Area swelling factor from the action of the solvent to uncurl the section. (or the ratio of the section area after swell to area before swelling)

L - volume percentage of black in compound

Note:
$$L = \frac{\text{Density of compound} \times \text{wt of black}}{\text{Density of black} \times \text{wt. of compound}} \times 100 \quad \dots 4.38$$

For badly dispersed compound, dispersion values of less than zero are obtained from the above equation. Equation 4.37 tacitly assumes that the agglomerates as well as the individual particles of blacks are compounds of solid carbon¹⁰⁰. This assumption is non-tenable, and one should arrive at the total volume of carbon blacks present in the agglomerates, rather than just the total volume of the agglomerates, to arrive at the fraction of undispersed black when division by L is effected.

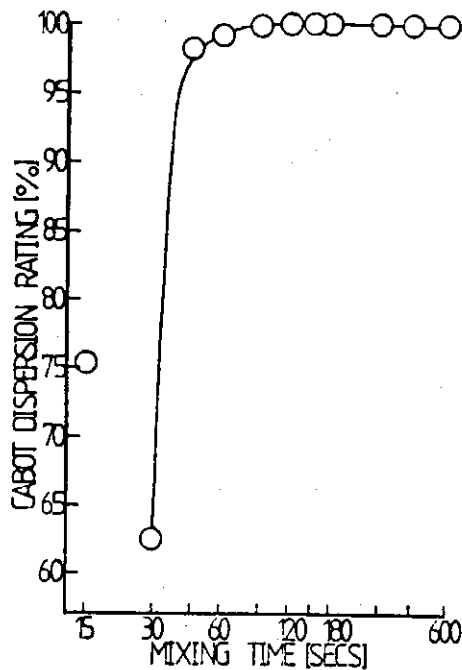
Medalia¹⁰⁸ assumed that the volume of black in the agglomerates is equal to 0.4 times the volume of the agglomerates. However, this value is not known with any accuracy and may be different in different stocks. There is no satisfactory method presently available for determining the precise amount of carbon black in each agglomerate^{99,108}. Consequently, Medalia¹⁰⁸ proposed the dispersion rating to be calculated as

$$D = 100 - \frac{v u s}{A L} \quad \dots 4.39$$

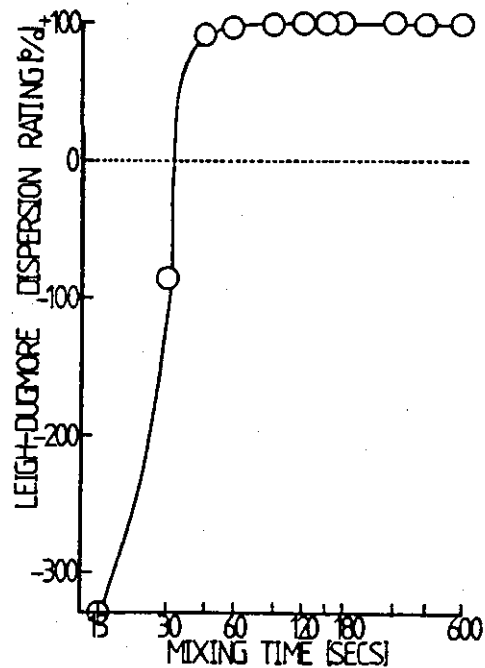
where v - volume fraction of carbon in agglomerates
A - areal swelling factor of agglomerates

Thus if $A = s$, the equation simplifies further. The equation still yields negative values for extremely badly dispersed compound, but the improvement is considerable^{8,108}. Carbon black dispersion determined by Medalia¹⁰⁸ is commonly known as the Cabot dispersion method.

Ebell⁸ in his mixing study used both the dispersion ratings. Figures 4.19 (a) and 4.19 (b) show the variation of dispersion with mixing time of SBR compound.



(a)



(b)

Figure 4.19 - (a) Cabot dispersion rating
(b) Leigh-Dugmore dispersion rating⁸.

As an alternative to the counting method, Medalia¹¹⁰ suggested the use of a classification chart to estimate dispersion ratings in transmitted light. Forty two comparators were developed, each of which bear a letter and number rating. The number rating (1 - 6), refers to agglomerate sizes whilst the letter rating (A - H), refers to the state of the dispersed black. Thus A1 would be an excellent dispersion while H6 would be very poor. Again, subjectivity enters the assessment especially when the sample being viewed consists of a different volume loading of black to that used in the standard.

4.4.3 Reflected Light Microscopy.

Carbon black dispersion is determined commonly by visual inspection of the cut or torn surfaces using a low power bright field reflected light microscope, or simply by means of a hand lens⁹⁷. The level of dispersion is obtained by comparing the images with photographic standards, which are rated numerically from very low to high degree of dispersion^{92,97}. However, Persson⁹⁸ has improved the photographic version of the cut surface test by means of a split field microscopy. With this method, the actual cut surface of a sample can be compared simultaneously to the photographic transparencies of the standards.

The reflected light technique is popular mainly because of quick and simple sample preparation, but it still remains very subjective, since it is based on the use of photographic comparators.

Recently Ebell and Hemsley^{8,99} developed a new method of

estimating carbon black dispersion in rubber. They employed the principle of dark field reflected light microscopy (DFRLM).

The DFRLM method will be adopted in this study for carbon black dispersion analyses. A short introduction of the subject will be described in this section, whilst further discussion will be dealt later in chapter 8.

Briefly, dark field microscopy uses a hollow cone of light rather than the usual solid cone to illuminate the sample. In reflected light, the hollow beam of light is produced by a stop situated in front of the illuminating source. This beam of light is diverted onto the sample by a system of reflective mirrors, such that it does not pass through the objective lens as shown in figure 4.20. On reflection from the sample, the non-diffracted light is returned outside the objective lens. The diffracted fraction passes through the objective and is admitted into the optical system, where an image is perceived at the eyepiece.

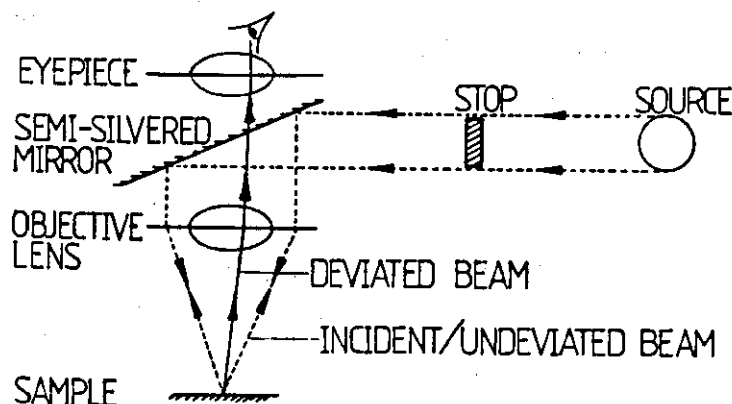


Figure 4.20 - Schematic representation of the principle of dark field reflected light microscopy⁸.

Irregular surfaces such as steps, hollows or craters act as diffracting centres for the incident light beams. A schematic diagram of such observation is illustrated in figure 4.21. No diffraction occurs from a flat area such as A, but the impingement of the incident beam at the idealized step caused its deviation and reflection, this being perceived by the DFRLM system. The intensity of the diffracted lights is proportional to the depth of the steps, which is an important criterion for surface characteristics.

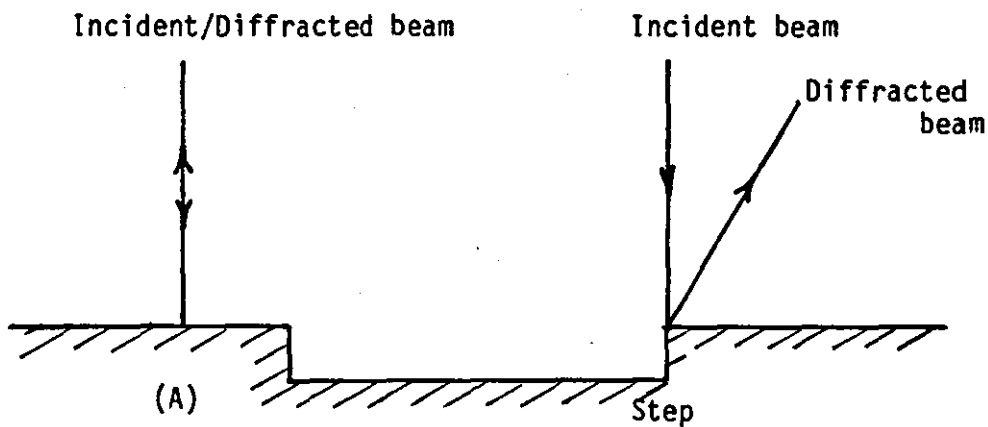


Figure 4.21 - Schematic diagram showing diffraction of an incident beam from a flat surface and step⁸.

The image obtained from the DFRL microscope is viewed on a monitor via a television camera system. A microcomputer is linked to the monitor which enables each line of the T.V. signal to be scanned and stored in the memory. A trace of each line can be obtained from a printer output, or viewed on another monitor interfaced with the microcomputer. Figure 4.22 illustrates typical trace of a compound surface.



No. of peaks (n) - 36
Mean height (\bar{h}) - 46
Std. deviation (SD) - 11.8

Figure 4.22 - A typical trace of compound surface.

The choice of parameters to characterize the traces were the mean peak height (\bar{h}), standard deviation of peak height (SD), and the number of peaks (n). For badly dispersed samples, larger peaky surfaces were observed and they should have high mean peak height. High standard deviation values were also noted for badly dispersed surfaces. The SD values measure the variability of roughness of the surface about the mean height.

As dispersion improves, aggregate sizes fall, creating more diffracting centres and consequently more peaks. Figure 4.23 illustrates the standard deviation versus mixing time for SBR compounds mixed under specified condition, where it levels off after about 2.5 minutes of mixing. In addition, Ebell⁸ utilized an empirical composite parameter C , which is a combination of the surface characteristics and expressed by

$$C = \frac{n \times \bar{h} \times S}{T \times 100} \quad \dots\dots\dots 4.40$$

where n - number of peaks
 \bar{h} - mean peak height
 S - standard deviation of peak height
 T - threshold

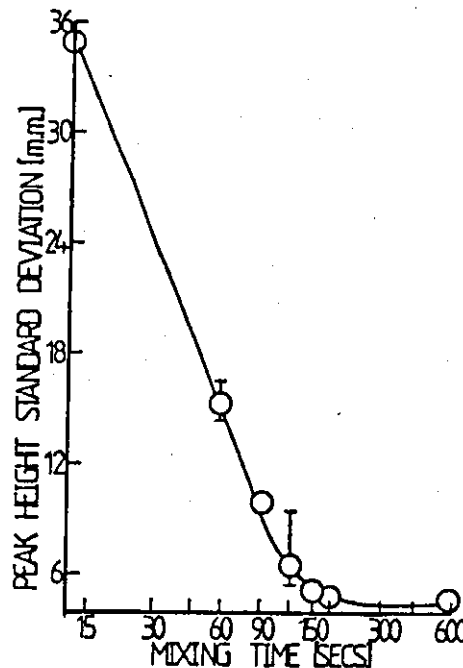


Figure 4.23 - Graph of standard deviation of peak heights against mixing time⁸.

Ebell⁸ observed that for SBR compound the composite parameter C decreases exponentially up to 2.5 minutes mixing after which it levels off, as shown in figure 4.24. However, for similar compound, the optimum mixing time derived by Leigh-Dugmore/Cabot method is at 1.5 minutes as illustrated earlier in figures 4.19 (a) and (b). On the other hand, Ebell⁸ noted that physical and processing properties measured were improving even after 1.5 minutes mixing, which is in agreement

with the optimum times indicated by the parameter C, and the standard deviation values.

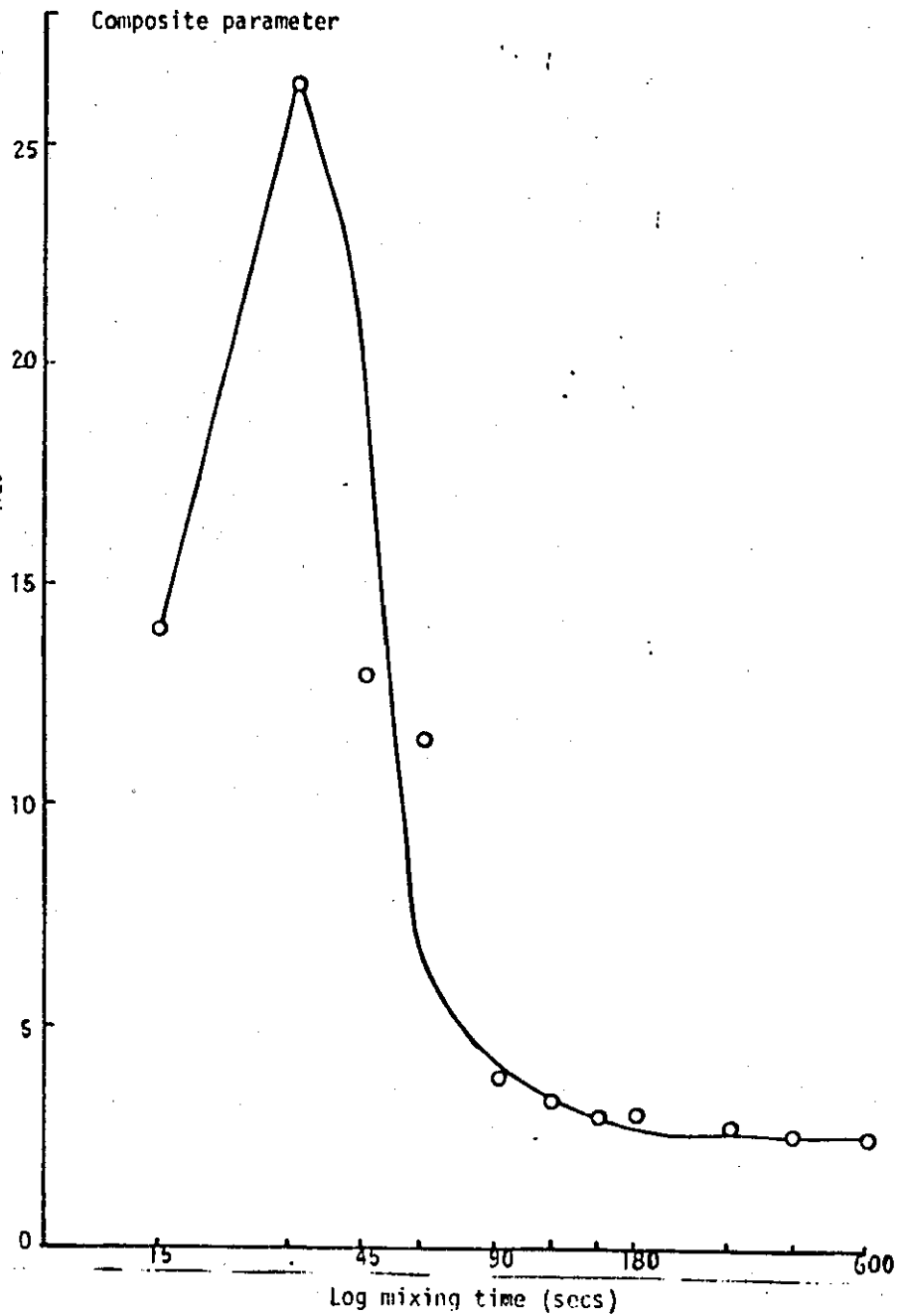


Figure 4.24 - Composite parameter vs mixing time⁸.

Hence the dark field reflected light microscopy was found to be effective and discriminating method for determining dispersion of carbon black over a wide range of dispersion level⁸. The counting method of Leigh-Dugmore/Cabot method is effective only for carbon black aggregates of size between 50 - 85 μm ^{97,100}. However, microdispersion exists during mixing, whereby further reduction in aggregate size occurs, which cannot be detected by the counting method. In addition sample preparation in DFRLM is rapid and it can also be used for unvulcanized compound. Recently, a photometric system was incorporated into the dark field microscope, whereby the dispersion level of carbon black can be determined. The photometric method will be discussed in chapter 8.

Another method for measuring black dispersion is by automated image analysis (AMEDA)¹⁰². For reflected light observation, Kadunce¹⁰² employed polished mirror like specimens. Thin sections may be used in the AMEDA system for transmitted light illumination. Long specimen preparation time of about 20 hours is required. However, there are limited informations on this method, where the references gave no correlation with rubber compound properties.

Literature Cited

(Chapter 4)

1. J.L. White, Rubb.Chem.Tech., 50,163(1977)
2. R.H. Norman and P.S. Johnson, Rubb.Chem.Tech., 54,493(1981)
3. C.M. Blow and C. Hepburn, 'Rubber Technology and Manufacture'
Butterworth Group, England (1977)
4. M.L. Studebaker and J.R. Beatty, Rubb. Age, 21, May (1976)
5. P.T. Dolezal and P.S. Johnson, Rubb.Chem.Tech., 53,252(1980)
6. B.B. Boonstra and A.I. Medalia, Rubb.Chem.Tech., 35,115(1963)
7. W.Y. Wan Idris, Ph.D Thesis Loughborough University (1978)
8. P.C. Ebell, Ph.D Thesis Loughborough University (1981)
9. E.S. Dizon and L.A. Papazian, Rubb.Chem Tech., 50,765(1977)
10. I. Drogin et.al, Rubber Age, 707, February (1954)
11. C.L. Baker, NR Technology, 8,24 (1977)
12. G.S. Williamson, M.Sc Thesis Loughborough University (1980)
13. ASTM 624 ; BS 903, Pt.A3 (1956)
14. E.M. Dannenberg, Ind.Eng.Chem., 40,2199(1948)
15. W.M. Hess et.al, Elastomerics, 24,January(1980)
16. G. Kraus, 'Science and Technology of Rubber', Chp. 8
Academic Press, New York (1978)
17. NR Technology, 4,41(1973)
18. S.D. Gehman. Rubb.Chem.Tech., 30,1202(1957)
19. A.I. Medalia, Rubb.Chem.Tech., 51,437(1978)
20. BS 903 Pt A10 and A11 ; D813
21. NR Technology, 4,42(1973)
22. A.R. Payne and R.E. Whittaker, Rubb.Chem.Tech., 44,2(1971)
23. A.I. Medalia, 'Elastomers-Criteria for Engineering Design'
Chp 15, Eds. C.Hepburn and C.W. Reynolds,App.Sci.(1979)
24. L.R. Barker et.al, J. I.R.I., 1,206 (1967)
25. A.R. Payne, Rubb.Plast. Age, 963, August (1961)
26. A.I. Medalia, Rubb.Chem.Tech., 46,877(1973)
27. B. Topcik, Rubber Age, 105,26 July (1973)

28. E.C.F. Wood, Int.Rubb.Conf., Brighton (1972)
29. S. Middleman, 'Flow of High Polymers',
Interscience Publ., New York (1978)
30. J.D. Ferry, 'Viscoelastic Properties of Polymers'
Wiley, New York (1961)
31. J.A. Brydson, 'Flow Properties of Polymer Melts'
ILIFFE, London (1970)
32. N. Tokita and I. Pilskin, Rubb.Chem.Tech., 46,1166(1973)
33. E.G. Kontus, Rubb.Chem.Tech., 43,1082(1970)
34. K. Ninomoya and G. Yasuda, Rubb.Chem.Tech., 42,714(1969)
35. J.L. White, Rubb.Chem.Tech., 42,257(1969)
36. M. Mooney, Physics (N.Y.) 7,413(1936)
37. M. Mooney, Ind.Eng.Chem.Anal.Ed., 6,147(1934)
38. S.M. Freeman and K.Weissenberg, Nature(London),161,324(1948)
39. J.M. McKelvey, 'Polymer Processing', John Wiley and Sons,
New York, (1962)
40. M. Mooney, 'Rheology' Vol.II. Chp 5, Eds F. Eirich,
Academic Publisher, New York (1956)
41. G.E. Decker and F.L. Roth, India Rubb. World, 128,339(1953)
42. D.M. Turner and A.C. Bickley, Plast.Rubb.Process.Appl.,
1,(4),357(1981)
43. R.W. Whorlow, Rubb.Chem.Tech., 27,20(1954)
44. J.H. Dillon and L.V. Cooper, Rubber Age(N.Y.) 41,306(1937)
45. D.C. Bogue, Ind.Eng.Chem.Fundam., 5,253(1966)
46. S. Middleman, Trans.Soc.Rheol., 13,123(1969)
47. N. Nakajima and E.A. Collins, Rubb.Chem.Tech., 47,333(1974)
48. K. Weissenberg, Nature 159,310(1947)
49. T.W. Spriggs et.al, Trans.Soc.Rheol., 10,191(1966)
50. A.B. Metzner et.al, Trans.Soc.Rheol., 5,133(1961)
51. F.N. Cogswell, Trans.Soc.Rheol., 18,383(1972)
52. G.R. Cotten and L.J.L. Thick, Rubb.Chem.Tech., 51,749(1978)
53. T. Alfrey, 'Mechanical Behaviour of High Polymer',
Wiley (Interscience), New York (1960)

54. A.V. Tobolsky, 'Properties and Structure of Polymer'
Wiley, New York (1960)
55. J.L. White, 'Science and Technology of Rubber', Chp 6,
Academic Press, New York(1978)
56. H. Leaderman, 'Rheology' Vol.II, Ed. F.Eirich, Chp 1
Academic Press, New York(1956)
57. D.M. Turner et.al, 'Elastomers-Criteria for Engineering
Design' Chp 3, Eds C.Hepburn and R.W.Reynolds,
Applied Science (1979)
58. A.V. Tobolsky and K. Murakami, J.Polym.Sci., 40,443(1959)
59. A. Turner Jr and E.F. Gurver, 'Rheology' Vol II,
Ed. F.Eirich, Academic Press, New York (1956)
60. A.B. Bestul and H.V. Belcher, J. Appl.Phys., 24,296(1953)
61. W. Philippoff and F.H. Gaskins, J.Polym.Sci., 21,205(1956)
62. J.L. White and N. Tokita, J.App.Polym.Sci., 9,1929(1965)
63. A.V. Zahrenko et.al, Rubb.Chem.Tech., 35,326(1962)
64. B. Marzetti, India Rubb. World, 68,776(1923)
65. I. Williams, Ind.Eng.Chem., 16,332(1924)
66. M. Mooney, Physics 7,413(1936)
67. G.H. Piper and J.R. Scott, J.Sci.Instru., 22,206(1945)
68. E.A. Collins and J.T. Oetzel, Rubber Age (N.Y.) 102,64(1970)
69. S. Einhorn and S.B.Turetzky, J.Appl.Polym.Sci., 8,1257(1964)
70. J.R. Hopper, Rubb.Chem.Tech., 40,463(1967)
71. M. Mooney and S.A. Black, J.Coll.Sci., 7,204(1952)
72. E.B. Bagley, Trans.Soc.Rheol., 5,355(1961)
73. G.R. Cotten, Plast.Rubb.Procc., 4,89(1979)
74. G.R. Cotten, Rubb.Chem.Tech., 52,199(1979)
75. J.C. Warner and J.A. Jedonek, Eur.Rubb.J., 162,11,July(1980)
76. ASTM D926
77. DIN 53514
78. H.C. Baker et.al, Trans.Inst.Rubb.Ind., 42,210(1966)
79. J.R. Scott, Trans.Inst.Rubb.Ind., 10,481(1935)
80. J.L. Leblanc and K. Price, Elastomerics, 112,27,Nov.(1980)

81. J.P. Berry et.al, Plast.Rubb.Process., 2,97(1977)
82. J. Meissner, Rheol. Acta 8,78(1969)
83. J. Stevenson, Am.Inst.Chem.Eng.J. 18,540(1972)
84. G.V. Vinogradov et.al, Rheol. Acta 11,286(1972)
85. S. Middleman, Trans.Soc.Rheol., 9(1),83(1965)
86. F.N. Cogswell, Plast.Polym.Process., 41,39(1973)
87. I.M. Krienger, Trans.Soc.Rheol. 12,5(1968)
88. J.D. Huppler et.al, Trans.Soc.Rheol., 11,1811(1976)
89. M. Mooney and R.H. Ewart, Physics(N.Y.), 5,350(1934)
90. G.E. Decker and F.L. Roth, India Rubb. World, 128,339(1953)
91. ASTM D1646 ; BS Pt. 3
92. N.A. Stumpe et.al, Rubber World, 151,41, December (1964)
93. G.M. Bristow, NR Technology 4.17(1973)
94. G. Kraus, 'Reinforcement of Elastomers', Interscience,
New York, (1965)
95. P.C. Vegravi et.al, Rubb.Chem.Tech., 51,817(1978)
96. W.M. Hess et.al, Elastomerics, 24,January (1980)
97. ASTM D2663
98. P.S. Persson, Eur.Rubb.J., 28,November(1978)
99. P.C. Ebell and D.A. Hemsley, Rubb.Chem.Tech., 54,698(1981)
100. C.H. Leigh Dugmore, Rubb.Chem.Tech., 29,1303(1956)
101. B.B. Boonstra, Rubb.Chem.Tech., 50,194(1977)
102. R.J. Kadunce, Rubb.Chem.Tech., 47,469(1974)
103. J. Janzen and G. Kraus, Rubb.Chem.Tech., 53,48(1980)
104. C.H. Leigh Dugmore, 'Microscopy of Rubber' Monograph
of IRI (1961)
105. W.A. Ladd and H.A. Braendle, Rubber Age(N.Y.), 57,681(1945)
106. C.W. Sweitzer et.al, Rubber World, 138,869,September(1958)
107. Mc.Graw-Hill, 'Encyclopedia of Science and Technology'
Volume 8.
108. A.I. Medalia, Rubb.Chem.Tech., 34.1134(1927)
109. J.S. Tidmus and D. Parkinson, Trans.IRI., 13,52(1937)
110. A.I. Medalia, Rubber Age, 97,1,82(1965)

CHAPTER 5

STATISTICAL ANALYSIS OF MULTIVARIABLE INTERNAL MIXING PROCESS

5.1 Introduction.

Rubber mixing, particularly in an internal mixer, is known to be a complex operation. It is a multivariable and non-steady state process where strong interactions between the process variables are usually found^{1,2}. Explaining the kinetics of internal mixing by mathematical functions, has been found to be arduous or unmanageable^{3,4}. Nevertheless, the theories derived are undoubtedly essential for scientific understanding and to provide valuable information for the machine designer.

However, processes which are too complicated to be analysed mechanistically, can be approached empirically by cause and effect studies. Frequently, statistical methods are used in this approach. They can provide numerically, a sound and logical assessment of results from an experiment, whereby statistical tests often give satisfactory judgement.

In a scientific investigation where the empirical approach is adopted, proper experimental design based on statistical principles, will offer an economical means of obtaining the necessary information. A good experimental design will furnish the required information with the minimum of experimental effort.

5.2 Experimental Design and Modelling.

5.2.1 Experimental Design.

The first step in planning any experiment is to form a clear picture of the object of the experiment, the factors which may affect the results, and the errors which will inevitably arise. The experiment should be able to show the effects of changing each variable at various levels of the other variables, and also enabling the effects to be measured with acceptable accuracy. By contrast, a haphazard arrangement of the experimental points leads to difficulties in extracting the information required and in the development of an appropriate model.

Usually the classical Edisonian approach to experimentation is adopted, whereby the effect of one variable is examined while holding the level of other variables constant. However, this approach is found to be ineffective and misleading particularly for multivariable processes, where interactions between the variables are expected^{5,6}.

Another class of design which is of great practical importance is the factorial experimental design⁵⁻⁸. The independent variables are commonly referred to as factors and the number of ways in which each factor is varied is referred to as the number of levels of the factor. Generally factorial experimental designs are important for several reasons:

- i. They require relatively few runs per factor studied, and although they are unable to explore a wide region in the factor space, they indicate major trends for further experimentation.

ii. If more thorough local exploration is needed, they can be suitably augmented to form composite designs as will be described at a later stage of this section.

iii. They form the basis for fractional factorial designs which is essential as preliminary experimentation for large number of factors.

iv. The preliminary analysis of the observations produced by the designs can be done by using common sense and elementary arithmetic.

v. It allows investigation for interactions between the factors, and even if there is no interaction, the factorial approach is more economical.

The simplest form of factorial design is that involving factors which are set at two levels. In a full factorial design with 'k' number of factors at two levels each factor, the total number of combinations is given by

$$N = 2^k \quad \text{.....5.1}$$

where N - number of combinations

k - number of factors

As for five or eight factors experiment, the total number of combinations will be 32 and 256 respectively. The number of combinations (trials) will increase geometrically as the number of variable increases. A full factorial experiment with 15 variables will require $2^{15} = 32,768$ trials, which is absurd. In cases like this, by fractioning the full factorial experiments, some useful informations can be obtained. This

procedure is termed as fractional factorial design^{5,6}. However, for multifactor experiments, the Plackett and Burman⁹ design offers an adequate method of experimental investigation. Stove and Mayer¹⁰ utilized this method for determining the effects of 15 factors at two levels, by using only 16 trials.

Two level factorial designs enable the main linear and interactive effects to be estimated. They can only model linear relationships between the response and the factors investigated. The effect which each individual factor has on the response is the main effect, and if the effect of one factor is different at different levels of another, the two factors are said to interact.

Generally, the two levels of each factor are coded +1 and -1, for the upper and lower level respectively. Coded values are used in order to give equal weighting of the factors, whose true levels differ widely in magnitude and units. Furthermore, regression analysis of the experimental data can be made easier.

In this study, the two level factorial experimental design is adopted. With eight factors (independent variables), the total rubber mixing trials required for full factorial experiment will be 256. However, after consultation with Buxton¹¹, the design was fractionated to one quarter, reducing it to 64 trials. A display of the experimental design matrix is shown partly in table 5.1. However, the full display of the design matrix is cited in appendix 5.1.

Table 5.1 - 1/4 Fractionated two-level factorial experimental design matrix of eight variables.

Mix Number	Fill Fact. F	Ram Press P	Cool. Temp. T	Rotor Speed S	Unit Work W	Fill. Load. L	Oil Load. O	Black Type B
R-1	-1	-1	-1	-1	-1	-1	+1	+1
R-2	-1	-1	-1	-1	-1	+1	+1	-1
R-3	-1	-1	-1	-1	+1	-1	+1	-1
↓								
R-18	-1	+1	-1	-1	-1	+1	-1	-1
R-19	-1	+1	-1	-1	+1	-1	-1	-1
R-20	-1	+1	-1	-1	+1	+1	-1	+1
↓								
R-28	-1	+1	+1	-1	+1	+1	+1	-1
R-29	-1	+1	+1	+1	-1	-1	-1	+1
R-30	-1	+1	+1	+1	-1	+1	-1	-1
↓								
R-38	+1	-1	-1	+1	-1	+1	+1	+1
R-39	+1	-1	-1	+1	+1	-1	+1	+1
R-40	+1	-1	-1	+1	+1	+1	+1	-1
↓								
R-48	+1	-1	+1	+1	+1	+1	-1	+1
R-49	+1	+1	-1	-1	-1	-1	+1	+1
R-50	+1	+1	-1	-1	-1	+1	+1	-1
↓								
R-55	+1	+1	-1	+1	+1	-1	-1	+1
R-56	+1	+1	-1	+1	+1	+1	-1	-1
R-57	+1	+1	+1	-1	-1	-1	-1	-1
↓								
R-62	+1	+1	+1	+1	-1	+1	+1	-1
R-63	+1	+1	+1	+1	+1	-1	+1	-1
R-64	+1	+1	+1	+1	+1	+1	+1	+1

Two level factorial designs do not enable any curvature which may exist in the relations between factors and responses to be modelled. Nevertheless, a composite design formed by augmenting the two level factorial design, enables estimation of quadratic curvature effects, thus improving the fitness of the model used⁵⁻⁷.

Composite design extends the experimental space of the factorial design. The high and low levels of the factors are increased and decreased respectively. These supplemented levels are known as 'star' points and they are calculated to ensure rotatability in the design, i.e. the precision of the fitted surface is constant for all points at a given distance from the centre of the design. A schematic representation of a three factor two level composite design is as shown in figure 5.1. The 'star' points can be determined by using equation 5.1 for full factorial, and equations 5.2 and 5.3 for fractional factorial designs

$$a = \pm 2^{k/4} \quad \text{full fractional} \quad \dots\dots 5.1$$

$$a = \pm 2^{(k-1)/4} \quad \text{half fractional} \quad \dots\dots 5.2$$

$$a = \pm 2^{(k-2)/4} \quad \text{quarter fractional} \quad \dots\dots 5.3$$

where a - 'star' points levels

k - number of factors

In this study, the one quarter fractional factorial design of eight variables is augmented by star points at levels $+ 2.8$ and $- 2.8$. The design matrix of these points is as shown in table 5.2 and in appendix 1. However, for the type of filler

factor (B), the minimum level is proportionally adjusted to -0.4 and keeping its maximum code value as $+2.8$. This is done mainly to allow fuller investigation of the influence of (N220) ISAF carbon black on the measured responses be more intensive, by moving it closer to the centre of the design and consequently omitting the minimum level at -2.8 coded value¹¹.

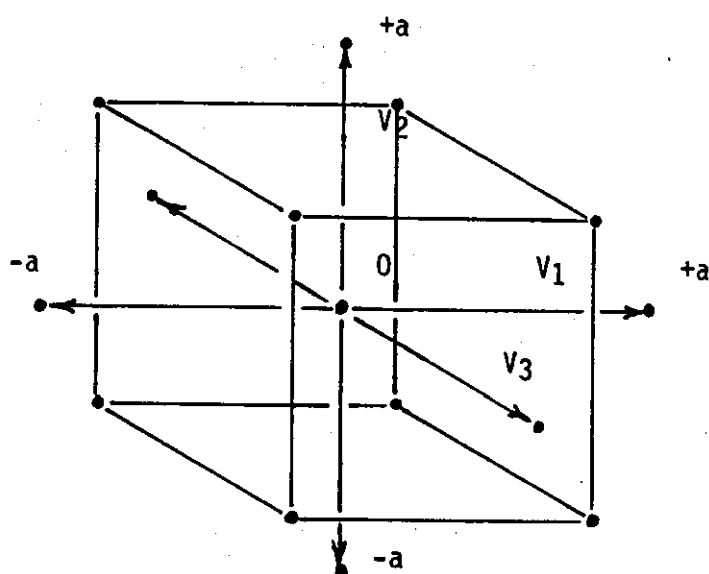


Figure 5.1 - Composite experimental design of three variables⁵.

Finally to augment the experimental area even further, a number of trials with all the factors are set at coded value 0, the origin of the experimental space were included. By genuinely replicating several trials at this level for all the factors, it is possible to estimate the experimental errors. Consequently the adequacy of fit of the nominated model can be determined. These augmented points are known as the centre points of the

composite experimental design, and its matrix is as shown in table 5.2.

Table 5.2 - Augmented points for composite experimental design matrix of eight variables.

Mix Number	Fill Fact. F	Ram Press P	Cool. Temp. T	Rotor Speed S	Unit Work W	Fill. Load. L	Oil Load. O	Black Type B
R-65	+2.8	0	0	0	0	0	0	0
R-66	-2.8	0	0	0	0	0	0	0
R-67	0	+2.8	0	0	0	0	0	0
R-68	0	-2.8	0	0	0	0	0	0
R-69	0	0	+2.8	0	0	0	0	0
R-70	0	0	-2.8	0	0	0	0	0
R-71	0	0	0	+2.8	0	0	0	0
R-72	0	0	0	-2.8	0	0	0	0
R-73	0	0	0	0	+2.8	0	0	0
R-74	0	0	0	0	-2.8	0	0	0
R-75	0	0	0	0	0	+2.8	0	0
R-76	0	0	0	0	0	-2.8	0	0
R-77	0	0	0	0	0	0	+2.8	0
R-78	0	0	0	0	0	0	-2.8	0
R-79	0	0	0	0	0	0	0	+2.8
R-80	0	0	0	0	0	0	0	-0.4
R-81	0	0	0	0	0	0	0	0
R-82	0	0	0	0	0	0	0	0
R-83	0	0	0	0	0	0	0	0
R-84	0	0	0	0	0	0	0	0
R-85	0	0	0	0	0	0	0	0
R-86	0	0	0	0	0	0	0	0
R-87	0	0	0	0	0	0	0	0
R-88	0	0	0	0	0	0	0	0
R-89	0	0	0	0	0	0	0	0
R-90	0	0	0	0	0	0	0	0
R-91	0	0	0	0	0	0	0	0
R-92	0	0	0	0	0	0	0	0

For each factor, the real (actual) values depend largely on the range of interest for investigation. The choice for minimum and maximum actual values of each factor were based on previous mixing studies^{1,2}, the rubber mixing conditions in industry and also on the capability of the machine used. This will be described further in chapter 6.

The minimum and maximum real values of each factor is related to - a and + a coded values respectively. 0 coded values represent the average between minimum and maximum real values. The two factorial levels were established by interpolating the real values proportionally. In this mixing study, the relationship between the real values and coded values of each factor is shown in table 5.3.

Table 5.3 - The real and coded values of the mixing variables and material variables.

Variables	Coded values				
	-2.8	-1	0	+1	+2.8
Fill factor (F)	0.5	0.63	0.7	0.77	0.9
Ram pressure (P) MPa	0.21	0.34	0.41	0.49	0.62
Cool. temperature (T) °C	20.0	40.0	50.0	60.6	80.0
Rotor speed (S) rpm	20.0	36.0	45.0	54.0	70.0
Unit work (W) MJ/m ³	400	594	700	806	1000
Filler level (L) phr	0	25.9	40.0	54.0	80.0
Oil level (O) phr	5.0	11.5	15.0	18.5	25.0
		-0.4	0	1.2	+2.8
Type of filler (B), mm		20	28	50	80
		N220	N330	N660	N762
		(ISAF)	(HAF)	(GPF)	(SRF)

5.2.2 Empirical Modelling.

Model building is an important part of any scientific investigation. Frequently, the mechanism underlying a process is not understood well, or is too complicated to allow an exact model to be postulated. In such circumstances, an empirical model may be useful particularly over the levels of the factors being studied. In general, the mathematical relationship between the response and the independent variables (factors) can be written as

$$Y = f (x_1 , x_2 , \dots x_k) \quad \dots\dots\dots 5.4$$

where Y - the response or dependent variable
 x_k - the independent variables or factors

In its simplest form, the response can be fitted by a straight line model or sometime known as the first order polynomial function. This can be expressed by

$$Y = B_0 + B_1 x_1 + B_2 x_2 + \dots B_k x_k \quad \dots\dots 5.5$$

When inadequacy arises due to the curvilinear nature of the experimental data, the second order polynomial function is used. The function takes the form of

$$\begin{aligned} Y = & B_0 + B_1 x_1 + B_2 x_2 + \dots B_k x_k \\ & \quad \quad \quad \text{(the first order terms)} \\ & + B_{11} x_1^2 + B_{22} x_2^2 + \dots B_{kk} x_k^2 \\ & \quad \quad \quad \text{(quadratic terms)} \\ & + B_{12} x_1 x_2 + \dots B_{k-1, k} x_{k-1} x_k \quad \dots\dots 5.6 \\ & \quad \quad \quad \text{(interaction terms)} \end{aligned}$$

The quantity B_0 is the grand mean or the zero order constant. $B_1 - B_k$ are the linear coefficients. $B_{12} - B_{k-1}$ are the quadratic coefficients. These coefficients can be estimated by regression analyses of the experimental data.

In this study, the second order polynomial function will be used to model the relationship between the properties of the rubber mixes and selected mixing condition and compounding ingredient factors. Previous studies by Ebell¹ and Williamson¹⁷ have shown that the second order polynomial function correlates the rubber vulcanizate properties to the mixer operating variables adequately. In addition, Freakley¹⁷ extended to include the third order terms into the polynomial equations. He observed that these terms improve the fit of the polynomial equations when relating the rheological properties of PVC/Nitrile rubber compounds with the mixer operating variables. However, for practical purposes a second order polynomial model is usually adequate⁷.

5.3 Multivariable Regression Analysis.

In the elementary case for one independent variable function, the best fit straight line can be obtained by the method of least squares, in which the sum of squares of deviation between the predicted and the experimental values are minimized. It is not intended to discuss in detail the derivation and the numerical techniques involved in the method of least squares, since they are accessible in many textbooks⁵⁻⁸. When more than two independent variables are considered, multiple linear regression analyses are used, whereby the number of least square equations to be solved

increase proportionally with the number of linear coefficients to be estimated. However, computer programs are now readily available for multiple linear regression calculations.

As for the case of curvilinear functions, a similar approach to linear regression is used in estimating the coefficients. The only difficulties which arise are the number of equations which have to be solved. Nevertheless, with the availability of computer programs, the user does not have to concern himself with the numerical techniques involved.

Generally a quadratic polynomial function with k variables (equation 5.6), contains k linear terms, k square terms and $1/2 k (k-1)$ interactive terms. For as few as three independent variables, fitting a quadratic function will require solving nine simultaneous (normal) equations, in order to estimate the coefficients. For four independent variables, the number of coefficients rises to fourteen and for five independent variables to twenty. There is a rapid increase in the number of coefficients as the order of the regression equation is increased. Fitting a multivariable model containing cubic or higher order terms is rarely attempted, and for practical purposes a quadratic equation is usually adequate⁷.

As mentioned earlier, there are a total of eight independent variables used in this rubber mixing study. Realizing the great number of equations to be solved, the coefficients of the quadratic polynomial function are estimated by means of a computer package. The package designated as GLIM (Release 3) was used, which was developed by the Royal Statistical Society London and the Numerical Algorithms Group¹².

Briefly the GLIM statistical package can accomplish the following tasks;

i. Perform a multivariable regression analysis (MVRA) and fit a curvilinear function relating the response to the nominated model terms. In this study, the analysis was carried out in two stages mainly due to the constraints and large file space required for the PRIME computer distributed terminal system operated by Loughborough University.

ii. It lists the estimated coefficients of the nominated model, together with their standard errors of the corresponding terms as shown in table 5.4. Since the analysis was performed in two stages, the standard errors have to be corrected by the following equations¹¹

$$C_{LQ} = \sqrt{\frac{D_2 (DF_1)}{D_1 (n - p)}} \quad \text{.....5.7}$$

$$C_I = \sqrt{\frac{DF_2}{n - p}} \quad \text{.....5.8}$$

where C_{LQ} - correction factor for linear and quadratic terms

C_I - correction factor for interactive terms

D_1, D_2 - deviance of first and second stage fitting respectively

DF_1, DF_2 - degree of freedom of first and second stage respectively

n - number of mixing trials

p - total number of coefficients of the nominated model

Table 5.4 - Estimated coefficients of reference viscosity.

First stage fitting			
Deviance = 57890		Degree of freedom = 78	
	Estimated coefficients	Standard error	Parameter
1	100.5*	7.14	%GM (Grand Mean)
2	0.6	3.05	F
3	2.4	3.05	P
4	-0.7	3.05	T
5	-2.6	3.05	S
6	-2.6	3.05	W
7	30.8*	3.05	L
8	-12.3*	3.05	O
9	-23.7*	3.34	B
10	-1.4	2.45	FF
11	-0.6	2.45	PP
12	-2.2	2.45	TT
13	-2.0	2.45	SS
14	-3.9	2.45	WW
15	-1.1	2.45	LL
16	-4.3	2.45	OO
17	0.5	2.7	BB
Second stage fitting			
Deviance = 21800		Degree of freedom = 67	
18	2.2	2.26	FP
19	-0.7	2.26	FT
20	-0.7	2.26	FS
21	-4.0	2.26	FW
22	1.0	2.26	FL
23	-4.4	2.26	FO
24	0.1	2.26	FB
25	2.4	2.26	PT
26	-1.9	2.26	PS
27	3.8	2.26	PW
28	2.3	2.26	PL
29	0.5	2.26	PO
30	-0.7	2.26	PB
31	-4.1	2.26	TS
32	1.5	2.26	TW
33	0.8	2.26	TL
34	-0.4	2.26	TO
35	-0.1	2.26	TB
36	-1.6	2.26	SW
37	-1.1	2.26	SL
38	1.8	2.26	SO
39	2.2	2.26	SB
40	1.1	2.26	WL
41	-0.8	2.26	WO
42	-2.3	2.26	WB
43	-6.2+	2.26	LO
44	-19.5*	2.26	LB
45	6.0+	2.26	OB

* indicates coefficient significance 99.9 %

+ indicates coefficient significance 97.5 %

The precision with which the regression coefficients are estimated depends upon the variance about the regression, the range of the values of the independent variables and the number of trials⁷. To test the significance of the regression, the ratio of the estimated coefficient to the corrected standard error of each polynomial term is determined by

$$t = \frac{\text{Estimated coefficients}}{\text{Standard error}} \quad \dots\dots\dots 5.9$$

By comparing this ratio with the constant value of Student's t-distribution at a particular degree of freedom, the reliability of the estimated coefficients, or of the predicted response can be assessed.

Consider the term L (black loading level) for the response, reference viscosity (refer table 5.4). The corrected standard error is 2.34 ($C_{LQ} = 0.767$), and its coefficient is 30.81. The ratio of which is 13.22, indicating that the probability of carbon black loading level has a real effect on reference viscosity is greater than 99 %, when referred to Student's t-table. For 99 % confidence limit with 50 degree of freedom (n-p), the regression coefficient of L can be between,

$$\begin{aligned} \text{Coefficient of L} &= 30.81 \pm (2.407 \times 2.34) \quad \dots\dots 5.10 \\ &= 36.41 \text{ and } 25.2 \end{aligned}$$

Similarly, the other variables such as O (oil loading level), B (type of black) and interactive terms, LO and LB, have indicated significant influence on reference viscosity. The estimated coefficients of the NR mixes' responses and their significant variables are presented in appendix (II).

iii. GLIM can list the observed values and the fitted values of each response predicted by the model. The algebraic difference between an observed value and the predicted value is known as residual. The residuals of each fitted value can be listed if required. However, in this study listing of these values was found to be unnecessary. By examining the plot of residuals as in figure 5.2, the signs of model inadequacy and inconsistent data can be detected, as explained later.

iv. GLIM programs calculate the deviance of the nominated model, i.e. the sum of squares of the residuals. In table 5.4, the deviance at each stage is 57890 and 21800 respectively. However, the deviance in the second stage of analysis represents the deviance of the model¹¹.

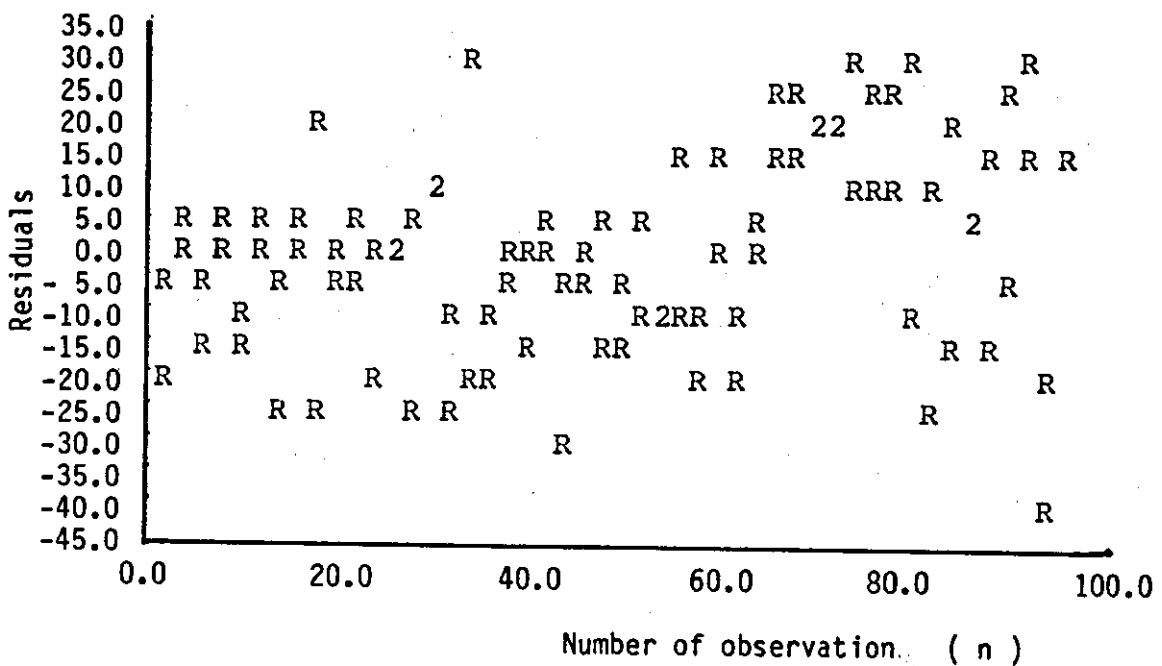


Figure 5.2 - Residual plot of reference viscosity.

v. A plot directive of GLIM programs produces scatter diagrams of up to 10 variables against another variable. A

scatter diagram of the residuals against the predicted values, or residuals against the observations is most valuable. It will indicate a systematic variation of the proposed model. For adequacy of fit of a model, the residual points should all lie within a horizontal band. In addition, outlying observations can be detected from the residuals plot. Outlying observations are usually due to gross experimental error at a single point and can have a serious distorting effect on the fitted response surface. Figure 5.2 illustrates the residuals plot of the reference viscosity against the observation numbers.

However, having reviewed some of the capabilities of the GLIM programs, it is necessary at this juncture to evaluate the goodness of fit of the nominated quadratic model used in this study. Goodness and adequacy of fit of a model can be verified by the analysis of variance from the residuals^{5,7}. There is one residual for each of the original observed values. The regression coefficients are actually estimated by minimizing the sum of squares of this residuals. Residuals are mainly due to pure experimental error and the inadequacy of fit of the nominated model⁵⁻⁷.

Pure experimental error can be detected by genuine replicates of experimental trials over the same conditions. Referring to the experimental design in section 5.2.1, twelve centre point mixing trials were replicated. The variance of the centre points V_c , is obtained by

$$\begin{aligned}
 V_c &= \frac{\sum_{n=1}^{n+1} (y_n - \bar{y})^2}{n - 1} \\
 &= \frac{SS_c}{d} \qquad \dots\dots\dots 5.11
 \end{aligned}$$

where y_n - observed values of centre points
 n - number of centre points
 \bar{y} - mean of observed values
 SS_C - sum of square of centre points
 d - degree of freedom

By subtracting SS_C from the sum of squares of the residuals SS_r , the sum of squares due to lack of fit SS_1 , can be obtained.

$$SS_1 = SS_r - SS_C \quad \text{.....5.12}$$

The degree of freedom⁵ for the residual sum of squares d_r , for a multiple curvilinear regression is given by

$$d_r = n - p \quad \text{.....5.13}$$

Therefore the variance V_1 , due to lack of fit can be derived from

$$V_1 = \frac{SS_1}{d_r - d} \quad \text{.....5.14}$$

A comparison of the variances V_1 and V_C can serve as a check to the adequacy of fit of the empirical model used^{5,7}. To determine the significance level, the ratio of the variances, V_1 / V_C is referred to the appropriate F - distribution. For a perfectly fitted model, the F-ratio will be close to unity. The larger the F-ratio, the higher is the degree of confidence that the model is inadequate^{5,7}. In such circumstances, other terms may have to be added to the model, or a transformation of the data is required. Also different models may have to be used to improve the fit.

The F-ratio of the response, reference viscosity is 1.72. With 39 and 11 degree of freedom, the probability level is between 0.1 and 0.25. This indicates that the probability level

Table 5.5 - Variance ratio of NR mixes.

Degree of freedom at 39 and 11.

Response	F-ratio	% lack of fit significance
<u>Mixer operating variables</u>		
Dump Temperature	2.57	95
Mixing time	1.20	< 75
<u>Viscous properties</u>		
Power law index	1.66	80
Reference viscosity	1.72	82
Apparent viscosity at 6.0 s^{-1}	2.14	91
Apparent viscosity at 12.0 s^{-1}	0.98	< 75
Apparent viscosity at 35.0 s^{-1}	2.68	96
Apparent viscosity at 44.0 s^{-1}	2.58	95
<u>Slip behaviour</u>		
Slip velocity at 3.0 s^{-1}	0.46	< 75
Slip velocity at 23.0 s^{-1}	1.06	< 75
Velocity ratio at 23.0 s^{-1}	1.07	< 75
<u>Elastic properties</u>		
Shear modulus	1.07	< 75
Relaxation rate	0.52	< 75
Relaxation time	1.97	88
<u>Carbon black dispersion</u>		
Photometer reading	2.37	93
Composite parameter	2.47	95

of the nominated model has an inadequacy of fit of approximately 82 % (when interpolating), which is a low statistical

significance. The variance ratio and the percentage lack of fit significance of other responses derived in this study is shown on table 5.5. However, by combining both the F-ratio test and examination of the scatter plots of residuals, will give a better judgement on the adequacy of a particular empirical model⁵⁻⁷.

5.4 Response Surfaces.

5.4.1 Introduction.

Geometrical presentation of results is widely used to visualize the relation between a response and its independent variables. For single variable experiments, a two dimensional graph will indicate the variation of the response over different levels of the variables. However, this technique can also be applied to multivariable experiments, simply by plotting the response versus one variable, holding the levels of the other independent variables constant^{5,7}. To observe any interactive effects between the variables on the response, this method was found to be inefficient¹. Furthermore, the two dimensional presentation fails to show the maximum response value of a multivariable function⁵.

Alternatively, the relationship between a response and a number of factor may be represented by a three dimensional surface called the response surface. The most common method of representing a response surface is the contour plot, which is frequently used in maps. Its use for rubber compounding¹³⁻¹⁵ and mixing studies^{1,2} has proved to be very useful. The polynomial function such as equation 5.6 will generate contour lines, generally consisting of either concentric ellipses or concentric hyperbolas, although these figures may not be complete within

the experimental region. Figure 5.3 illustrates the response contours of a polynomial function of second order.

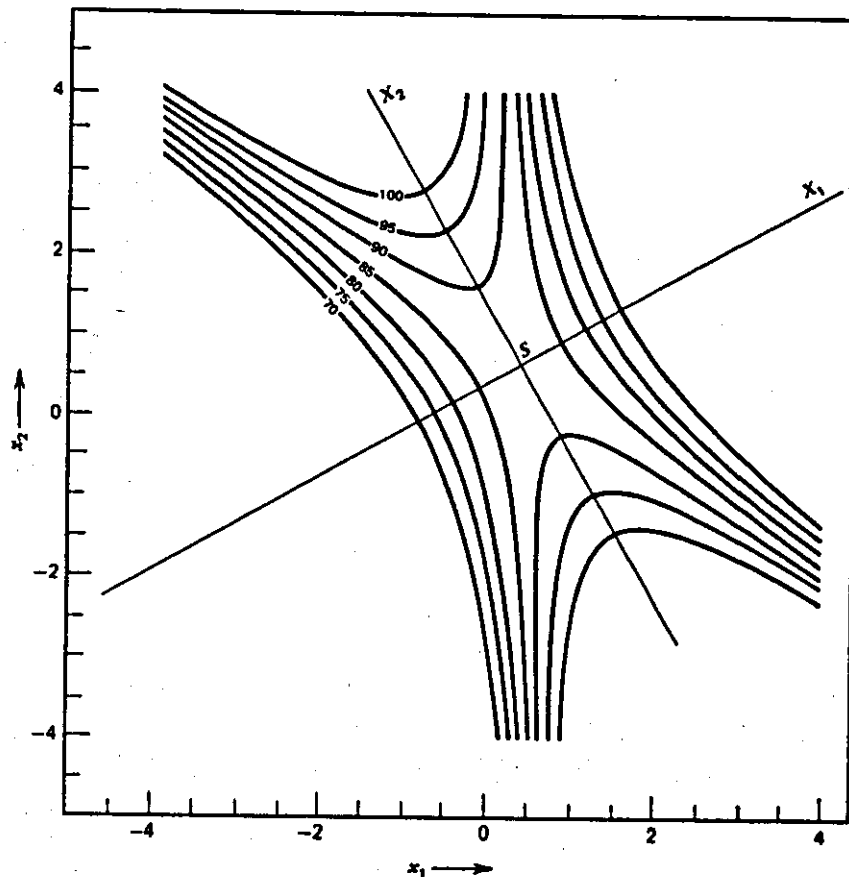


Figure 5.3 - A typical response contour representation⁵.

Another form of response surface is the isometric projection. In this case, the graph will have three axes, the z-axis showing the response whilst the independent variables on the x and y axes. Figure 5.4 shows a typical isometric projection presentation.

With the current trend of computer graphics, mathematical models which describe the responses can be pictorially represented by shading diagrams of various colours, creating an effect similar to response contours. This method of response presentation is adopted in this study and will be described in the following section.

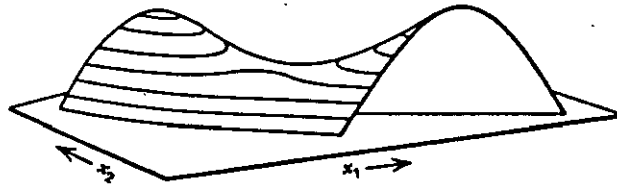


Figure 5.4 - An isometric projection of a response⁵.

5.4.2 Shading Diagrams.

The graphical technique used in generating shading diagrams is based on a newly developed computer program known as Interactive Graphics for Process Simulation (IGPS) ¹⁶. In this program, rectangular blocks of colours are arranged according to the response's values. A single shading diagram can show how two variables affect a response. However, additional variables can be incorporated by combining several shading diagrams in a single display. The shading diagrams on the visual display unit of the computer were photographed and are shown in figure 5.5.

The program offers several facilities, however the method displayed in figure 5.5 is more appropriate in this study. This method of display is called 'parallel' sections, and is easily extended to regimes of four or even five dimensions. A single response can be plotted against four variables in an array of the shading diagram. The third and fourth variables are adjusted between adjacent diagrams in any row and column respectively. Thus showing the influence of these non-axial variables on the

response in the form of a 3 x 3 matrix. For simplicity, each shading diagram is numbered accordingly as shown in figure 5.6.

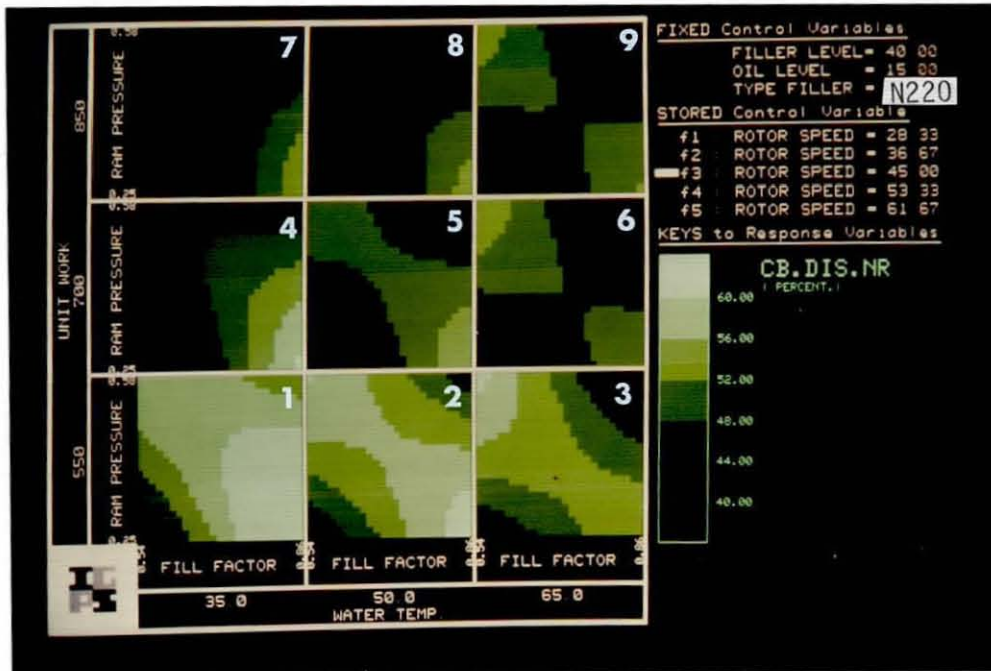


Figure 5.5 - Typical shading diagrams of the response carbon black dispersion.

A schematic representation of the shading diagram in three dimensions is as shown in figure 5.7. For five-dimension surfaces, the effects of the fifth variable on the response are stored in the computer memory. A shading diagram at a particular level of the fifth variable can be recalled at any time. The fifth variable can be adjusted up to five levels, in which case successive displays will indicate its influence on the response over the same level of the other four variables. Figure 5.5 illustrates the level of the fifth variable at f3.

As mentioned in chapter 1 (section 1.4), this study is concerned with the influence of machine and material parameters on the properties of rubber mixes. Consequently, the shading

diagrams of either parameters are examined separately. After which the combined influence of both the parameters is examined. The choice of the variables on the axes of the shading diagram is based on the GLIM analyses. The variables with high level of significance, indicating a strong influence on the response are then considered as the axes of the shading diagram.

7	8	9
4	5	6
1	2	3

Figure 5.6 - 3 x 3 matrix of shading diagram
in a single display.

Extrapolation outside the range covered by the experimental data should be made with considerable caution. The only occasion in which extrapolation may be made with greater confidence, is when it is known that the fitted relationship is of the correct functional form, but this is seldom the case when a multivariable curvilinear regression is fitted⁶.

In addition, experimental region can be defined to give a greater confidence of the response predicted by the nominated model. The experimental area conservatively defined¹¹, for the coded values of the variables by

$$V_1^2 + V_2^2 + V_3^2 + V_4^2 + V_5^2 + V_6^2 + V_7^2 + V_8^2 \leq 8 \quad \dots 5.15$$

where V_{1-8} - the independent variables

If six of the variables are set to their centre point values (coded value = 0), as indicated by shading diagram number 5 in figure 5.5, and the remaining two are used as the axes of the diagram, then they can vary within the experimental region between +2.0 and -2.0 coded values. In fact, the experimental region is defined for this case by a circular area having a radius of $(2.0^2 + 2.0^2)^{0.5}$. The experimental region is reduced when more non-zero coded values are considered. For shading diagram number 1 and number 4 of figure 5.5, the experimental region are ± 1.32 and ± 1.414 coded values respectively.

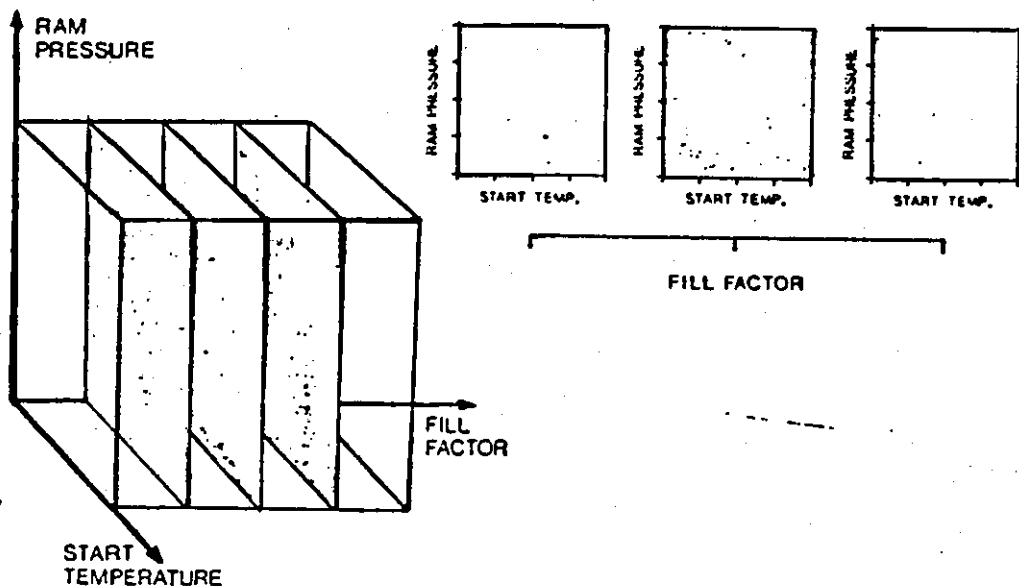


Figure 5.7 - Schematic representation of three-dimension 'parallel' section shading diagram

Literature Cited.

(Chapter 5)

1. P.C. Ebell, Ph.D Thesis Loughborough University (1981)
2. K.B. Basir and P.K. Freakley, Kautschuk + Gummi Kunststoffe, March (1982)
3. J.M. McKelvey, 'Polymer Processing' John Wiley & Sons (1962)
4. W.R. Bolen and R.E. Colwell, SPE J., 24, August (1958)
5. G.E.P. Box, W.G. Hunter and J.S. Hunter, 'Statistic for Experimenters', John Wiley & Sons, New York (1978)
6. O.L. Davies, 'The Design and Analysis of Industrial Experiments' Oliver and Boyd (ICI), Edinburgh (1963)
7. O.L. Davies and P.L. Goldsmith, 'Statistical Methods in Research and Production', Oliver and Boyd (ICI), Edinburgh, (1972)
8. B.E. Cooper, 'Statistics for Experimenters', Pergamon Press (1969)
9. R.L. Plackett and T.P. Burman, Biometrika, 33, 305 (1946)
10. R.A. Stove and R.P. Mayer, Ind.Eng.Chem., 58, 36, February (1966)
11. J.R. Buxton, Private communication, Engineering Maths Department Loughborough University.
12. R.J. Baker and J.A. Nelder, 'GLIM Release 3', Numerical Algorithms Group, Oxford (1978)
13. P.F. Bertsch, Rubber World, 75, June (1961)
14. G.C. Derringer, Rubb.Chem.Tech., 47, 825 (1974)
15. J.R. Hopper, Rubb.Chem.Tech., 40, 463, (1967)
16. J.M. Holt and J.R. Buxton, Private communication, Eng.Maths Department, Loughborough University.
17. P.K. Freakley, Private communication, Loughborough University.

CHAPTER 6

COMPOUND SELECTION AND PREPARATION OF NR MIXES

6.1 Introduction.

A high percentage of natural and synthetic rubber produced is consumed for tyre production and other related products. Haynes¹ evaluated that about 63 % of the rubber (natural and synthetic) produced during this decade is for this application. Consequently, in this mixing study, the author felt that an investigation on the influence of process and material variability on the properties of tyre compound is most suitable. Furthermore, tyre producers have commented that the reduction in processing inconsistency and variability of stock properties are favourable particularly with the rapidly rising cost of both energy and labour².

A tyre comprises several rubber components, such as tread, sidewall, chafer, linings and strips³. Each component is made up of a different compound formulation. Nevertheless, the choice of an NR tread formulation was preferred in this mixing study, the tread being the major critical rubber component.

6.2 Experimental Work.

6.2.1 Compounding Materials.

The base polymer used for the tread formulation was technically specified natural rubber of grade 20 (SMR 20), which was acquired from the Malaysian Rubber Producers and Research Association. To examine the influence of material variables on the mixes properties, the types of carbon black (B), carbon black loading level (L), and process oil loading level (O), were varied over a wide range.

The types of carbon black used were N220 (ISAF), N330 (HAF), N660 (GPF) and N762 (SRF), obtained directly from the University's stock. Their properties were not evaluated, but the specifications given by the suppliers were utilized⁴. The average particle diameter was used to characterize these blacks, and it ranges from 20.0 to 80.0 nm. The filler loading level was varied from 0 to 80.0 phr. In addition, the level of processing oil in the formulation varies from 5.0 to 25.0 phr.

As mentioned earlier, the composite experimental design was adopted in this investigation. The levels of the material variables over the whole experimental range are shown in Chapter 5 (section 5.2.1). However, the formulation of the compound is shown in table 6.1.

The processing oil was the aromatic type with tradename Dutrex 729 supplied by the Shell Oil Limited.

Zinc oxide and stearic acid were supplied by Anchor Chemical Company.

The antioxidant was N-(1,3-Dimethylbutyl)-N-phenyl-p-phenylenediamine, tradename Santoflex 13 obtained from Monsanto Industrial Chemical Company.

Table 6.1 - NR mixes formulation.

	parts by weight
TSR 20 (SMR 20)	100.0
Carbon blacks	0 - 80.0
Process oil (Dutrex 729)	5.0 - 25.0
Zinc oxide	5.0
Stearic acid	3.0
Antioxidant (Santoflex 13)	2.0
Retarder (Santogard PVI)	0.5

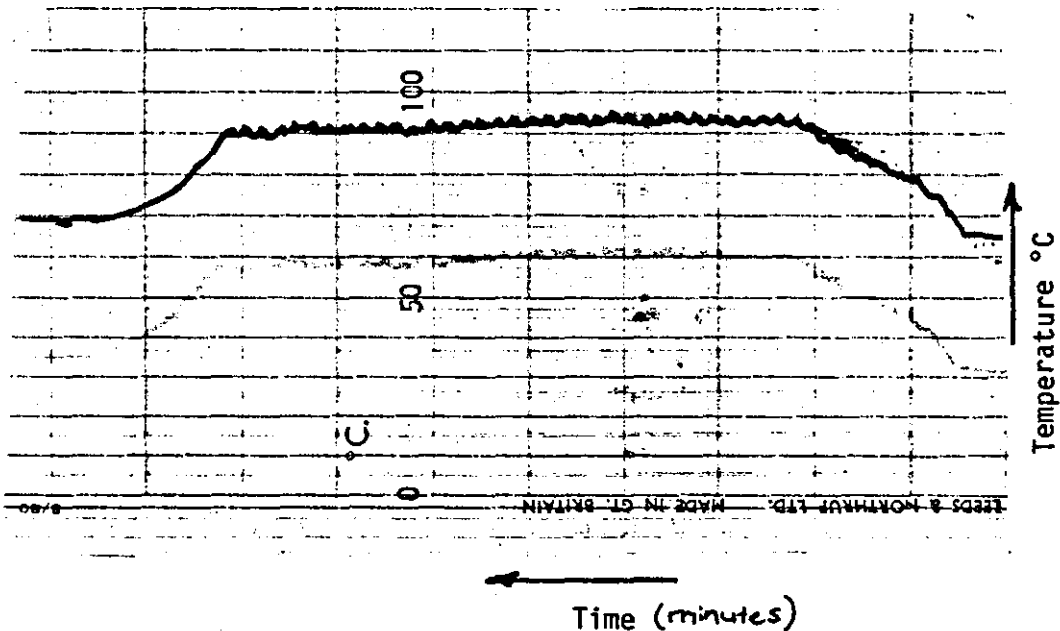
N-Cyclohexylthio-phthalimide, tradename as Santogard PVI, was the retarder. It was supplied by Monsanto Industrial Chemical Company. At 0.5 phr of PVI, it will safely inhibit scorching of the compound during mixing^{5,6}.

No curative and accelerator were added in the formulation, primarily to avoid crosslinking and degradation of the compound during mixing and storage.

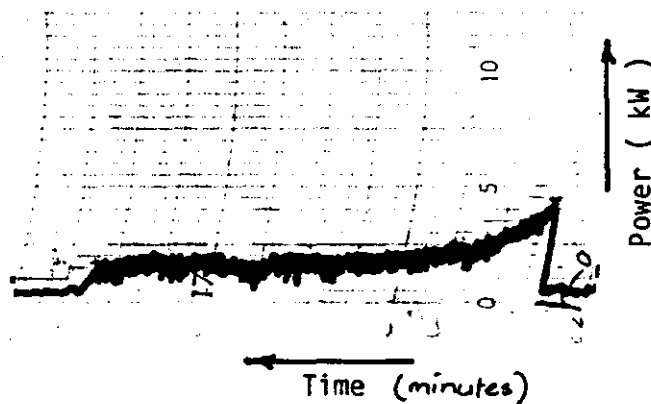
6.2.2 Mixing Equipment and Method.

The NR mixes were prepared in a Farrel Bridge BR Banbury internal mixer with free chamber volume of 1.57 litres. This machine was equipped with manual controls for variable rotor speeds, cooling water system, energy measurements and ram pressure. Temperature in the mixing chamber is measured by a thermocouple probe fixed to the chamber wall. In addition,

instantaneous power is measured by an induction wattmeter. Both the chamber temperature and power traces for each mixing cycle can be obtained from the chart recorders. Typical temperature and power traces of a mixing cycle are illustrated in figure 6.1 (a) and (b) respectively.



(a)



(b)

Figure 6.1 - (a) Typical temperature trace and
(b) power trace of a mixing cycle.

The upper and lower limits of the mixer operating variables, F, P, T, S and W are tabulated in table 6.2. Nevertheless, the whole range of their levels used in this study can be referred in Chapter 5 (section 5.2.1). Several trial runs were made at the extreme levels of the operating variables, together with the material variables. Initially, visual inspection of the mixing stock, noting whether the batch crumbles or held together as a lump was a good indicator. However, drastic temperature rise and sudden increase in power would further indicate the acceptable operating levels for investigation. The choice of upper and lower levels were also based on the findings of other mixing studies; and together with the operating conditions used in industry⁷⁻⁹. In addition the capability of the equipment was also considered in selecting these levels.

Table 6.2 - Mixer operating variables.

Variables	range
Fill factor (F)	0.5 - 0.9
Ram pressure (P) MPa	0.21- 0.62
Coolant temperature (T) °C	20.0- 80.0
Rotor speed (S) rpm	20.0- 70.0
Unit work (W) MJ/m ³	400.0- 1000.0

The starting temperature of a mixing cycle has an effect on the final properties of a compound^{7,8}. The required starting temperature was effected by heating electrically the circulating water using an immersion heater. A pump circulates the water to the mixer chamber wall and the rotors. If the required

temperature is exceeded, cooling water from the mains was automatically admitted into the reservoir via the control valve. The control valve and the amount of current input into the immersion heater enables the right circulating water temperature to be obtained. A schematic diagram of the circulating water system is as shown in figure 6.2. The starting temperature was allowed to stabilize for 10.0 minutes before commencing each mixing cycle.

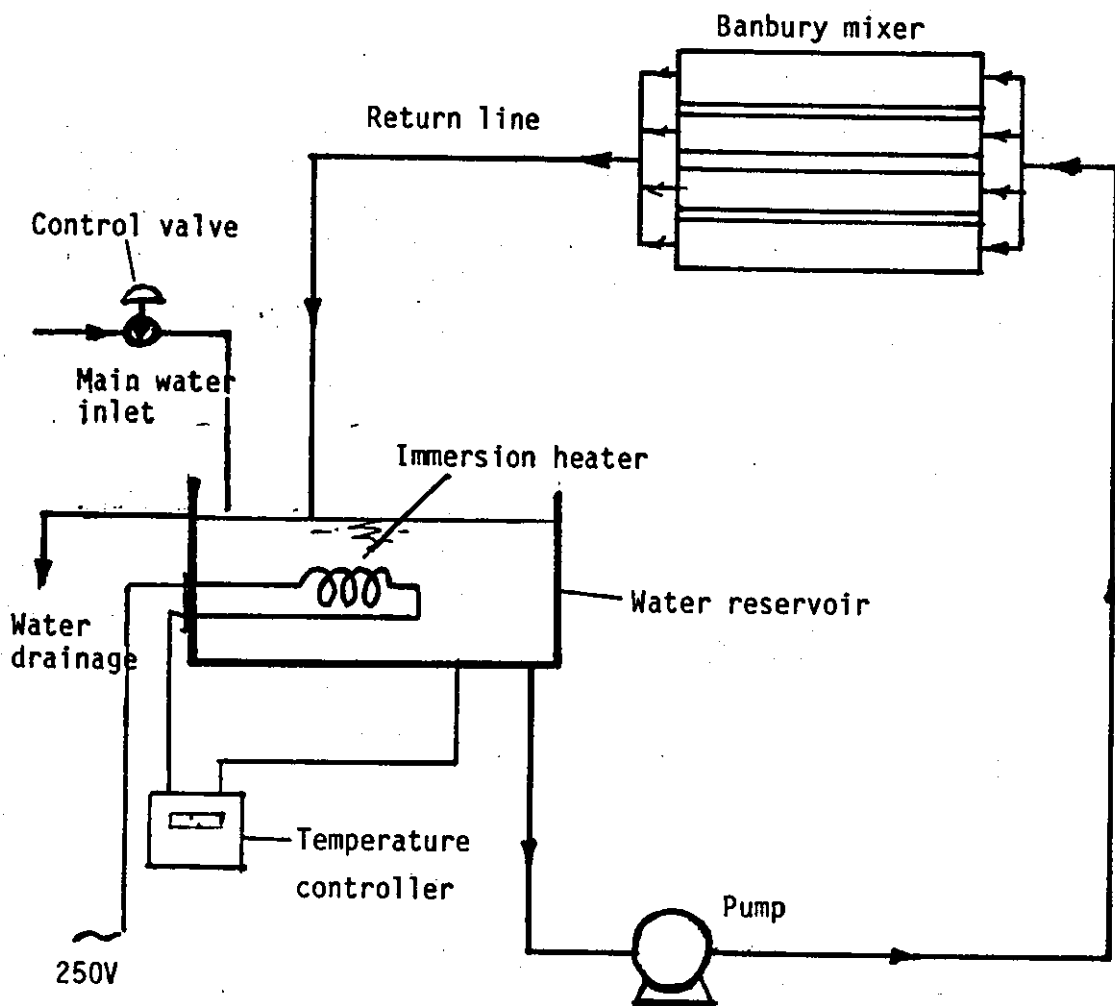


Figure 6.2 - Schematic diagram of circulating water system.

The use of power integrator for energy measurements and control in rubber mixing operation has shown to improve the mixing efficiency^{10,11}. In this study the amount of work or energy input was used as the dump criteria. It was measured by a counter connected to the kilowatt-hour meter of the mixer. The number of rotations of the disc in the meter was measured by means of a light source and photocell assembled opposite to each other. A hole in the disc allows the light passing through to be sensed by the photocell thus enabling the number of rotations of the disc to be determined. The rotations were indicated by the counter, and calibrated with reference to the kilowatt-hour meter. This gave a measure on the amount of energy input into the mixer. Sensitivity of the measurement can be improved by increasing the number of holes in the disc.

The energy obtained by the counter method was compared to the instantaneous power-time trace of the mixer. Both measurements were found to be compatible with each other. The specific energy or unit work can be calculated by dividing the energy input to the batch volume as described in chapter 1 (section 1.3.1).

The mixing method employed for the NR mixes was single stage *dump* mixing technique. The levels of each run is indicated by the experimental design matrix illustrated in chapter 5 (section 5.2.1). However, the sequence of mixing the compound was selected randomly, based on the random number tables¹², as commonly used in statistical analysis technique.

The mixing procedures for the compound were as follows:

1. Select the run corresponding to random number 1 of the experimental design.

2. The ingredients of each experimental run were identified and weighed. The rubber was cut into small pieces of about 6.0 mm cubes, for ease of feeding.
3. Ensure that the machine is clean.
4. Set the starting temperature and the rotor speed. Ample time of 10.0 minutes was given for the temperature to stabilize.
5. Bring the ram down onto the empty chamber and set the required air line pressure to generate the required specific ram pressure. Raise the ram when equilibrium pressure is reached.
6. Check that the timer is set to zero.
7. Switch on the recorders.
8. Close the discharge door.
9. Start rotors and adjust speed.
10. Load all ingredients together into the mixer (upside-down mixing). Rubber first followed by carbon black and oil and lastly the other additives.
11. Bring the ram down.
12. Start timer and the energy counter.
13. Check rotor speed and make fine adjustment if necessary
14. At prescribed energy level (calculated for each mix), dump batch.
15. Note the time of mixing.
16. Check batch temperature by using a portable pyrometer. The probe was stuck into the mix at several points and the average temperature was noted. This gave the dump temperature of the batch.
17. Check the batch weight.
18. Sheet by passing once through a mill with 5.0 mm nip.
19. Identify mixed batch and store for further testing.

The above procedures were followed in all the experimental runs made in this study.

Literature Cited.

(Chapter 6)

1. R.Haynes, Prog. of Rubb.Tech.,46,1 (1984)
2. G.M. Bristow, NR Technology, 12(3),45(1981)
3. C.M. Blow and C.Hepburn, 'Rubber Technology and Manufacture'
2nd Edition, Butterworth Group, England (1982)
4. ASTM Section 9:D1765
5. NR Technology, 9,41-42 (1978)
6. ibid, 11,15-16 (1980)
7. P.C. Ebell, Ph.D thesis Loughborough University (1981)
8. W.Y. Wan Idris, Ph.D thesis Loughborough University (1978)
9. M.L. Studebaker and J.R. Beatty, Rubb.Age, 107(5),131(1976)
10. G.E. Oconor and J.R. Putman, Rubb.chem.tech., 51,799(1978)
11. P.R. Van Buskirk, Rubb.Chem Tech., 48,577 (1977)
12. R.A. Fischer and Yates, 'Statistical Tables for Biological
and Medical Research',Oliver and Boyd Ltd.,
Edinburgh.

CHAPTER 7

RHEOLOGICAL BEHAVIOUR OF NR MIXES

7.1 Rheological Testing Methods.

7.1.1 TMS Rheometer.

The TMS rheometer is a variable speed rotational instrument which was developed at Avon Rubber Company, Melksham. It has the basic configuration of the Mooney Viscometer, but differs mainly in its rotor design. The material is injected into the testing cavity by means of a transfer moulding system as shown in figure 7.1. This system offers several advantages over the compression moulding cavity filling method used with the Mooney viscometer; i) freshly created material surfaces are in contact with the rotor and cavity, ii) the injection of material prior to test allows precise dimension of the cavity to be maintained, iii) the hydrostatic pressure of the material in the cavity can be controlled and iv) the system eliminates error due to the operator during filling of the test materials¹.

The biconical rotor is designed to reduce the influence of the edge section (couette region). Furthermore, it produces a constant shear rate over the rotor surfaces. The apex angle of each cone of the rotor is 168 degrees, developing a shear rate of 1 s^{-1} for each rotor revolution per minute (rpm). The rheometer can be used with rotors of different surface texture. A radial grooved rotor is used to derive shear stress-shear rate relationships for the no slip condition. Polished and smooth rotors are then used to predict the wall slip behaviour of a

material, which is normally encountered in polymer processing^{2,3}.

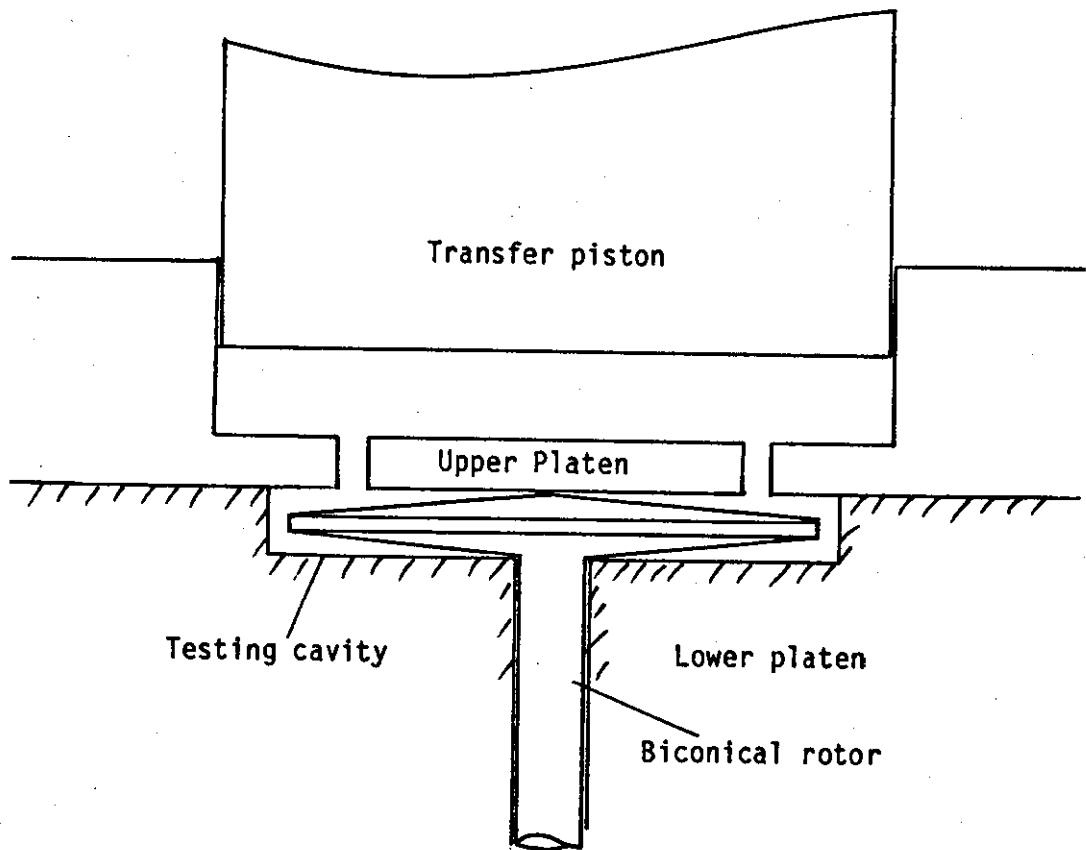


Figure 7.1 - Schematic diagram of the TMS rheometer¹.

In addition to the viscous and slip properties, the rheometer can measure stress relaxation behaviour. Turner and Bickley⁴ have also shown the effect of shear history of rubber by adopting a test routine developed for the rheometer.

Mechanical drives are used to vary the rotor rotation from

0.3 rpm to 44 rpm, corresponding to 0.3 s^{-1} and 44 s^{-1} shear rate respectively. A later version of the rheometer incorporates a DC stepper motor for the rotational variation. This allows precise control and programmable test routines to be made. In addition a higher shear rate of about 100 s^{-1} can be achieved⁵. However, in this study the mechanical drive model was used for rheological evaluation of the NR mixes. The testing temperature in the rheometer can vary from 60°C to 160°C .

7.1.2 Determination of Viscous Flow Behaviour.

The shear stress values at each shear rate were extracted from the raw plots generated by the rheometer, as shown in figure 7.2. A sequential increase in rotational rates from 3 s^{-1} to 44 s^{-1} enables the stress values to be determined. The sequence and procedure of rotational variation is shown in appendix V.

Generally, at low shear rate the shear stress builds up steadily to an equilibrium value whilst at higher shear rate the shear stress increases to a peak before levelling to a steady value^{4,11,18}. The steady stress value was taken as the 'typical' shear stress for each shear rate.

During testing of the NR mixes, a short period of 4 seconds was allowed at each rotational rate. Within such period the stress reaches a peak and decreases, where no steady stress value was obtained (refer to figure 7.2). As such, to allow consistency in establishing the shear stress at each shear rate level, the stress at 0.5 second after the peak was taken.

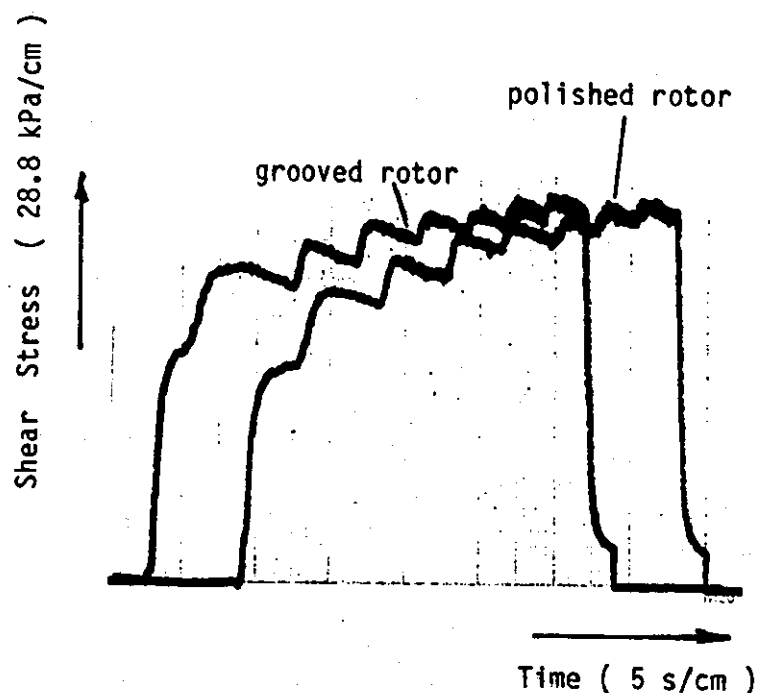


Figure 7.2 - Shear stress vs time at a range of shear rates.

The log shear stress - log shear rate plot of a material is commonly known as the 'flow curve'. The figure 7.3 shows typical flow curves of a mix tested with grooved and polished rotors. Within the shear rates of 3 s^{-1} and 44 s^{-1} , regression analysis was performed over the experimental values. For the no slip condition (grooved rotor), regression lines of correlation coefficients greater than 0.98 were observed for 72 % of the NR mixes. These mixes obey closely the power law relationship mentioned in chapter 4 (section 4.3.1) and expressed again by equation 7.1.

$$\tau = \eta_0 \dot{\gamma}^n \quad \text{.....7.1}$$

where τ - shear stress

η_0 - reference viscosity

$\dot{\gamma}$ - shear rate

n - flow or power law index

In this investigation, the lowest shear rate was at 3 s^{-1} . Thus the reference viscosity (apparent viscosity at 1 s^{-1}) of each mix was derived from the regression analysis. The y-intercept of the regression equation represents the reference viscosity of the mixes. Similarly the flow index n , was determined by the slope of the fitted straight line, represented by the regression coefficient. Apparent viscosity at other shear rates was derived from the equation

$$\eta_a = \eta_0 \dot{\gamma}^{n-1} \quad \text{.....7.2}$$

where η_a - apparent viscosity

7.1.3 Measurement of Wall Slip Behaviour.

The slippage of rubber stocks on hot metal surfaces is known to occur during processing, and it is found to be difficult to measure^{2,3}. Wall slip can be determined by the difference in shear stress values of the grooved and polished rotor of the TMS rheometer at constant shear rate. Under constant shear rate, Mooney⁶, Decker and Roth⁷ described that the lower shear stress values of the polished rotor was attributed to wall slip. Turner et.al¹ and Nadiri⁸ postulated that slip behaviour arises due to the viscous boundary layer formed between the rubber bulk and the metal wall.

The raw plot of figure 7.2 was again utilized, to extract

the shear stresses of the polished rotor over the whole range of shear rates. The log shear stress - log shear rate values were plotted and superimposed with the flow curves of the grooved rotor as shown in figure 7.3. Similarly, regression analysis was performed over the experimental values. It was observed that 73 % of the mixes have correlation coefficient of greater than 0.98, indicating a good fit.

Turner and Moore¹ proposed that wall slip is manifested by the difference in rotational rates of the grooved and polished rotor at constant shear stress level as shown in figure 7.3. The slip velocity in this case was determined by the expression

$$V_{st} = R (w_p - w_g) \quad \text{.....7.3}$$

where V_{st} - slip velocity at constant shear stress
 R - rotor radius
 w_p - angular velocity of polished rotor
 w_g - angular velocity of grooved rotor

However, in this study the author found that slip velocity determined at constant shear rate was more favourable and adaptable to the slippage theory to be discussed later. At constant shear stress, the difference in rotational rate of grooved and polished rotor can be attributed to both wall slip and the change in apparent viscosity of the compound. Furthermore, recognising that temperature rise during testing, the variation in apparent viscosity with temperature change at constant shear stress is much greater than that at constant shear rate^{9,10}. For this reason, the difference in stress level of the grooved and polished rotor at constant shear rate was utilized in evaluating the slip behaviour of the mixes.

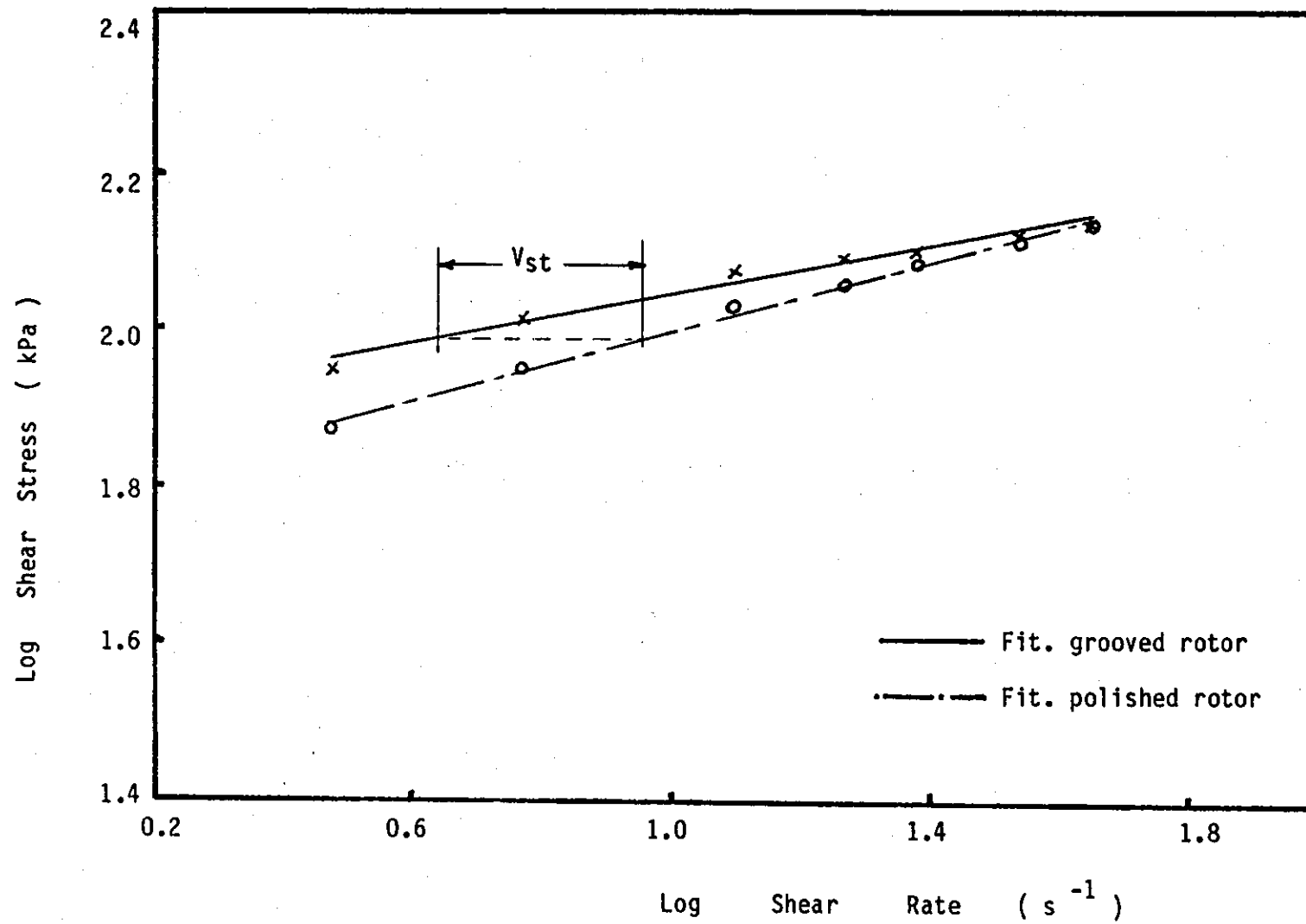


Figure 7.3 - Typical Flow Curves Of A NR Mix (R-20).

Moreover, it is in line with the theory developed by Mooney⁶ and Nadiri⁸ and will be described in the next section.

7.1.4 Measurement of Stress Relaxation Behaviour.

When a viscoelastic material is constrained to a constant deformation, the stress required to hold it decays gradually with time. Stress relaxation of the mixes tested in TMS rheometer was measured by stopping and clamping the rotor after a short period of rotation. The values of stress decay with respect to time can then be recorded. In each test, a shear rate of 10 s^{-1} was imposed on the mix for approximately 4 seconds before cessation of the flow. The amount of stress decay for a period of 8 seconds after cessation was recorded. A typical plot of stress decay with time is as shown in figure 7.4.

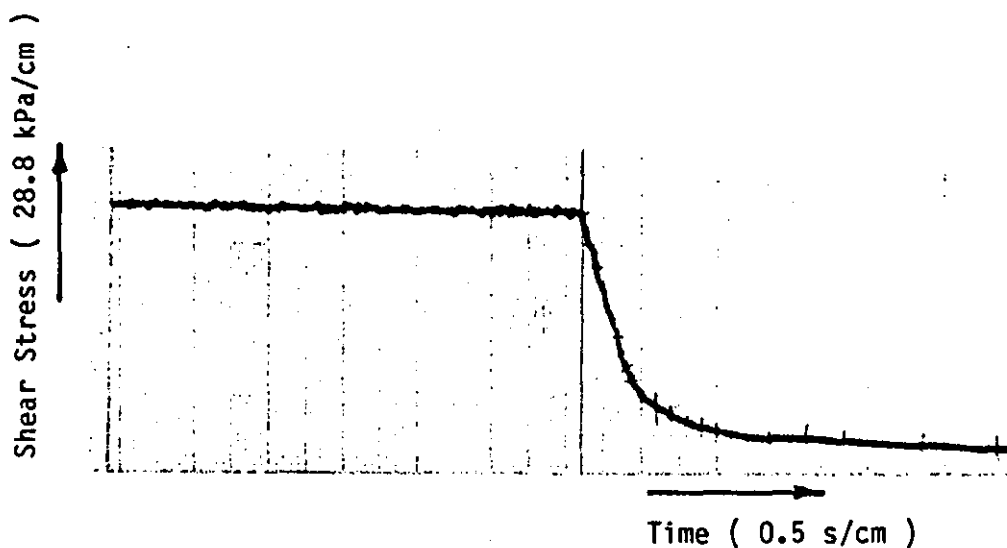


Figure 7.4 - Shear stress vs time at 10 s^{-1} shear rate.

An initial sharp drop in shear stress was observed for the first 0.5 second. A constant shear stress was normally reached 8 seconds after cessation. The shear stresses at an interval of

0.05 second were extracted from the above plot (figure 7.4) for the first 0.6 second after cessation. Stress values at an increase interval of 0.1, 0.25, 0.5 and 1 seconds were further noted until the full period of 8 seconds was reached.

A plot of log decay shear stress against log time was established as shown in figure 7.5. Regression analysis was performed on these experimental values. Correlation coefficients of greater than 0.98 were observed for 74 % of the NR mixes. These stress relaxation plots are necessary for evaluation of viscoelastic behaviour of the mixes which will be described later.

In addition, based on the rheological equation of a simple Maxwell model, the time required for the stress to decay to 37 % of its initial value represents the relaxation time of the material⁹. Consequently, the relaxation times of the NR mixes can be derived from the raw plots of stress decay versus time (as in figure 7.4).

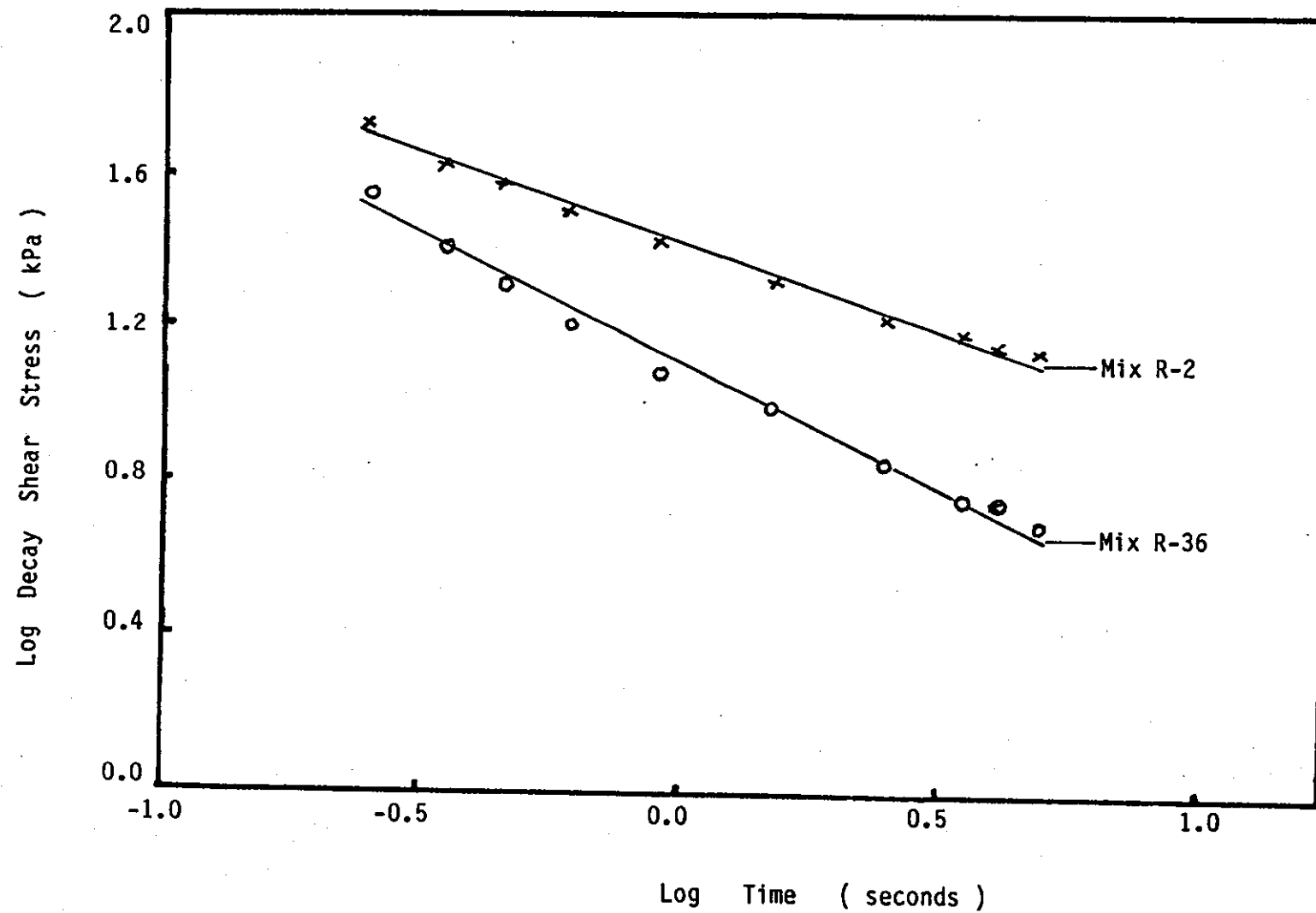


Figure 7.5 - Stress Relaxation Plots Of NR Mixes.

7.2 Analysis of Viscoelastic and Slip Behaviour.

7.2.1 Mechanical Modelling of Viscoelastic Behaviour.

As mentioned in chapter 4 (section 4.3.1), mechanical models can be used to simulate the viscoelastic behaviour of a material. A simple Maxwell model with a Hookean spring and power-law dashpot as shown in figure 7.6 was used in the rheological characterization of the NR mixes. The parameters of the model can be determined from the flow curves and the stress relaxation plots. Consequently, these parameters would be used to compare the rheological properties between the mixes studied.

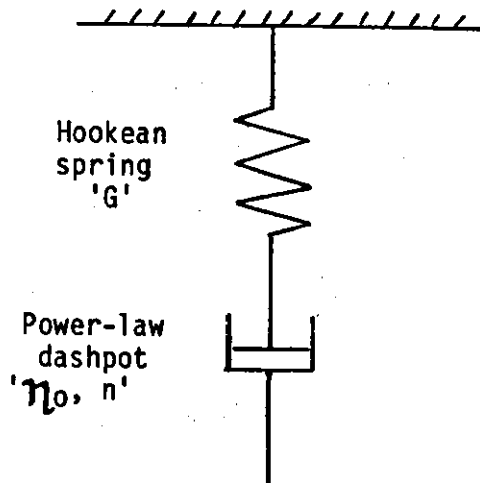


Figure 7.6 - Maxwell model with power-law dashpot.

The rheological equation of state for the model is defined by:

$$\frac{d\gamma}{dt} \text{ (total)} = \frac{d\gamma}{dt} \text{ (dashpot)} + \frac{d\gamma}{dt} \text{ (spring)} \quad \dots 7.4$$

For the dashpot the shear rate is related to shear stress by the familiar power law equation

$$\tau = \eta_0 \left(\frac{d\delta}{dt} \right)^n \quad \dots\dots\dots 7.5$$

and the Hookean behaviour of the spring is defined by

$$\tau = G \delta \quad \dots\dots\dots 7.6$$

Substituting equations 7.5 and 7.6 in to equation 7.4 and recognizing that $d\delta/dt$ (total) is zero in a stress relaxation experiment gives

$$\left(\frac{\tau}{\eta_0} \right)^{1/n} = - \frac{1}{G} \frac{d\tau}{dt} \quad \dots\dots\dots 7.7$$

The shear modulus G can be found by the following route:

$$\int \frac{d\tau}{\tau^{1/n}} = - \frac{G}{\eta_0^{1/n}} \int dt \quad \dots\dots\dots 7.8$$

giving, on integration

$$\frac{\tau^{-(1-n)/n}}{-(1-n)/n} = - \frac{G}{\eta_0^{1/n}} \cdot t + C \quad \dots\dots\dots 7.9$$

The constant of integration can be evaluated from $\tau = \tau_{\max}$ at $t = 0$, giving after rearrangement:

$$\frac{1}{\tau^{(1-n)/n}} - \frac{1}{\tau_{\max}^{(1-n)/n}} = \frac{(1-n)}{n} \frac{G \cdot t}{\eta_0^{1/n}} \quad \dots\dots\dots 7.10$$

It was observed experimentally that for time $t > 0.3$ second

$$\frac{1}{\tau^{(1-n)/n}} \gg \frac{1}{\tau_{\max}^{(1-n)/n}} \quad \dots\dots\dots 7.11$$

allowing the term containing τ_{\max} to be neglected. This simplifies equation 7.10 to

$$\frac{1}{\tau^{(1-n)/n}} = \frac{(1-n)}{n} \cdot \frac{G \cdot t}{\eta_0^{1/n}} \quad \dots\dots\dots 7.12$$

and rearranging

$$\tau = \left(\frac{1-n}{n} \cdot \frac{G}{\eta_0^{1/n}} \right)^{-n/(1-n)} \cdot t^{-(n/(1-n))} \quad \dots\dots\dots 7.13$$

so a plot of $\log \tau$ vs $\log t$ (the stress relaxation plot) gives a negative slope of $(n/(1-n))$ and an intercept D , expressed by

$$D = \left(\frac{(1-n)}{n} - \frac{G}{\eta_0^{1/n}} \right)^{-n/(1-n)} \quad \dots\dots\dots 7.14$$

The term $(n/(1-n))$ can be equated to a , the numerical value of the slope of the stress relaxation plot. Rearranging equation 7.14, the shear modulus G , can be determined from

$$G = \eta_0^{(a+1)/a} \cdot a \cdot D^{-1/a} \quad \dots\dots\dots 7.15$$

The reference viscosity η_0 was obtained from the flow curves described earlier.

7.2.2 Wall Slip Analysis in the TMS Rheometer.

Mooney⁶ developed the slippage theory that the slip velocity obeys a power law relationship as

$$V_s = k \tau^m \quad \dots\dots\dots 7.16$$

where V_s - slip velocity

τ - the shearing stress

k, m - material constants (characteristic of the elastomer and the surface on which it is slipping)

The above relationship was used to evaluate the amount of slip exhibited by the polished rotor in the TMS rheometer. The equation 7.17 was derived, and it enabled the shear stress of the polished rotor to be predicted.

$$\eta_a k \tau(r)^m + r \tan \alpha \tau(r) - \eta_a r w = 0 \quad \text{.....7.17}$$

where η_a - apparent viscosity

r - radius of rotor

$\tau(r)$ - shear stress of polished rotor at radius r

α - rotor cone angle

w - angular velocity of the rotor

The derivation of equation 7.17 can be referred to in appendix VI. Shear stress of the polished rotor $\tau(r)$, material constant k and m , can only be evaluated by numerical methods. A computer program as shown in appendix VII was utilized in solving this equation.

The closeness of the predicted shear stress to the experimental values of the polished rotor would depend on the right choice of the material constant k and m . Having established these constants, the slip velocity of the polished rotor can be calculated using equation 7.16.

The amount of computation required to predict the shear stress and the slip velocity of the polished rotor was enormous,

particularly for the whole series of the NR mixes. However, slip velocity can be approximated from the shear stresses and linear velocity of the grooved and polished rotors. An equation was derived in determining the slip velocity which takes the form of

$$V_{se} = V_L \times \frac{\tau_{ge} - \tau_{pe}}{\tau_{ge}} \quad \text{.....7.18}$$

where V_{se} - slip velocity derived from experimental result

V_L - linear velocity of the polished rotor

τ_{ge} - experimental shear stress of grooved rotor

τ_{pe} - experimental shear stress of polished rotor

For low shear rate of less than 12.5 s^{-1} , a reasonable approximation was observed between the slip velocity derived from stress function (equation 7.17), and the one calculated by equation 7.18. This is illustrated by column 3 and 4 of table 7.1. Larger deviations were observed between V_{se} and V_s at high shear rate. This may be due to the change in flow behaviour of the mixes at higher shear rate (shear stress), from primary laminar flow to secondary 'rotational' flow⁴. Further discussion on this behaviour will be discussed in the coming section.

Generally slip velocity V_{se} overestimated the calculated value V_s . Nevertheless, the velocity V_{se} was used in this study to characterize the slip behaviour of the mixes. In addition, the ratio of slip velocity V_{se} to the linear velocity V_L of the rotor, known as the velocity ratio was also used to describe this behaviour.

Table 7.1 - Slip velocity of mix number R-32.

Shear rate s ⁻¹	Linear Vel. mm/s	Slip Vel. predict. from equation 7.17, V _s mm/s	Slip Vel. predict. from equation 7.18, V _{se} mm/s	Velocity ratio.	% tage error of V _s to V _{se}
3.0	7.2	0.83	1.0	13.9	17.0
5.9	14.2	1.23	1.5	10.5	18.0
12.5	30.1	1.67	2.05	7.2	18.5
18.5	44.6	2.33	2.1	7.2	11.0
23.5	57.3	1.14	1.98	4.8	42.0
34.5	83.1	0.75	1.2	1.4	38.0
44.0	107.0	0.02	0.06	1.4	67.0

7.3 Discussion of Results.

7.3.1 General form of Rheological and Slip Behaviour of NR Mixes.

During testing of SMR 20 and the associated mixes in the TMS rheometer, an initial peak rise in shear stress was observed when sequential increases in rotational rates were made. The stress drops gradually after reaching the peak, and does not attained an equilibrium value within the testing period. However, a characteristic stress level was determined at each shear rate, using the procedure described previously, giving consistency in establishing the flow curves of the mixes.

The behaviour of the NR mixes differed from that observed with compounds of PVC/Nitrile¹¹, Butyl¹², and SBR¹⁴ when tested

in the TMS rheometer, where rapid drop in the stress levels after the peak were observed. This transient peak behaviour of rubber is attributed to its non-linear viscoelastic effect which is more pronounced at larger deformation^{18,21}.

As mentioned earlier, 72 % of the flow curves have a high correlation coefficients (0.98). However, deviation from the power law relationship was observed, where 20 % of the curves exhibited inflexion points occurring between 10.0 s^{-1} to 15.0 s^{-1} shear rate. Consequently, there is a change in gradient of the curves indicating this deviation as shown in figure 7.7. Within the shear rates investigated, it was found insufficient to establish numerically the amount of gradient change in these flow curves. Only two points of the curves at low shear rates indicate the difference in gradient. Perhaps additional tests at lower shear rates ($<3 \text{ s}^{-1}$) would have allowed this difference in gradient be established. Nevertheless, the best fitted straight lines were plotted over the experimental values.

The flow index n , indicates the amount of deviation from the Newtonian flow behaviour. It varies from a minimum value of 0.02 to a maximum value of 0.27, which were exhibited by mixes R-24 and R-43 respectively. By referring to the experimental design matrix in appendix I, these mixes (R-24 and R-43) differed mainly in types of black (B) and the black loading level (L). Both of these variables were found to have a strong influence on flow index n . However, the variation of the flow index n with the variables studied will be discussed in the forthcoming section.

The flow index n also shows the rate of decrease in

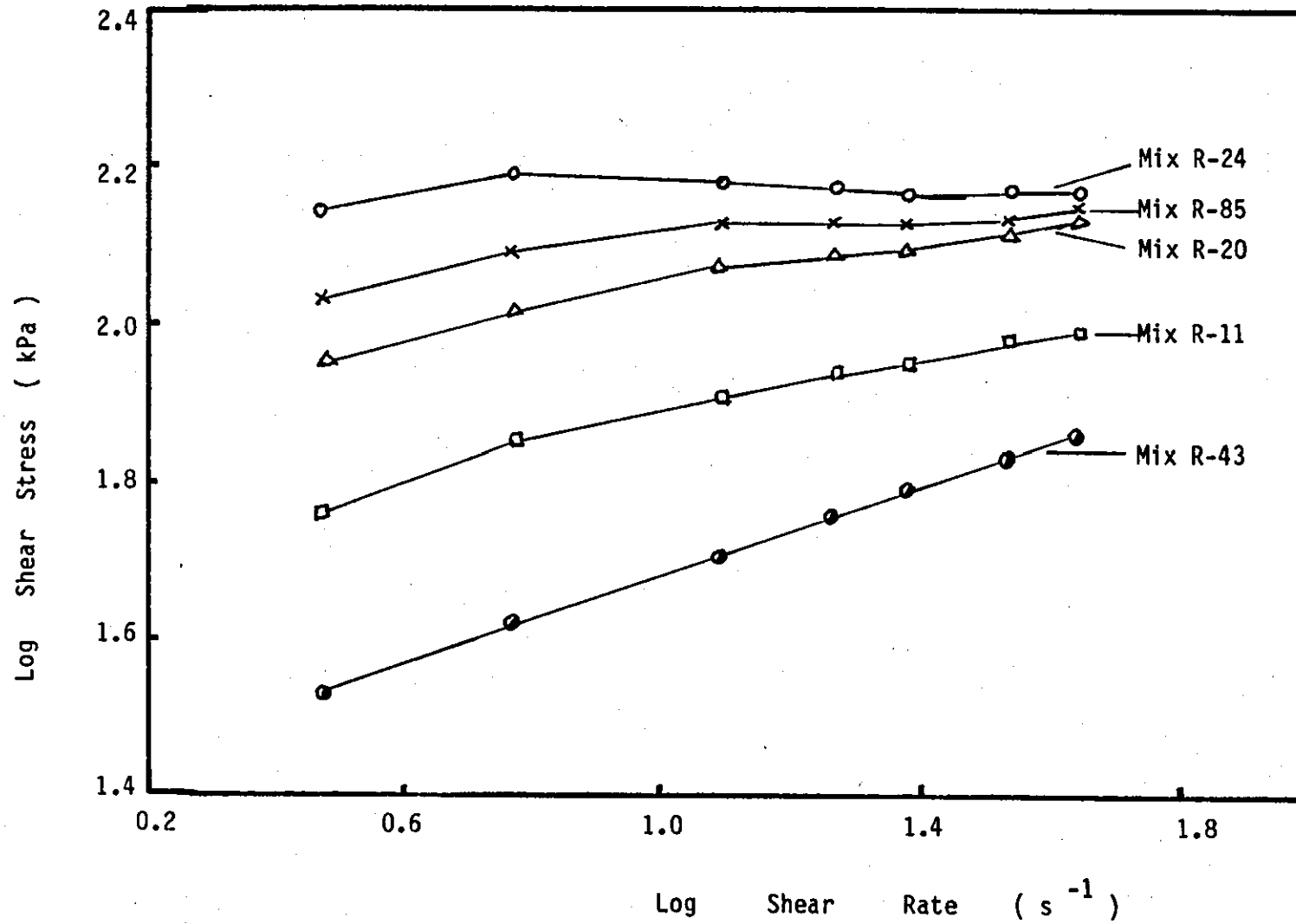


Figure 7.7 - Flow Curves Of Mixes With Changing Of Slopes.

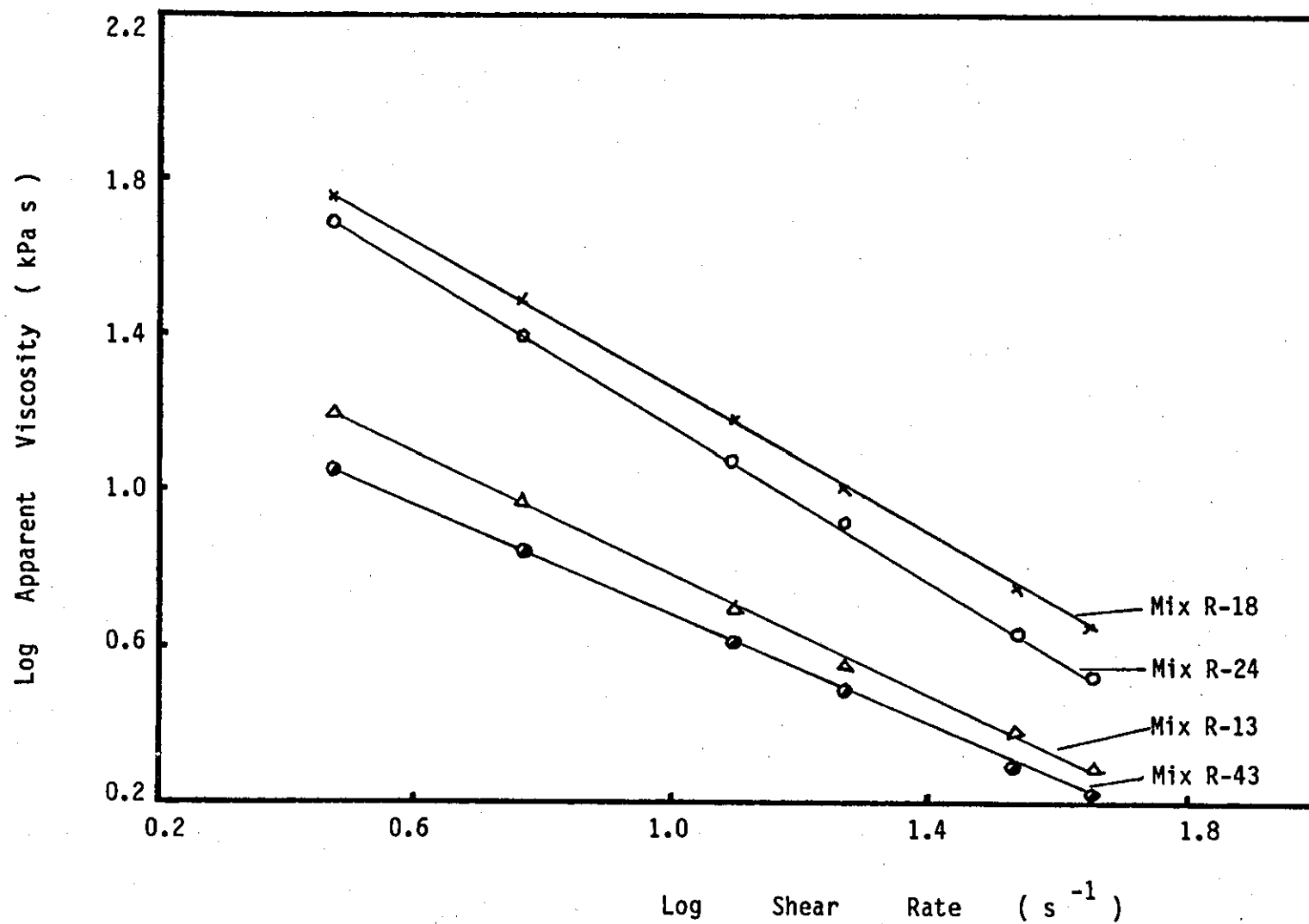


Figure 7.8 - Apparent Viscosity Of NR Mixes.

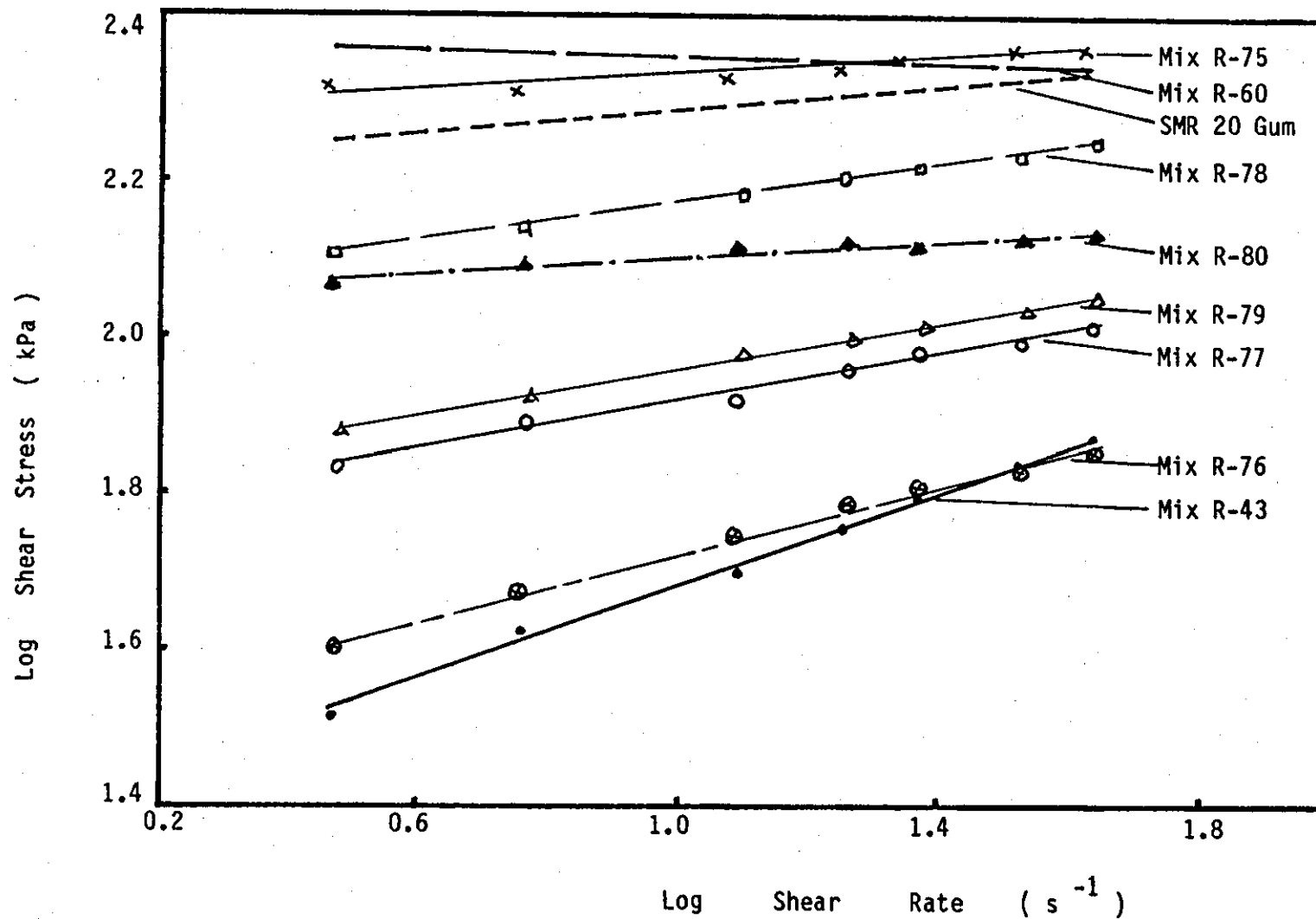


Figure 7.9 (a) - Flow Curves Of Mixes At Extreme Levels Of Material Variables.

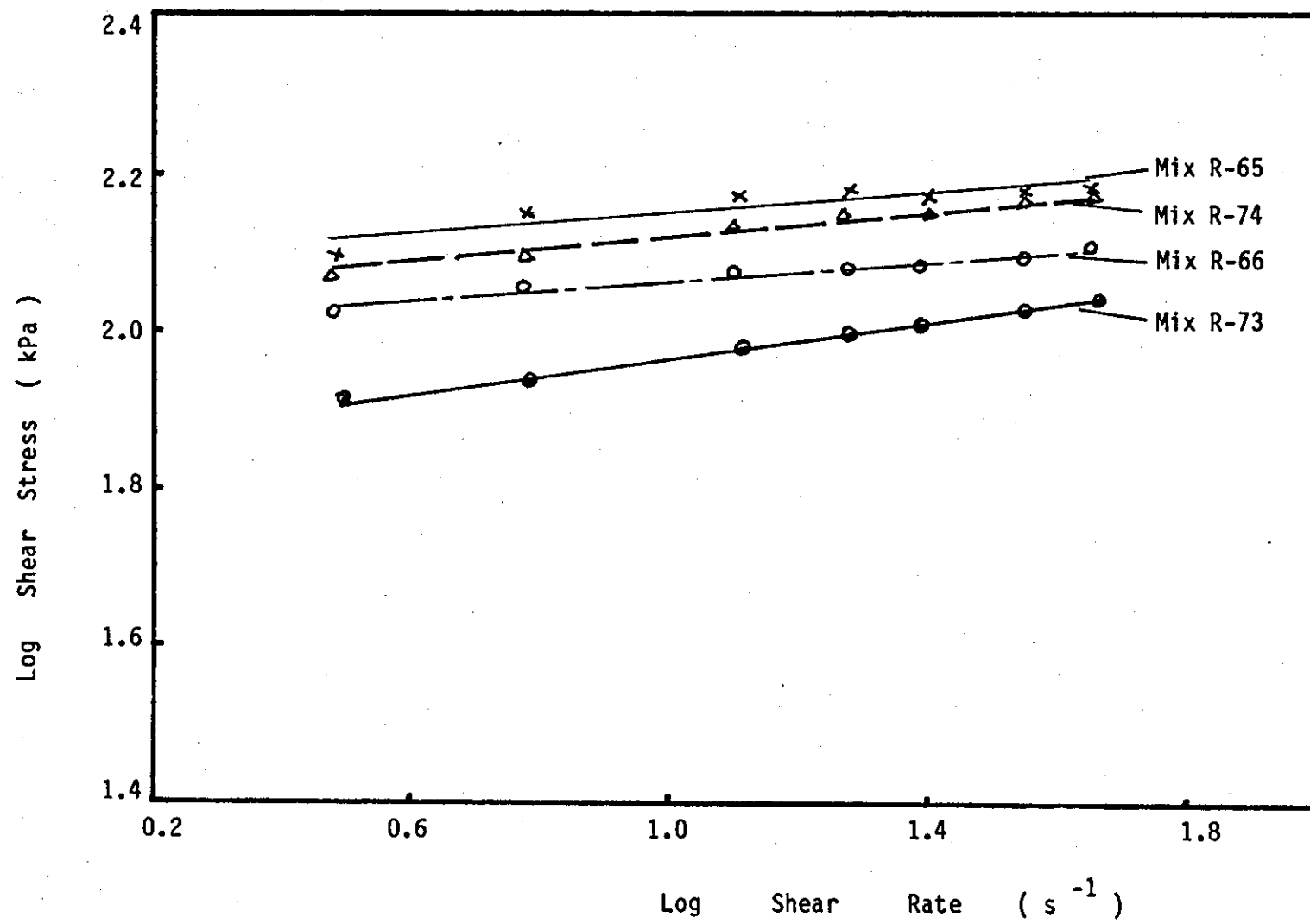


Figure 7.9 (b) - Flow Curves Of Mixes At Extreme Levels Of Machine Variables.

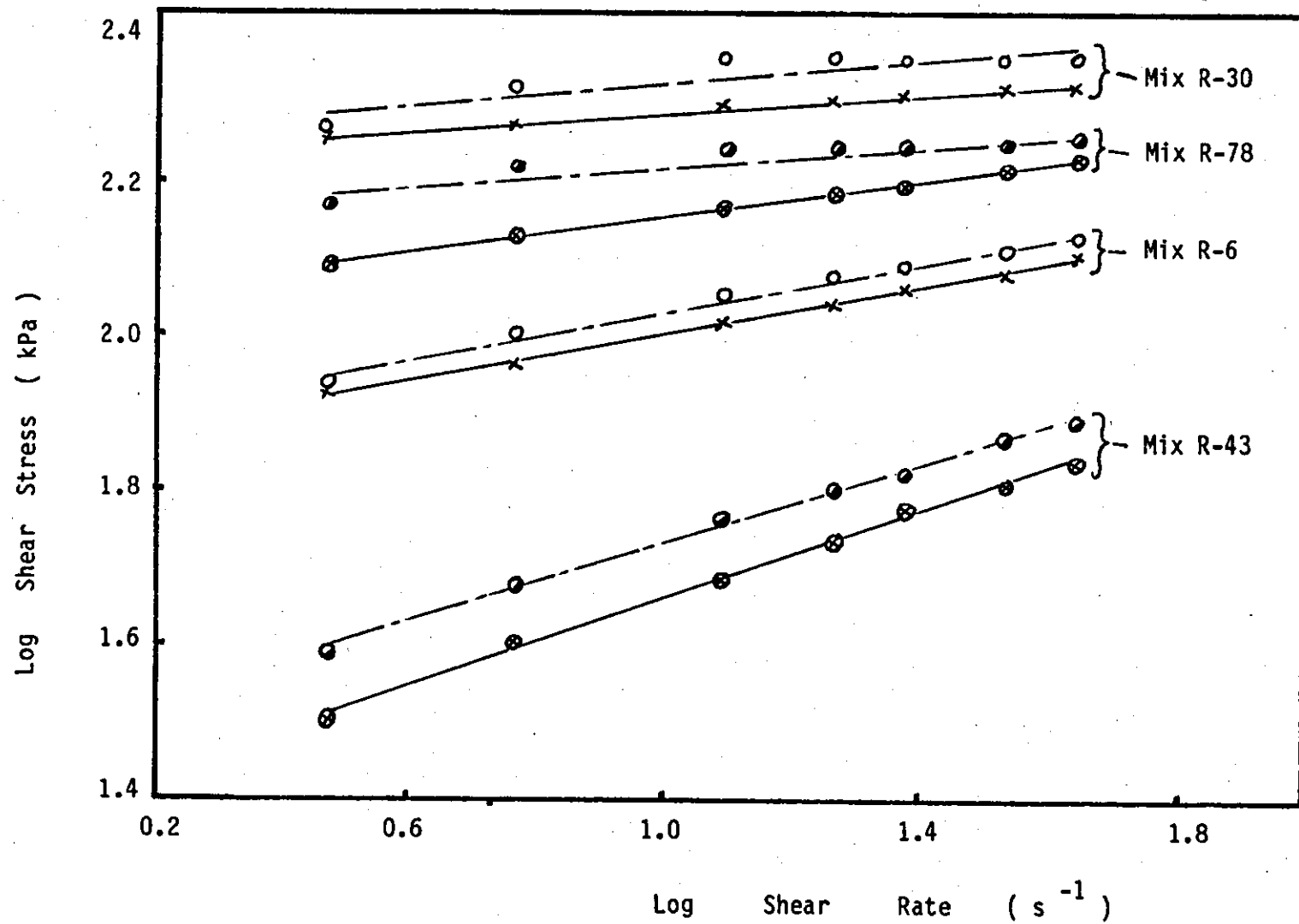


Figure 7.10 - Flow Curves Of Polished Rotor Above Grooved Rotor.

apparent viscosity at increasing shear rate. A reduction by 90 % and 85 % in apparent viscosity was observed for mixes R-24 and R-43 respectively, between the values of 3 s^{-1} and 44 s^{-1} shear rates. The variation of apparent viscosity with shear rates are shown in figure 7.8.

The flow curves of the star point mixes, at each two extreme levels of both the material and machine variables are shown in figure 7.9 (a) and 7.9 (b) respectively. All the mixes exhibited flow behaviour within the range defined by the flow curves at high ($L = 50.0 \text{ phr}$) and low ($L = 0 \text{ phr}$) carbon black loading level, represented by mixes R-75 and R-76 respectively.

In general, based on these star point mixes the material variables strongly influenced the flow behaviour, particularly the filler loading level. The deviation from Newtonian behaviour was greater for small particle size and highly black loaded compounds. Amongst the machine variables unit work and ram pressure affect the flow behaviour considerably. However, the main and combined effects of these variables on flow properties will be discussed further in the coming section.

A peculiar phenomenon was observed in the log shear stress - log shear rate curves of the polished rotor (slip condition). About 20 % of the mixes were found to have shear stress values above the no slip condition (grooved rotor) at each shear rate level. This behaviour as shown in figure 7.10 occurred mainly for flow curves of mixes with high black concentration, leading to higher shear stress at each shear rate.

As mentioned earlier, slip behaviour arises due to the formation of a viscous boundary layer. At high shear stress,

there may be a reduction or non-existence of this layer, resulting in a decrease or absence of the wall slip. Recently, Turner and Bickley⁴ described the change of slopes of flow curves at increasing shear rates is due to the formation of the secondary 'rolling' flow. They observed this phenomenon experimentally by using coloured rubber tested in the capillary and TMS rheometer. With increasing shear rates the flow changes from primary laminar flow to secondary 'rolling' flow.

The flow line in the TMS rheometer for both the laminar and 'rolling' flow can be safely assumed to be as in figure 7.11. For the no-slip condition (grooved rotor), initially laminar flow existed, with further increase in shear rate the change to 'rolling' flow may occur, reducing the shear stress values. Whilst for the slip condition (polished rotor), laminar flow persists and thus no change in the flow characteristic. The onset of laminar to 'rolling' flow may occur at a particular shear rate value, and it varies for different compounds.

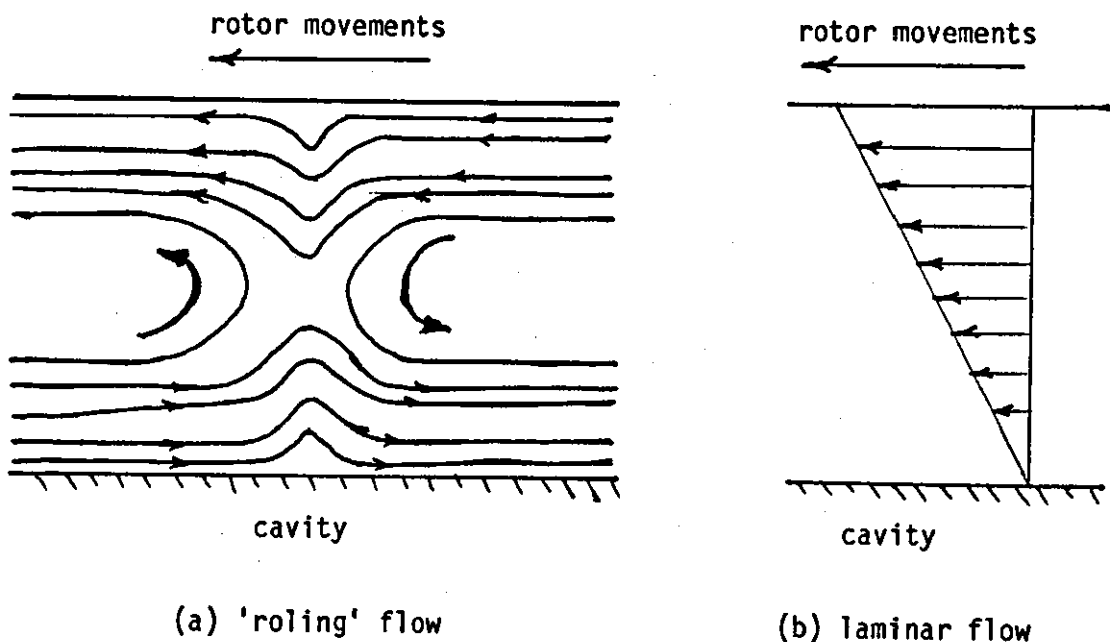


Figure 7.11 - The flow line in TMS rheometer⁴.

Base on the above hypothesis, the phenomenon where the flow curves of the polished rotor are above those of the grooved rotor may be due to early onset of 'rolling' flow from the laminar flow behaviour. As such, lower shear stress values of the grooved rotor were observed as compared to the polished rotor at the same shear rate. Nevertheless, further investigation is required to confirm these phenomenon.

Similarly, the cross-over of the polished rotor curves as shown in figure 7.12, may be attributed to the above hypothesis. About 15 % of the mixes exhibited such cross-over points in their flow curves. As the shear stress increases, the viscous boundary layer may be reduced due to the onset of the secondary 'rolling' flow. In this case, slip velocities at shear rate levels of up to the cross-over points were determined. Whilst zero slip velocity was assumed for curves which have shear stresses for which the polished rotor exceeded the grooved rotor shear stress values.

In this study, it was observed that the slip velocity increases rapidly up to a maximum value with increasing shear rate, as shown in figure 7.13. Some mixes do not attain the maximum slip velocity within the shear rate investigated. These findings conform with the results established by Mooney⁶ and Turner et.al⁴. Here again the drop in slip velocity at increasing shear rate may be attributed to similar hypothesis. Further investigation would be necessary to correlate the change in the flow behaviour from laminar to 'rolling' flow with respect to the slip behaviour of the compound.

However, it is important to note that slip analysis is only valid when laminar flow occurs with both the grooved and polished rotors of the TMS rheometer.

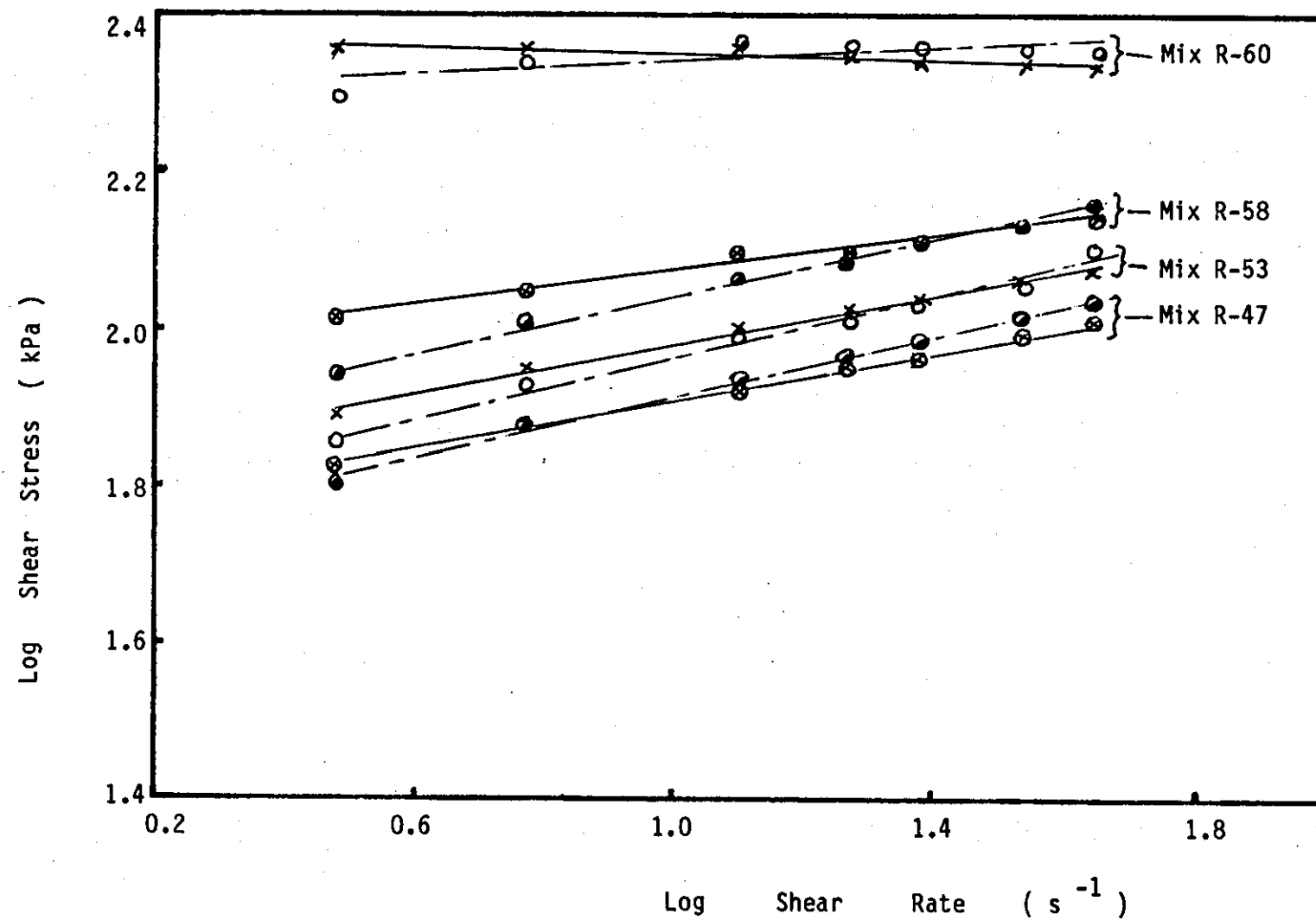


Figure 7.12 - Flow Curves Of Polished Rotor Crosses Grooved Rotor.

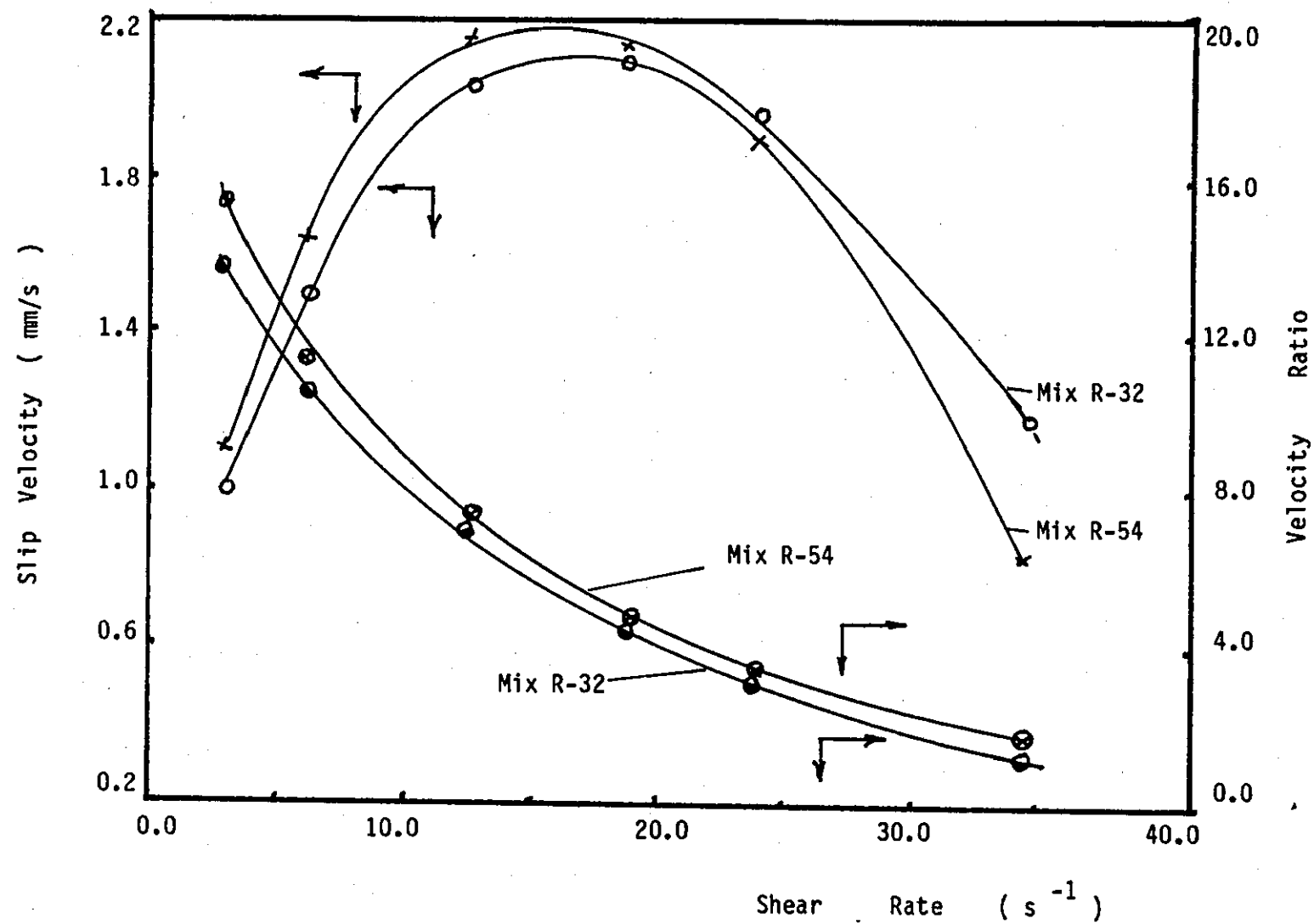


Figure 7.13 - Variation Of Slip Velocity And Velocity Ratio With Shear Rates.

7.3.2 General Form Of Viscoelastic Behaviour.

Viscoelastic behaviour of the NR mixes can be described by stress relaxation experiments. An approximately linear zone of the plot log decay shear stress against log time was utilized to characterise this viscoelastic behaviour. The linear zones vary between mixes, and were observed to be within 0.3 seconds and 7 seconds after cessation of flow. A high correlation coefficient (0.98) was obtained from the straight lines drawn within this linear zone. Negative slopes were observed, with a maximum value of 0.96 and a minimum value of 0.43 for mixes R-13 and R-18 respectively. Stress relaxation plots of other mixes were within these limits. Typical stress relaxation plots are shown in figure 7.14.

The mechanisms of stress relaxation have been distinguished to be due: i)the presence of irrecoverable viscous flow in the material, ii)the presence of reinforcing fillers, iii)the breakdown of crosslinked network due to chemical reaction and iv)the physical process in the attainment of equilibrium in the crosslinked network by rearrangement of the whole chains or filler aggregates^{13,23}. However, mechanism (i) and (ii) are more relevant in ascribing the relaxation behaviour of the unvulcanised mixes in this study. This behaviour was characterized by the slopes of the relaxation curves (the relaxation rate) and by the time for 37 % (derived from single Maxwell model) reduction in shear stress.

The combination of viscous and elastic effects on the relaxation behaviour of the mixes can be seen in both figures 7.8 and 7.14. A comparatively higher viscosity compound, such as mix R-18 would have a longer relaxation time and lower

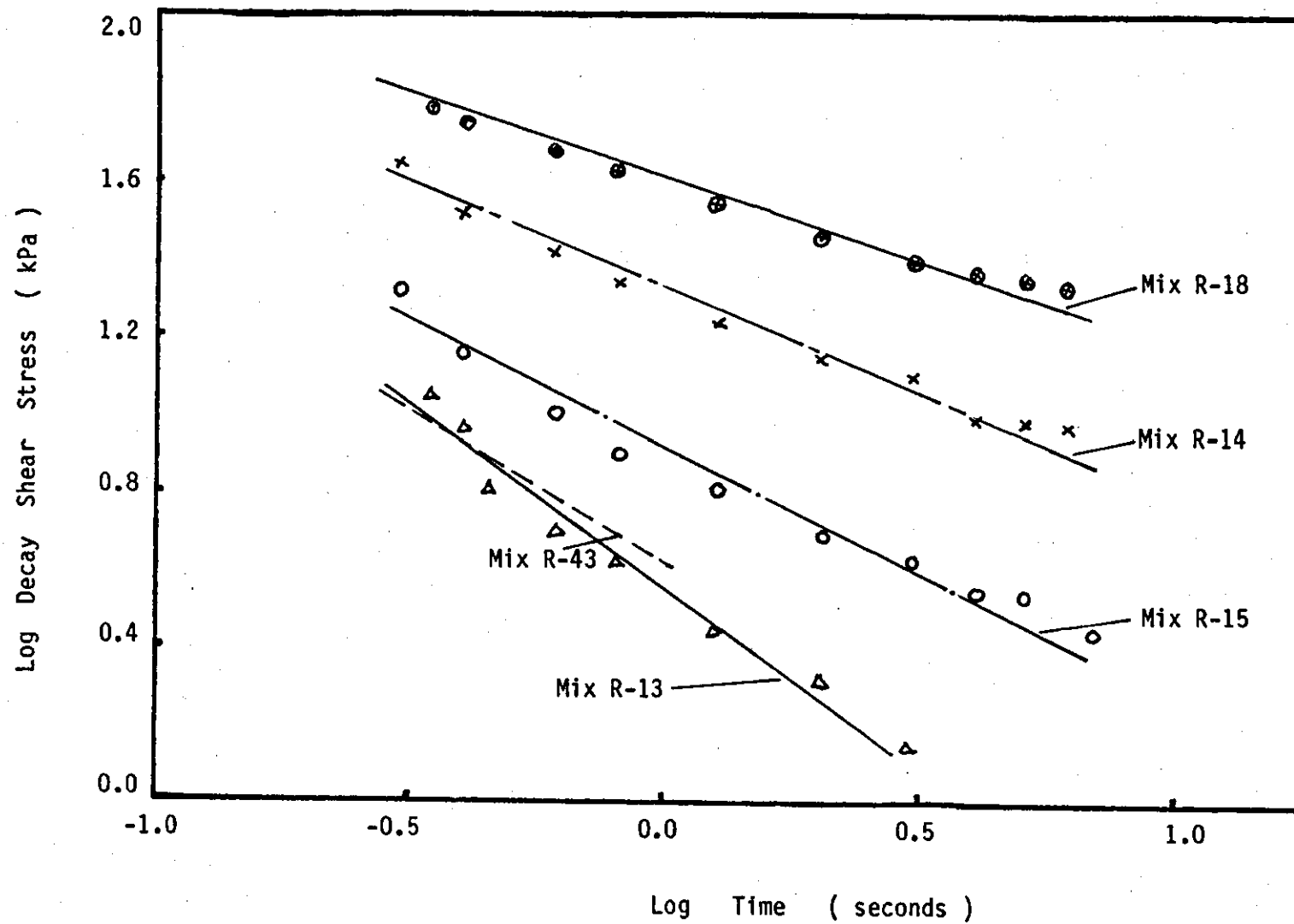


Figure 7.14 - Stress Relaxation Plots Of NR Mixes.

relaxation rate. Lower viscosity compounds such as mix R-43, have a shorter relaxation time and high relaxation rate¹⁵. However, the difference in types of black and their loading level between these mixes (R-18 and R-43) would obviously have great effect on the filler-rubber interaction^{17,22} which causes such variation in the viscoelastic properties.

Table 7.2 - Viscous and elastic value of mixes.

Mixes	Flow index 'n'	Apparent Viscosity at 10 s ⁻¹	Shear Modulus kPa.	Relax. Rate*	Relax. Time s.
R-13	0.23	4.9	340.8	0.94	0.3
R-18	0.07	13.9	1179.1	0.43	0.45
R-24	0.02	11.8	2547.6	0.59	0.33
R-43	0.27	4.0	171.9	0.77	0.28
R-75	0.05	17.17	1264.2	0.45	0.5

* slope of log decay shear stress vs log time plot.

The mechanical model in section 7.2.1 predicts the shear modulus G , of the mixes. Higher shear modulus increases the relaxation time and reduces the rate of relaxation. Table 7.2 illustrates the variation in viscous and elastic values of the above mentioned mixes.

7.3.3 Effect Of Temperature.

Temperature has an important effect on the rheological properties of a rubber compound. The flow curves of a centre point mix, with temperature varying from 80 to 140 °C, are shown in figure 7.15. Shearing stress decreases with increasing temperature at all levels of shear rates. A reduction by 57 % and 35 % in shear stress was observed at 3 s⁻¹ and 44 s⁻¹ shear rate respectively, with increasing temperature from 80 to 140 °C. The flow index n , increases with increasing temperature and it varies from 0.05 to 0.21 at 80 and 140 °C respectively.

The variation in apparent viscosity with changes in temperature was greater at low shear rates. A converging band of this variation was observed with increasing shear rate as depicted in figure 7.16. A reduction by 92 % in apparent viscosity with increasing shear rate from 3 s⁻¹ to 44 s⁻¹ was observed at temperature 80 °C based on the apparent viscosity at 3 s⁻¹ shear rate. At 140°C, a slightly lower reduction in apparent viscosity by 88 % was observed for similar increase in shear rate. These results could be an artifact of shear heating at higher shear rate (shear stress). The apparent viscosities of the mix R-85 at different temperatures and shear rates are shown in table 7.3.

The elementary mechanism of the flow process consists of accumulation of energy in the molecule required to overcome the barrier to transition from one equilibrium position to the next. This accumulation of energy is called the energy of activation¹⁴. As mentioned in chapter 4 (section 4.3.1), the activation energy derived at constant shear rate for

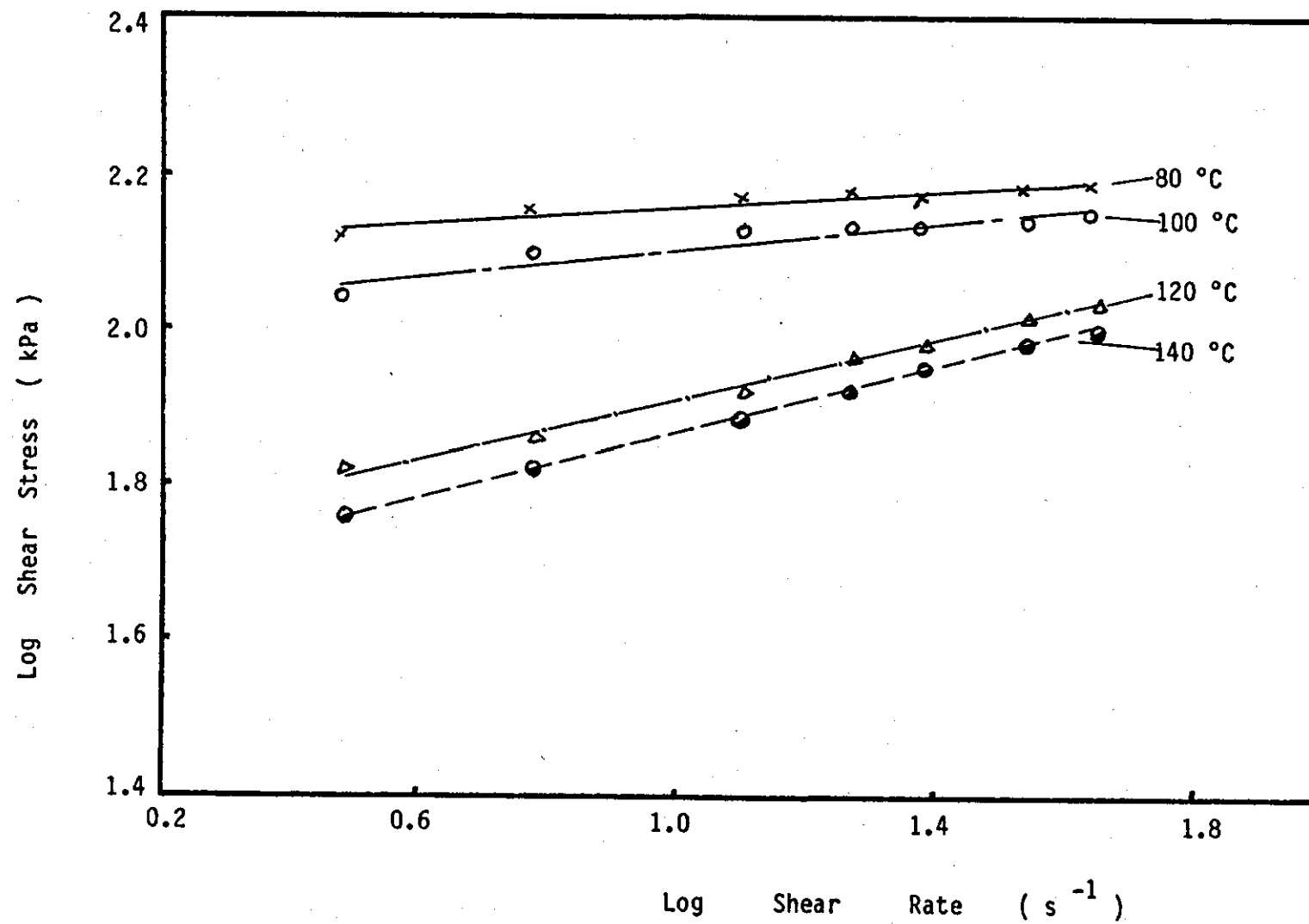


Figure 7.15 - Flow Curves Of Centre Point Mix At Different Temperatures.

non-Newtonian material was preferred than at constant shear stress⁹, particularly in describing its temperature viscosity behaviour.

Table 7.3 - Viscosity variation with temperature.

Shear rates sec.-1.	Testing Temperatures (° C)			
	80.0	100.0	120.0	140.0
	Apparent Viscosity (kPa s)			
1.0	127.6	103.6	52.6	45.6
3.0	44.9	37.8	21.5	19.1
5.9	23.6	20.3	12.4	11.2
12.6	11.6	10.2	6.7	6.2
18.5	8.0	7.1	4.9	4.5
35.5	4.4	4.0	3.0	2.8
44.0	3.5	3.2	4.0	2.3

The activation energy was determined from the Arrhenius formula expressed by

$$\eta_a = A \exp E/RT \quad \text{.....7.19}$$

where η_a - apperent viscosity

A - material constant

E - activation energy

T - absolute temperature (°K)

R - gas constant

On the basis of the above equation 7.19, log apparent viscosity was plotted against the reciprocal of the absolute temperature at fixed shear rate. This is shown in figure 7.17.

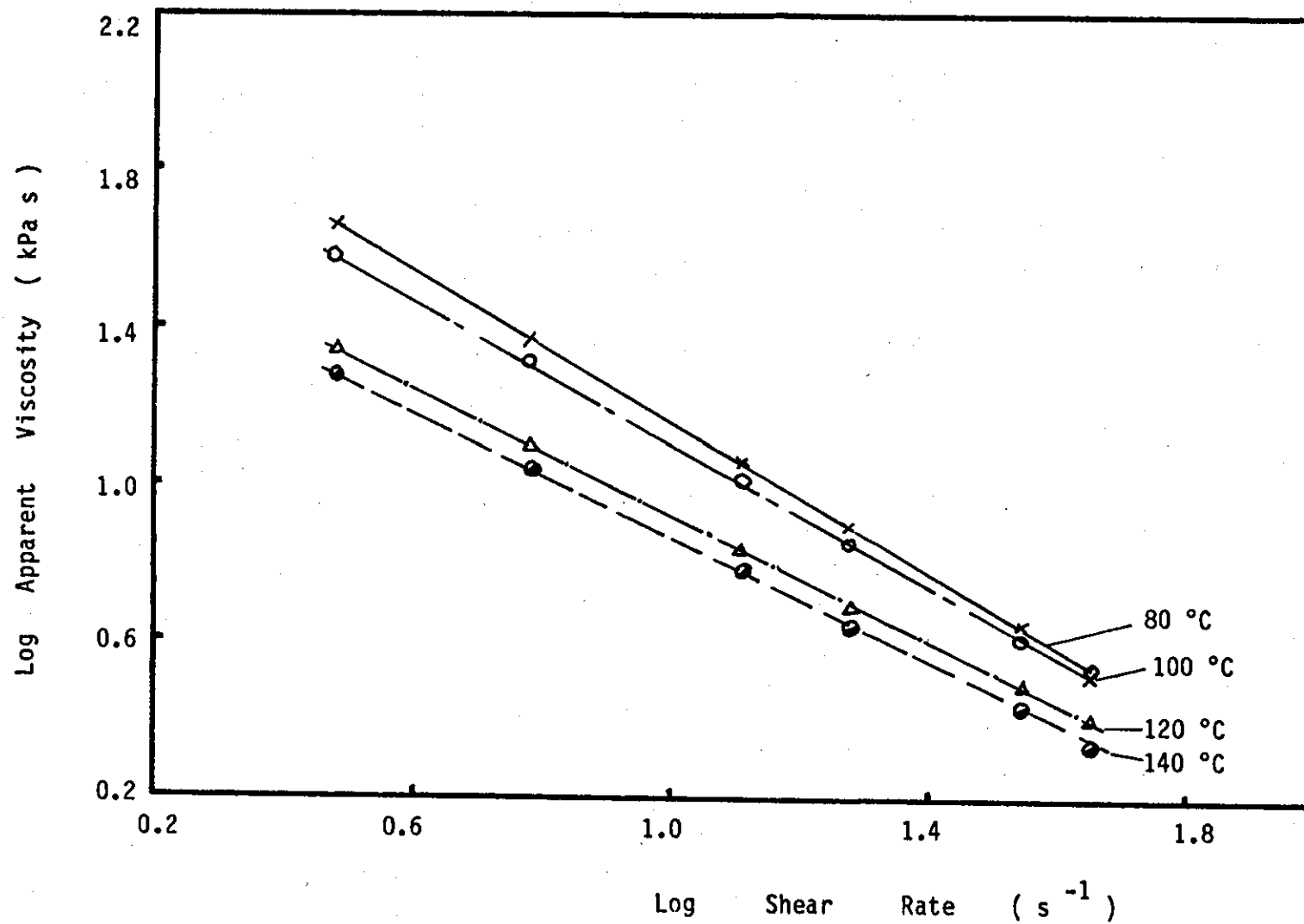


Figure 7.16 - Variation Of Apparent Viscosity With Temperatures Of A Centre Point Mix.

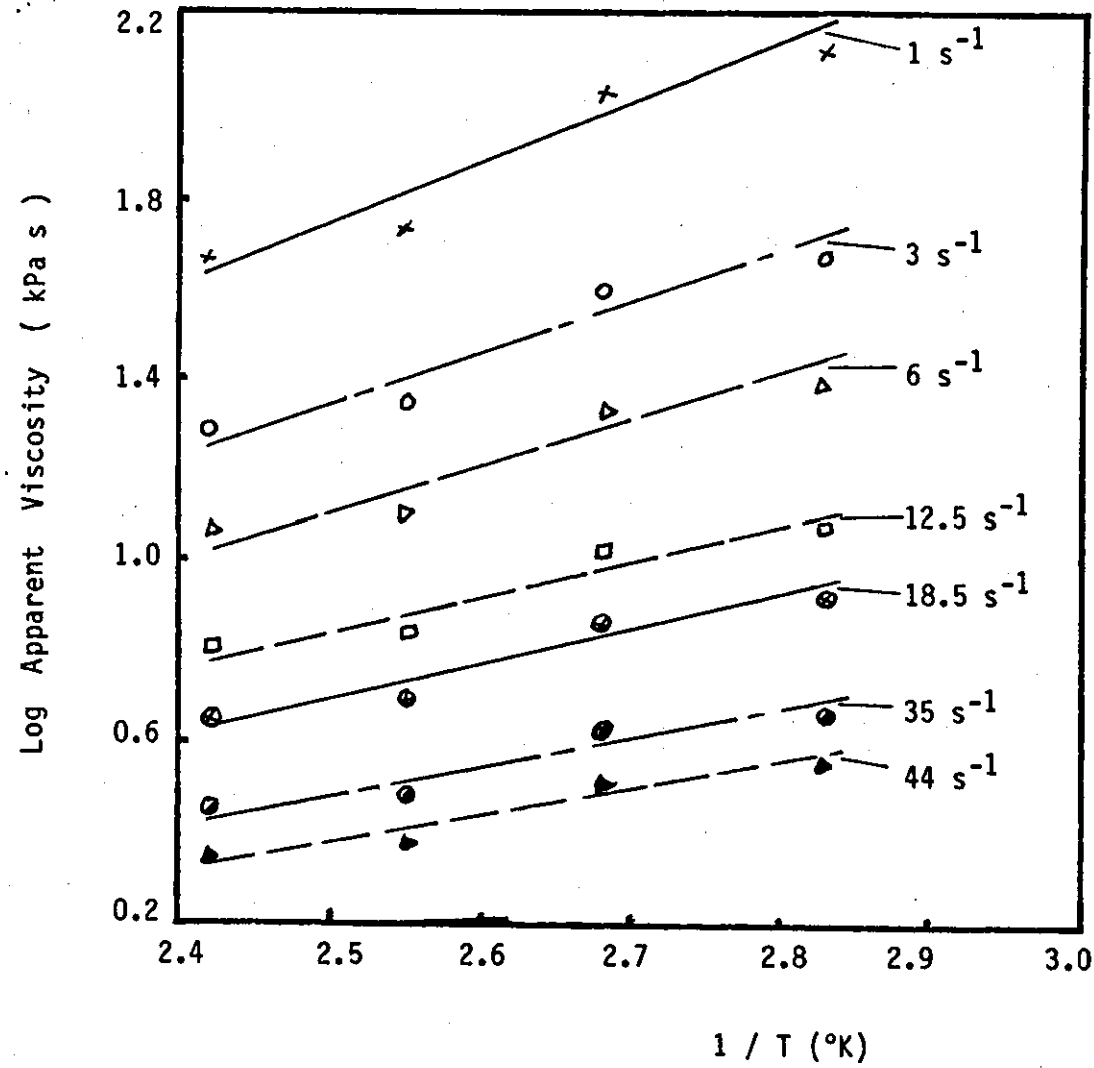


Figure 7.17 - Variation Of Apparent Viscosity With 1/T At Different Shear Rates.

The activation energy was obtained by multiplying the slope of the best straight line plotted over the experimental values by 2.3 (ln to log conversion factor). Within the shear rates investigated, the flow activation energies are listed in table 7.4.

Table 7.4 - Activation energy at constant shear rate.

Shear rates s^{-1}	Activation Energy kJ/mol
1.0	7.57
3.0	0.42
5.9	0.21
12.5	0.085
18.5	0.055
35.0	0.027
44.0	0.02

7.3.4 Influence Of Mixer Operating Variables.

As mentioned in chapter 3 (section 3.2), the main effect of a variable should be interpreted individually only if there is no evidence that the variable interacts with other variables. The statistical analysis performed earlier would indicate these effects. Moreover, the most influential variables can therefore be identified accordingly.

In this study, the mixer operating variables were found to have less influence on the flow behaviour of the NR mixes, as compared to the material variables (refer to appendix II).

Furthermore the interactive effects observed between the mixer variables on this behaviour were smaller than the main effects. Among these variables, unit work and ram pressure showed a strong influence on the reference and apparent viscosities of the NR mixes.

At ram pressure 0.28 MPa, increasing unit work reduces the reference viscosity substantially, irrespective of rotor speed and fill factor as shown in figure 7.18 (a). A lesser reduction in reference viscosity at this condition was observed at high ram pressure. Considering the shading diagram number 5 of figure 7.18(a) and (b), at the centre points of both diagrams, increasing unit work from 700.0 to 900.0 MJ/m³ reduces the reference viscosity by 18 % (from 102.0 to 84.0 kPa s), at ram pressure 0.28 MPa, whilst the reference viscosity remains unchanged at 102.2 kPa s for ram pressure 0.41 MPa.

The effect of increasing ram pressure is to increase the contact force between the mixture and the rotor surface. At high ram pressure, effective mixing begins much earlier in the cycle and because the stock temperature is lower at this point, the viscosity is higher. At low ram pressure the rotors tend to slip past the stock, increasing its temperature and leading to a lower viscosity, as compared to at high ram pressure, for the same amount of unit work²⁵.

Varying the rotor speed, particularly at higher unit work (>700.0 MJ/m³) does not change the reference viscosity, except at high coolant temperature (65°C), where increasing rotor speed would cause a reduction in reference viscosity. At such high rotor speed and high coolant temperature the unbalance of heat energy may occur²⁴, the amount of heat build up in the stock being greater than the amount of heat removal, leading to

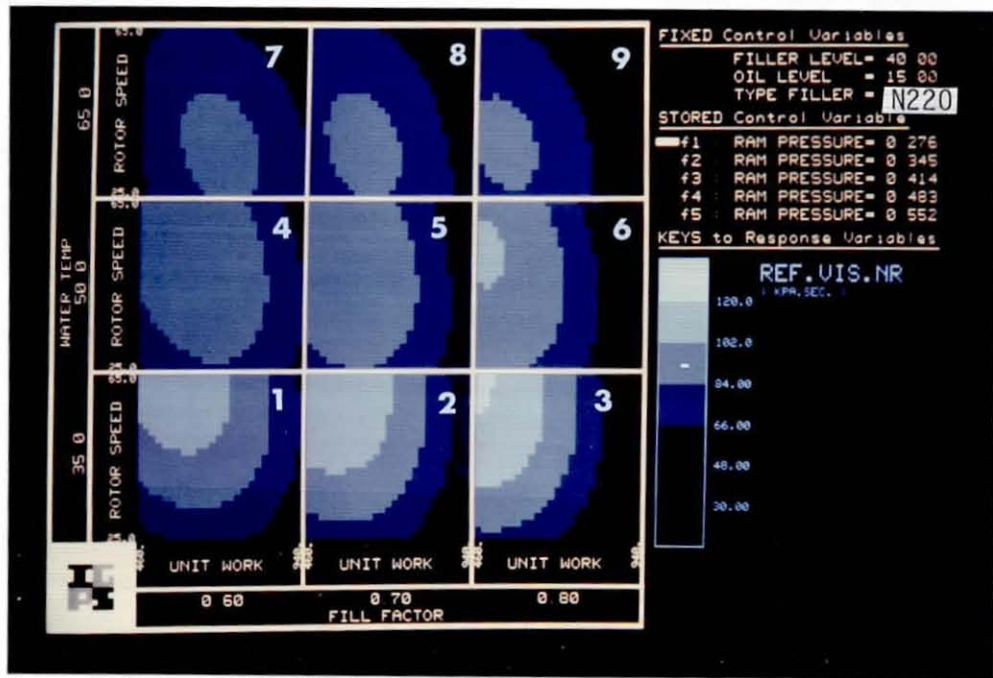


Figure 7.18 (a) - Influence of mixer variables on reference viscosity at 0.28 MPa ram pressure.

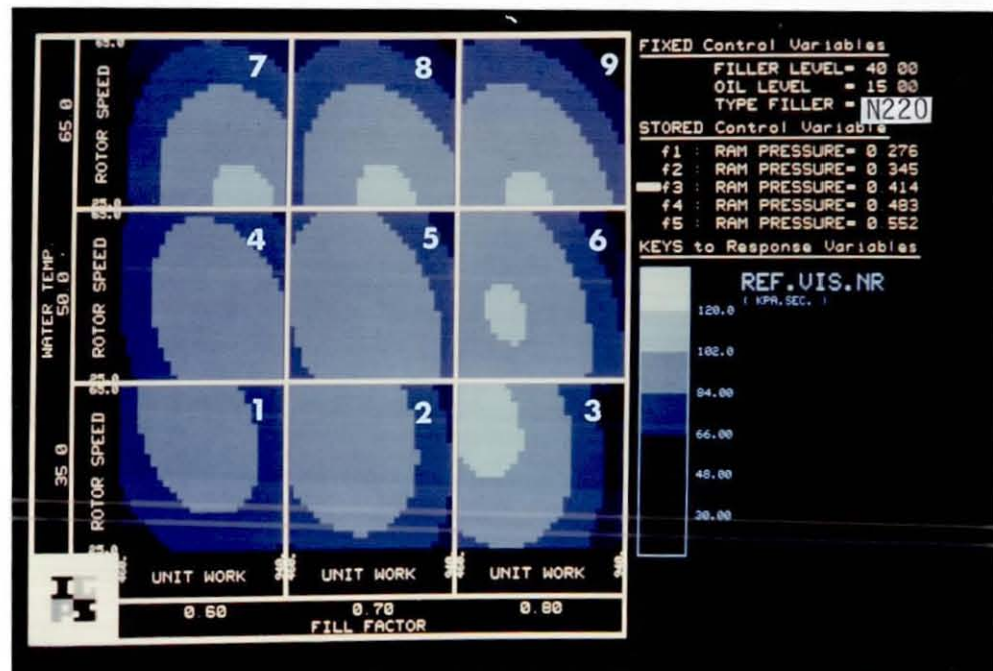


Figure 7.18 (b) - Influence of mixer variables on reference viscosity at 0.41 MPa ram pressure.

a reduction in viscosity. This argument is supported by high dump temperature of the mixes at this conditions and this will be discussed in chapter 9.

Considering the non-axial variables of figure 7.18, increasing fill factor from 0.6 to 0.8 showed a drop in viscosity at high unit work ($>700.0 \text{ MJ/m}^3$). Reference viscosity increases with increase in fill factor at low unit work. At low unit work, the material experienced a low level of dispersive mixing, thus with additional loading, the viscosity increases. The phenomenon of viscosity increase with increasing fill factor at low unit work was more pronounced at high shear rate (i.e. at 6 and 35 s^{-1} in TMS rheometer).

By inspection of the diagrams in figure 7.18, the variation of viscosities were affected more by changing the amount of energy input to the mixer as compared to the change in ram pressure and rotor speed.

Similarly, it was observed that the mixer operating variables have less influence on the flow index n , as compared to the influence of material variables. An interaction between coolant temperature and the rotor speed (TR) existed in this response. By referring to figure 7.19 a minimum region was generally noted within the centre range of the axial variables (W and S), particularly at 50°C coolant temperature and fill factor 0.7.

The minimum region of $n = 0.08$ covers a wide range of energy and rotor speed levels. Within this region ($n=0.08$) the reduction in reference viscosity is greater as compared to region of higher n values. This is favourable at the early stage

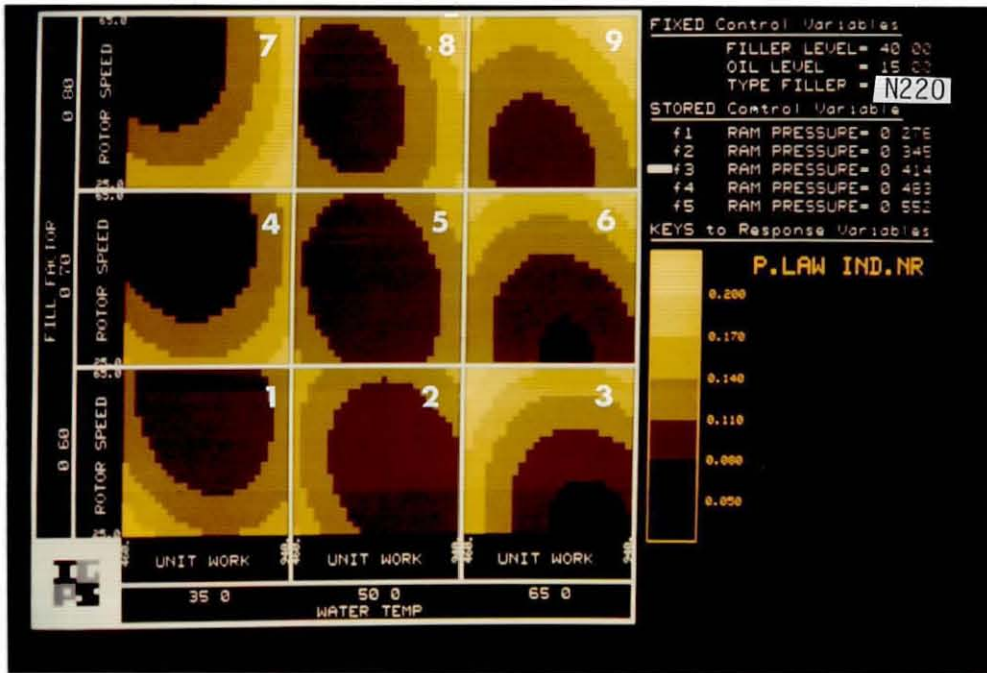


Figure 7.19 - Influence of mixer variables on power law index at 0.41 MPa ram pressure.

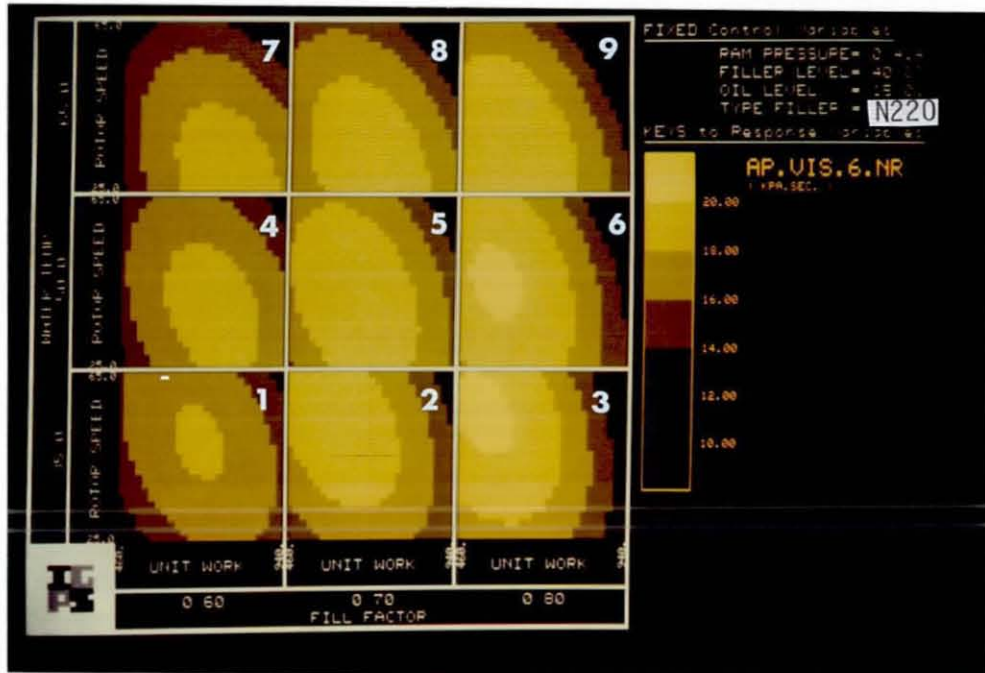


Figure 7.20 - Influence of mixer variables on apparent viscosity at 6 s⁻¹ shear rate.

of mixing, where the fillers can be incorporated rapidly into the rubber matrix.²⁵

The elastic behaviour of the mixes is represented by the shear modulus G , derived from the model described in earlier section 7.2.1. Here again, the mixer operating variables have less influence as compared to the material variables. However, the effect of the mixer variables on shear modulus can be observed in figure 7.21.

A similar effect was observed in the variation of shear modulus and the apparent viscosities with respect to the changes in the mixer operating variables. Several shading diagrams in figure 7.20 and 7.21 have a close resemblance to each other. High shear modulus compound corresponds with high viscosity, and low shear modulus compound corresponds with low viscosity.

Considering shading diagram number 2 and number 5 of figures 7.20 and 7.21 respectively, for a rough comparison, at 40 rpm increasing unit work from 700 to 900 MJ/m³, decreases the apparent viscosity from 18 to 14 kPa s, and reduces the shear modulus from 920 to 540 kPa. Both the responses, viscosity and modulus decreases by 22 % and 41 % respectively. At that level of energy, the mixes would have passed the incorporation stage, and the formation of occluded rubber in the void space of the carbon blacks would cause immobilization of the rubber chain⁷. Consequently this would reduce the elasticity of the compound considerably. Hence, a greater reduction in the modulus as compared to the viscosity was observed for such increase in the unit work.

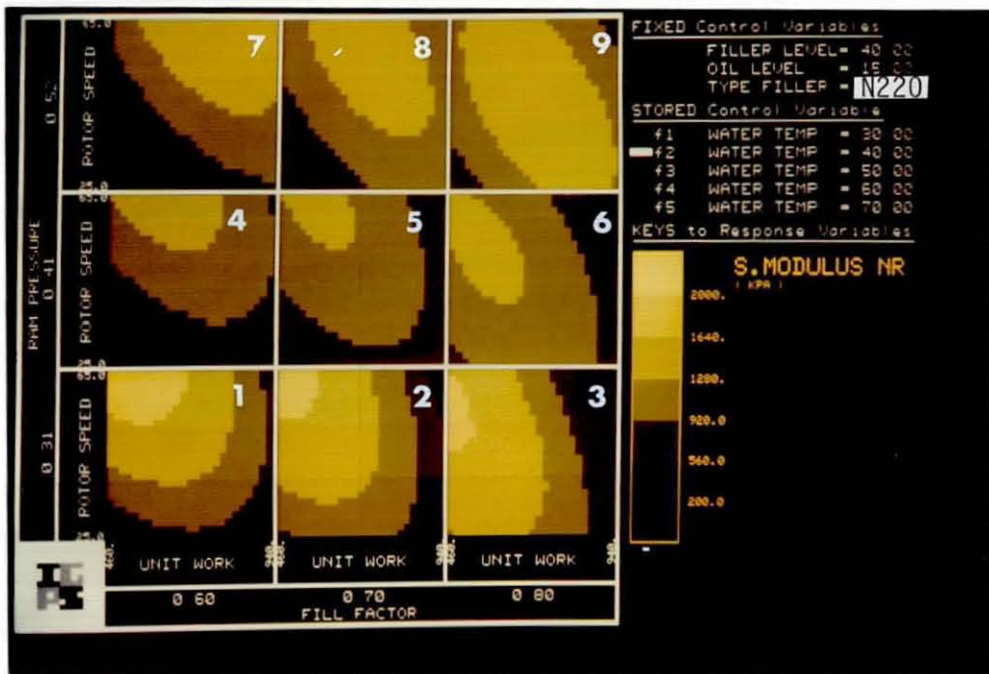


Figure 7.21 - Influence of mixer variables on shear modulus at 40°C coolant temperature.

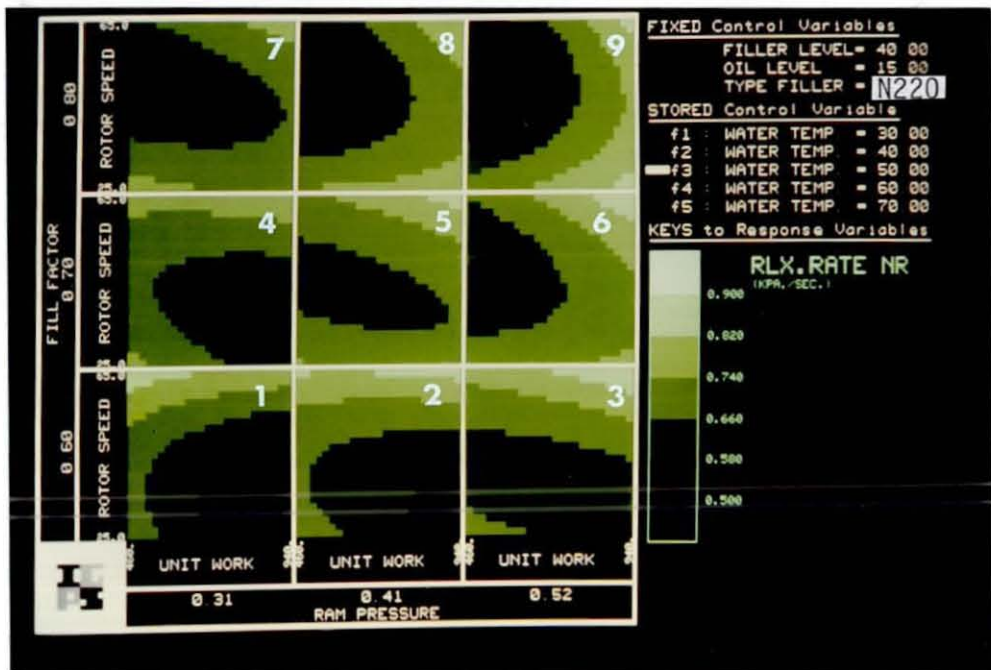


Figure 7.22 - Influence of mixer variables on relaxation rate at 50°C coolant temperature.

The variation of shear modulus with increasing ram pressure is more pronounced at high coolant temperature. By referring to the centre points of diagrams number 2, 5 and 8 in figure 7.21, increasing ram pressure from 0.31 to 0.41 MPa causes a reduction in shear modulus from 1280 to 920 kPa. However, with further increase in ram pressure to 0.52 MPa the shear modulus increases to 1280 kPa. Such variation in moduli may be due to the different time of commencement of the dispersive mixing stage in a mixing cycle, which varies with different ram pressure levels²⁵.

The influence of coolant temperature and rotor speed on shear modulus can be seen in figure 7.27. Increasing coolant temperature from 35 to 65°C resulted in an increasing shear modulus for rotor speed of less than 45 rpm. However, at higher rotor speed of 57.5 rpm, an equal increase in coolant temperature (from 35 to 65°C) showed a drastic drop in shear modulus. Such behaviour can be similarly explained as that encountered in the rapid drop of viscosity at high coolant temperature and at high rotor speed.

Relaxation time and relaxation rate can be used to characterise the viscoelastic behaviour of the mixes¹⁵. At low fill factor (i.e. <0.6), increasing unit work decreases the relaxation rate, as shown by shading diagrams 1 and 2 of figure 7.22. However, at higher fill factor (>0.70), the inverse was observed where increasing unit work increases the relaxation rate. As mentioned earlier with reference to figure 7.18 and 7.20, increasing the energy input reduces the viscosity of the mixed stock, thus correspondingly reducing the relaxation time and giving a high relaxation rate value.

From the statistical analysis (appendix II), the slip behaviour is largely influenced by ram pressure and filler loading level. Interaction effects between fill factor and oil loading (F0), together with fill factor and ram pressure (FP), also have a strong influence on the wall slip behaviour of the compound.

The combined effects of ram pressure and fill factor on slip behaviour of the mixes are clearly illustrated in figure 7.23. As mentioned earlier in chapter 1 (section 1.2.1), at low ram pressure the internal mixer's rotors tend to slip past the mixing stock. With high ram pressure, the contact force between the rubber and the rotor surface increases and consequently reduces the slippage between the mixing stock and the rotor surface.

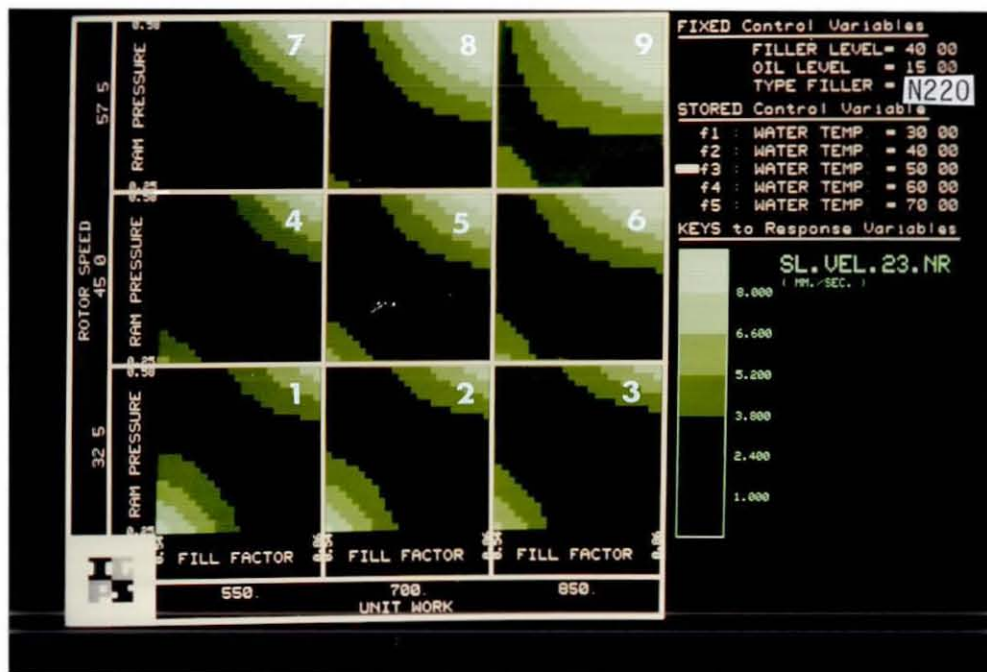


Figure 7.23 - Influence of mixer variables on slip behaviour.

By referring to figure 7.23, at low ram pressure (< 0.41 MPa), increasing fill factor decreases the slip velocity of the mixes. A region of low slip velocity of 1 mm/s was distinct at fill factor greater than 0.7. It can be said that the increase in stock loading at sufficient ram pressure, in this case between 0.28 to 0.41 MPa, increases the contact force causing a reduction in wall slip.

However, at high ram pressure (i.e. > 0.41 MPa), increasing fill factor (i.e. > 0.7), the inverse was observed where slip velocity increases drastically. This is magnified at high rotor speed as shown by shading diagrams number 8 and 9 of figure 7.23. To the author's best knowledge, no explanation can be ascribed to such phenomenon. Nevertheless, ram pressures of up to 0.41 MPa. and fill factors greater than 0.7 are shown to give the most favourable low slippage (approximately 1 mm/s slip velocity) mixing conditions.

7.3.5 Influence Of Compounding Variables.

The rheological properties of a compound are greatly influenced by its material composition^{16,17}, particularly by the type of filler, base polymers, processing oils and their loading levels.

A rapid increase in reference viscosity with increasing filler concentration was observed for the NR mixes loaded with small particle blacks, such as N220 (ISAF). For larger particle blacks, such as N660 (GPF), a more gradual increase in reference viscosity was noted with increasing black loading. Both behaviours are illustrated in figure 7.24 and 7.25.

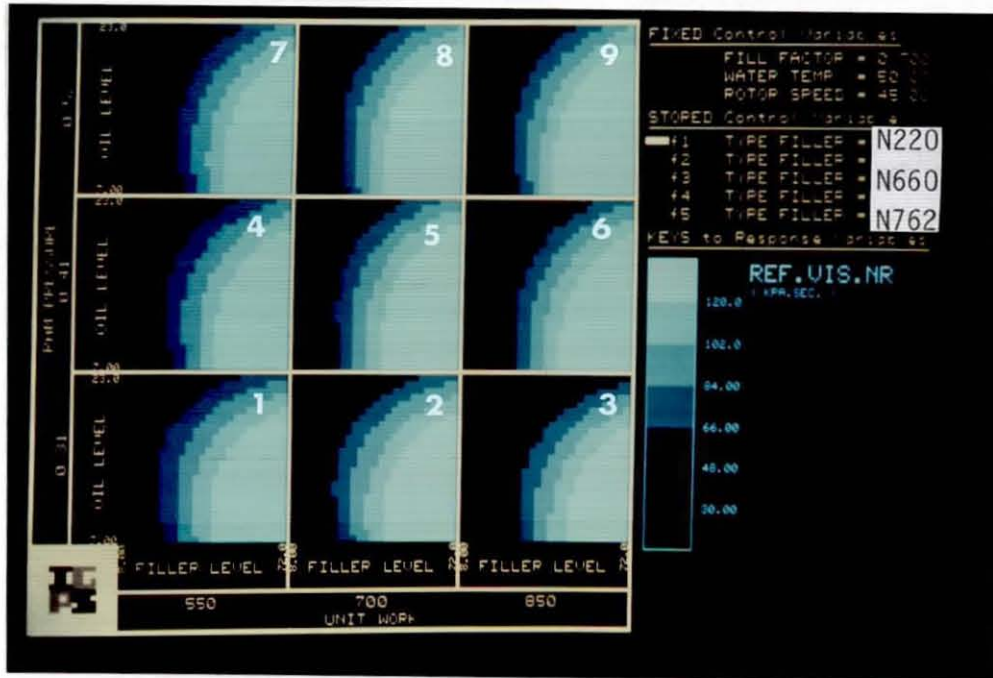


Figure 7.24 - Combined influence of mixer/material variables on reference viscosity of N220 (ISAF) black loaded mix.

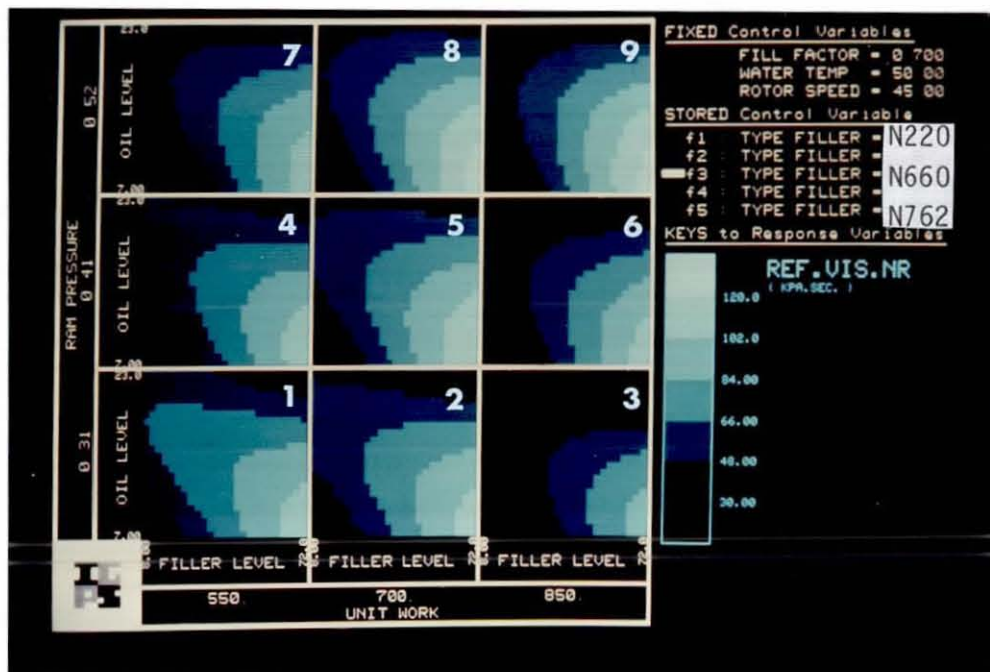


Figure 7.25 - Combined influence of mixer/material variables on reference viscosity of N660 (GPF) black loaded mix.

These behaviours have been widely acknowledged^{17,22} and were attributed mainly to the extent of filler-rubber interaction. Small particle blacks, such as N220 (ISAF) have larger facial area and are in closer proximity with the rubber as compared to the larger particle blacks. As such, with increasing filler concentration, the rate of increase in viscosity is higher for compound loaded with the former blacks than the latter.

For a particular black concentration, a critical oil loading level was observed below which the oil loading does not influence the reference viscosity. Above this critical loading, the oil has the expected effect of reducing reference viscosity. This critical limit of oil loading level decreased with increasing black concentration. Such behaviour is more pronounced for compounds loaded with larger particle blacks, in this case N660 (GPF), as illustrated in figure 7.25.

Considering shading diagram number 5 of the above figure, at 40, 56 and 64 phr black loading level, the critical oil limits are approximately at 19, 15 and 11 phr loading respectively. Below these oil levels, the reference viscosity remains at 84, 102 and 120 kPa s for the respective black concentrations.

As mentioned in chapter 2 (section 2.5), carbon black and oil have an opposing effect on the viscosity of a rubber compound²⁵. By inspecting figures 7.24 and 7.25, such opposing effect are obvious, where increasing filler levels increases viscosity and increasing oil levels decreases the viscosity. Generally for the same level of black and oil loading, the

viscosity of the smaller particle size black compounds are higher than compound loaded with larger particle size blacks. This conform to the common findings of viscosity variation with types of carbon black generally expressed by¹⁸,

$$\eta(\text{SAF}) > \eta(\text{ISAF}) > \eta(\text{HAF}) > \eta(\text{FEF}) \quad \text{.....7.20}$$

At higher shear rates, as measured by the TMS rheometer, the apparent viscosities follow similar behaviours as at 1 s^{-1} shear rate. However, gradual changes in the apparent viscosities were observed with varying filler and oil loading levels. This is also true for all types of carbon black investigated.

The deviation from Newtonian behaviour indicated by flow index n , intensified with increasing filler loading. A minimum plateau region exists, whose level increases with increase in particle size of carbon blacks. This is illustrated by figure 7.19 and 7.26. By referring to shading diagrams number 5 of both figures, at the centre points, the flow index n increases from 0.08 to 0.1 and 0.2 for the N220(ISAF), N660(GPF) and N762(SRF) compounds respectively. It can be seen from both figures that a big working range of black and oil concentration can be utilized where the flow index remains constant, which is an important criteria for processing of rubber.

The influence of compounding variables on the shear modulus of the mixes resembled closely their influence on the viscosities. The interaction effect between black concentration and types of black on this response is significant, as shown in the statistical analysis in appendix II. Such resemblance in the elastic and viscous properties of the NR mixes can be explained by the widely known theoretical studies of Guth²⁶ and

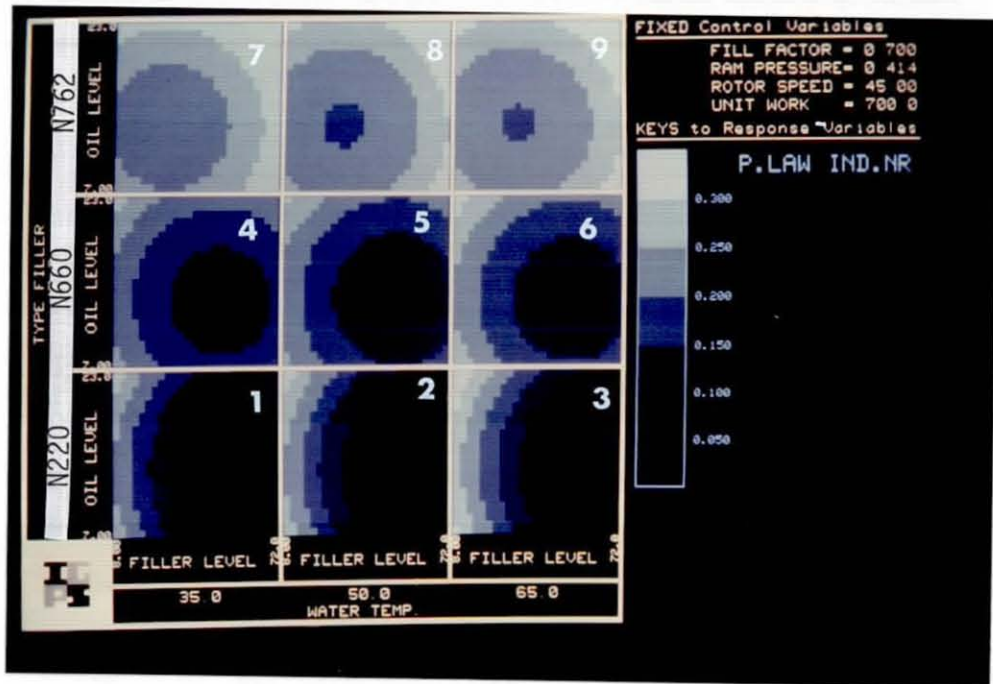


Figure 7.26 - Combined influence of mixer/material variables on power law index.

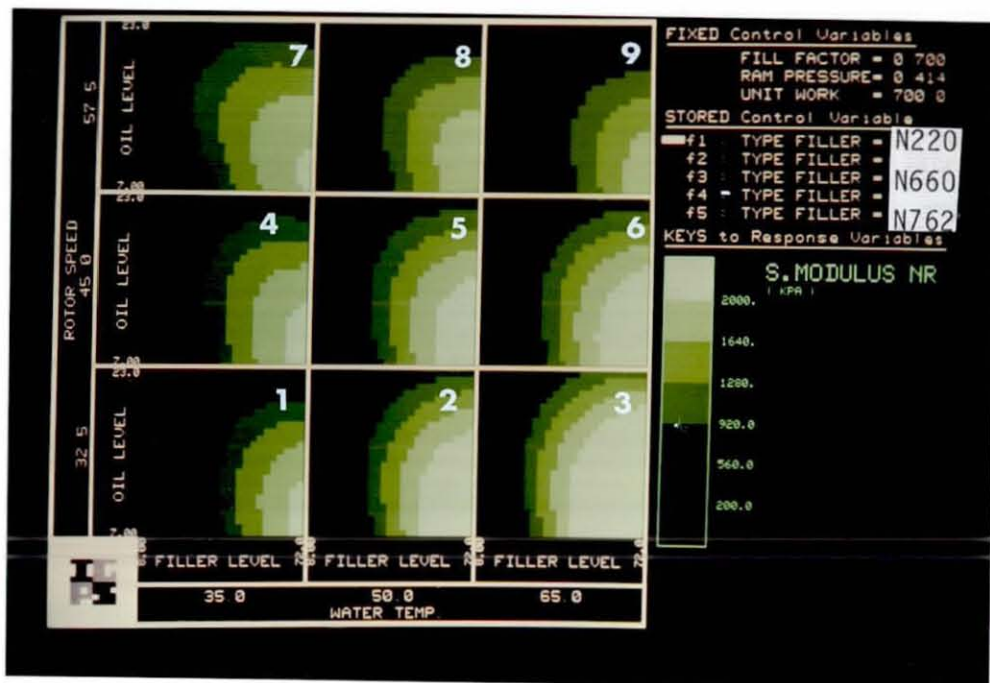


Figure 7.27 - Combined influence of mixer/material variables on shear modulus of N220 (ISAF) black loaded mix.

Smallwood²⁷. They proposed that the elastic variation of filled rubber can be analogous to that of the viscous variation of the compound.

The rate of increase in shear modulus with increasing black loading was higher for small particle size blacks N220 (ISAF). A more gradual rate of increase was observed with bigger particle blacks. At constant oil loading, shear modulus increases with increasing black concentration.

The variation of shear modulus with types of black shows that, at constant oil and black loading, shear modulus decreases with increasing blacks particle size. However, a peculiar behaviour was noted for compound loaded with N762 (SRF) carbon black. Increasing the N762 (SRF) black levels, decreases the shear modulus. The highest shear modulus values were at low black level and at high oil loading. Similar behaviour was observed by Bristow^{19,20} in his mixing study of NR with SRF carbon blacks.

A comparison can be made with regards to the influence of filler and oil levels on reference viscosity and shear modulus of a N220(ISAF) black loaded mixes. Considering the centre points (reference viscosity=102 kPa s and shear modulus=1280 kPa), of shading diagrams number 5 in figure 7.24 and 7.27, increasing the filler level from 40 to 55 phr resulted in 18 % increase of reference viscosity (120 kPa s) and 28 % increase in shear modulus (1680 kPa). The higher increase in modulus may be due to the reinforcement ability of the N220 (ISAF) carbon black, where more grafting of carbon blacks with the free radicals of rubber would readily occurs with increasing filler levels¹⁷.

Again, referring to the above shading diagrams, increasing oil level from 15 to 19 phr would markedly reduced the reference viscosity by 35 % (from 120 to 66 kPa s). Such high reduction in viscosity with increasing oil level may be attributed to the increase in absorption of the oil in the rubber matrix. Furthermore at such a mixing condition, the critical oil loading level is at 15 phr, above which the reference viscosity of the N220 (ISAF) loaded mixes reduces rapidly. For the same amount of increase in oil level, the shear modulus reduces by 28 % (920 kPa) which is comparatively smaller than the amount of viscosity reduction. This finding would further justify the well known fact of the opposing effect of black and oil in a rubber compound²⁵.

As mentioned in the previous section, filler loading level and the interaction between fill factor and oil loading level were among the most influential variables on the slip behaviour. At a particular oil loading level, increasing carbon black loading decreases wall slip velocity, as illustrated in figure 7.28. Wall slippage is presumed to be due to the formation of viscous boundary layer^{1,8}. With increase filler loading, the carbon black aggregates may interfere with the boundary layer causing the reduction in slip velocity. However, further investigation is required to confirm such tentative explanation.

The expected increase in slippage with increasing oil level can be seen clearly in the above figure. Also, high oil content in the compound would facilitate the formation of the viscous boundary layer resulting in high wall slippage.

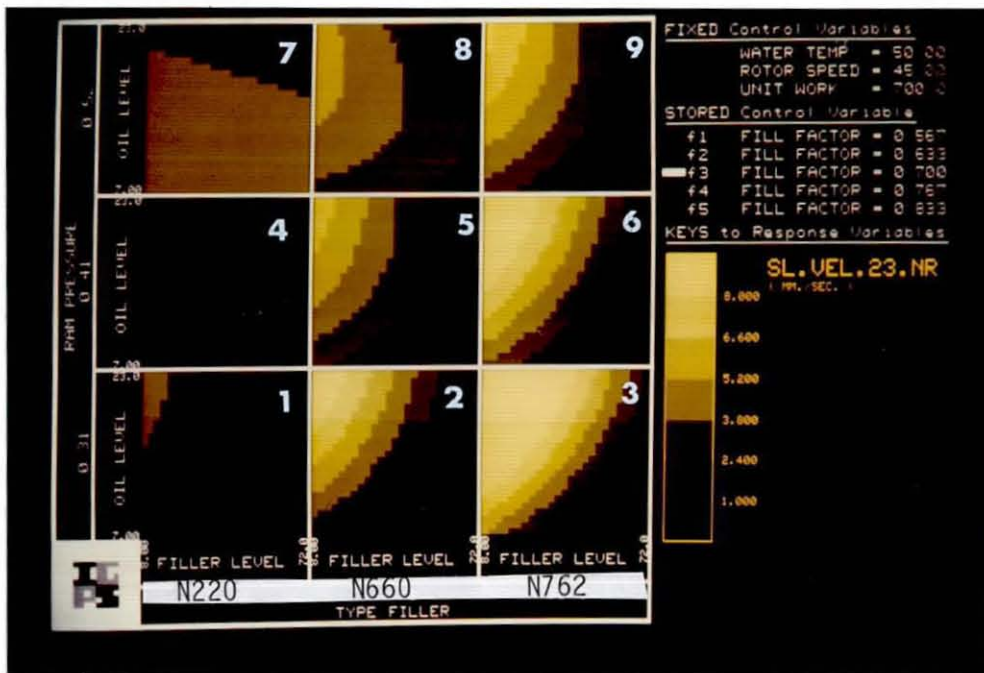


Figure 7.28 - Influence of material variables on wall slip velocity at 23 s⁻¹ shear rate.

With regards to the influence of types of black on slip behaviour, lesser variations in slip velocity were observed with small particle size blacks N220 (ISAF). A large minimum area of less than 2.4 mm/s was observed as shown in figure 7.28. For N660 (GPF) and N762 (SRF) blacks loaded mixes, increasing black loading levels decreases the slip velocity. The rate of reduction in slip velocity increases as the particle size of the blacks increase.

7.3.6 Combined Influence Of The Mixer And The Compounding Variables.

In earlier sections, the influence of material variables and mixer operating variables were treated separately. The combined influence of these variables on the rheological properties will be interpreted here by visual inspection of the shading diagrams. However, an alternative and systematic approach to identifying the strongest affecting variables would be based on the statistical analysis cited in appendix II.

The influence of material variables on the reference viscosity of a small particle black N220 (ISAF) compound can be seen in figure 7.24. Only slight variation in reference viscosity was observed by changing the level of ram pressure and unit work, though they were among the most influential mixer variables. However, the combined influence of these variables (ram pressure and unit work) can be seen for mixes loaded with larger particle size blacks, as shown in figure 7.25.

It is widely known that compound loaded with smaller particle size blacks require a higher energy level for changes in their flow behaviour to occur^{7,9,25}. This is so mainly due to the morphological characteristics of carbon black and the extent of rubber-filler interaction¹⁷. For N660 (GPF) blacks mixes, the reference viscosity decreases as unit work reaches 850 MJ/m^3 , as shown in figure 7.25. The energy level in figure 7.24 may be comparatively low to indicate any changes in the reference viscosity of the N220(ISAF) blacks loaded compound.

The reduction in reference viscosity of a compound can be effected either by varying the mixer operating variables or the

material variables. By inspecting figures 7.24 and 7.25, the extent of influence of these variables on reference viscosity can be approximated. Considering the centre points of shading diagrams number 5 and 6 of figure 7.25, in order to reduce the reference viscosity of a N660 (GPF) compound from 84 to 66 kPa s, it can be done by increasing the oil loading level from 15 to 19 phr (27 % increase) or by lowering the filler loading level from 40 to 24 phr (40 % decrease). Alternatively, the unit work can be increased from 700 to 850 MJ/m³ (22 % increase) for effecting equal amount of viscosity reduction.

Hence, in reducing the reference viscosity from 84 to 66 kPa s of N660 (GPF) black loaded NR compound, a lower percentage increase in unit work was required as compared to the percentage increase in oil loading and percentage decrease in filler loading levels.

However, for a N220 (ISAF) black loaded compound a higher percentage of mixer variable change is required for the same percentage of reduction in reference viscosity, as compared to the percentage of variation in the materials variables. This argument is supported by the centre points of shading diagrams number 5 and 6 of figure 7.24. To reduce the reference viscosity from 102 to 84 kPa s, the oil level can be increase from 15 to 16 phr (7 % increase), and also by decreasing the filler loading level from 40 to 36 phr (10 % reduction). Alternatively, for effecting the same amount of viscosity reduction, the unit work is increased from 700 to 850 MJ/m³ i.e. a 21 % increased.

Consequently, in addition to either varying the mixer variables of material variables for effecting viscosity reduction of a compound, other criteria such as the processing

economics and physical properties of the end products must be taken into consideration.

An approximation can also be made on the extent of moduli reduction by either varying the mixer operating variable or the material variables. Such approximation can be made by referring to the centre points of the shading diagrams number 2 and 5 of figure 7.21 and the centre point of shading diagram number 5 of figure 7.27. Both figures represent the variation of shear modulus for N220 (ISAF) black loaded compound. With reference to appendix II, ram pressure is one of the influential mixer variable on shear modulus. In order to reduce shear modulus from 1280 to 920 kPa (refer to shading diagrams 2 and 5 of figure 7.21), the ram pressure is increased from 0.31 to 0.41 MPa, i.e. an increase by 31 %.

Alternatively, for similar amount of modulus reduction the filler loading level has to be reduced by 25 %, i.e. from 40 to 30 phr (refer shading diagram 5 of figure 7.27). In addition an increase by 13 % (from 15 to 17 phr) of the oil loading level is required for effecting an equal amount of reduction in shear modulus.

Here again a higher level of mixer variable is required for the same amount of modulus reduction as compared to the variation required in the material variables of a compound. This is similar to the behaviour in viscosity reduction mentioned earlier for a N220 black loaded NR compound.

7.4 Summary.

- i. Within the shear rate investigated, (from 3 to 44 s^{-1}), the rheological properties of the NR mixes were influenced strongly by the material variables as compared to the mixer variables. Similarly this trend was also observed for the viscoelastic properties of these mixes. However, in the case of the slip behaviour, the compounds were influenced by both the material variables and the mixer operating variables.
- ii. The flow curves of the mixes obey the power law equation, with flow index n ranging from a minimum value of 0.02 to maximum value of 0.27. Greater deviation from the Newtonian behaviour (i.e. low flow index) was observed in compound loaded with smaller particle size blacks. For a particular type of carbon black, a large area of a constant flow index value was observed, over which a wide working range of both the mixer variables and the material variables can be utilised.
- iii. The variation of viscosity (reference and apparent viscosity) of a compound can be effected either by varying the the mixer operating variables or the material variables. Among the mixer variables, unit work and ram pressure strongly affect the viscosity of the compound. The extent of influence of these variables, particularly on viscosity reduction, depends largely on the type of carbon black. For larger particle black loaded compound, viscosity reduction is effectively done by varying the mixer variables (i.e. unit work). Whilst for compound loaded with small particle black, variation in the material variables is preferred for effecting the same amount of viscosity reduction.

- iv. Increasing filler loading level increases the viscosity of a compound. However the rate of increase in viscosity with increasing filler levels is higher for compound loaded with smaller particle size blacks (eg.N220), as compared to compound loaded with larger particle size blacks (eg.N660).
- v. The addition of oil into the rubber mixes generally decreases its viscosity. For a particular black concentration, a critical oil loading level was observed, below which the oil does not influenced the viscosity. Above the critical loading level, the oil has the expected effects of reducing the compound viscosity.
- vi. Increasing the temperature of a compound leads to decreasing the shear stress and its viscosity, irrespective of the shear rate levels. The variation in apparent viscosity with change in temperature was greatest at lower shear rates.
- vii. The influence of mixer variables and the material variables on shear modulus were observed to be similar to that of their influence on the viscosity of the NR mixes. High shear modulus compound corresponds with high viscosity and low shear modulus corresponds with low viscosity. Shear modulus increases with decreasing carbon black particle size and with increasing black loading level. However, for N762 (SRF) loaded compound increasing black concentration decreases the shear modulus.
- viii. The slip behaviour of the NR mixes was measured in the TMS rheometer by means of a polished rotor. Wall slip velocity increases up to a maximum value, and after which it drops with increasing shear rates (shear stress). The drop in slip velocity

with increasing shear rates may be attributed to the change in flow phenomenon, from laminar to the hypothetical secondary 'rolling' flow.

ix. It was observed that filler loading level was the main affecting variable on slip behaviour. In addition, interaction effects between fill factor and oil loading level and between fill factor and ram pressure also have a strong influence on the wall slippage.

Literature Cited.

(Chapter 7)

1. D.M. Turner and M.D. Moore, ' Practical Rheology in Polymer Processing ' Conference, Loughborough (1980)
2. R.A. Worth and H.A. Helmy, Proceed.Polym.Rheol. and Plast. Process., 147, September (1975)
3. G.M. Bristow, NR Technology, 12 (1981)
4. D.M. Turner and A.C. Bickley, Plast.Rubb.Process.Appl., 1,(4), (1981)
5. P.K. Freakley, Private Communication
6. M. Mooney, 'Rheology - Theory and Application' Ed.Eirich, Chp. 9, Academic Press, New York.
7. G.E. Decker and F.L. Roth, India Rubber World, 128,339(1953)
8. F. Nadiri, Dept. Mechanical Engineering, Imperial College of Science and Technology, London. (1979)
9. J.M. McKelvey, 'Polymer Processing', John Wiley & Sons, New York (1962)
10. A.B. Bestul and H.V. Belcher, J.Appl.Phys., 24,696,(1953)
11. K.B. Basir and P.K. Freakley, Kautschuk + Gummi Kunststoffe March (1982)
12. K.B. Basir, Unpublished information
13. J.D Ferry, ' Viscoelasticity of Polymers', Wiley New York (1961)
14. G.V. Vinogradov and A.Ya. Malkin, ' Rheology of Polymers' , Mir Publishers, Moscow (1980)
15. J.L. Leblanc, Elastomerics, 27, November (1980)
16. J. B. Horn, 'Rubber Technology and Manufacture' ed. C.M.Blow and C.Hepburn. Chp. 6, 2nd Edition (1982)
17. G. Kraus, 'Science and Technology of Rubber',Chp. 8, Academic Press, New York, (1978)

18. J.L. White, 'Science and Technology of Rubber', Chp. 6,
Academic Press, New York (1978)
19. G.M. Bristow, NR Technolgy, 11, 81 (1980)
20. ibid, 11, 45 (1980)
21. D.C. Bogue, Ind.Eng.Chem.Fundam., 5,253 (1966)
22. L. Mullins, 'The Chemistry and Physics of Rubber-like
Substances', Chp.11, Ed. L.Bateman, McLaren & Sons,
London, (1963)
23. ibid, Chapter 8.
24. M.G. Peakman, J. I.R.I., 4(1),35, February (1970)
25. J.M. Funt, 'Mixing of Rubber', RAPRA Publication (1977)
26. E. Guth, J.Appl.Phys., 16,20 (1945)
27. H.M. Smallwood, J.Appl.Phys., 15,758, (1944)

CHAPTER 8

DISPERSION OF CARBON BLACK IN THE NR MIXES

8.1 Carbon Black Dispersion Testing Methods.

The degree of dispersion of carbon blacks in the NR mixes was determined by the dark field reflected light microscopy (DFRLM) technique. Referring to chapter 4.0 (section 4.4.3), a brief description of its principle and advantages over other black dispersion testing methods can be found.

The DFRLM system used, which is shown in figure 8.1, comprised of a Leitz Epvert inverted microscope fitted with a triocular head. A closed circuit T.V. system was incorporated to view the area of the sample to be analysed and to ensure that it was representative, free of pores and bubbles and always in focus during measurements. The inverted microscope simplified the necessary levelling of the sample on the microscope stage. In addition, the light entering the objective can be directed either to the photocell or the T.V. camera system, where dispersion level can be determined separately in each case. The determination of black dispersion level in both cases will be described in the coming section.

In a previous study by Ebell¹, the dispersion of blacks in vulcanized compounds of SBR were evaluated by the DFRLM method, where sample preparation was much easier as compared to the present compounds of unvulcanized NR. However, bigger samples of

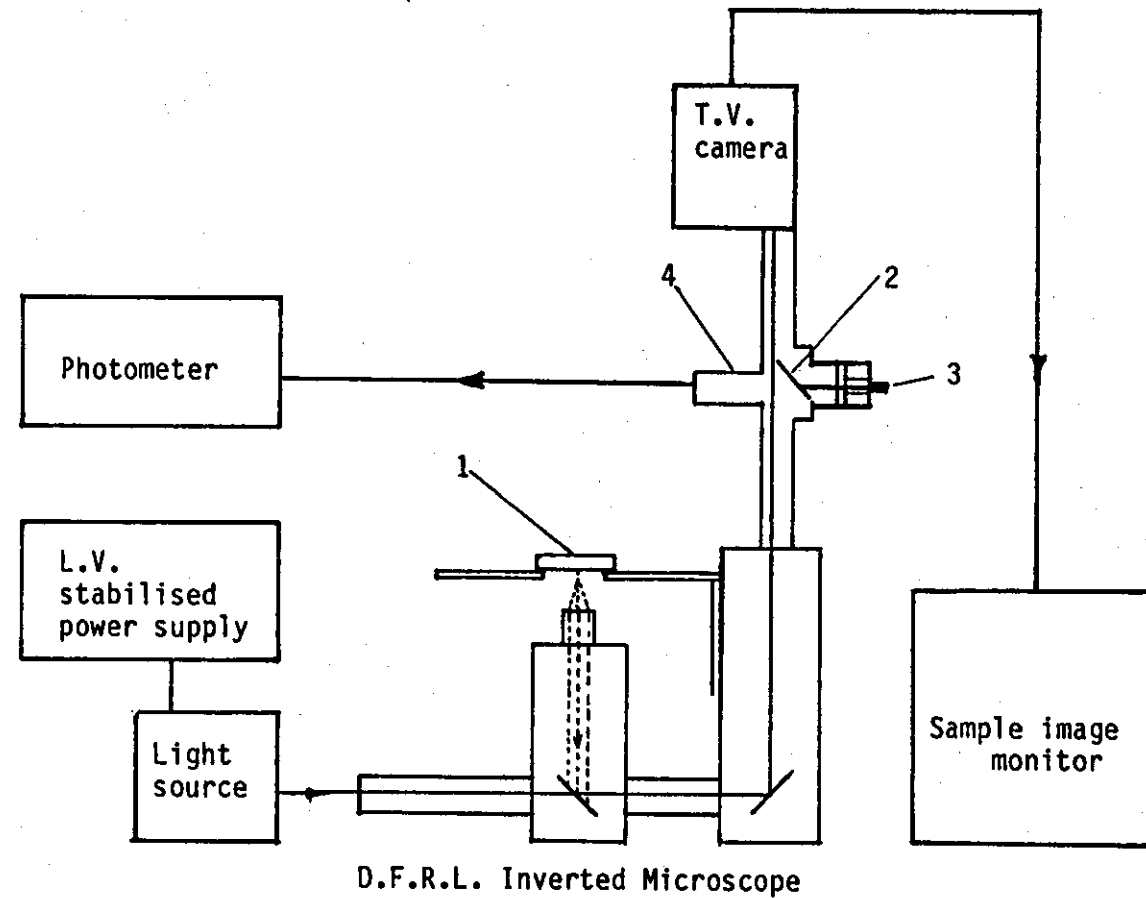


Figure 8.1 - Block Diagram Of Dark Field Reflected Light Microscopy System.
 1 - sample, 2 - mirror, 3 - push button, 4 - photocell

approximately 10.0 x 10.0 x 15.0 mm was initially prepared and immersed in a solution of methanol for about 10 minutes. This hardened the samples slightly, after which the sample was placed on the anvil of the cutter, as shown in figure 8.2, and cut by means of a new degreased razor blade. This operation produced a small block which was then clamped on a sample holder. The first cut surface was faced downward ready for microscopical observation. Prior to the observation, a short period was allowed so as to ensure that the methanol evaporated leaving a dry sample surface.

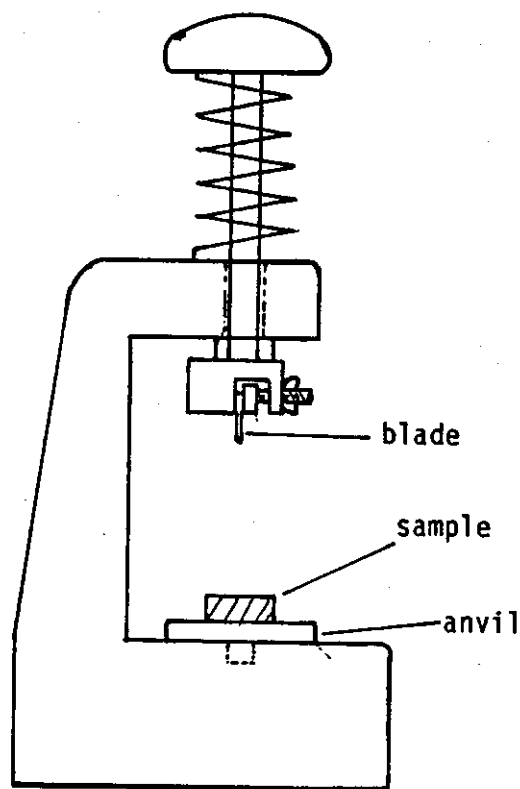


Figure 8.2 - Sample cutter.

Before any measuring session, a standard test piece was used to calibrate for good and bad dispersion level. A photographic film (ILFORD FP4) which was exposed and developed

was found to be a good 'standard' surface². The silver grain size gives scattering characteristics similar to those of cut rubber surfaces. The calibration was achieved by taking a number of measurements of the film and adjusting the stabilized lamp current to give a photometer output reading of 65 %. Calibration in this way generally results in a reading of around 75 % and 30 % for bad and good dispersion level respectively.

8.2 Determination And Analysis Of Carbon Black Dispersion.

8.2.1 Dispersion Analysis By Photometric Method.

The reflected light from a rough sample surface passes through the objective lens of the dark field microscope, where its intensity can be measured by means of a photometer. The intensity of the reflected light is found to be closely related to the level of carbon black dispersion in a compound¹⁻³.

With the sample on the microscope stage, a representative surface is selected by viewing the image on the T.V. monitor. A pushrod on the microscope head facilitates the photometric reading PR, to be taken. The photometer output is indicated by the light intensity meter. The average of several readings is noted, thus representing the photometer reading (PR) of the sample. This reading expressed as a percentage is then used as a parameter to characterize the level of black dispersion in the NR mixes. Low photometer values correspond to well dispersed compound and vice versa.

The photometer reading for the NR mixes varied between 33 % to 74.5 %. These values represent the dispersion level of the mixes number R-55 and R-74 (refer to appendix I) respectively.

Both the mixes differ in their mixer operating variables and the material variables. However, the photometer readings derived were analysed statistically by the GLIM programme as previously done to enable the influence of mixer operating variables and compound variables on carbon black dispersion level to be evaluated. This response (dispersion level) will be presented in the form of shading diagrams and will be discussed in the coming section.

8.2.2 Automatic dispersion analysis by microcomputer.

In addition to the photometric method, black dispersion level was evaluated concurrently by means of a microcomputer linked with the T.V. system. The changes of image intensity in a line scanned vertically across the microscopical image on the T.V. monitor indicates the surface roughness of the section. It has been generally recognized that surface roughness of a compound is closely related to the dispersion level of carbon black^{1,4}. In order to perform this task, the image signals from the T.V. system were digitized and stored in the memory of the computer. The software (held on a disk) manipulates the digitized signals, and computes the surface roughness characteristics. Also, the software allows several choices of processing functions necessary for interactive operations. A block diagram of the system is as shown in figure 8.3.

In the automatic mode, the computer will take a number of sampling lines (i.e. 20 lines) at regular intervals across the television image and calculate the output parameters for each scan, as shown in table 8.1.

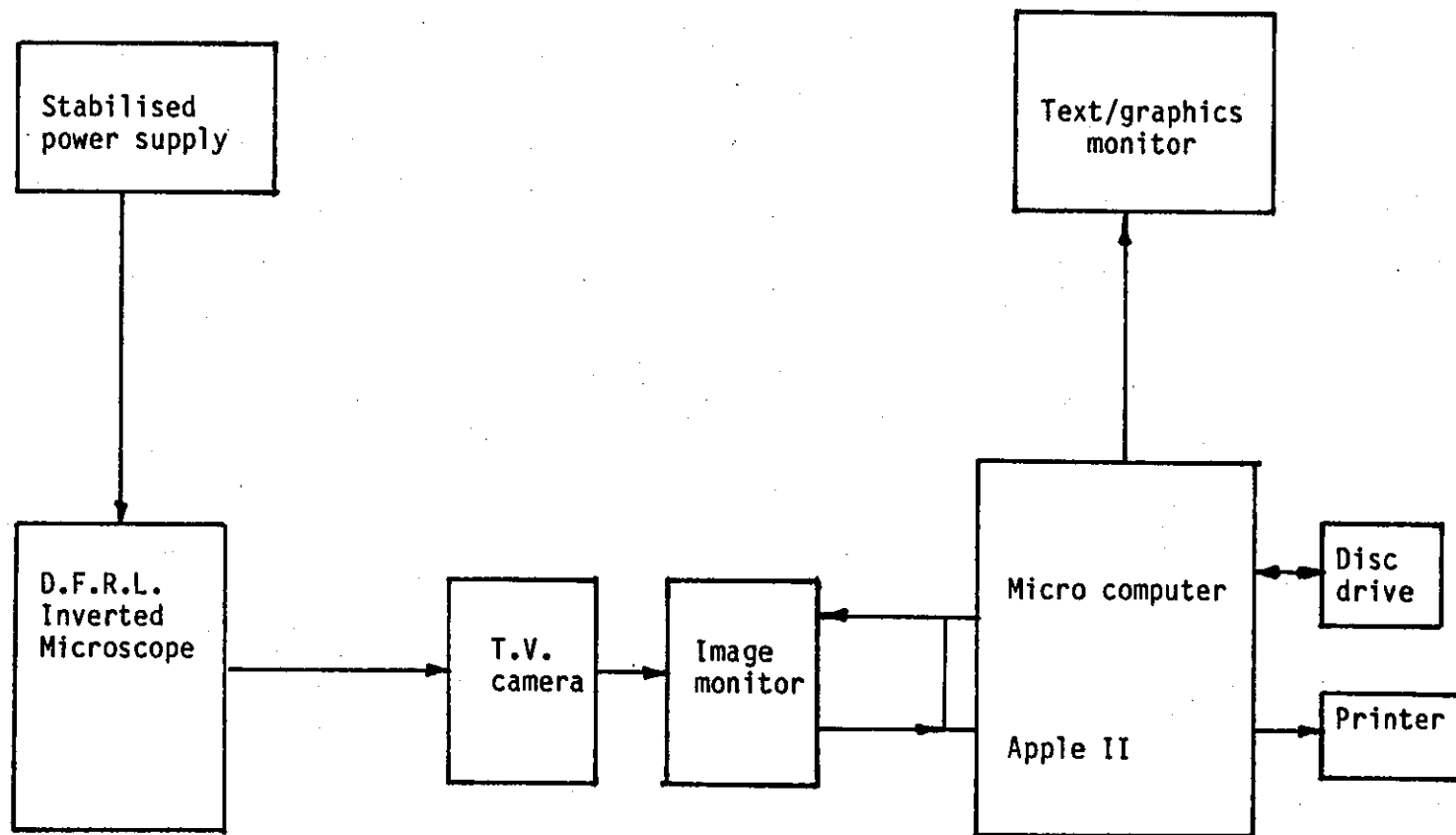
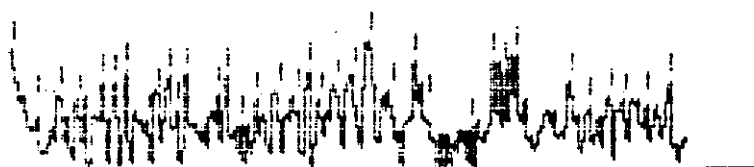


Figure 8.3 - Block Diagram Of Automatic Dispersion Method.

Table 8.1 - Typical output parameters of a scanned image. *

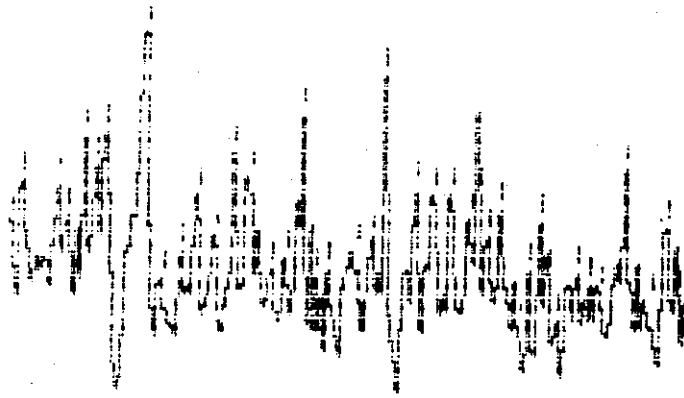
	no. of peaks n	mean height h	variance	std. devia. SD
1.	35	41.4	112.2	10.6
2.	34	43.5	96.4	9.9
3.	33	47.4	158.5	12.7
4.	33	39.7	100.7	10.1
5.	35	44.5	274.5	16.7
6.	37	44.6	179.8	13.5
7.	40	47.7	501.8	22.5
8.	36	43.8	139.9	11.9
9.	38	57.1	1537.6	39.4
10.	33	50.7	1223.2	35.2
11.	35	44.5	214.5	14.8
12.	34	56.8	1164.9	34.3
13.	38	45.3	239.3	15.6
14.	37	49.3	818.8	25.0
15.	33	51.9	785.4	28.2
16.	38	47.1	605.3	24.7
17.	37	48.2	292.6	17.2
18.	38	55.2	1203.5	34.6
19.	38	53.2	790.8	28.3
20.	34	54.8	1148.8	34.1
Mean Values	35.7	48.4	564.7	23.8

* output parameters of mix number R-70.



No. of peaks (n) - 36
Mean peak height (\bar{h}) - 46
Std. deviation (SD) - 11.8

Figure 8.4 (a) - Typical traces of a good dispersion compound, such as mix number R-70.



No. of peaks (n) - 42
 Mean peak height (\bar{h}) - 98
 Std. deviation (SD) - 38.5

Figure 8.4 (b) - Typical trace of a bad dispersion compound, such as mix number R-39.

Typical traces of the line scanned across the image are in figure 8.4 (a) and (b), for good and bad dispersion respectively. As mentioned earlier in chapter 4 (section 4.4.3), the parameters to characterize the traces are the mean peak height \bar{h} , the number of peaks n , and the standard deviation of the peak height SD.

Hess et.al⁵ and Ebell⁴ utilized these parameters (n , \bar{h}) to derive an index in order to evaluate the level of carbon black dispersion in rubber compounds. Recently Cembrola⁶ reported that a composite parameter $n^2 \bar{h}$, was sufficient to describe the dispersion level. Based on Cembrola's findings, a similar composite parameter was used in this study and it takes the form of

$$CP = k n^2 \bar{h} \quad \text{.....8.1}$$

where k - constant (10^{-3})
 n - number of peaks
 \bar{h} - mean height of peaks

Similarly the CP values for the series of NR mixes were determined and analysed statistically by the GLIM programme. Lower CP values indicate a high degree of carbon black dispersion in the compound.

8.3 Discussion Of Results.

8.3.1 General Form Of Dispersion Analysis.

The dispersion analysis of the NR mixes has shown that the photometric reading PR and the composite parameter CP, exhibits similar trends with respect to the influence of both the mixer operating variables and the material variables. Recently, by using the same DFRLM system, Mutagahywa² observed that the photometric reading PR is more sensitive at 'good' levels of dispersion as compared to the composite parameter CP. As such, the present author decided to use the photometric reading PR in evaluating the dispersion level of the NR mixes.

Nevertheless, the use of either parameter would depend greatly on the level of precision required, availability of equipment and its adaptability into routine quality control during rubber processing^{1,2}.

8.3.2 Influence Of Mixer Operating Variables.

During mixing of a rubber compound, the dispersion of carbon black can be achieved by optimizing the level of mixer operating variables^{1,7,9}. The statistical analysis in appendix IV shows that, the degree of dispersion indicated by both the photometric reading PR and the composite parameter CP were

strongly influenced by types of black (B), unit work (W), fill factor (F) and the coolant temperature (T). Significant interactions between fill factor and ram pressure (FP), and interaction between unit work and coolant temperature (WT) were observed.

The requirement of high energy level during mixing of small particle size black, such as N220 (ISAF), loaded compound is widely acknowledged^{6,9}. With reference to figure 8.5, good dispersion levels of less than 40 % PR value occur at high unit work (700.0 MJ/m³). At such energy level, adequate force is achieved to overcome the cohesive forces between the filler aggregates, enhancing dispersive mixing. Moreover, high energy reduces the viscosity of the compounds as mentioned in chapter 7 (section 7.3.4), contributing to the incorporation of carbon black into rubber to form a coherent mass.

In addition to high unit work, good dispersion level of 40 % PR value for the N220 (ISAF) loaded compound, was observed at low fill factor of less than 0.7 and at low coolant temperature of 35°C , as shown in figure 8.5.

From the preceding chapter 7 (section 7.3.4), the viscosity of N220 (ISAF) loaded compound decreases with increasing unit work. Greater reduction in viscosity was observed at high unit work for fill factor above 0.7 than at lower fill factor. As such, for the same high level of unit work, higher viscosity was observed for compound mixed at low fill factor than at high fill factor (refer to figure 7.18 in chapter 7.0). Thus, this supports the argument that for small particle size black loaded compound, better dispersion is achieved when mixing at low fill factor. However, the

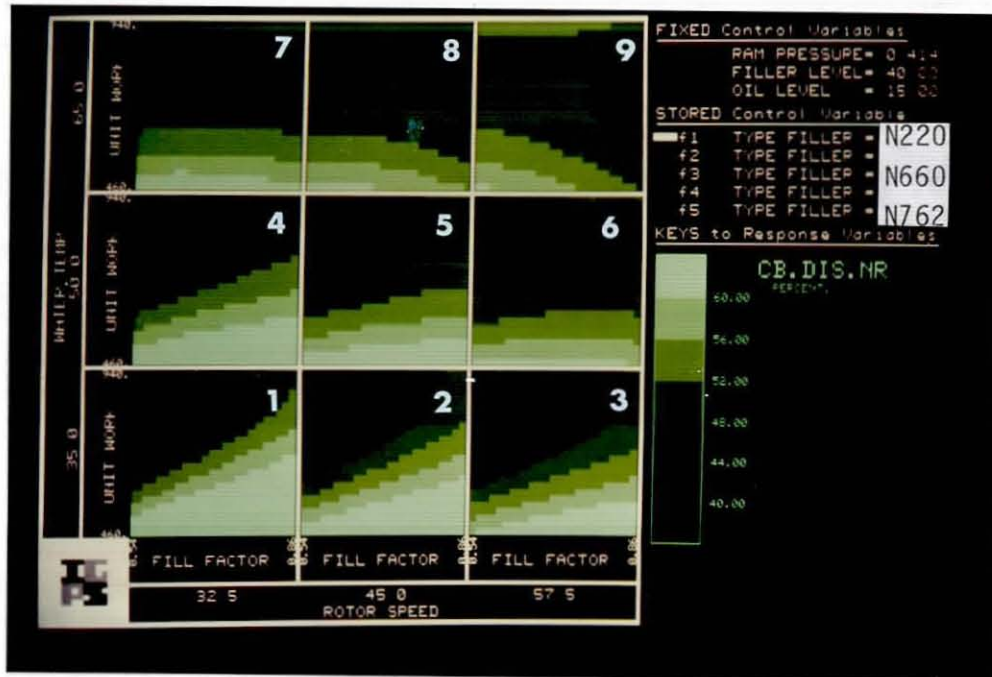


Figure 8.5 - Influence of mixer variables on carbon black dispersion of N220 (ISAF) black loaded mix.

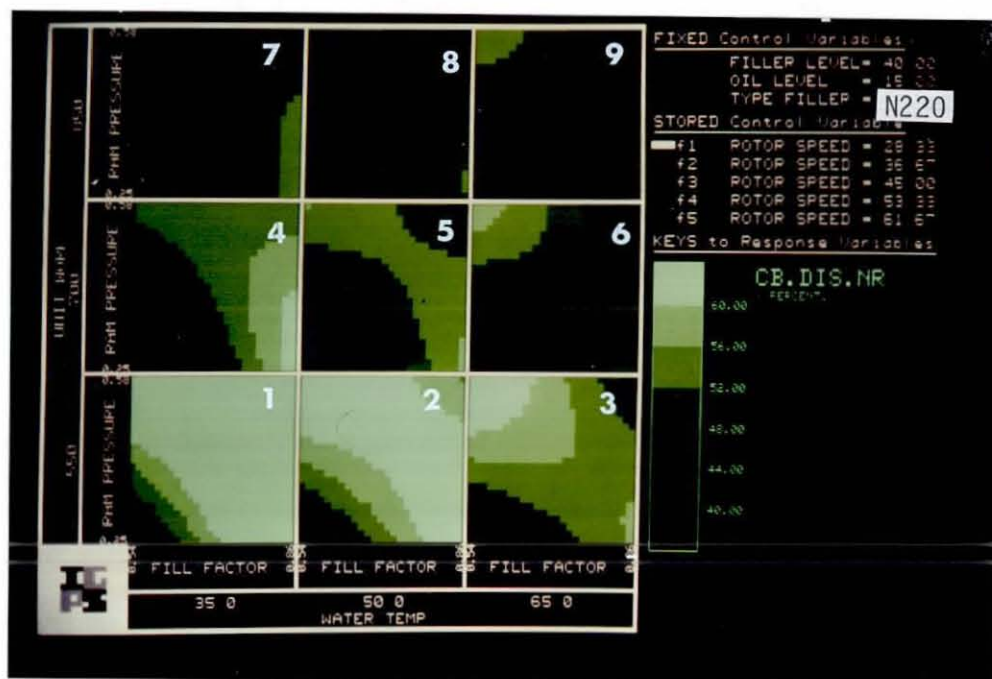


Figure 8.6 - Influence of mixer variables on carbon black dispersion at low mixer rotor speed (≈ 30 rpm).

characteristics of the carbon black are also responsible for such behaviour¹⁰.

Mixing at low coolant temperature allows better heat transfer¹¹, maintaining the desired high viscosity favourable for effective dispersive mixing. Only slight variation in dispersion levels were observed with increasing rotor speed at low coolant temperature. Substantial reduction in dispersion level occurs when increasing rotor speed at high coolant temperature i.e. 65°C, as shown in figure 8.5.

The influence of ram pressure on dispersion level for small particle size black, such as N220 (ISAF) compound, mainly occurs at low fill factor of less than 0.7, as shown in figure 8.6. Nevertheless, it can be safely said that at high energy level of greater than 700 MJ/m³, a wide range of ram pressure of up to 0.41 MPa. and fill factor of up to 0.7 can be utilized to produce a well dispersed N220 (ISAF) black loaded compound.

8.3.3 Influence Of Compounding Variables.

The statistical analysis in appendix IV shows that, amongst the variables investigated, the types of carbon black (B) were found to be the most influential factor on level of dispersion in the NR mixes.

The level of dispersion of each type of black depends largely on the effectiveness of each stage in the mixing operation, i.e. incorporation, dispersive and distributive mixing. All of which are related to the properties of base polymers and the morphological characteristics of the carbon black. As mentioned earlier in chapter 2 (section 2.4.1), high

structure and large particle size blacks can be rapidly incorporated into the rubber matrix^{8,13}. Small particle size blacks are incorporated at slower rate. Furthermore, the inter-aggregate cohesive forces are higher in small particle blacks¹², demanding intensive dispersive mixing as compared to coarser blacks.

Considering figures 8.5, 8.7 and 8.8, different types of black attained a dispersion level of PR value 40 % at different level of fill factor, coolant temperature and unit work. For easy reference and comparison these levels are summarized in table 8.2 for compounds loaded with N220 (ISAF) and N660 (GPF) blacks. It clearly illustrates the variation of mixer operating variables required for compounds loaded with small and large particle blacks particularly in achieving similar dispersion level (i.e. 40 % PR value). However, dispersion level at 40 % PR value can also be achieved for the N660 (GPF) black, at low fill factor but at low coolant temperature of 35°C and higher unit^{work} of greater than 700 MJ/m³. This arguments are supported by shading diagrams number 1-3 and 7-9 of figure 8.7.

Table 8.2 - Summary of mixer operating variables required to achieve 40 % PR value.

Variables	N220 (ISAF) compound	N660 (GPF) compound
Fill factor	0.54 - 0.7	> 0.7
Ram pressure (MPa)	0.28 - 0.41	0.28 - 0.41
Cool. temperature °C	35	50 - 60
Rotor speed (rpm)	30 - 45	40 - 60
Unit work (MJ/m ³)	>700	560 - 840

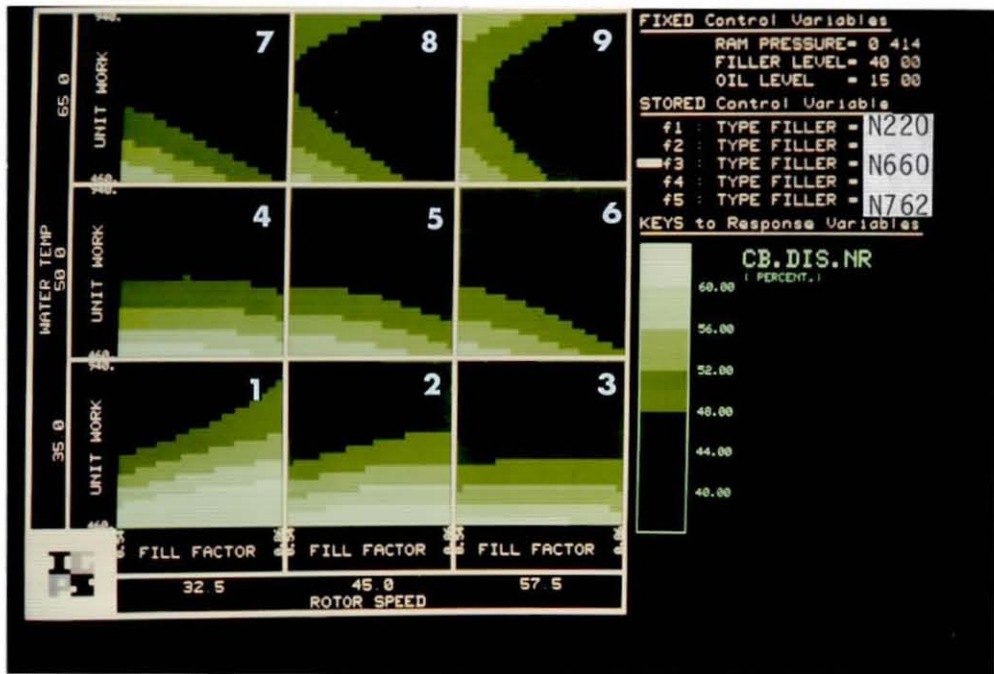


Figure 8.7 - Influence of mixer variables on carbon black dispersion of N660 (GPF) black loaded mix.

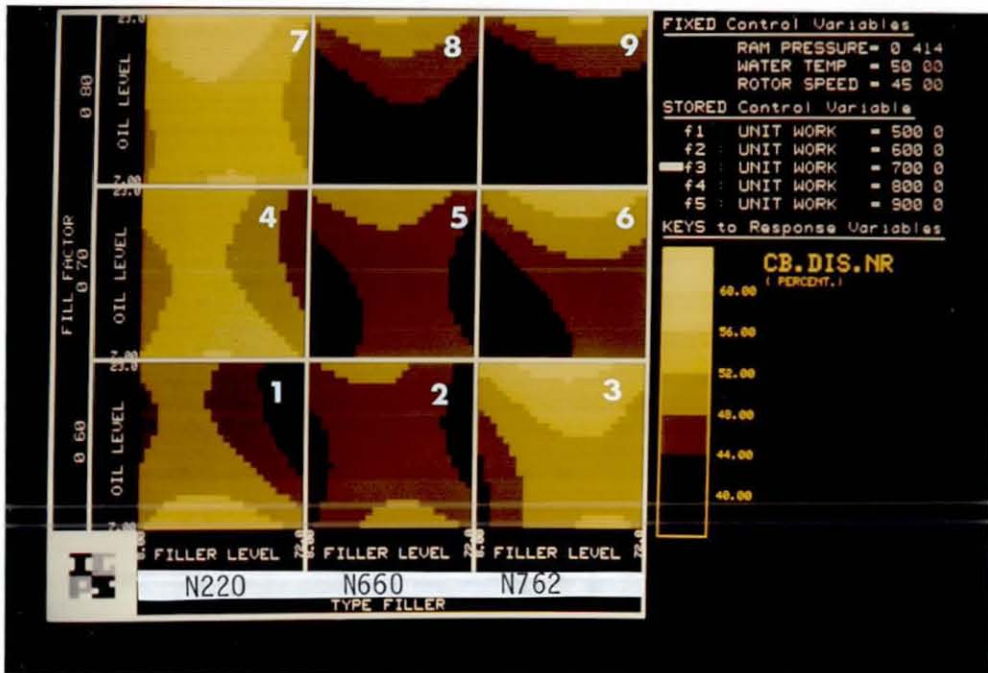


Figure 8.8 - Combined influence of mixer/material variables on carbon black dispersion.

In addition to earlier explanation regarding the extent of viscosity reduction at low fill factor for the N220 (ISAF) black loaded compound, the slow rate of incorporation of the fine carbon black also has an effect on the dispersion level. At high fill factor, Dizon¹³ showed that the percentage of loose black, determined after the second power peak in the mixing power profile, is higher for compound loaded with small particle size than the larger particle size blacks. As such, mixing at high fill factor of the fine blacks would prolong the incorporation stage and hind dispersive mixing. Alternatively, large particle size black, such as N660 (GPF) is incorporated faster in the compound, thus it can be processed at higher fill factor than the fine blacks¹³.

During mixing, the temperature buildup in a compound is also influenced by the characteristics of carbon blacks^{7,13}. Small particle size and high structure blacks have a higher rate of temperature buildup as compared to large particle size blacks. Consequently, to achieve a well dispersed compound loaded with fine black such as N220 (ISAF), it was found necessary to mix at low coolant temperature. For large particle black loaded compound, effective mixing occurs at high coolant temperature, as mentioned earlier.

Within the range of variables studied, the dispersion level of the NR mixes was found to be slightly influenced by the black and oil concentration. For a particular dispersion level a wide range of oil and filler loading levels can be utilized as shown in figure 8.8. In compounds loaded with N660 (GPF) and N762 (SRF) blacks, dispersion level of less than 40 % PR values can be obtained over a range of 8 to 72 phr filler loading. An oil loading of between 7 to 15 phr was found acceptable for the

same compounds to achieve 40 % PR value, as shown by shading diagrams number 8 and 9 of figure 8.8. For compound loaded with small particle black, such as N220 (ISAF), increasing filler loading level improved the dispersion level of the compound at similar mixing conditions.

In earlier study by Ebell¹, when mixing at high energy ($>700 \text{ MJ/m}^3$), carbon black concentration has minor influence on the dispersion level determined by the DFRLM system. The variation in the surface parameters (n , \bar{h} and SD) with black loading level vanishes as mixing energy increases. Well dispersed compound corresponds to high energy mixing condition. As such, the dispersion measurement for well dispersed NR mixes in this study at different black concentration is therefore, due to the variation in mixer variables and material variables and not due to the inherent characteristics of the dispersion testing method.

The variation in the degree of dispersion with respect to filler and oil loading is primarily due to the extent of filler rubber interaction, together with the extent of oil absorption in the compound. All of which are directly related to the rheological properties of the compound, as described in chapter 7 (section 7.3).

By referring to figure 7.24 in chapter 7, it can be seen that increasing filler loading increases the viscosity of the N220 (ISAF) black loaded compound. Higher dispersion of 40 % PR values were observed at black loading level of about 56 phr, as shown in figure 8.8. A comparison between these figures (7.24 and 8.8) would further justify the need for a higher viscosity stock for effective dispersive mixing, so as to achieve a well dispersed N220 (ISAF) compound.

However, for large particle black (N660 and N762) loaded compound, the level of filler loading is not critical in achieving similar dispersion level of 40 % PR value. By inspecting figure 7.25 in chapter 7, it would seem that these compounds can be effectively mixed at lower viscosity as compared to small particle black (N220) loaded compound. This conclusion is in line with earlier discussion where mixing of large particle blacks is favourable at higher temperature, i.e. at lower viscosity.

8.4 Summary.

- i. The Dark Field Reflected Light Microscopy (DFRLM), was well-adapted to evaluating the dispersion level of the large number of NR mixes, particularly with respect to fast sample preparation and proven reliability of results obtained. The photometric reading PR was utilized since it is more sensitive at good level of dispersion as compared to the composite parameter CP. Furthermore, both responses exhibit similar trends with respect to the influence of mixer operating variables and the material variables.
- ii. The favourable mixing conditions in producing a well dispersed compound loaded with small particle size black, such as N220 (ISAF) were found to be at high unit work of above 700.0 MJ/m³, low fill factor of less than 0.7 and at low coolant temperature of lower than 50°C.
- iii. For compound loaded with large particle size black, such as N660 (GPF) and N762 (SRF), effective mixing conditions were at lower range of unit work i.e. between 560 to 840 MJ/m³, high fill factor of greater than 0.7 and at high coolant temperature of 65°C.

iv. Increasing filler concentration improves the dispersion level of compound loaded with small particle blacks, such as N220 (ISAF). However, for compound loaded with larger particle blacks, such as N660 and N762, a wide range of filler loading level between 8 and 72 phr can be utilized to achieve similar dispersion level i.e. 40 % PR value. High oil loading level of greater than 15 phr reduces the level of dispersion of the NR mixes.

v. Carbon black dispersion is closely related to the rheological properties of the compound. This is clearly illustrated when comparison were made between the effective mixing conditions for good dispersion level with that of similar mixing conditions in the rheological properties in chapter 7. High viscosity level is conducive to efficient dispersive mixing leading to good dispersion, particularly for small particle size blacks. Comparatively, lower viscosity is sufficient to achieve similar dispersion level for compound loaded with larger particle blacks.

Literature Cited.

(Chapter 8)

1. P.C. Ebell, Ph.D Thesis Loughborough University (1981)
2. B.M. Mutagahywa, Private communication, research paper to
be published in Polym.Proc.Appl., April (1985)
3. P.C. Ebell and D.A. Hemsley, Rubb.Chem.Tech., 54,698 (1981)
4. N.A. Stumpe and H.G. Railback, Rubber World, 151,3,41(1964)
5. W.M. Hess et.al, Elastomerics, 112,(1) 24 (1980)
6. R.J. Cembrola, Rubb.Chem.Tech., 55,233(1982)
7. W.M. Wiedman and H.M. Schmid, Rubb.Chem.Tech., 55,363(1982)
8. A.I. Medalia, Rubb.Chem.Tech., 47,411(1974)
9. E.S. Dizon and L.A. Papazian, Rubb.Chem.Tech., 50,715(1977)
10. N. Tokita and I. Pilskin, Rubb.Chem.Tech., 46,1166(1973)
11. N. Nakajima et.al, Rubb.Chem.Tech., 55,546(1982)
12. J.M. McKelvey, 'Polymer Processing', John Wiley & Sons,
New York, (1962)
13. E.S. Dizon, Rubb.Chem.Tech., 49,12(1976)

CHAPTER 9

CORRELATION BETWEEN RHEOLOGICAL PROPERTIES AND CARBON BLACK DISPERSION WITH REGARD TO MIXER RESPONSES AND MIXER PERFORMANCE

9.1 Measurement Of Mixer Responses.

The set up of the BR Banbury internal mixer used in this study has been described earlier in chapter 6 (section 6.2.2). A thermocouple probe fixed to the chamber wall measures the temperature in the mixing chamber. It is connected to a chart recorder which indicates the temperature profile of a mixing cycle. However, after each mixing cycle, a portable pyrometer was used to determine the temperature of the mix. The pyrometer sensor was poked into the mix at several positions and the average reading was taken. This reading was used as the dump temperature of the compound; and it was found to be several degrees higher than the temperature measured by the thermocouple fixed in the mixer chamber wall.

In this mixing study, unit work was used as the dump criteria. The total mixing time after reaching the required energy level was measured by using a stop clock. Alternatively, the mixing time of each cycle can be determined from the power traces derived from the induction wattmeter. Both measurements were found to be close to each other. However, the time indicated by the power traces was taken as the mixing time of each mixing cycle.

9.2 Discussion Of Results.

9.2.1 General Form Of Variation Of The Mixer Responses.

Here again the responses dump temperature and mixing time were analysed by means of the GLIM computer package, and they are presented, as with previous results, in the form of shading diagrams. The coefficients of the terms in the postulated polynomial model of the responses were estimated and are as shown in appendix IV. From this analysis it was found that the dump temperature and mixing time of the NR compound were strongly influenced by both the mixer operating variables and the material variables. Comparatively small interactive effects between these variables on the mixer responses were observed.

Within the levels of the variables studied, the highest dump temperature was 135°C exhibited by the mix R-75 (refer to appendix I). This compound has the highest filler loading level of coded value +2.82 (80.0 phr) and all other variables were at 0 coded value. The lowest dump temperature recorded was 80°C corresponding to mix R-1, which was loaded with 26 phr of N660 (GPF) black. Compound R-1 was mixed at minimum levels of the mixer operating variables, with -1 coded values, and at high loading of the processing oil.

As for the mixing time, the longest time recorded was at 1005 seconds exhibited by mix R-73 which was mixed at the highest energy level of 1000 MJ/m³ (coded value +2.82). On the other hand, the minimum mixing time was 190 seconds corresponding to mix R-74 obviously with the lowest mixing energy of 400 MJ/m³ (-2.82 coded value).

9.2.2 Influence Of Mixer Variables and Material Variables On Dump Temperature.

The level of rotor speed, coolant temperature and fill factor were the most influential variables on dump temperature. This is indicated by their high linear coefficient values (refer appendix IV). These are then followed by the filler loading and the oil loading levels.

Generally, increasing rotor speed, irrespective of the level of other variables, increases the dump temperature of the compound. The rate of increase in dump temperature is higher at high coolant temperature (above 50°C) and also at high fill factor (above 0.7). This is illustrated clearly in figure 9.1.

Rotor speed is directly related to the magnitude of the shear rates experienced by the compound¹. The relative motion of the compound against the rotor surfaces and the chamber wall generates frictional heat and also combine with hysteristic heat loss during deformation to generate the temperature rise in the mixing compound. Consequently, the amount of heat generated, which is indicated by the compound temperature (batch temperature), is proportional to the level of rotor speed².

However, the amount of heat generated can be balanced by the amount of heat removal. This can be effected either by the design of the mixer itself or by controlling the level of coolant temperature passing through the mixer^{2,3}. High temperature difference between the compound and the coolant temperature leads to better heat transfer, consequently lowering the compound temperature as observed during dumping.

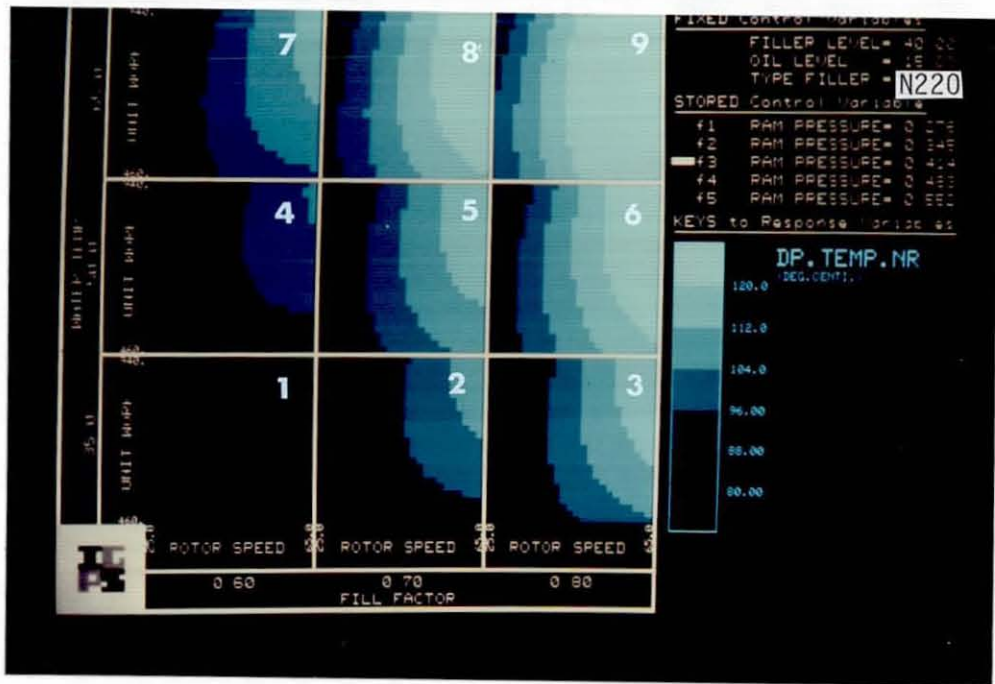


Figure 9.1 - Influence of mixer variables on dump temperature of N220 (ISAF) black loaded mix.

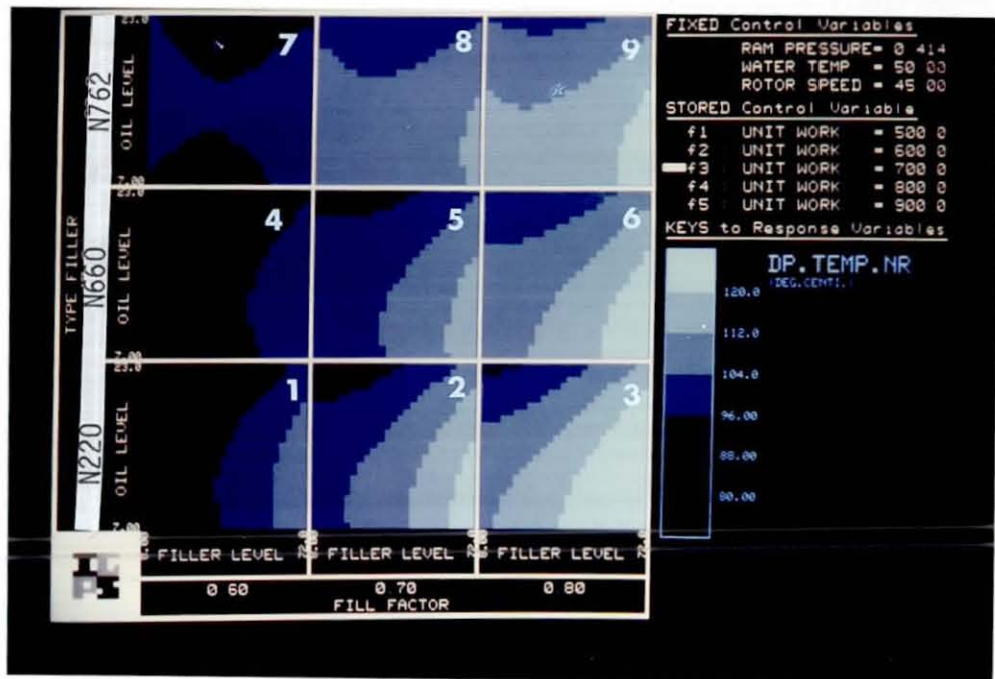


Figure 9.2 - Combined influence of mixer/material variables on dump temperature.

Below a particular rotor speed level, unit work has little influence on the dump temperature, as shown in figure 9.1. Nevertheless, at any mixing condition the highest dump temperature values occur at high rotor speed and at high unit work as compared to those at low rotor speed and low unit work. This is presumably because of heat generation exceeding the mixer cooling capacity.

By referring to figure 9.2, the influence of material variables on dump temperature can be evaluated, where increasing filler loading level increases the dump temperature of the compound. However, greater variation was observed for compound loaded with smaller particle size black, such as N220 (ISAF), as compared to large particle size black such as N762 (SRF). It is also interesting that a wide range of filler and oil loading levels in the large particle size black N762 (SRF) loaded compound yield a constant dump temperature. This behaviour is depicted by shading diagrams number 7, 8 and 9 of figure 9.2.

The addition of fillers in a compound significantly increases the hysteristic losses, which are then transformed into heat, resulting in temperature buildup of the compound. In this study a high rate of increase in batch temperature with small particle size black loaded compound was observed, as compared to compound loaded with larger particle black, as shown in figure 9.2. Presumably this is due to the amount of hysteristic heat loss, which is directly related to the loading level, structure and surface area of carbon black in the compound⁹.

For a particular black concentration, a critical oil loading level was also observed, below which the oil loading

does not influence the dump temperature. Above this loading level, the oil has the expected effects of reducing the dump temperature of the compound. The critical limit of oil loading level decreases with increasing black concentration. The influence of oil on dump temperature follows similar trend as to its influence on the reference viscosity as described in chapter 7 (section 7.3.5).

The changes in dump temperature of a compound can be effected either by varying the mixer operating variables or the material variables. An approximation on the extent of influence of these variables on dump temperature can be made by comparing the diagrams in figure 9.1 and figure 9.2.

Considering the center points of shading diagram number 5 and number 2 of the above figures 9.1 and 9.2 respectively. In order to reduce the dump temperature from 104 to 96 °C, the rotor speed was decreased from 45 to about 44 rpm, i.e. 2 % reduction. Alternatively, for effecting equal reduction on dump temperature, the filler loading level was reduced from 40 to 37.5 phr, a reduction of 6 %. Whilst 13 % increase in oil loading level from 15 to 17 phr would effectively reduce the same amount of dump temperature.

Hence, in reducing the dump temperature of N220 (ISAF) black loaded compound from 104 to 96 °C, a lower percentage decrease in rotor speed was required as compared to the percentage decrease in filler loading level and percentage increase in oil loading level. Consequently, a conclusion can be drawn that mixer variables have a greater influence on the variation of dump temperature than the material variables for a compound loaded with N220 (ISAF) black.

In addition, figure 9.1 illustrates the extent of increase in dump temperature with respect to the change in coolant temperature. Increasing coolant temperature from 35 to 50 °C, i.e. 30 % increase would only increase the dump temperature from 96 to 104 °C i.e. about 8 % increase. Thus this is in line with the finding of Wiedman et.al¹⁰, where the change in dump temperature was lesser as compared to the change in circulating coolant temperature.

9.2.3 Influence Of Mixer Variables And Material Variables On The Mixing Time.

The level of unit work, rotor speed and fill factor strongly influenced the mixing time of the NR compound. Amongst which unit work has the highest linear coefficient value as compared to other variables as shown in appendix IV, indicating its strongest influence on mixing time. As for the material variables, filler loading level affects mixing time considerably.

In this study, unit work is used as the dump criteria. As such, increasing unit work has the expected effect of increasing mixing time irrespective of the levels of other variables. At a constant level of unit work, mixing time decreases with increasing rotor speed as shown in figure 9.3. This observation is similar to previous findings by other researchers^{4,5}.

However, the influence of fill factor at similar mixing conditions was found to be the inversed from that observed by Freakley⁵ and Ebell⁴. Increasing fill factor decrease the mixing time of the compound. Whilst earlier studies by the above

researchers^{4,5} showed that mixing time increases with increasing fill factor.

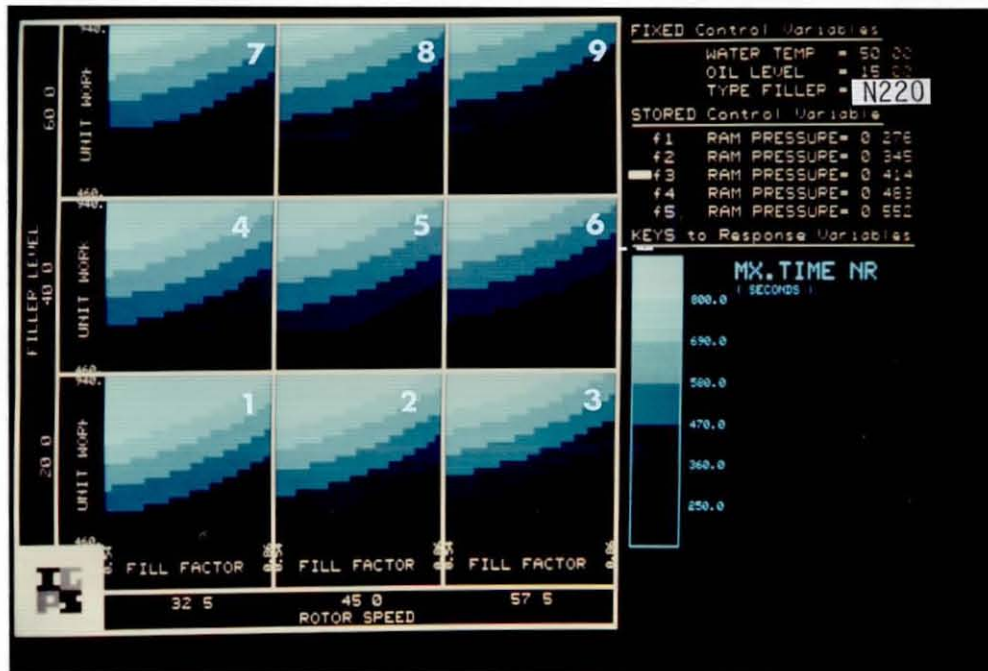


Figure 9.3 - Combined influence of mixer/material variables on mixing time at 0.41 MPa ram pressure.

Considering the centre points of the shading diagram number 5 of figure 9.3, increasing fill factor from 0.7 to 0.8 decreases the mixing time from 470 to 360 seconds respectively. The decrease in mixing time with increasing fill factor can be explained by the difference in power profiles of the mixing cycles. This can be verified by referring to the power traces of mixes R-65 and R-66, as shown by figure 9.4.

At constant unit work, the peaks of the power trace for the same compound mixed at high fill factor are higher as compared to mixing at low fill factor. As such, a shorter mixing time is observed for compound loaded at high fill factor than at

low fill factor when process at similar mixing conditions. The influence of fill factor on the output of the process controlled to achieve a certain black dispersion level will be discussed in the coming section.

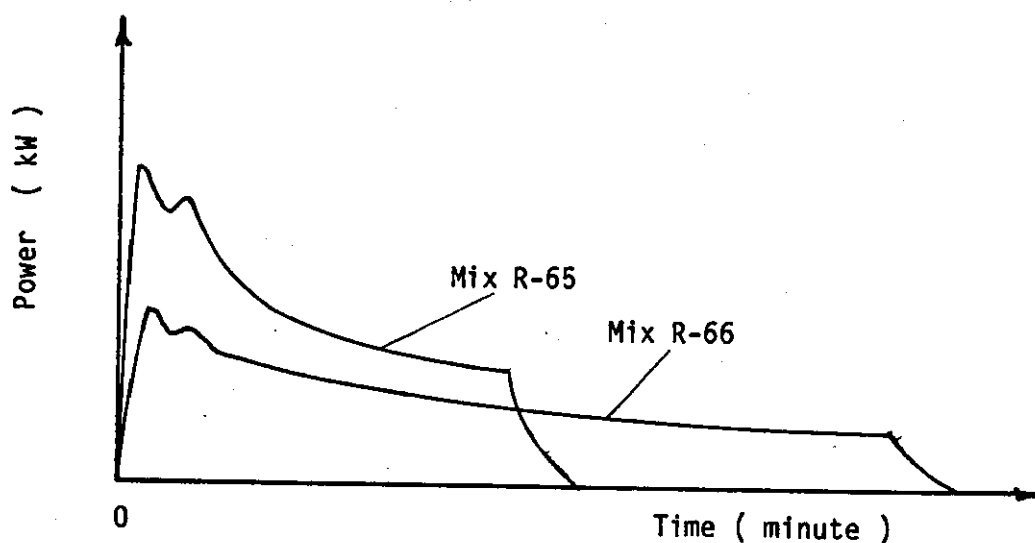


Figure 9.4 - Power traces of mixing cycle.

The requirement of an adequate level of ram pressure for effective mixing has been discussed in earlier chapter 7 (section 7.3.4) and chapter 8 (section 8.3.). Such requirement also applies to the mixing time of the NR compound. It is widely acknowledged that mixing at high ram pressure reduces the mixing time as compared to mixing at low ram pressure^{6,7}.

Increasing coolant temperature increases the mixing time of the compound. This is related to the rheological properties of the compound where high temperature lowers the compound viscosity leading to longer mixing time.

With regards to the influence of the material variables on mixing time at constant unit work and constant filler and oil

loading level, increasing the the particle size of the blacks prolongs the mixing time. Such variation can be ascribed to the extent of rubber filler interaction and also due to the different time of commencement of each mixing stage. Compounds loaded with small particle black such as N220 (ISAF) experience more intensive dispersive mixing than compounds loaded with coarser blacks, such as N660 (GPF).

The power trace in figure 9.5 illustrates such variation, where mixes R-79 and R-80 only differed in the types of carbon black. The mix R-80 was loaded with N220 (ISAF) black and mix R-79 was loaded with N762 (SRF) carbon black. Consequently at constant unit work the mixing time of compound loaded with large particle size black is longer than for compound loaded with small particle size black. However, the comparison only applies when disregarding the black dispersion level of such compounds. Bearing in mind that large particle size blacks are dispersed at faster rate as compared to compound loaded with finer black.

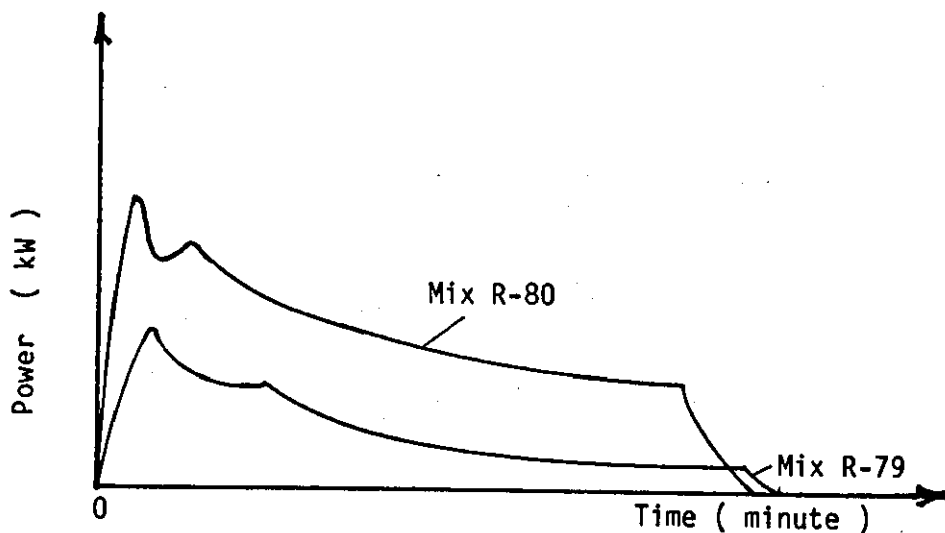


Figure 9.5 - Power traces of mixing cycles.

Oil loading level has little influence on the mixing time, particularly for compound loaded with larger particle size blacks. When the oil loading level was varied from 7 to 20 phr of N762 (SRF) black loaded compound, the mixing time was found to remain unchanged. This is depicted in shading diagram number 7-9 of figure 9.6.

Increasing filler level decreases the mixing time of a compound for a given level of unit work. This effect was more pronounced for compounds loaded with small particle size blacks such as N220 (ISAF) as compared to compound loaded with coarser black such as N762 (SRF) black. However, in some cases the filler loading can be varied over a substantial range without influencing strongly the mixing time, as shown in figure 9.6.

The mixing time of a compound can either be affected either by varying the mixer variables or the material variables. By inspecting figure 9.3 a comparison can be made on the extent of influence of these variables on mixing time. Considering the centre points of shading diagrams number 5 and 6 of figure 9.3, in order to reduce the mixing time of a N220 (ISAF) loaded compound from 470 to 360 seconds, the fill factor must be increased from 0.7 to 0.74 (6.5 % increase). Alternatively increasing the rotor speed from 45 to 57.5 rpm (27 % increase) effects the same amount of reduction of the mixing time. However, an increase of 50 % in the filler loading level was needed for effecting a similar reduction in the mixing time (i.e. increase from 40 to 60 phr).

From the above observations, it can be deduced that the mixer operating variables, particularly unit work, rotor speed and fill factor affect mixing time strongly as compared to the

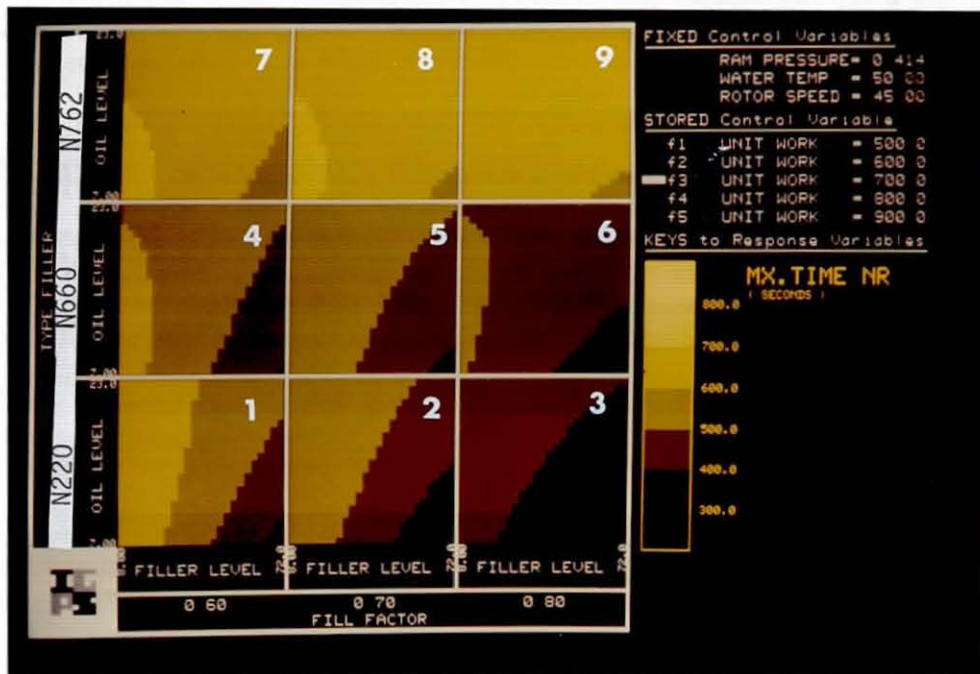


Figure 9.6 - Influence of material variables on mixing time at 700 MJ/m³ unit work.

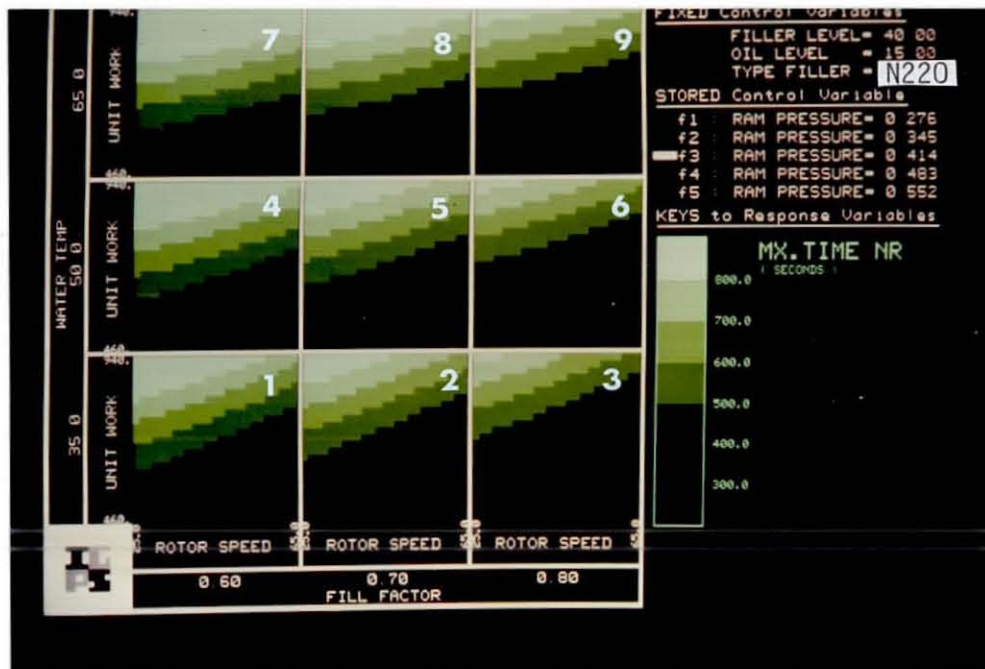


Figure 9.7 - Influence of mixer variables on mixing time at 0.41 MPa ram pressure.

material variables. High mixing time will increase excessively the temperature of the compound resulting in pre-vulcanization in cases where curatives are added. In addition high mixing time lowers the compound viscosity and hinders dispersive mixing.

During mixing, the throughput is directly related to mixing time and batch volume (fill factor). A shorter mixing time and high fill factor would obviously lead to high output mixing, as compared to mixing at longer duration. However, other criteria such as the rheological properties and carbon black dispersion level of the compound must be taken into consideration. The correlation between these criteria and the mixer performance will be discussed in the following sections.

9.2.4 The Variation Of Rheological Properties With Respect To The Mixer Responses And Mixer Performance.

As mentioned earlier in chapter 7 (section 7.3) the rheological properties of the NR compounds are strongly influenced by the material variables, but the mixer responses (dump temperature and mixing time), are more strongly influenced by the mixer operating variables. Thus for a particular compound, such as one loaded with N220 (ISAF) black, within the levels studied, a greater proportional variation in dump temperature was observed as compared with the variation in reference viscosity. This is illustrated in figure 7.18 (a) in chapter 7 (section 7.3) and figure 9.1.

At high unit work (850 MJ/m^3) increasing rotor speed increases the dump temperature of up to 120°C for the N220 (ISAF) black loaded compound (refer figure 9.1). Such variation

in batch temperature substantially reduces the viscosity of the compound as described in chapter 7 (section 7.3.3). However, at similar mixing conditions (i.e. 850 MJ/m^3 unit work, increasing rotor speed), the reference viscosity measured at constant temperature (100°C) in the TMS rheometer remained within the same range of 66 to 84 kPa s. Thus it can be deduced that during mixing of N220 (ISAF) black loaded compound, the viscosity reduction is dominated effectively by the variation in batch temperature as compared to the viscosity reduction due to chain extension and rupture of rubber molecules.

From the above argument, it justifies further that mixing at high rotor speed is not favourable particularly for N220 (ISAF) black loaded compound. In addition the rotor speed can be used to control the batch temperature for effective mixing and this has been adopted in the variable speed mixing system².

A comparison can be made on the extent of influence of mixer operating variables on mixing time and the reference viscosity of a N220 (ISAF) black loaded compound. Greater variation in mixing time was observed as compared to the variation in reference viscosity particularly when changes in unit work, rotor speed and fill factor were made. This is illustrated in figure 7.18 (b) and figure 9.3.

Consider the centre points of the shading diagrams number 5 of the above figures. Increasing unit work from 700 to 820 MJ/m^3 increases the mixing time from 470 to 690 seconds, whilst the reference viscosity remains within the same colour band value (i.e. between 84 to 102 kPa s). Similarly increasing rotor speed from 45 to 57.5 rpm and increasing fill factor from 0.7 to 0.8 reduces the mixing time from 470 to 360 seconds (23 %

decrease), and the reference viscosity still remains within the colour band of the same value as above. However, if a smaller scale was used in representing the reference viscosity, a more accurate evaluation could be made. Nevertheless the present scale is adequate to verify that a larger proportional variation in mixing time occurs as compared to the variation of reference viscosity when the levels of unit work, rotor speed and fill factor were changed.

As mentioned earlier in chapter 5 (section 5.4), an 'operating window' can be identified from the shading diagrams where a compound can be produced to satisfy both the process productivity and mixed compound specification. Within the limit of variables studied, a large throughput of the N220 (ISAF) black loaded compound of reference viscosity value within the range of 48 to 66 kPa s can be produced by referring to the figures 7.18 (b), 9.3 and 9.7. High throughput can be achieved at low mixing time and high batch volume.

To produce the above compound of reference viscosity within 48 to 66 kPa s, the shading diagram number 3 of figure 7.18 (b) is preferred to other shading diagrams, primarily based on the acceptable levels of the responses dump temperature and mixing time. From this shading diagram the level of the mixer variables at unit work 900 MJ/m^3 , fill factor 0.7 and coolant temperature of 35°C were required, irrespective of the level of rotor speed. A choice of rotor speed will be based on the mixing time, which is directly related to the throughput. However, the dump temperature will indicate the safety margin for the mix to prevent scorching. As such an optimum level of the rotor speed at 45 rpm was derived to meet these requirements. Table 9.1 illustrates the selected levels of the mixer operating variables

in producing N220 (ISAF) black loaded compound with an acceptable level of throughput and rheological properties.

Table 9.1 - Acceptable levels of mixer operating variables.

<u>Mixed Product</u>	
<u>Specification</u>	
Reference viscosity (kPa s)	48 - 66
<u>Mixer Operating</u>	
<u>Variables</u>	
Fill factor	0.8
Ram pressure (MPa)	0.41
Coolant Temperature (°C)	35
Rotor Speed (rpm)	45
Unit work (MJ/m ³)	900
<u>Mixer Responses</u>	
Dump Temperature (°C)	96 - 104
Mixing time (seconds)	600 - 700
Photometric Reading (%)	44 - 48
(carbon black dispersion)	

The above procedure demonstrate the use of the shading diagrams to identify an 'operating window' in which a N220 (ISAF) compound can be mixed to meet the rheological properties specification, at an acceptable level of mixing time. In addition, combination of specified limit values of carbon black dispersion with those for reference viscosity would further define the processing window.

9.2.5 The Variation Of Carbon Black Dispersion With Respect To The Mixer Responses And Mixer Performance.

It has been discussed earlier in chapter 8 that carbon black dispersion in the NR compound is strongly influenced by the amount of energy input, fill factor, coolant temperature and the characteristics of the filler itself. In addition significant interaction between fill factor/ram pressure and unit work/coolant temperature were observed. It is clear that the mixer operating variables are the most influential variables as compared to the material variables on the black dispersion level. It was also observed that in sections 9.2.3 and 9.2.4, the mixer operating variables strongly affect the dump temperature and mixing time. Therefore, these observations show that a direct correlation exists between carbon black dispersion and the mixer responses. Moreover it is widely known that dispersion is closely related to the rheological properties of the compound. In addition, the physical properties of a rubber compound depend greatly on the level of the carbon black dispersion.

Here again the variation of the mixer responses in relation to the dispersion level of the N220 (ISAF) black loaded compound was evaluated. This compound is chosen because it has greater variability and inconsistency during processing as compared to compounds loaded with larger particle blacks¹¹. As such, it is necessary to refer to the figures cited in preceding chapter 7 and chapter 8.

High energy level is a requirement for 'good' dispersion of compound loaded with N220 (ISAF) black. At energy level of

above 700 MJ/m^3 , the dispersion level was observed to be well within 40 % photometric reading (PR), representing a 'good' dispersion level. This is illustrated by the shading diagrams number 1-3 in figure 8.5 (chapter 8).

Considering 40 % to 44 % PR values as the mixed product specification required of the compound, the optimum mixing conditions were found to be as shown in table 9.2. The values of mixer and rheological responses at similar mixing conditions can be derived from figures 9.1, 9.2 and 7.18 (b) respectively, and they are also shown in table 9.2.

Table 9.2 - Tentative optimum mixing conditions.

<u>Mixed Product</u>	
<u>Specification</u>	
Photometric Reading PR (%) (Carbon black dispersion)	40 - 44
<u>Mixer Operating</u>	
<u>Variables</u>	
Fill factor	0.7
Ram pressure (MPa)	0.41
Coolant Temperature (°C)	35
Rotor speed (rpm)	45
Unit work (MJ/m^3)	900
<u>Mixer and Rheological</u>	
<u>Responses</u>	
Dump temperature (°C)	88 - 96
Mixing time (seconds)	700 - 800
Reference viscosity (kPa s)	66 - 84

As mentioned earlier, the main objective of mixing is to

produce a homogenously mixed compound with high black dispersion level at a high level of productivity. However, the goal of high productivity often counters the goal of improved quality. Nevertheless, an optimal level of both product quality and processing efficiency can be achieved by investigating systematically and by understanding the mixing process and processibility of the rubber compound.

In the case of N220 (ISAF) black loaded compound, by inspecting all the figures stated above and intelligently selecting the level of the mixer operating variables, an optimum level of both the compound quality and processing efficiency (high throughput) can be achieved.

Consider a dispersion level of within 40 % to 44 % PR value and a reference viscosity of between 66 to 84 kPa s to be the required mixed product specification of the N220 (ISAF) black loaded compound. From the tables 9.1 and 9.2, a higher dump temperature level can be utilised which can be effected either by increasing the rotor speed or the fill factor as shown in figure 9.1. Looking back at figure 8.5, increasing rotor speed from 45 to 57.5 and at fill factor 0.7, the dispersion level between 40 % and 44 % PR value is still maintained. However, increasing the fill factor to 0.8 would have reduce the dispersion level to within 44 % and 48 % PR value. The effect of increasing rotor speed at fill factor 0.7 causes a reduction in mixing time from 700 to 600 seconds, as shown in figure 9.7. Consequently optimum mixing conditions for N220 (ISAF) black loaded compound were derived and are tabulated in table 9.3.

The optimum mixing conditions (refer table 9.3) indicate too high a mixing time of above 600 seconds. However, setting

the mixed compound specification to within 44 % to 48 % PR values (dispersion levels), the mixing time is drastically reduced to between 300 and 400 seconds (refer to figure 8.5 and figure 9.7). In addition to shorter mixing time, the increase in fill factor from 0.7 to 0.8 obviously adds to the process productivity. Generally the mixed compound specification depends greatly on the requirement of downstream processes and the end product quality.

Table 9.3 - Optimum mixing conditions of N220 (ISAF) black loaded compound.

<u>Mixed Product</u>	
<u>Specification</u>	
Photometric reading PR (%)	40 - 44
Reference viscosity (KPa.s)	66 - 84
<u>Mixer Operating</u>	
<u>Variables</u>	
Fill factor	0.7
Ram pressure (MPa)	0.41
Coolant temperature (°C)	35
Rotor speed (rpm)	57.5
Unit work (MJ/m ³)	900
<u>Mixer Responses</u>	
Dump temperature (°C)	96 - 104
Mixing time (secs)	600 - 700

As mentioned earlier in chapter 8 (section 8.3.3) and from above discussion, the optimum mixing conditions for compound loaded with N220 (ISAF) black were at 900 MJ/m³ unit work and at fill factor 0.7. However, to achieve 40 % PR value for a compound loaded with N660 (GPF) black, mixing at lower range of

unit work, between 560 to 840 MJ/m³ and at high fill factor greater than 0.7 is indicated. Both the variables unit work and fill factor are related closely to the output of the mixing process. As such, it can be deduced that for the same dispersion level, a higher throughput can be achieved for compound loaded with large particle size blacks as compared to compound loaded with small particle size blacks.

Though the above procedure may be considered as a crude method of determining the optimum level of a mixing operation, it is adequate to identifying an 'operating window' within which a compound will meet both the process productivity and mixed product specification. Nevertheless the postulated polynomial model for each response can be computed so as the optimum mixing conditions can be precisely established. This would be an interesting area for future investigations of the rubber mixing process.

9.3 Summary.

i. During mixing of rubber compound, the dump temperature and mixing time are strongly influenced by the mixer operating variables as compared to the influence of material variables. High dump temperature occurs at high rotor speed and high unit work and it increases with increasing coolant temperature and fill factor. However, a higher percentage increase in coolant temperature is required for effecting a given percentage increase in dump temperature. In the case of mixing time, at constant unit work increasing rotor speed reduces the mixing time. Similarly increasing fill factor decreases the mixing time but at the expense of black dispersion level particularly for N220 (ISAF) black loaded compound.

ii. Increasing filler loading level increases the dump temperature of the NR compound. Greater variation in dump temperature was observed for compound loaded with smaller particle size black as compared to compound loaded with large particle size black. The influence of oil loading level on dump temperature is similar to its influence on reference viscosity, where a critical limit of oil loading level was observed.

iii. At constant unit work mixing time decreases with increasing filler concentration. Again, at constant unit work, irrespective of filler dispersion level, the extent of decrease in mixing time was higher for compound loaded with smaller particle size blacks such as N220 (ISAF), as compared to compound loaded with large particle size blacks such as N762 (SRF). Oil loading level, within the range investigated, has little influence on the mixing time.

iv. Within the level of variables studied, comparatively greater variation in dump temperature and mixing time was observed than the variation of reference viscosity. The viscosity reduction of a compound due to batch temperature variation is greater than the viscosity reduction due to chain extension and rupture of rubber molecules.

v. The shading diagrams generated in this study enable an 'operating window' to be identified within which a compound will meet both the process productivity and mixed product specification. By combining the shading diagrams of these responses i.e. rheological properties, carbon black dispersion levels and mixer responses, an optimum mixing condition can be established. The optimum mixing condition of N220 (ISAF) black loaded compound are shown in table 9.3.

Literature Cited.

(Chapter 9)

1. H. Palmgren, Rubb.Chem.Tech., 48,462(1975)
2. P. Whitaker, J.I.R.I., 4(4),153,August(1970)
3. N. Nakajima et.al, Rubb.Chem.Tech., 55,456(1982)
4. P.C. Ebell, Ph.D.Thesis Loughborough University, (1981)
5. P.K. Freakley, Int.Rubb.Conf. Harrogate England, Paper F3-1,
5-12 June(1981)
6. J.M. Funt, 'Mixing of Rubber' RAPRA Publication (1977)
7. R.N. Comes, Rubber World, 135,4,565(1957)
8. W.F. Busse, Ind.Eng.Chem., 24,140,(1973)
9. E.S. Dizon, Rubb.Chem.Tech., 49,12(1976)
10. W.M. Wiedman and H.M. Schmid, Rubb.Chem.Tech., 55,363(1982)
11. G.M. Bristow, NR Technology, 12(3),45(1981)

CHAPTER 10

SUMMARY AND CONCLUSION

Internal mixing of rubber is known to be a complex operation. It is a multivariable and non-steady state process. The empirical approach adopted in this study has shown some promise, perhaps adding to a better understanding of the mixing operation and the processability of the NR compound. Furthermore, the statistical experimental design (factorial design) and analysis (multivariable regression analysis) techniques have made this investigation possible, where the influence of eight independent variables on the compound properties were evaluated. However, the empirical approach renders specifically to the mixer and the compound used for the mixing trials. Nevertheless it forms the basis for fractioning and modification of the experimental design, eventually reducing the number of mixing trials and omitting some process variables in the experimental design.

In addition, the use of computer graphics, in this case the colour shading diagrams, have proved to be a useful technique in presenting pictorially the variation of measured responses with the independent variables. Although the hard copy of the diagrams are in the form of colour photographs, the availability of colour computer printers will in future reduce its preparation time considerably.

The TMS rheometer and the dark field reflected light microscopy (DFRLM) used were able to characterize each mix,

discriminating the compounds rheological properties and black dispersion level satisfactorily. However, in evaluating the wall slip behaviour of the compound, the data extracted from both the grooved and polished rotors of the TMS rheometer should be treated with great care, whereby the flow characteristic of the compound changes at high shear rates from laminar to hypothetical 'rolling' flow.

The extent of influence of mixer operating variables and material variables on the NR compounds differ for each response measured. The influence of these variables on rheological properties, viscoelastic behaviour and wall slip behaviour can be referred to in chapter 7, whilst carbon black dispersion and the mixer performance are in chapter 8 and 9 respectively. In addition, a comparative influence between the mixer operating variables and the material variables on the measured responses was also evaluated and discussed in the respective chapters. By inspecting the shading diagrams, the responses can be correlated with one another, consequently enabling an optimum level of the mixer operating variables and the material variables ^{to} be established, meeting both the process productivity and mixed product specification.

Alternatively, as mentioned earlier the optimum level can be determined mathematically, thereby opening an avenue for future rubber mixing study. The wide range of mixer variables and material variables used in this study is beneficial to the NR product manufacturers, particularly when the results obtained are collaborated with mechanical properties of the NR compound.

On the whole, this study is extravagant of materials and time; however, the analysis and results derived are very useful

particularly when they are stored in computers and are accessible for references and controls during processing. Furthermore, these results can be manipulated to simulate several mixing conditions generating valuable informations for NR processing in the coming future.

Finally to the authors best knowledge and experience the following future research works are suggested;

i. Further investigation on the hypothetical 'rolling' flow phenomenon of rubber compound is necessary. Its correlation with the wall slip behaviour will give a better insight and understanding of the compound behaviour during processing.

ii. Having identified the 'go' and 'no go' mixing areas of the NR compound, it is useful to undertake further experiments in order to establish a comprehensive relationship between the flow behaviour of the mixing stock and its cured compound property. In addition, extending the work to internal mixer of bigger volume will be obviously of commercial importance.

iii. In this study the prototype TMS rheometer was used, and it has shown great potential as a process control and research instrument. As such it will be advantageous if further refinement and development are made on this rheometer before pursuing further rheological study such as mentioned in (i) and (ii) above.

iv. It will be interesting to note whether the coefficients of the polynomial functions of the measured responses derived in this study, are related in any way to those results established by other researchers. Consequently, a closer coordination between researchers is encouraged so that the present and future research findings can be fully exploited.

APPENDICES

APPENDIX I

1/4 FRACTIONAL TWO-LEVEL FACTORIAL AND COMPOSITE EXPERIMENTAL
DESIGN MATRIX OF 8 VARIABLES.

	Mix Number	Random Order	Fill Fact. F	Ram Press P	Cool. Temp. T	Rotor Speed S	Unit Work W	Fill. Load. L	Oil Load. O	Black Type B
Two-Level Factorial Points	R-1	50	-1	-1	-1	-1	-1	-1	+1	+1
	R-2	74	-1	-1	-1	-1	-1	+1	+1	-1
	R-3	63	-1	-1	-1	-1	+1	-1	+1	-1
	R-4	9	-1	-1	-1	-1	+1	+1	+1	+1
	R-5	36	-1	-1	-1	+1	-1	-1	-1	-1
	R-6	61	-1	-1	-1	+1	-1	+1	-1	+1
	R-7	38	-1	-1	-1	+1	+1	-1	-1	+1
	R-8	5	-1	-1	-1	+1	+1	+1	-1	-1
	R-9	82	-1	-1	+1	-1	-1	-1	-1	-1
	R-10	21	-1	-1	+1	-1	-1	+1	-1	+1
	R-11	70	-1	-1	+1	-1	+1	-1	-1	+1
	R-12	37	-1	-1	+1	-1	+1	+1	-1	-1
	R-13	6	-1	-1	+1	+1	-1	-1	+1	+1
	R-14	91	-1	-1	+1	+1	-1	+1	+1	-1
	R-15	71	-1	-1	+1	+1	+1	-1	+1	-1
	R-16	83	-1	-1	+1	+1	+1	+1	+1	+1
	R-17	66	-1	+1	-1	-1	-1	-1	-1	+1
	R-18	64	-1	+1	-1	-1	-1	+1	-1	-1
	R-19	18	-1	+1	-1	-1	+1	-1	-1	-1
	R-20	84	-1	+1	-1	-1	+1	+1	-1	+1
	R-21	77	-1	+1	-1	+1	-1	-1	+1	-1
	R-22	44	-1	+1	-1	+1	-1	+1	+1	+1
	R-23	10	-1	+1	-1	+	+1	-1	+1	+1
	R-24	17	-1	+1	-1	+1	+1	+1	+1	-1
	R-25	11	-1	+1	+1	-1	-1	-1	+1	-1
	R-26	65	-1	+1	+1	-1	-1	+1	+1	+1
	R-27	45	-1	+1	+1	-1	+1	-1	+1	+1
	R-28	1	-1	+1	+1	-1	+1	+1	+1	-1
	R-29	23	-1	+1	+1	+1	-1	-1	-1	+1
	R-30	22	-1	+1	+1	+1	-1	+1	-1	-1
	R-31	87	-1	+1	+1	+1	+1	-1	-1	-1
	R-32	43	-1	+1	+1	+1	+1	+1	-1	+1

</																			

APPENDIX II

Polynomial Coefficients Of Viscous Parameters.

Polynomial Terms	Flow Index n	Apparent Viscosity kPa s			
		1s ⁻¹	6s ⁻¹	35s ⁻¹	44s ⁻¹
B ₀ (%GM) (Grand Mean)	0.08*	100.5*	19.5*	3.8*	3.0*
B ₁ (F)	0.004	0.6	0.2	0.06	0.05
B ₂ (P)	-0.0009	2.4	0.5	0.09	0.07
B ₃ (T)	0.002	-0.7	-0.1	-0.02	-0.01
B ₄ (S)	0.002	-2.6	-0.4	-0.05	-0.04
B ₅ (W)	0.003	-2.6	-0.7+	-0.2*	-0.1*
B ₆ (L)	-0.04*	30.8*	5.0*	0.8*	0.6*
B ₇ (O)	0.01+	-12.3*	-2.1*	-0.4*	-0.3*
B ₈ (B)	0.04*	-23.7*	-3.5*	-0.5*	-0.3*
B ₁₁ (FF)	0.005	-1.4	-0.2	-0.02	-0.01
B ₂₂ (PP)	0.0003	-0.6	-0.2	-0.05	-0.04
B ₃₃ (TT)	0.006	-2.2	-0.3	-0.04	-0.03
B ₄₄ (SS)	0.005	-2.0	-0.3	-0.04	-0.03
B ₅₅ (WW)	0.008	-3.9	-0.6+	-0.07	-0.05
B ₆₆ (LL)	0.01*	-1.1	-0.1	0.005	0.007
B ₇₇ (OO)	0.01+	-4.3	-0.6+	-0.05	-0.03
B ₈₈ (BB)	0.002	0.5	0.01	0.008	-0.007
B ₁₂ (FP)	-0.006	2.2	0.3	0.02	0.01
B ₁₃ (FT)	-0.0009	-0.7	-0.04	0.003	0.003
B ₁₄ (FS)	-0.0006	-0.7	-0.02	0.02	0.02
B ₁₅ (FW)	0.008	-4.0	-0.6	-0.08	-0.05
B ₁₆ (FL)	0.0004	1.0	0.3	0.05	0.04
B ₁₇ (FO)	0.006	-4.4	-0.6	-0.06	-0.04
B ₁₈ (FB)	-0.003	0.1	-0.07	-0.04	-0.03
B ₂₃ (PT)	-0.004	2.4	0.3	0.04	0.03
B ₂₄ (PS)	0.006	-1.9	-0.3	-0.05	-0.04
B ₂₅ (PW)	-0.003	3.8	0.5	0.05	0.04
B ₂₆ (PL)	-0.002	2.3	0.4	0.07	0.06
B ₂₇ (PO)	0.0008	0.5	0.01	-0.002	-0.003
B ₂₈ (PB)	-0.004	-0.7	-0.2	-0.04	-0.04

	n	η_0	η_6	η_{35}	η_{44}
B ₃₄ (TS)	0.01+	-4.1	-0.4	0.01	-0.001
B ₃₅ (TW)	-0.004	1.5	0.04	-0.04	-0.004
B ₃₆ (TL)	-0.002	0.8	0.2	0.03	0.02
B ₃₇ (TO)	-0.0003	-0.4	-0.1	-0.02	-0.02
B ₃₈ (TB)	-0.004	-0.1	-0.1	-0.04	-0.03
B ₄₅ (SW)	0.003	-1.6	-0.3	-0.05	-0.04
B ₄₆ (SL)	0.003	-1.1	0.02	0.04	0.03
B ₄₇ (SO)	-0.003	1.8	0.3	0.05	0.04
B ₄₈ (SB)	-0.005	2.2	0.2	-0.006	-0.01
B ₅₆ (WL)	-0.003	1.1	0.04	-0.02	-0.02
B ₅₇ (WO)	0.002	-0.8	-0.04	0.01	0.01
B ₅₈ (WB)	0.008	-2.3	-0.06	0.05	0.05
B ₆₇ (LO)	0.0005	-6.2+	-0.8+	-0.1+	-0.08+
B ₆₈ (LB)	0.02*	-19.5*	-2.8*	-0.4*	-0.26*
B ₇₈ (OB)	0.0004	6.0+	0.8+	0.1+	0.08+

* indicates coefficient significance 99.9 %

+ indicates coefficient significance 97.5 %

APPENDIX III

Polynomial Coefficients Of Wall Slip and Elastic Parameters.

Polynomial Terms	Wall Slip V_{s3} mm/s	Wall Slip V_{s23} mm/s	Shear Modul. G kPa	Relax. Rate a	Relax. Time t sec.
B_0 (%GM) (Grand Mean)	0.83*	2.7*	1256*	0.7*	0.33*
B_1 (F)	-0.04	0.2	-10.5	-0.0004	-0.0003
B_2 (P)	0.1	0.8+	60.5	0.005	0.007
B_3 (T)	-0.05	-0.5	26.5	0.002	-0.0007
B_4 (S)	0.1	0.3	-70.6	0.01	-0.002
B_5 (W)	0.1	0.3	32.9	0.01	-0.009
B_6 (L)	-0.3*	-0.9+	449.0*	-0.07*	0.02*
B_7 (O)	0.1	0.3	-145.5+	0.03*	-0.01+
B_8 (B)	0.3*	0.4	-427.0*	0.06*	-0.02*
B_{11} (FF)	-0.04	-0.01	1.1	-0.009	-0.0008
B_{22} (PP)	0.06	0.2	77.2	-0.002	-0.006
B_{33} (TT)	-0.02	-0.0003	-25.1	0.003	-0.006
B_{44} (SS)	0.0003	0.2	-38.3	0.02+	-0.004
B_{55} (WW)	0.07	-0.07	-64.0	0.003	-0.004
B_{66} (LL)	0.03	-0.04	-85.9	0.005	0.004
B_{77} (OO)	-0.08	-0.2	-96.8	0.008	0.002
B_{88} (BB)	-0.04	0.04	57.7	-0.02+	0.0001
B_{12} (FP)	0.1	0.8	41.2	-0.006	-0.0004
B_{13} (FT)	0.07	0.03	-50.2	-0.03+	-0.0004
B_{14} (FS)	-0.007	0.4	-73.6	-0.02	0.004
B_{15} (FW)	-0.1	-0.03	-54.7	0.02	-0.005
B_{16} (FL)	-0.02	0.1	-3.0	-0.01	0.007
B_{17} (FO)	-0.07	-0.8	-132.0	0.008	-0.003
B_{18} (FB)	0.008	-0.3	28.0	-0.004	-0.001
B_{23} (PT)	0.1	-0.04	85.2	-0.02	-0.005
B_{24} (PS)	-0.05	0.3	18.0	-0.005	-0.002
B_{25} (PW)	-0.05	0.2	97.0	0.02	-0.003
B_{26} (PL)	0.04	0.4	73.4	-0.003	0.002
B_{27} (PO)	-0.04	-0.4	-8.2	0.003	-0.003
B_{28} (PB)	0.02	-0.5	-46.4	-0.003	0.002

	V_{s3}	V_{s23}	G	a	t
B ₃₄ (TS)	-0.1	-0.6	-169.1+	0.0004	0.007
B ₃₅ (TW)	-0.05	-0.8	81.2	0.02	-0.001
B ₃₆ (TL)	0.07	-0.4	45.4	0.004	0.002
B ₃₇ (TO)	-0.04	0.3	-20.8	0.02	-0.006
B ₃₈ (TB)	-0.1	0.1	-35.6	-0.003	-0.003
B ₄₅ (SW)	0.02	0.4	-55.1	0.01	-0.004
B ₄₆ (SL)	-0.02	0.6	-68.1	0.01	-0.004
B ₄₇ (SO)	0.04	-0.1	18.4	-0.02	0.002
B ₄₈ (SB)	0.002	-0.3	97.5	-0.01	-0.005
B ₅₆ (WL)	0.02	0.4	88.1	0.007	-0.004
B ₅₇ (WO)	-0.07	-0.7	22.8	-0.03*	-0.002
B ₅₈ (WB)	0.03	-0.3	-115.5	-0.02	-0.0004
B ₆₇ (LO)	-0.02	-0.2	-106.7	0.01	-0.007
B ₆₈ (LB)	0.05	-0.4	-369.0*	0.05*	-0.02*
B ₇₈ (OB)	0.008	0.4	91.1	0.01	0.01+

* indicates coefficient significance 99.9 %

+ indicates coefficient significance 97.5 %

APPENDIX IV

Polynomial Coefficients Of Black Dispersion And Mixer Responses.

Polynomial Terms	Carbon Black Dispersion		Mixer Responses	
	Photo.Read. (PR) %	Comp.Para. (CP) %	Dump.Temp. °C	Mix.Time sec.
B ₀ (%GM) (Grand Mean)	48.8*	79.7*	104.6*	491.4*
B ₁ (F)	1.1	6.4+	6.4*	-47.9*
B ₂ (P)	0.08	-0.1	0.2	-12.8
B ₃ (T)	-0.4	4.8	6.8*	24.0+
B ₄ (S)	-0.9	-1.4	7.0*	-43.8*
B ₅ (W)	-3.8*	-7.4+	1.0	138.3+
B ₆ (L)	-0.5	-1.1	3.8*	-37.4*
B ₇ (O)	0.2	3.3	-2.9*	16.4
B ₈ (B)	-4.1*	-15.7*	-1.7+	4.4
B ₁₁ (FF)	-0.3	-1.0	-0.7*	-6.0
B ₂₂ (PP)	-0.6	-1.0	-0.9	-1.0
B ₃₃ (TT)	-0.03	0.4	0.08	3.7
B ₄₄ (SS)	0.2	-0.8	-0.9	-2.8
B ₅₅ (WW)	1.2+	1.9	-0.7	11.3
B ₆₆ (LL)	-0.9	-5.8+	0.8	0.2
B ₇₇ (OO)	0.5	-1.8	-0.8	-3.1
B ₈₈ (BB)	1.2+	4.5+	0.8	20.5*
B ₁₂ (FP)	-1.8+	-3.5	-0.2	-5.4
B ₁₃ (FT)	-1.3	-3.8	0.8	-5.4
B ₁₄ (FS)	-0.5	-3.0	1.4	1.1
B ₁₅ (FW)	0.3	-0.8	-0.1	-9.6
B ₁₆ (FL)	0.3	-0.6	0.5	5.0
B ₁₇ (FO)	-0.9	-1.4	-0.9	3.2
B ₁₈ (FB)	-1.7+	-5.5	-0.3	18.0
B ₂₃ (PT)	0.02	-2.2	0.5	1.2
B ₂₄ (PS)	-1.0	1.0	0.6	6.3
B ₂₅ (PW)	0.05	-1.2	0.7	-10.0
B ₂₆ (PL)	-0.06	0.4	0.6	4.6
B ₂₇ (PO)	-0.3	2.2	-0.2	-16.2
B ₂₈ (PB)	-1.1	-4.7	0.2	5.2

	(PR) %	(CP) %	Dm.Temp°C	Mx.Time s
B ₃₄ (TS)	0.5	-3.7	1.0	7.5
B ₃₅ (TW)	1.4+	2.6	-0.4	8.1
B ₃₆ (TL)	-0.4	-2.5	0.2	-6.8
B ₃₇ (TO)	-0.04	-4.1	0.6	3.0
B ₃₈ (TB)	-1.3	4.0	1.1	4.0
B ₄₅ (SW)	0.8	-0.9	1.0	-2.2
B ₄₆ (SL)	0.3	2.7	0.8	7.0
B ₄₇ (SO)	0.8	-1.4	0.5	10.1
B ₄₈ (SB)	0.05	1.9	-0.4	-2.1
B ₅₆ (WL)	0.4	4.3	0.7	-12.2
B ₅₇ (WO)	0.7	-3.5	-0.2	-3.0
B ₅₈ (WB)	1.2	2.9	0.6	-4.7
B ₆₇ (LO)	-0.4	1.4	-0.3	7.8
B ₆₈ (LB)	0.7	0.2	-1.0	7.8
B ₇₈ (OB)	0.9	-4.1	0.5	-5.0

* indicates coefficient significance 99.9 %

+ indicates coefficient significance 97.5 %

APPENDIX V

Testing Procedure In the TMS Rheometer.

Time (seconds)	Procedure
0	<ol style="list-style-type: none"> 1. Set the temperature control to the required testing temperature. Insert the rotor into the testing cavity and allow ample time for the testing temperature to ^{be}reached 2. Inject rubber at 80 psi for a short period of time into the testing cavity. In this study the time varies from 6 seconds to 30 seconds.
30	<ol style="list-style-type: none"> 3. Start the rotor rotation at 3 rpm
35	<ol style="list-style-type: none"> 4. Increase rotor rotation to 4 rpm
39	<ol style="list-style-type: none"> 5. Increase rotor rotation to 10 rpm
42	<ol style="list-style-type: none"> 6. Increase rotor rotation to 15 rpm
44	<ol style="list-style-type: none"> 7. Increase rotor rotation to 20 rpm
46	<ol style="list-style-type: none"> 8. Increase rotor rotation to 30 rpm
48	<ol style="list-style-type: none"> 9. Increase rotor rotation to 40 rpm
49	<ol style="list-style-type: none"> 10. Stop rotor rotation (motor)
49	<ol style="list-style-type: none"> 11. Reverse motor rotation
170	<ol style="list-style-type: none"> 12. Restart rotor rotation at 10 rpm
174	<ol style="list-style-type: none"> 13. Stop motor for stress relaxation test
184	<ol style="list-style-type: none"> 14. Reverse motor rotation
185	<ol style="list-style-type: none"> 15. Raise transfer mould and that is the end of a test.

APPENDIX VI

Derivation Of Stress Function In Wall Slip Behaviour.

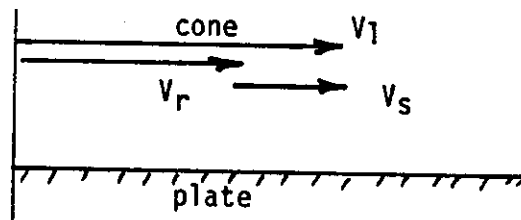
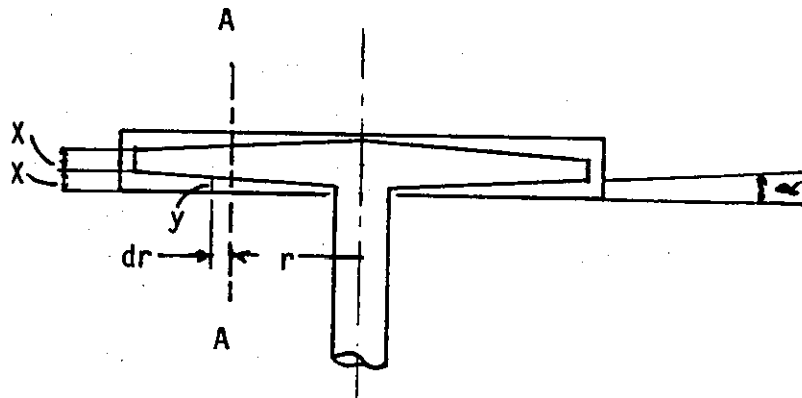
Referring to chapter 7 (section 7.2.2), the slip velocity obeys power law relationship as

$$V_s = k \tau^m \quad \dots\dots\dots 1$$

where V_s - slip velocity

τ - shearing stress

k, m - material constant



Section AA

Consider section-AA at radius r from the centre of the rotor.

$$V_r = V_1 - V_s \quad \dots\dots\dots 2$$

where V_r - resultant linear velocity
 V_l - linear velocity of rotor
 V_s - wall slip velocity

Shear rate at radius r

$$\dot{\gamma} = V_r / y \quad \dots\dots\dots 3$$

Assuming Newtonian boundary layer

$$\tau(r) = \eta_a \dot{\gamma} \quad \dots\dots\dots 4$$

$$= \eta_a \frac{V_l - V_s}{y} \quad \dots\dots\dots 5$$

$$y = r \tan \alpha$$

where α - 1/2 cone angle

ω - angular velocity of rotor

$$\tau(r) = \eta_a \frac{V_l - V_s}{r \tan \alpha} \quad \dots\dots\dots 6$$

$$\tau(r) = \eta_a \frac{r\omega - k \tau(r)^m}{r \tan \alpha} \quad \dots\dots\dots 7$$

Rearranging equation 7,

$$\eta_a k \tau(r)^m + r \tan \alpha \tau(r) - \eta_a r \omega = 0 \quad \dots\dots\dots 8$$

Equation 8 is the stress function and it can only be solved numerically. In this study a computer programme in appendix VII was utilised to solve for $\tau(r)$.

APPENDIX VII

A) Computer Programme For Linear Regression Of Experimental Data And Plotting Of Flow Curves.

```

LIBRARY 'GINOGRAF'
LIBRARY 'GINO'
LIBRARY 'VAPPLB'
LIBRARY 'LUSUBV'
IMPLICIT REAL*4(A-H,O-Z)
C THIS PROGRAM IS SINGLE PRECISION
DIMENSION D(7),G(7),F(7)
DIMENSION X(10),Y(10),XL(10),YL(10),SQXL(10),SQYL(10),PXL(10),PYL(10)
DIMENSION YF(7),YFL(7),P(7),PL(7),SQPL(7),PXLPL(7),PF(7),PFL(7)
DIMENSION AS(7),SG(7),TG(7),TP(7),VISC(7),AT(150),SP(7)
DIMENSION C(150),DELTOP(150),AR(21),TI(21),SHS(21),SN(7),ST(150)
DIMENSION XR(10),YFS(10),VS(10),XP(10),VSQ(10),YSQ(10),DS(10)
DIMENSION VSL(10),YFSL(10),VSF(10),PVY(10),VSFL(10),VST(150)
DIMENSION VISA(10)
OPEN(UNIT=5,IOSTAT=IOS,ERR=90,FILE='DNRO',STATUS='OLD')
READ(5,*)IL
DO 1 I=1,7
1 READ(5,*)D(I),G(I),F(I)
C CONVERT TO ABSOLUTE VALUES
DO 5 I=1,7
X(I)=D(I)*1.0
Y(I)=G(I)*57.5/20.0
P(I)=F(I)*57.5/20.0
5 CONTINUE
C CONVERT LINEAR VALUES TO LOG10
DO 10 I=1,7
XL(I)=ALOG10(X(I))
YL(I)=ALOG10(Y(I))
PL(I)=ALOG10(P(I))
SQXL(I)=XL(I)*XL(I)
SQYL(I)=YL(I)*YL(I)
PXL(I)=XL(I)*YL(I)
SQPL(I)=PL(I)*PL(I)
PXLPL(I)=XL(I)*PL(I)
10 CONTINUE
C SUMMATION OF THE VALUES
C
C
SUMX=0
SUMY=0
SUMP=0
SUMXX=0
SUMYY=0
SUMPP=0
SUMXP=0
SUMXY=0
C
DO 100 I=1,7
SUMX=SUMX+XL(I)
SUMY=SUMY+YL(I)
SUMP=SUMP+PL(I)
SUMXX=SUMXX+SQXL(I)
SUMYY=SUMYY+SQYL(I)
SUMPP=SUMPP+SQPL(I)
SUMXY=SUMXY+PXL(I)
SUMXP=SUMXP+PXLPL(I)
100 CONTINUE
C
T=SUMX*SUMY/7

```

```

WRITE(1,452)
452  FORMAT(1H1,/,10X,'APPARENT VISCOSITY',5X,'SHEAR RATE',/,15X,
1    'KPA SEC',12X,'SEC')
DO 453 I=1,7
WRITE(1,454)VISA(I),X(I)
454  FORMAT(/,10X,F11.3,12X,F6.3)
453  CONTINUE
C    PLOT OF SHEAR RATE WITH SH.STRESSES (REGRESSED)
C
C
WRITE(1,500)
500  FORMAT(/,2X,'5.T4014',/,2X,'6.T4010',/,2X,'7.TREND',
1    /,2X,'8.C1051N',/,2X,'9.VDU',/,2X,'10.SE281',/,2X,'11.NO PLOT')
LDV=8
IF(LDV.EQ.5)CALL T4014
IF(LDV.EQ.6)CALL T4010
IF(LDV.EQ.7)CALL TREND
IF(LDV.EQ.8)CALL C1051N
IF(LDV.EQ.9)CALL VDU
IF(LDV.EQ.10)CALL SE281
IF(LDV.EQ.11)GO TO 502
C
C
CALL PICCLE
CALL DEVPAP(297.0,210.0,1)
CALL WINDO2(0.0,297.0,0.0,210.0)
CALL ERRMAX(1)
CALL CHASIZ(2.0,2.0)
C
C
CALL AXIPOS(1,60.0,50.0,200.0,1)
CALL AXIPOS(1,60.0,50.0,120.0,2)
CALL AXISCA(3,10,0.0,2.0,1)
CALL AXISCA(3,10,1.4,2.4,2)
CALL AXIDRA(2,1,1)
CALL AXIDRA(-2,-1,2)
C
CALL GRASYH(XL,YL,7,4,0)
CALL GRAPOL(XL,YFL,7)
CALL GRASYM(XL,PL,7,7,0)
CALL BROKEN(3)
CALL GRAPOL(XL,PFL,7)
C
C
CALL MOVTO2(160.0,33.0)
CALL CHASIZ(2.5,2.5)
CALL CHAHOL('LOG SHEAR RATE (SEC-1.)*.')
CALL CHAANG(90.0)
CALL MOVTO2(40.0,80.0)
CALL CHAHOL('LOG SHEAR STRESS (KPA.)*.')
CALL CHAANG(0.0)
CALL MOVTO2(100.0,180.0)
CALL CHASIZ(3.0,3.0)
CALL CHAHOL('FLOW CURVES OF NR MIXES. RUN 63 *.')
CALL CHASIZ(2.0,2.0)
CALL MOVTO2(230.0,80.0)
CALL BROKEN(0)
CALL LINTO2(245.0,80.0)
CALL MOVTO2(250.0,80.0)
CALL CHAHOL('F*LIT. *UG*LROOVED *UR*LOTOR*.')
CALL MOVTO2(230.0,70.0)
CALL BROKEN(3)
CALL LINTO2(245.0,70.0)
CALL MOVTO2(250.0,70.0)
CALL CHAHOL('F*LIT. *UP*LOLISHED *UR*LOTOR*.')
CALL BROKEN(0)
CALL DEVEND

```


B) Programme For Analysis Of Wall Slip Behaviour In TMS Rheometer.

```

C
C
C      ANALYSIS OF SLIP BEHAVIOUR IN TMS RHEOMETER WITH DOUBLE CONE ROTOR
C
C
C      800 DO 505 I=1,7
C          SN(I)=X(I)
C          SG(I)=Y(I)
C          SP(I)=P(I)
C      505  CONTINUE
C
C
C      SET NUMBER OF EXPERIMENTAL POINTS
C      NT=7
C
C
C      READ IN EXPT. VALUES FOR ROTATIONAL SPEED AND SHEAR STRESS
C
C      SET THE ROTOR GEOMETRY (DIMS. IS IN METERS)
C      PI=4.0*ATAN(1.)
C      A=0.02302
C      AL=0.00242
C      AH=0.00160
C      ALPHA=6.00*PI/180
C      RSTEP=A/20
C
C
C      DIVIDE EQUALLY ROTOR RADIUS TO EVALUATE THE TORQUE BY INTEGRATION
C
C      DO 570 M=1,21
C      570  AR(M)=RSTEP*FLOAT(M-1)
C
C
C      START THE MAIN LOOP FOR EACH EXP. POINT
C
C      READ(5,*) EPS,ST11,ST22,SM,ITMAX
C      DO 530 N=1,NT
C
C          CONVERT EXP. SHEAR STRESS INTO TORQUE VALUES
C          TG(N)=4.0*PI*A*A*SG(N)*1000.0*(A+1.5*AH)/3.0
C          TP(N)=4.0*PI*A*A*SP(N)*1000.0*(A+1.5*AH)/3.0
C
C          CONVERT ROTOR SPEEDS FROM R.P.M. TO RADIAN/SEC.
C          AS(N)=SN(N)*PI/30.0
C
C          CALCULATE THE APPARENT VISCOSITY OF MATERIAL USING
C          IGROOVED ROTOR RESULTS ASSUMING NO SLIP CONDITION
C
C          VISC(N)=SG(N)*1000.0*SIN(ALPHA)/COS(ALPHA)/AS(N)
C
C          LOOP FOR INCREMENT VALUES OF "K"(THE CONSTANT IN SLIP FUNCTION)
C          CK=0.0
C          DO 540 I=1,10
C          C(I)=CK+1.00E-8
C          CK=C(I)
C
C          LOOP FOR INCREMENT RADIUS VALUES
C          DO 560 M=1,21
C
C          SET THE TWO SHEAR STRESS LIMITS FOR THE "REGULAR FALSI METHOD"
C          ST1=ST11
C          ST2=ST22
C          SM=SM
C
C          TEST IF THE UPPER SHEAR STRESS LIMIT IS A NEGATIVE STRESS FUNCTION
C          STF1=ST1*AR(M)*SIN(ALPHA)/COS(ALPHA)+VISC(N)*C(I)*ST1**SM
C          1  -VISC(N)*AR(M)*AS(N)
C          STF2=ST2*AR(M)*SIN(ALPHA)/COS(ALPHA)+VISC(N)*C(I)
C          1  *ST2**SM-VISC(N)*AR(M)*AS(N)

```

```

C      IF(STF2.LT.0.0)GO TO 600
C      SOLUTION OF SHEAR STRESS USING "REGULAR FALSI METHOD"
C
C      DO 610 NI=1,ITMAX
C      ST(I)=(ST1*STF2-ST2*STF1)/(STF2-STF1)
C      STF=ST(I)*AR(M)*SIN(ALPHA)/COS(ALPHA)+VISC(N)*C(I)*ST(I)
1     **SH-VISC(N)*AR(M)*AS(N)
C
C      STF=STF
C
C      TEST FOR MAXIMUM NUMBER OF ITERATION
C
C      IF(NI.GE.ITMAX) GO TO 574
C
C      TEST IF ROOT HAS BEEN FOUND
C
C      IF(ABS(STFN).LE.EPS) GO TO 579
C      IF(ST1*STFN.LE.0.0) GO TO 572
C      ST1=ST(I)
C      STF1=STFN
C      GO TO 610
572    ST2=ST(I)
C      STF2=STFN
C
C      610 CONTINUE
C
C      GO TO 579
574    WRITE(1,577)NI
577    FORMAT(5X,'ITERATION NOT CONVERGE AT ',2X,I5)
C
C      GO TO 680
C 575    WRITE(1,578)ST
C 578    FORMAT(5X,'SHEAR STRESS =',2X,F20.6)
579    VST(I)=C(I)*(ST(I)**SH)
C      SHS(M)=ST(I)
580    TI(M)=AR(M)*AR(M)*SHS(M)
C
C      CAL. THE TORQUE VALUES BY INTEGRATION
C      TIS=0
C      DO 590 M=2,21
590    TIS=TIS+(TI(M-1)+TI(M))*RSTEP/2
C      AT(I)=4.0*PI*TIS+2.0*PI*VISC(N)*AS(N)*A*A*AH/SIN(ALPHA)/
1     COS(ALPHA)
C
C      COMPARE THE CALCULATED TORQUE WITH THE EXPERIMENTAL TORQUE VALUES
C      DELTOP(I)=AT(I)-TP(N)
540    CONTINUE
C
C      PRINT THE EXPERIMENTAL TORQUE VALUES
C      NC=N
C      WRITE(1,720)
720    FORMAT(////,10X,'EXPERIMENTAL VALUES')
C      WRITE(1,730)SN(NC),VISC(NC)
730    FORMAT(//,10X,'ROTOR SPEED (R.P.M.) =',F6.3,//10X,
1     'APPARENT VISCOSITY (PA.SEC) =',2X,F11.3)
C      WRITE(1,740)TG(NC),TP(NC)
740    FORMAT(/,10X,'TORQUE ON GROOVED ROTOR =',F8.4,2X,'NM',
1     /,10X,'TORQUE ON POLISHED ROTOR =',F8.4,2X,'NM')
C
C      PRINT OUT THE CALCULATED(PREDICTED) TORQUE VALUES
C      WRITE(1,750)SH
750    FORMAT(///,10X,'PREDICTED VALUES',5X,'M - VALUE =',F5.3)
C      WRITE(1,550)
550    FORMAT(/,14X,'K',8X,'TORQUE',8X,'DELTOP',8X,'STRESS',3X,'ITR NO.',
1     2X,'SL.VEL.')
C      WRITE(1,560)(C(I),AT(I),DELTOP(I),ST(I),NI,VST(I),I=1,10)
560    FORMAT(/,8X,E10.5,4X,F8.4,5X,F8.4,4X,E12.6,I5,5X,E8.3)
530    CONTINUE
C
C      GO TO 680
600    WRITE(1,620)
620    FORMAT(1X,'SHEAR STRESS FUNCTION IS NEGATIVE')
C      GO TO 680
C 660    WRITE(1,670)
C 670    FORMAT(1X,'NO CONVERGENCE AFTER ITMAX CYCLES')
680    CLOSE(UNIT=5,Iostat=IOS,ERR=90)
C      CALL EXIT
90     CALL RUMERR(IOS)
C      END
BOTTOM
FIL
KBBNRO
OK,

```

